The Development of Vanadium and Titanium Containing Metal Organic Frameworks for Applications in Adsorption and Heterogeneous Catalysis

Dissertation submitted in fulfillment of the requirements for the degree of Doctor of Science: Chemistry
by

Karen Leus

Department of Inorganic and Physical Chemistry
Faculty of Sciences

Promoter: Prof. Dr. Pascal Van Der Voort
Promoter: Prof. Dr. ir. Guy B. Marin

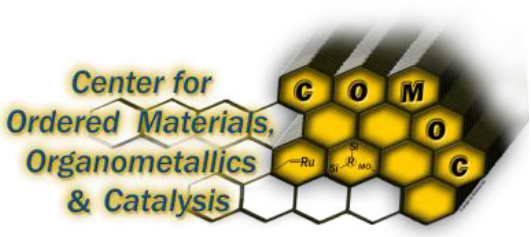

This dissertation work has been performed in the Center for Ordered Materials, Organometallics and Catalysis (COMOC) under the supervision of Prof. Dr. Pascal Van Der Voort and the Laboratory for Chemical Technology under the supervision of Prof. Dr. ir. Guy B. Marin.

Members of the dissertation jury

Prof. Dr. A. Adriaens	Ghent University (chairperson)
Prof. Dr. P. Van Der Voort	Ghent University (promoter)
Prof. Dr. ir. G. B. Marin	Ghent University (promoter)
Prof. Dr. ir. H. Vrielinck	Ghent University
Prof. Dr. ir. J. F. M. Denayer	Vrije Universiteit Brussel
Prof. Dr. ir. V. Van Speybroeck	Ghent University
Prof. Dr. R. Van Deun	Ghent University
Prof. Dr. ir. B. Weckhuysen	University of Utrecht
Prof. Dr. F. Kapteijn	TU Delft

This research was funded by the Long Term Structural Methusalem Grant Nr. 01M00409. Funding by the Flemish Government.

Scientific publications

A1 publications-articles indexed by the Thomson Reuters citation index

J. De Gelder, P. Scheldeman, K. Leus, M. Heyndrickx, P. Vandenabeele, L. Moens, P. De Vos, *Raman spectroscopic study of baterial endospores*, Analytical and Bioanalytical Chemistry, **2007**, 389 (7-8), 2143-2151.

K. Leus, I. Muylaert, M. Vandichel, G. B. Marin, M. Waroquier, V. Van Speybroeck, P. Van Der Voort, *The remarkable catalytic activity of the saturated metal organic framework V-MIL-47 in the cyclohexene oxidation*, Chemical Communications, **2010**, 46, 5085–5087.

K. Leus, I. Muylaert, V. Van Speybroeck, G.B. Marin, P. Van Der Voort, *A coordinative saturated vanadium containing metal organic framework that shows a remarkable catalytic activity*, Studies in Surface Science and Catalysis, **2010**, 175, 329-332 (WOS proceeding paper).

Y. Y. Liu, K. Leus, M. Grzywa, D. Weinberger, K. Strubbe, H. Vrielinck, R. Van Deun, D. Volkmer, V. Van Speybroeck, P. Van Der Voort, *Synthesis, Structural Characterization, and Catalytic Performance of a Vanadium-Based Metal–Organic Framework (COMOC-3)*, European Journal of Inorganic Chemistry, **2012**, 16, 2819-2827.

I. Muylaert, J. Musschoot, K. Leus, J. Dendooven, C. Detavernier, P. Van Der Voort, *Atomic Layer Deposition of Titanium and Vanadium Oxide on Mesoporous Silica and Phenol/Formaldehyde Resins – the Effect of the Support on the Liquid Phase Epoxidation of Cyclohexene*, European Journal of Inorganic Chemistry, **2012**, 2, 251-260.

K. Leus*, M. Vandichel*, Y.Y. Liu, I. Muylaert, J. Musschoot, S. Pyl, H. Vrielinck, F. Callens, G. B. Marin, C. Detavernier, P. V. Wiper, Y. Z. Khimyak, M. Waroquier, V. Van Speybroeck, P. Van Der Voort, *The coordinatively saturated vanadium MIL-47 as a low leaching heterogeneous catalyst in the oxidation of cyclohexene*, Journal of Catalysis, **2012**, 285, 196–207.
*both authors contributed equally to this work

M. Vandichel, K. Leus, P. Van Der Voort, V. Van Speybroeck, M. Waroquier *Mechanistic insight into the cyclohexene epoxidation with VO(acac)$_2$ and tert-butyl hydroperoxide,* Journal of Catalysis, **2012**, 294, 1-18.

R. Decadt, K. Van Hecke, D. Depla, K. Leus, D. Weinberger, I. Van Driessche, P. Van Der Voort, R. Van Deun, *Synthesis, crystal structures and luminescence properties of carboxylate based rare-earth coordination polymers*, Inorganic Chemistry, **2012**, 51, 11623-11634.

K. Leus, S. Couck, M. Vandichel, G. Vanhaelewyn, Y. Y. Liu, G. B. Marin, I. Van Driessche, D. Depla, M. Waroquier, V. Van Speybroeck , J. Denayer, P. Van Der Voort*, Synthesis, characterization and sorption properties of NH$_2$-MIL-47,* Physical Chemistry Chemical Physicals, **2012**, 14, 15562-15570.

K. Leus, G. Vanhaelewyn, T. Bogaerts, Y. Y. Liu, D. Esquivel, F. Callens, G. B. Marin, V. Van Speybroeck, H. Vrielinck, P. Van Der Voort, *Ti-functionalized NH$_2$-MIL-47: an effective and stable epoxidation catalyst*, Catalysis Today, **2012**, accepted.

Y.Y. Liu, S. Couck, M. Vandichel, M. Grzywa, K. Leus, S. Biswas, D. Volkmer, J. Gascon, F. Kapteijn, J. F. M. Denayer, M. Waroquier, V. Van Speybroeck, P. Van Der Voort, *A new V^{IV} based metal-organic framework having framework flexibility and high CO$_2$ adsorption capacity*, Inorganic Chemistry, **2012**, under revision.

M. Vandichel, K. Leus, P. Van Der Voort, M. Waroquier and V. Van Speybroeck *A combined experimental and theoretical approach to elucidate the influence of linker substituents on the epoxidation performance of V-MIL-47,* ChemPlusChem, **2012**, under revision.

National and international oral presentations

K. Leus and M. Vandichel, *Synthesis of new Vanadium containing Metal Organic Frameworks (V-MOFs) for applications in oxidation catalysis and adsorption/separation processes* , PhD symposium Sciences, 22 March, **2012**, Ghent, Belgium.

H. Vrielinck, G. Vanhaelewyn, K. Leus, Y.Y. Liu, F. Callens, P. Van Der Voort, *Electron paramagnetic resonance study of the active vanadium sites in MIL-47*, E-MRS Spring meeting, 14-18 May, **2012**, Strasbourg, France.

K. Leus, Y.Y. Liu, S. Biswas, G.B. Marin, P. Van Der Voort, *Metal Organic Frameworks in adsorption and catalysis – focus on Vanadium containing MOFs,* Dutch Zeolite Association Symposium (DZA symposium), 22 November, **2012**, Utrecht, The Netherlands.

National and international poster presentations

K. Leus, M. Vandichel, V. Van Speybroeck, P. Van Der Voort, *Development of Metal-Organic Frameworks as heterogeneous catalysts*, Doctoraatsymposium UGent Faculteit Wetenschappen, **2009**, Ghent, Belgium.

K. Leus, I. Muylaert, M. Vandichel, V. Van Speybroeck, G.B. Marin, P. Van Der Voort, *Development of Metal Organic Frameworks as heterogeneous catalysts*, The Netherlands Catalysis and Chemistry Conference NCCC-XI, 1-3 March, **2010**, Noordwijkerhout, The Netherlands.

A. Verberckmoes, K. Leus, P. Van Der Voort, *Catalytic performance of CuBTC and CuBDC Metal Organic Frameworks in cyclohexene oxidation*, The Netherlands Catalysis and Chemistry Conference NCCC-XI, 1-3 March, **2010**, Noordwijkerhout, The Netherlands.

K. Leus, I. Muylaert, V. Van Speybroeck, G.B. Marin, P. Van Der Voort , *A coordinative saturated vanadium containing Metal Organic Framework that shows a remarkable catalytic activity*, 10 the International Symposium of Preparation of Catalysts PREPA-X, 11-15 July, **2010**, Louvain-La-Neuve, Belgium.

K. Leus, I. Muylaert, A. Verberckmoes, G.B. Marin, Y.Y. Liu, V. Van Speybroeck, P. Van Der Voort, *A detailed study of the catalytic performance of V, Co and Cu MOFs in the oxidation of cyclohexene*, 2nd International Conference on Metal-Organic Frameworks and Open Framework Compounds, 5-8 September, **2010,** Marseille, France.

M. Vandichel, K. Leus, I. Muylaert, Pascal Van Der Voort, M. Waroquier, V. Van Speybroeck, *How does alkene epoxidation with TBHP occur in MIL-47?*, 2nd International Conference on Metal-Organic Frameworks and Open Framework Compounds, 5-8 September, **2010,** Marseille, France.

K. Leus, M. Vandichel, Y.Y Liu, G.B. Marin, M. Waroquier, V. Van Speybroeck, P. Van Der Voort, *A study of the effect of electron donating and electron withdrawing groups on the catalytic performance of V-MIL-47*, 5th International FEZA (The Federation of the European Zeolite Association) Conference, 3-7 July, **2011**, Valencia, Spain.

M. Vandichel, K. Leus, Y.Y. Liu, M. Waroquier, P. Van Der Voort, V. Van Speybroeck, *Effect of linker substituents on the epoxidation performance of V-MIL-47*, 5th International FEZA (The Federation of the European Zeolite Association) Conference, 3-7 July, **2011**, Valencia, Spain.

K. Leus, M. Vandichel, Y.Y. Liu, G.B. Marin, M. Waroquier, V. Van Speybroeck, P. Van Der Voort, *A study of the effect of electron donating and electron withdrawing groups on the catalytic performance of V-MIL-47*, The Netherlands Catalysis and Chemistry Conference NCCC-XII, 28 February-2 March, **2011**, Noordwijkerhout, The Netherlands.

Y.Y. Liu, K. Leus, P. Van Der Voort*, Synthesis, structural characterization and catalytic performance of a new vanadium based Metal-Organic Framework; COMOC-3*, International Symposium on Advanced Complex Inorganic Nanomaterials, 11-14 September, **2011**, Namen, Belgium.

Y.Y. Liu, S. Couck, M. Vandichel, M. Crzywa, K. Leus, S. Biswas, D. Volkmer, J. Gascon, F. Kapteijn, J. Denayer, M. Waroquier, V. Van Speybroeck, P. Van Der Voort, *COMOC-2, a flexible vanadium based metal-organic framework*, The Netherlands Catalysis and Chemistry Conference, NCCC-XIII, 5-7 March*,* **2012**, Noordwijkerhout, The Netherlands.

K. Leus, S. Couck, M. Vandichel, Y.Y. Liu, J. Denayer, M. Waroquier, V. Van Speybroeck, P. Van Der Voort, *Synthesis, characterization, adsorption and catalytic properties of an amino functionalized metal-organic framework: NH_2-MIL-47 (V),* 3rd International Conference on Metal-Organic Frameworks and Open Framework Compounds, 16-19 September, **2012**, Edinburgh, Scotland.

Acknowledgements

De laatste uurtjes van mijn doctoraat tikken langzamerhand weg. Het was een hele reis die ik niet had kunnen maken zonder de steun van verschillende personen allerhande. Een woordje van dank is dan ook hier meer dan ooit op zijn plaats. Vooreerst wil ik mijn dank betuigen aan mijn promotor Prof. Dr. Pascal Van Der Voort, voor de kans die u me heeft gegeven deel uit te maken van uw jonge, dynamische onderzoeksgroep COMOC. U heeft me volledig ondergedompeld in de wereld van de poreuze materialen en heeft mijn interesse aangewakkerd voor het onderzoek naar wat wij MOF's noemen. Het eerste jaar was een jaar waarin ik veel nieuwe zaken heb moeten leren met vele ups en downs. Zonder uw vertrouwen en geloof in mij tijdens die periode (en gedurende heel dit doctoraat) zou dit proefschrift (nu 4 jaar later) nooit op tafel gelegen hebben. Ook u, Prof. Guy Marin, wil ik danken voor de kans die u me gegeven heeft om deel uit te maken van het prestigieuze Methusalem project. Uw visie vanuit het standpunt "ingenieur" gaf vaak een heel andere, verhelderende kijk op de verkregen resultaten. Dit heeft er dan ook voor gezorgd dat ik geleerd heb de zaken vanuit een ander perspectief te bekijken.

De leden van mijn leescommissie, Prof. Vrielinck, Prof. Denayer en Prof. Marin, jullie wil ik danken voor het grondig en kritisch nalezen van dit proefschrift. Verder betuig ik ook mijn dank aan Prof. Weckhuysen, Prof. Kapteijn, Prof. Van Deun, Prof. Van Speybroeck en mijn promotor Prof. Van Der Voort om te willen zetelen in mijn jury en Prof. Adriaens om mijn openbare verdediging in goede banen te leiden.

Ik heb ook het geluk gehad om met diverse onderzoeksgroepen te mogen samenwerken gedurende mijn doctoraat. Hierbij wil ik vooreerst mijn samenwerkingspartner, het CMM, bedanken. Michel, Veronique en Matthias, samen met jullie heb ik mijn eerst "stapjes" in de MOF-wereld gezet. Nu 4 jaar later kunnen we terugkijken op een heel intense maar vruchtbare samenwerking met veel memorabele momenten. Daarnaast wil ik de EMR onderzoeksgroep bedanken. Freddy, Henk en Gauthier, jullie lieten me kennismaken met de EPR techniek! Verder wil ik ook Joeri en Sarah bedanken voor de uitgevoerde adsorptiemetingen. Ook Tineke, Steven en Jan wil ik danken voor de misschien wel korte, maar heel leuke samenwerking! Last but

not least, i would like to express my gratitude toward Prof. Khimyak and Paul Wiper for the performed solid state NMR measurements.

Uiteraard mogen mijn S3 collega's niet ontbreken in dit dankwoord. Ilke, Els, Frederik, Matthias, Ying-Ya, Dolores en Shyam alsook de jongere garde: Thomas, Isabelle en Jeroen. Bedankt voor de vele wetenschappelijke babbels, maar ook en vooral voor de leuke momenten tussendoor: de praatjes doorloops met soms een glimlach of een traan zullen me voor altijd bijblijven! Danny en Tom, ook jullie verdienen een woordje van dank om te helpen met de apparatuur toen die het op bepaalde momenten liet afweten, alsook voor de uitgevoerde metingen. Ook mijn masterstudenten: Kim, Roel Decadt, Babs, Roel De Smedt en Hannes wil ik bedanken voor de aangename samenwerking.

Verder heb ik op S3 ook heel veel nieuwe contacten kunnen leggen en vrienden mogen maken buiten de COMOC groep. Het afhandelen van administratieve zaken en zoveel meer werd altijd in goede banen geleid door mijn maatjes Pierre en Claudine van het secretariaat! Bedankt hiervoor! Maar bovenal zullen de vele middagpauzes mij bijblijven! De babbels (van soms heel uiteenlopende aard☺) onder de middag in de koffiekamer met de verschillende onderzoeksgroepen en de andere ATP leden maken S3 tot een echte hechte groep! S3 is the best☺!

Buiten S3 wil ik ook mijn vrienden en in het bijzonder mijn familie danken voor de steun die ze me de afgelopen 4 jaar gegeven hebben. Aan opa en oma een hele dikke merci voor alles! Dankjewel! Ook gaat een speciaal woordje van dank uit naar mijn neef Brecht Leus en Niels De Mayer voor het nalezen van mijn thesis. Tot slot mogen ook mijn ouders niet ontbreken in dit dankwoord. Mama en papa bedankt voor al de steun die jullie me altijd geven! Zonder jullie zou ik hier nooit hebben gestaan! Bedankt!

Karen Jacqueline Stella Leus

Preface

Porous materials were already known by the ancient Egyptians. The presence of voids of controllable dimensions at the atomic, molecular or nanometer scale makes them of high scientific and technological importance. The pores of the solids are classified by the IUPAC according to their sizes. Pores with a diameter below 2nm are called micropores, between 2-50 nm mesopores and above 50 nm they are called macropores.

Zeolites are crystalline inorganic materials with well defined microporous structures. The natural zeolites already exist for millions of years and were discovered 250 years ago. With the upcoming of the synthetic zeolites in 1948-1955 an increasing interest raised towards their applications. They can be utilized as purifiers of water, molecular sieves, drying materials, in separations and catalysis. However, a big disadvantage is the difficulty to tune the pores (pores < 1 nm) what makes it impossible to use them in catalysis of larger molecules. Since 1992 various "meso structured" materials have been developed with larger pores but amorphous walls. The pure silica materials were followed in 1999 by the hybrid organosilica materials.

In 2000 a new class of materials was developed, the so called Metal Organic Frameworks were born. These are porous materials with a robust, crystalline structure. MOFs combine the advantages of zeolites with the possibility to control the pore dimensions. This type of materials is constructed by linking organic ligands with metal ions or metal clusters to form infinite network structures. As MOFs are also hybrid materials, they cannot be used in high temperature applications, but find typical applications in mild heterogeneous catalysis, adsorption, gas storage…

At the start of this PhD work, very few V-MOFs were reported. In spite of the potential of vanadium in oxidation catalysis, a V-MOF was never investigated. The main goal of this research work is to evaluate the catalytic performance of V-MOFs and V/Ti-MOFs in oxidation catalysis.

A combined experimental and modeling approach has been applied throughout this research work to evaluate their potential in the oxidation of cyclohexene and to elucidate the plausible catalytic mechanism. The influence of the oxidant and amount of catalyst has been investigated along with stability and regenerability tests. Finally, these MOFs were compared with other solid V-based reference catalysts (zeotypes and silica materials) and homogeneous analogues. This research work may hopefully contribute to a better knowledge toward the development of the ultimate catalyst.

Karen Leus
Ghent, November 2012

Outline

This PhD thesis consists of seven chapters. In the first chapter a general introduction to MOFs is presented. In the second chapter an extensive literature overview is given concerning the use of MOFs in catalysis. The three following sections, chapter 3 to 5, comprise the results of this research work illustrating the use of vanadium and vanadium/titanium based MOFs as potential candidates in heterogeneous catalysis and adsorption. Finally, a general conclusion and a Dutch summary are provided in chapter 6 and 7 respectively.

Chapter 1 gives an introduction to MOFs. The potential advantages and disadvantages are presented, followed by the most commonly applied synthesis methods. Finally, the broad range of potential applications for this novel class of porous materials is presented.

Chapter 2 gives a general overview on catalysis. Firstly, the different types of catalysts and oxidants are discussed. Secondly, the employment of MOFs in catalysis, and more specifically their use in oxidation catalysis is highlighted. A state of the art is presented of the utilization of MOFs in the oxidation of cycloalkanes, benzylic compounds, alcohols, thiols, sulfides, cycloalkenes and linear alkenes.

Chapter 3 surveys the use of the V-MOF, MIL-47, in the oxidation of cyclohexene using different types of oxidants and amounts of catalyst. Furthermore, the catalytic performance of MIL-47 is compared with other V-based reference catalysts (VAPO-5, $VO(acac)_2$, VO_x/SiO_2) and regeneration and stability test have been carried out. Finally an intensive computational part is presented to define the active sites for catalysis and to propose the plausible reaction pathways for the epoxidation of cyclohexene.

Chapter 4 focuses on the synthesis and characterization of the amino functionalized V-MOF, NH_2-MIL-47.

The CO_2 and CH_4 adsorption properties have been evaluated and compared to MIL-47. DFT- based molecular modeling calculations were performed to obtain more insight into the adsorption positions for CO_2 in NH_2-MIL-47.

Chapter 5 presents the post-functionalization of NH_2-MIL-47 with $TiO(acac)_2$ to create a bimetallic oxidation catalyst. Furthermore, the catalytic performance of this bimetallic MOF is evaluated and compared to the non-functionalized material NH_2-MIL-47 and the homogeneous catalyst $TiO(acac)_2$. Additionally regenerability and stability tests have been done. Finally a plausible mechanism is given.

Chapter 6 summarizes the most important conclusions made throughout this work.

Chapter 7 provides a Dutch summary of this PhD research work.

List of abbreviations

A

AQDS	Anthraquinone-2,6-disulfonate

B

Bped	1,2-bis(4-pyridyl)-1,2-ethanediol
H_2bpb	1,4-bis(4'-pyrazolyl)benzene
Bipy	Bipyridine
Bpy	4,4′-bipyridine
H_2btec	1,2,4,5-benzenetetracarboxylic acid
H_2bdpb	1,4-bis[(3,5-dimethyl)-pyrazol-4-yl]benzene
BDC	1,4-benzenedicarboxylate
BTC	1,3,5-tricarboxylate

C

^{13}C CP/MAS NMR	Cross Polarization Magic Angle Spinning Nuclear Magnetic Resonance
CIF	Crystallographic Information Framework

D

DMF	Dimethylformamide

Dhtp	2,5-dihydroxyterephthalate
DFT	Density Functional Theory
DRIFTS	Diffuse Reflectance Infrared Fourier Transform Spectroscopy
Dipy-pra	1,3-bis(4-pyridyl)propane

E

EPR	Electron Paramagnetic Resonance

G

GC-FID	Gas-Chromatograph(y)-Flame Ionization Detector

H

H_2O_2	Hydrogen peroxide
HTC	High temperature cavity
HF	Hyperfine
HT	High throughput

I

Im	Imidazole
IR	Infrared
IRMOF	IsoReticular Metal Organic Framework

M

MOF	Metal Organic Framework
MIL	Materials of Institut Lavoisier
MTBS	Methyltributylammonium methyl sulfate

N

NHPI	*N*-hydroxyphthalimide
Nds	Naphthalenedisulfonate
Hnic	Nicotinic acid

P

2-pymo	2-pyrimidinolate
PhIM	Phenylimidazolate
POM	Polyoxometalate
pht^{2-}	Dianion of *o*-phthalicacid
PBE	Perdew, Burke and Ernzerhof
PHVA	Partial Hessian Vibrational Analysis
PCP	Porous Coordination Polymer

R

RT	Room temperature

S

SEM	Scanning Electron Microscopy
SBU	Secondary Building Unit

T

TBHP	*Tert*-Butyl hydroperoxide
TON	Turnover number
TEMPO	(2,2,6,6-tetramethylpiperidin-1-yl)oxidanyl
TOF	Turnover frequency
TGA	Thermogravimetric analysis
TOF-MS	Time-of-flight mass spectrometry

U

UV/Vis	Ultraviolet-visible

V

VASP	Vienna Ab Initio Simulation Package

X

XRPD	X-ray powder diffraction
XRD	X-ray diffraction
XRF	X-ray fluorescence
XPS	X-ray photoelectron spectroscopy

Z

ZMOF	Zeolite-*like* Metal–Organic Frameworks
ZIF	Zeolitic Imidazolate Framework

Table of contents

Chapter 1: Introduction to Metal Organic Frameworks

Abstract

In this chapter a general introduction to Metal Organic Frameworks (MOFs) is presented. Firstly, a brief insight into the history of MOFs is given. Secondly the design of these materials and some general features, such as their high porosity and surface area is described. Thirdly several ways are depicted to synthesis MOFs ranging from the classical hydrothermal and solvothermal synthesis to high-throughput synthesis methods. Finally various applications of MOFs are illustrated.

1.1 History

Metal Organic Frameworks, abbreviated as MOFs, are a recent class of crystalline materials containing metal ions or metal clusters which are connected with each other by rigid organic linkers. The resulting structures can have a zero-dimensional (0D), one-dimensional (1D), two-dimensional (2D) or three-dimensional (3D) architecture.
The first "MOF", denoted as MOF-5, was synthesized by the group of Yaghi (see Fig. 1.1)[1]. As can be seen from Fig. 1.1 MOF-5 consists of Zn_4O tetraheda clusters connected with each other by 1,4- benzenedicarboxylate organic linkers[1].

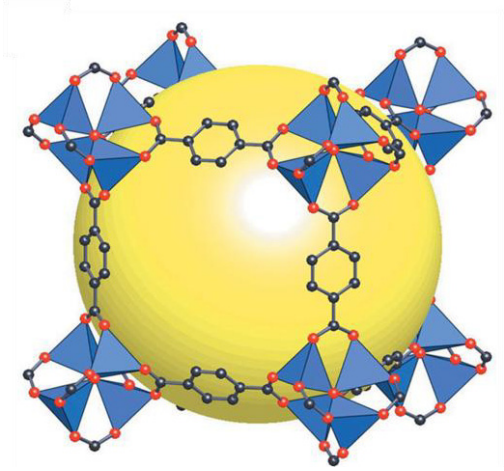

Fig. 1.1. Ball-and-stick representation of the framework of MOF-5[1].

In literature many derived acronyms are introduced: IRMOF (IsoReticular Metal Organic Framework), MOP (Metal Organic Polyhedra), ZIF (Zeolitic Imidazole Framework), PMOF (Porous Metal Organic Framework), CP (Coordination Polymers), PCP (Porous Coordination Polymers), MMOF (Microporous Metal Organic Framework) and more[2-7].
Nevertheless, there were already some earlier reports on coordination polymers.

The term coordination polymer was already used in a paper in 1916 [8], but there was no means of demonstrating infinite frameworks without single-crystal-X-ray-crystallography. Later on in 1936, the well-known Prussian Blue compounds, based on Fe-CN-Fe linkages, were introduced which had a three-dimensional coordination framework [9].
However, it was not until the early 1990 that research into materials with polymeric, sometimes porous, structures based on metal ions and organic bridging ligands increased intensively [10]. Early papers by Robson [11-13], Moore [14, 15], Yaghi [16] and Zawarotko [17] contributed to the field of MOFs, which nowadays witnesses an exponential growth as can be seen from Fig.1.2.

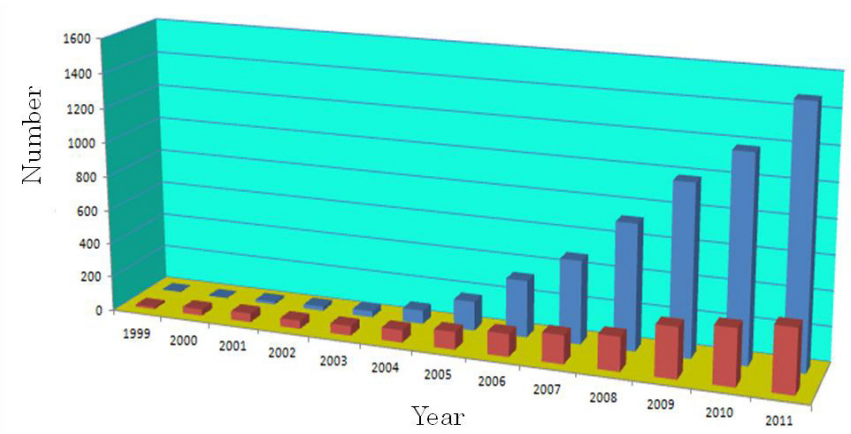

Fig. 1.2. Number of papers containing the key word "Metal-organic Frameworks (blue) and Porous coordination polymers (red) in the Web Of Science.

1.2 Design of MOFs

From the above described definition, it can be seen that MOFs consist of two main components: the organic linkers and the metal ions. The linkers act as "struts" that bridge the metal ions, which in turn act as "joints" in the resulting MOF architecture[7]. The synthesis of new MOF materials is sometimes more an art than a science due to the discovery of many compounds by trial and error techniques. Nevertheless, there is an increasing desire to produce materials designed to perform highly specific functions. In other words, research into the design of MOFs for specific purposes is becoming of a paramount importance.

In general, crystal engineering involves the design and construction of crystal structures from molecular building blocks. These building blocks can be seen as the "bricks" to build up a house[18]. Many scientists in the field of MOFs applied this approach for the design and synthesis of new components[19] . The group of O'Keeffe and Yaghi introduced in 2002 the concept of reticular synthesis (reticular: form a net), described as the process of assembling designed rigid secondary building units (SBU) into predetermined ordered structures (networks) which are held together by strong bondings[20]. The successful design of rigid frameworks based on such SBUs was demonstrated for the first time in MOF-2 and MOF-5[1]. In MOF-5 the $Zn_4O(CO_2)_6$ units containing four ZnO_4 tetrahedra with a common vertex and six carboxylate C atoms define an octahedral inorganic SBU (see Fig. 1.3). Other examples of highly symmetrical inorganic SBUs are the $Cu_2(OH)_2(CO_2)_4$ brick from HKUST-1, the $Cr_3O(OH)_3(CO_2)_6$ SBU from MIL-88 and the $Zr_6O_4(OH)_4(CO_2)_{12}$ SBU in UiO-66 and UiO-67[21-24].

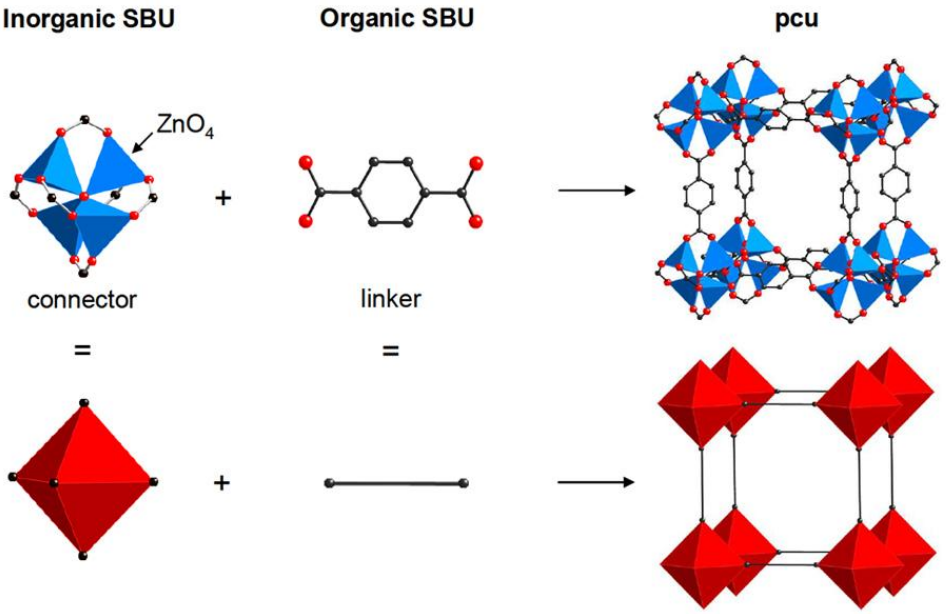

Fig. 1.3. Illustration of the combination of inorganic and organic secondary building units (SBUs) into a 3D connected network of **pcu** topology. A Zn_4O cluster, red octahedral, represents the inorganic SBU and the bidentate benzenedicarboxylic acid (bdc) linker represents the organic SBU.

These inorganic and organic SBUs are formed *in situ* under well defined reaction conditions. Moreover, once the *in situ* synthesis of an SBU has been established, it is possible to reproduce this unit, and reproduce it in combination with new linkers. The latter has been demonstrated by the elegant isoreticular synthesis of the IRMOF-1-16 in which the pore sizes and functionality could be varied without changing the original topology[25]. Other examples of isoreticular synthesis can be found elsewhere[26-28].

Although methods as reticular synthesis exist, it is not always easy to control the orientation of building blocks in the solid state and thus prediction of the resulting structure is sometimes difficult. This is specifically the case for flexible linkers such as 4,4- bipyridine where the flexible nature of the angles within the metal coordination sphere resulted in less predictable and more flexible framework topologies[29].

1.3 Features of MOFs

1.3.1 Porosity of MOFs

The most striking difference to other porous materials (such as activated carbons and zeolites) is their very low density, giving them exceptionally high porosities and surface areas[30]. Many attempts have been made to enlarge the pores and surface areas of MOFs. In principle, expansion of the organic linker should give rise to MOFs with bigger pores and higher surface areas. However some difficulties can arise: (i) expanded linkers often yield too fragile frameworks and (ii) the large void spaces within the crystal framework makes it generally susceptible to self-interpenetration (two lattices grow and interpenetrate each other)[31]. Pioneering work to enlarge the pores has been executed by the group of Yaghi which resulted in the isoreticular series of MOF-5 in which the pores could be incrementally varied from 3.8 to 28.8 angstroms [25]. Furthermore, his group was able to bring new functionalities into the framework without changing the original topology of the structure. Today many other mesoporous MOFs and MOFs with very high surface areas have been reported [32-34]. In Table 1.1. the porosity data of some highly porous MOFs are shown.

Table 1.1. Porosity data of some highly porous MOFs.

MOF	Linker	Void volume (%)	Langmuir Surface area (m^2/g)	Reference
MOF-177	4,4′,4″-benzene-1,3,5-triyltribenzoate	83	5340	Furukawa *et al.* [35]
MOF-200	4,4′,4″-(benzene-1,3,5-triyl-tris (benzene-4,1-diyl))tribenzoate	90	10400	Furukawa *et al.* [31]
MOF-205	2,6-naphthalenedicarboxylate and 4,4′,4″-benzene-1,3,5-triyltribenzoate	85	6170	Furukawa *et al.*[31]
MOF-210	biphenyl-4,4′-dicarboxylate and 4,4′,4″-(benzene-1,3,5-triyl-tris (ethyne-2,1-diyl))tribenzoate	89	10400	Furukawa *et al.*[31]
UMCM-2	thieno[3,2-b]thiophene-2,5-dicarboxylate and 4,4′,4″-benzene-1,3,5 triyltribenzoate	83	6060	Koh *et al.*[36]
Cr-MIL-101	1,4-benzene dicarboxylate	83	5900	Férey et al.[37]

1.3.2 Hard versus soft MOFs

A remarkable feature of MOFs is that besides hard and rigid MOF structures, some MOFs reveal a flexible, "breathing" framework. These compounds are categorized as soft porous crystals, having a highly ordered network and reversible structural transformability[38]. When guest species are introduced they can ether show a sigmoidal or double-sigmoidal adsorption profile with a hysteresis. The latter has been detected for CH_3OH, C_2H_5OH, CO_2, O_2, N_2, Ar, CH_4 and H_2O on a range of MOFs[39-47]. Sigmoidal adsorption profiles have been observed for materials showing a transition from a non-porous to a porous state and are characterized by a certain "gate opening pressure" depending on the adsorbate and temperature[42, 48-50]. Double-sigmoidal adsorption profiles are related to crystal-to-crystal transitions accompanied by a change in cell volume, which have been reported for the adsorption of CO_2 [51], C2-C4 alkanes[52] and C8 alkyl aromatic compounds in MIL-53[53]. Next to the introduction of guest species, other external stimuli, such as light, pressure and an electric field can also result in the reversible change of the channels and pores in soft porous materials.

In other words, the functions of soft porous crystals are not necessarily restricted to structural properties but also involve electric and magnetic properties. In the review of Horike *et al.*[38] a perspective overview of the functions of these materials is shown (see Fig. 1.4).

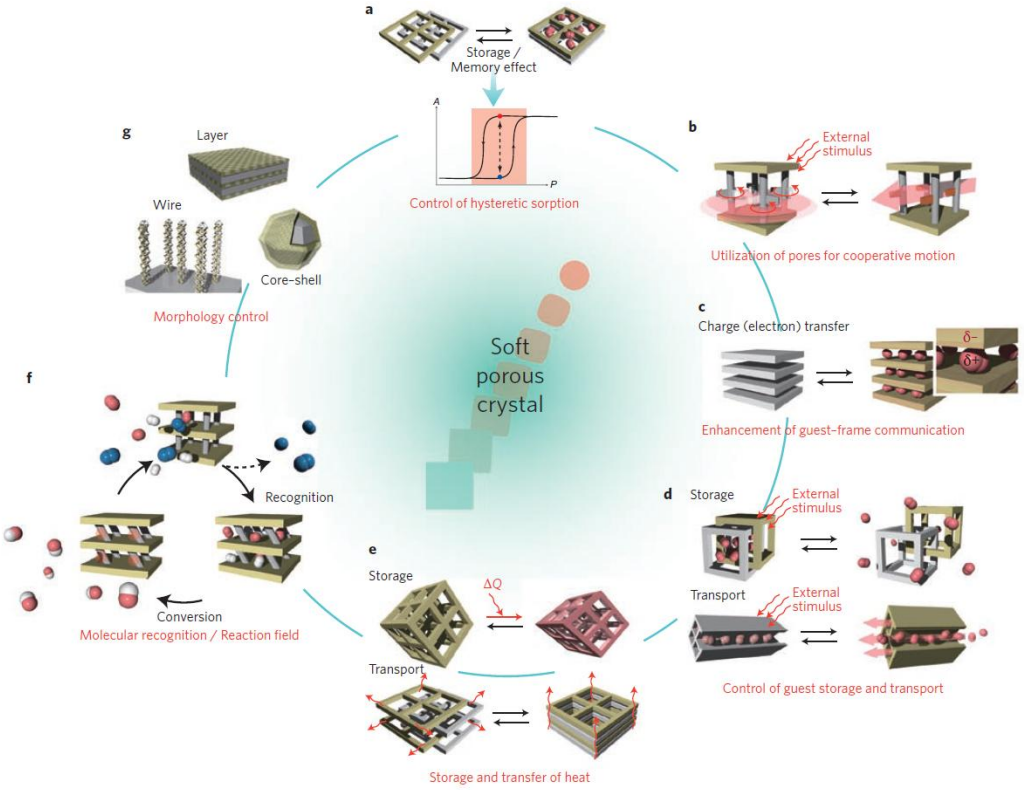

Fig. 1.4. Perspectives in functions of soft porous crystals[38].

1.3.3 Weaknesses of MOFs

For most applications, mentioned later on in section 1.5, pure-phase MOF materials are required that retain their full porosity after guest removal. However, some MOFs show the disadvantage to collapse after removal of the guest molecules. To overcome this problem Nelson *et al.*[54] introduced a supercritical treatment method.

Furthermore, an approach was developed, based on density differences, to obtain phase-pure MOF materials within a few tens of seconds[55]. The only requirements are (a) density differences between product and impurities and (b) the availability of an appropriate solvent. Although this density-based separation is a powerful technique it does not address one of the principal problems of MOFs, which is the formation of multiphase products. Another disadvantage of a MOF is, the more porous the MOF is, the easier interpenetration would likely to happen. This interpenetration or catenation imposes severe limitations on efforts to expand the surface area and/or decrease density by employing bigger ligands. Two and three-fold catenation are routinely encountered in MOF structures and even higher degrees of catenation have been observed [56, 57]. Many methods have been employed to prevent interpenetration. For example, Yaghi and co-workers utilized very diluted synthesis conditions to produce a reasonable quantity of a noncatenated version of IRMOFs[25]. However, this dilution method could not be generalized to avoid interpenetration[58]. Another example describes the use of templating agents (oxalic acid) to produce noninterpenetrated materials[59]. Furthermore, some reports confirmed that the presence of a bulky substituent on the organic linker can suppress the formation of interpenetrated frameworks[60, 61].

The relatively poor stability is an additional disadvantage of MOFs. Besides their low thermal stability (limited to 350-400°C), few MOFs are known to be stable in the presence of water. Only a small number of MOFs: ZIF-8, MOF-74, Al-MIL-110, Cr-MIL-101 and Al-MIL-53 have been identified to be stable toward water vapor during steam stability tests. Their high hydrothermal stability was due to the high bond strength between the metal oxide and the bridging linker. On the other hand, MOF-69C, MOF-5 and MOF-508 were very unstable[62].

1.4 Preparation of MOFs

There are many methods to synthesize MOFs. In the following, the most commonly used synthetic approaches will be discussed briefly: hydro- and solvothermal synthesis, microwave synthesis, electrochemical synthesis and high-throughput synthesis. Furthermore, some of the approaches for the preparation of multifunctional frameworks will be presented.

For more extended details on the different synthesis routes and other synthetic methods (e.g. mechanochemical route, sonochemical way...) to obtain MOF structures, the reader is referred to the recent review of Stock *et al.*[63]

1.4.1 Classical method: hydro- and solvothermal synthesis

In general MOFs are synthesized using well soluble salts as the source for the metal compounds e.g. metal nitrates, sulfates or acetates together with the organic linker (mostly carboxylic acids or pyridyl-based linkers) in a solvent or mixture of solvents[30]. Hydrothermal synthesis involves water as solvent, whereas the solvothermal synthesis refers to the use of organic solvents (for example: alcohols, dialkylformamides and pyridine)[64]. The choice of the solvent depends on its ability to dissolve the organic ligand. In both cases the reaction takes place in a Teflon-lined stainless autoclave in which an autogeneous pressure is built up. The self-assembly of the frameworks is mostly influenced by the temperature, the concentration of the metal-salt, the extent of solubility of the reactants in the solvent and the pH of the solution[65]. The operational temperature range is between 80-260°C, during a time scale of several hours and several days [66]. Thus the classical synthesis is rather slow in comparison to other synthesis routes (microwave, electrochemical and high-throughput synthesis).

1.4.2 Microwave-assisted synthesis

Microwave techniques have attracted growing attention for the rapid synthesis of MOFs and nanoporous materials in general. The microwave-assisted synthesis of MOFs, was recently summarized in a perspective of Klinowski *et al.*[67]. The main advantage of microwave heating is its energy efficiency, because power is only applied within the reactive mixture. The energy is generated directly throughout the bulk of the material instead of by conduction from the external surface (see Fig. 1.5)[67].

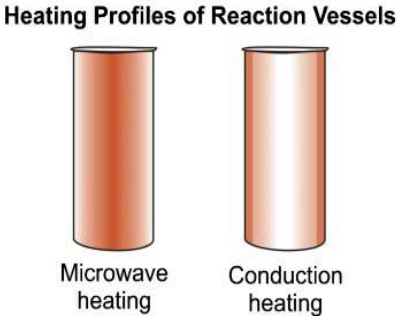

Fig. 1.5. Comparison of the heating profiles inside the reaction vessel for standard conductive and microwave heating[67].

Consequently, microwave heating allows short crystallization times, narrow particle size distribution, high yields and selectivities and facile morphology control[68-73].

The very first microwave synthesis of MOFs dealt with the Cr-MIL-100[74]. The compound was synthesized in 4 hours at 220°C with a yield comparable to the conventional synthesis method of 4 days. Yet, many other metal (III) carboxylate (M= Fe, Al, Cr, V, Ce) MOFs have been prepared[75-82].

Furthermore, a wide variety of metal (II) carboxylate based MOFs were synthesized by applying microwave irradiation[83-86]. Among them MOF-5 and HKUST-1 are the most studied materials[87-93]. For both materials the influence of the power level, irradiation time, temperature and composition of reaction mixture was examined.

Most of the times, microcrystalline powders or nano-sized crystals are obtained under microwave heating due to the fast kinetics of crystal nucleation and growth[67]. Thus one challenge with microwave heating is to get crystals in the size range comparable to the ones obtained by solvothermal heating. Because structural elucidation is crucial in the research of MOFs, microwave heating may be considered as unsuitable for the investigation of new phases. Nevertheless, there are already some reports on the synthesis of single-crystals of MOFs[94-97].

1.4.3 Electrochemical synthesis route

The earliest report on the electrochemical synthesis of MOFs was carried out by researchers at BASF in 2006 for the synthesis of HKUST-1[30, 98]. Bulk copper plates were arranged as the anodes in an electrochemical cell with the carboxylate linker dissolved in methanol as the solvent and a copper cathode. After 150 min. the greenish blue precipitate was formed. The big advantage is that no anions from added salts can block the pores[30, 98]. By the same method the successful synthesis of Zn-EZIF (electrochemically made ZIF) with 2-methylimidazole as linker was reported[99].
Later on, Ameloot *et al.* modified the electrochemically produced HKUST-1 of BASF, to enable the preparation of thin films[100]. By applying an anodic voltage to the Cu-electrode, Cu^{II} ions were introduced into the synthesis solution containing the carboxylate linker and methyltributylammonium methyl sulfate (MTBS) as a conduction salt. By varying the voltage, the crystal size could be controlled. Besides offering the advantage of self-completion, the electrochemical synthesis is also remarkably fast and the coatings can be formed continuously what makes them applicable in industry. However, one major problem was identified by the group of Tangermann applying the electrochemical route of Ameloot *et al.*.They observed that during the fast electrochemical synthesis of HKUST-1, the organic linker and MTBS coprecipitate with the MOF, resulting in pore blockages.
In contrast to the anodic deposition approach of Ameloot *et al.*, Li *et al.* described a cathodic electrodeposition method of MOF-5, which was deposited in only 15 min. at room temperature[101].

1.4.4 High-throughput synthesis

As mentioned earlier, for MOF materials it is well known that subtle changes in the reaction parameters (temperature, pH, concentration of the reactants…) can have a considerable impact on the resulting products. For a given combination of metal-salt and organic ligand, different crystalline phases are often possible (besides the formation of undesired side-products).

Unfortunately, each increase in the number of studied parameters, raises the number of necessary experiments exponentially. In such cases, high-throughput (HT) methods can be implemented. The methodology is characterized by low reagent consumption and a complete set of parallel reactors can be set to work under identical conditions, allowing the efficient discovery of new components, the fast optimization of the synthesis conditions and facilitate the observation of reaction trends. Parallel reactors, often based on the 96 well-plate format have been employed in which the handling of small amounts of reactants and rapid characterization of the materials by means of XRD has been automated[102]. The most HT studies on MOFs were performed to elucidate the role of certain parameters, such as the influence of temperature, pH, concentration and reaction time[103-107]. This resulted in the discovery of new phases as observed by Forster *et al.*[103] on the cobalt succinate system and a more profound know-how on the influence of these reaction parameters during the synthesis of MOF-5, HKUST-1 and the Fe-based MOFs, namely MIL-53, MIL-88 and MIL-101 [104, 106]. Furthermore, the influence of guest species as structure-directing agents on the synthesis of the anionic framework $NaLa[(PO_3H)_2CH\text{-}C_6H_4\text{-}CH(PO_3H)_2].4H_2O$ was investigated using HT methods [108].

Additionally, HT experiments were carried out to discover new MOFs and hence the optimization of the synthesis conditions [102, 109-113]. In one of these reports, Maniam *et al.*[110] demonstrated for the first time, besides the conventional heating high-throughput system, high-throughput experiments using microwave heating in the search for new Ni^{2+} based MOFs exhibiting a paddle-wheel structure similar to HKUST-1 [110].

1.4.5 Preparation of multifunctional frameworks

1.4.5.1 Mixed ligands and mixed metals

In principle, MOF frameworks can be constructed from multiple organic ligands and metal ions. However, there are a limited number of reports on frameworks having more than two kinds of ligands or metal ions. In a first report Kleist *et al.*[114] described a synthesis route at ambient pressure to make mixed-linker MOFs (called MIXMOFs).

Based on MOF-5, they performed a partial substitution of the terephthalate linkers by 2-aminobenzene-1,4-dicarboxylate linkers to obtain a series of MIXMOFs with a loading up to 40% of 2-aminobenzene-1,4-dicarboxylate[114]. The potential of the mixed-ligand approach in the MOF-5 framework was extended by the group of Yaghi by using a high-throughput technique[115]. They were able to obtain 18 multivariate MOF-5 type structures that contain up to eight distinct functionalities in one phase. Other examples that apply this ligand doping approach to prepare multifunctional frameworks can be found elsewhere[77, 116-119].

In addition to ligand mixing, the mixing of metal species has been reported to result in mixed MOFs. Botas *et al.*[120] describe the partial substitution of Zn in MOF-5 by Co-ions during the solvothermal synthesis procedure of MOF-5[120]. However, the amount of Zn that could be substituted was limited to 25%. In other words the substitution occurs to a maximum degree of 1 Co atom/Zn_4O cluster on average. Another example of metal-doping was achieved in $[Cu_3(btc)_2]$[121]. The Cu-MOF was doped with low levels (up to 1%) of Zn using a slightly modified solvothermal method which was already established in the literature for$[Cu_3(btc)_2]$[21].

1.4.5.2 Core-Shell

In addition to the integration of different functional moieties described above, combinations of multiple distinct functional MOF frameworks are also of interest for the preparation of multifunctional frameworks. This can be achieved by the synthesis of a core MOF crystal with a different shell crystal by epitaxial growth at the single-crystal level, thus creating core-shell MOF heteroepitaxial crystals. The first synthesis of core-shell MOF single crystals by epitaxial growth was carried out by Furukawa *et al.*[122]. In this report a series of tetragonal frameworks $[\{M_2(dicarboxylate)_2(N\text{-}ligand)\}_n]$, have been employed for core-shell fabrication (see Fig. 1.6). The hybridization of two frameworks into one single crystal was successfully achieved by a step-by-step solvothermal reaction of $[\{Zn_2(ndc)_2(dabco)\}_n]$ and $[\{Cu_2(ndc)_2(dabco)\}_n]$ to afford clear core (Zn)-shell (Cu) crystals, in which the nitrogen ligands were used as coordination sites to grow the shell crystal.

Furthermore [Zn_4O(dicarboxylate)$_3$]-type frameworks were also found to be a good platform to prepare the core-shell-type frameworks [118, 123]. This resulted in the core-shell MOFs: IRMOF-3@MOF-5 and MOF-5@IRMOF-3 and the multilayered crystals: MOF-5@IRMOF-3@MOF-5 and IRMOF-3@MOF-5@IRMOF-3.

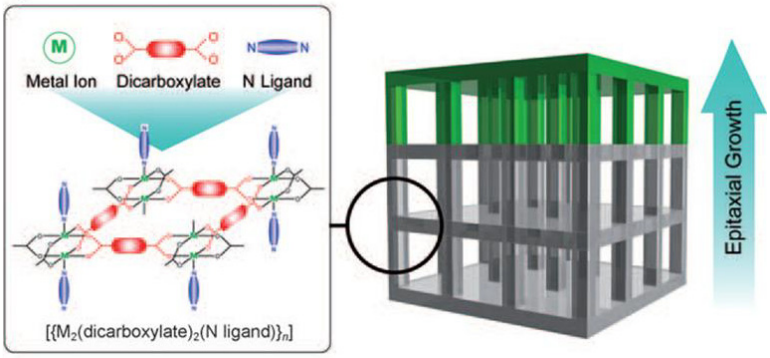

Fig. 1.6. Schematic illustration of the epitaxial growth of [{M_2(dicarboxylate)$_2$(N-ligand)}$_n$][122].

1.4.5.3 Nanoparticles in MOFs

Another approach to obtain multifunctional frameworks is the preparation of MOFs with well dispersed nanoparticles in their nano-cages [124-131]. In most reports this inclusion is achieved by a metal organic chemical vapor deposition or *via* an "incipient wetness" impregnation as an alternative method to avoid the use of highly reactive and air sensitive precursors. By means of a reduction or hydrogenation of the metal precursors, the "naked" metal-nanoclusters are obtained. Besides the inclusion of "naked" metal particles, many papers present the encapsulation of polyoxometalates (POMs) into the MOF framework[132-134]. For example, Sun *et al.*[135] reported a one-step hydrothermal reaction to encapsulate different Keggin POMs into HKUST-1 resulting in crystalline materials with the chemical formula $[Cu_2(BTC)_{4/3}(H_2O)_2]_6[H_nXM_{12}O_{40}].(C_4H_{12}N)_2$ with X=Si, Ge, P, As and M= W, Mo. Another example is the loading of ammonia borane into [Y(BTC)], called JUC-32, by infusion.

The Y^{3+} metal sites interact with the ammonia borane to prevent the formation of ammonia (which poisons the catalyst) and small particles of ammonia borane were obtained as a result of the nano-confinement effect of the MOF [136].

1.5 MOFs :applications

While the initial focus in the field of MOFs was the synthesis and structural characterization, an increasing number of MOFs are now being explored for their interesting properties, including optic[137],[138-141] magnetic,[142-148] and electronic properties[149-153] as well as their various potential applications such as catalysis [154-156], ion exchange[141, 157, 158] gas storage [159-165] separation [16, 166, 167] sensing [168-174], polymerization [175-177] and drug delivery [178-180]. As the discussion of each application falls beyond the scope of this thesis, the reader is referred to some important reviews on each application (see Table 1.2). Since the main focus of this thesis is on the use of MOFs in catalysis and more specifically oxidation catalysis, a state of the art of MOFs in oxidation catalysis and catalysis in general is presented in chapter 2.

Table 1.2. References to recent reviews dedicated to applications of MOFs.

MOF application	Reference
Luminescence	181-183
Biomedical applications	184-190
Adsorption/separations and storage	165, 167, 191-207
Catalysis	208-211

1.6 References

1. H. Li, M. Eddaoudi, M. O'Keeffe and O. M. Yaghi, *Nature*, 1999, **402**, 276-279.
2. O. M. Yaghi, H. L. Li, C. Davis, D. Richardson and T. L. Groy, *Accounts Chem Res*, 1998, **31**, 474-484.
3. S. Kitagawa, R. Kitaura and S. Noro, *Angew Chem Int Edit*, 2004, **43**, 2334-2375.
4. M. J. Rosseinsky, *Micropor Mesopor Mat*, 2004, **73**, 15-30.
5. D. J. L. Tranchemontagne, Z. Ni, M. O'Keeffe and O. M. Yaghi, *Angew Chem Int Edit*, 2008, **47**, 5136-5147.
6. M. Eddaoudi, D. B. Moler, H. L. Li, B. L. Chen, T. M. Reineke, M. O'Keeffe and O. M. Yaghi, *Accounts Chem Res*, 2001, **34**, 319-330.

7. N. W. Ockwig, O. Delgado-Friedrichs, M. O'Keeffe and O. M. Yaghi, *Accounts Chem Res*, 2005, **38**, 176-182.
8. Y. Shibata, *Journal of the College of Science, Imperial University of Tokyo*, 1916, **37**, 1-31.
9. J. F. Keggin and F. D. Miles, *Nature*, 1936, **137**, 577-578.
10. S. L. James, *Chem Soc Rev*, 2003, **32**, 276-288.
11. B. F. Hoskins and R. Robson, *J Am Chem Soc*, 1989, **111**, 5962-5964.
12. B. F. Hoskins and R. Robson, *J Am Chem Soc*, 1990, **112**, 1546-1554.
13. B. F. Abrahams, B. F. Hoskins, D. M. Michail and R. Robson, *Nature*, 1994, **369**, 727-729.
14. D. Venkataraman, G. B. Gardner, S. Lee and J. S. Moore, *J Am Chem Soc*, 1995, **117**, 11600-11601.
15. G. B. Gardner, D. Venkataraman, J. S. Moore and S. Lee, *Nature*, 1995, **374**, 792-795.
16. O. M. Yaghi, G. M. Li and H. L. Li, *Nature*, 1995, **378**, 703-706.
17. S. Subramanian and M. J. Zaworotko, *Angew Chem Int Edit*, 1995, **34**, 2127-2129.
18. G. Ferey, *J Solid State Chem*, 2000, **152**, 37-48.
19. J. A. Brant, Y. L. Liu, D. F. Sava, D. Beauchamp and M. Eddaoudi, *J Mol Struct*, 2006, **796**, 160-164.
20. O. M. Yaghi, M. O'Keeffe, N. W. Ockwig, H. K. Chae, M. Eddaoudi and J. Kim, *Nature*, 2003, **423**, 705-714.
21. S. S. Y. Chui, S. M. F. Lo, J. P. H. Charmant, A. G. Orpen and I. D. Williams, *Science*, 1999, **283**, 1148-1150.
22. S. Surble, C. Serre, C. Mellot-Draznieks, F. Millange and G. Ferey, *Chem Commun*, 2006, 284-286.
23. J. H. Cavka, S. Jakobsen, U. Olsbye, N. Guillou, C. Lamberti, S. Bordiga and K. P. Lillerud, *J Am Chem Soc*, 2008, **130**, 13850-13851.
24. D. J. Tranchemontagne, J. L. Mendoza-Cortes, M. O'Keeffe and O. M. Yaghi, *Chem Soc Rev*, 2009, **38**, 1257-1283.
25. M. Eddaoudi, J. Kim, N. Rosi, D. Vodak, J. Wachter, M. O'Keeffe and O. M. Yaghi, *Science*, 2002, **295**, 469-472.
26. S. Biswas, T. Ahnfeldt and N. Stock, *Inorg Chem*, 2011, **50**, 9518-9526.
27. M. Kandiah, M. H. Nilsen, S. Usseglio, S. Jakobsen, U. Olsbye, M. Tilset, C. Larabi, E. A. Quadrelli, F. Bonino and K. P. Lillerud, *Chem Mater*, 2010, **22**, 6632-6640.
28. D. N. Dybtsev, M. P. Yutkin, E. V. Peresypkina, A. V. Virovets, C. Serre, G. Ferey and V. P. Fedin, *Inorg Chem*, 2007, **46**, 6843-6845.
29. J. Kim, B. L. Chen, T. M. Reineke, H. L. Li, M. Eddaoudi, D. B. Moler, M. O'Keeffe and O. M. Yaghi, *J Am Chem Soc*, 2001, **123**, 8239-8247.

30. A. U. Czaja, N. Trukhan and U. Muller, *Chem Soc Rev*, 2009, **38**, 1284-1293.
31. H. Furukawa, N. Ko, Y. B. Go, N. Aratani, S. B. Choi, E. Choi, A. O. Yazaydin, R. Q. Snurr, M. O'Keeffe, J. Kim and O. M. Yaghi, *Science*, 2010, **329**, 424-428.
32. O. I. Lebedev, F. Millange, C. Serre, G. Van Tendeloo and G. Ferey, *Chem Mater*, 2005, **17**, 6525-6527.
33. N. Klein, I. Senkovska, K. Gedrich, U. Stoeck, A. Henschel, U. Mueller and S. Kaskel, *Angew Chem Int Edit*, 2009, **48**, 9954-9957.
34. W. M. Xuan, C. F. Zhu, Y. Liu and Y. Cui, *Chem Soc Rev*, 2012, **41**, 1677-1695.
35. H. Furukawa, M. A. Miller and O. M. Yaghi, *J Mater Chem*, 2007, **17**, 3197-3204.
36. K. Koh, A. G. Wong-Foy and A. J. Matzger, *J Am Chem Soc*, 2009, **131**, 4184-+.
37. G. Ferey, C. Mellot-Draznieks, C. Serre, F. Millange, J. Dutour, S. Surble and I. Margiolaki, *Science*, 2005, **309**, 2040-2042.
38. S. Horike, S. Shimomura and S. Kitagawa, *Nat Chem*, 2009, **1**, 695-704.
39. T. Loiseau, C. Serre, C. Huguenard, G. Fink, F. Taulelle, M. Henry, T. Bataille and G. Ferey, *Chem-Eur J*, 2004, **10**, 1373-1382.
40. S. Bourrelly, P. L. Llewellyn, C. Serre, F. Millange, T. Loiseau and G. Ferey, *J Am Chem Soc*, 2005, **127**, 13519-13521.
41. K. S. Walton, A. R. Millward, D. Dubbeldam, H. Frost, J. J. Low, O. M. Yaghi and R. Q. Snurr, *J Am Chem Soc*, 2008, **130**, 406-+.
42. D. Li and K. Kaneko, *Chem Phys Lett*, 2001, **335**, 50-56.
43. D. Tanaka, K. Nakagawa, M. Higuchi, S. Horike, Y. Kubota, L. C. Kobayashi, M. Takata and S. Kitagawa, *Angew Chem Int Edit*, 2008, **47**, 3914-3918.
44. J. P. Zhang and X. M. Chen, *J Am Chem Soc*, 2008, **130**, 6010-6017.
45. T. K. Maji, R. Matsuda and S. Kitagawa, *Nat Mater*, 2007, **6**, 142-148.
46. A. J. Fletcher, E. J. Cussen, T. J. Prior, M. J. Rosseinsky, C. J. Kepert and K. M. Thomas, *J Am Chem Soc*, 2001, **123**, 10001-10011.
47. X. B. Zhao, B. Xiao, A. J. Fletcher, K. M. Thomas, D. Bradshaw and M. J. Rosseinsky, *Science*, 2004, **306**, 1012-1015.
48. R. Kitaura, K. Seki, G. Akiyama and S. Kitagawa, *Angew Chem Int Edit*, 2003, **42**, 428-431.
49. S. Horike, D. Tanaka, K. Nakagawa and S. Kitagawa, *Chem Commun*, 2007, 3395-3397.
50. K. Nakagawa, D. Tanaka, S. Horike, S. Shimomura, M. Higuchi and S. Kitagawa, *Chem Commun*, 2010, **46**, 4258-4260.

51. C. Serre, S. Bourrelly, A. Vimont, N. A. Ramsahye, G. Maurin, P. L. Llewellyn, M. Daturi, Y. Filinchuk, O. Leynaud, P. Barnes and G. Ferey, *Adv Mater*, 2007, **19**, 2246-+.
52. P. L. Llewellyn, G. Maurin, T. Devic, S. Loera-Serna, N. Rosenbach, C. Serre, S. Bourrelly, P. Horcajada, Y. Filinchuk and G. Ferey, *J Am Chem Soc*, 2008, **130**, 12808-12814.
53. V. Finsy, C. E. A. Kirschhock, G. Vedts, M. Maes, L. Alaerts, D. E. De Vos, G. V. Baron and J. F. M. Denayer, *Chem-Eur J*, 2009, **15**, 7724-7731.
54. A. P. Nelson, O. K. Farha, K. L. Mulfort and J. T. Hupp, *J Am Chem Soc*, 2009, **131**, 458-+.
55. O. K. Farha, K. L. Mulfort, A. M. Thorsness and J. T. Hupp, *J Am Chem Soc*, 2008, **130**, 8598-8599.
56. K. L. Mulfort, T. M. Wilson, M. R. Wasielewski and J. T. Hupp, *Langmuir*, 2009, **25**, 503-508.
57. S. R. Batten, *Crystengcomm*, 2001.
58. D. J. Tranchemontagne, J. R. Hunt and O. M. Yaghi, *Tetrahedron*, 2008, **64**, 8553-8557.
59. S. Q. Ma, D. F. Sun, M. Ambrogio, J. A. Fillinger, S. Parkin and H. C. Zhou, *J Am Chem Soc*, 2007, **129**, 1858-1859.
60. R. K. Deshpande, J. L. Minnaar and S. G. Telfer, *Angew Chem Int Edit*, 2010, **49**, 4598-4602.
61. O. K. Farha, C. D. Malliakas, M. G. Kanatzidis and J. T. Hupp, *J Am Chem Soc*, 2010, **132**, 950-+.
62. J. J. Low, A. I. Benin, P. Jakubczak, J. F. Abrahamian, S. A. Faheem and R. R. Willis, *J Am Chem Soc*, 2009, **131**, 15834-15842.
63. N. Stock and S. Biswas, *Chem Rev*, 2012, **112**, 933-969.
64. G. Ferey, *Chem Soc Rev*, 2008, **37**, 191-214.
65. R. J. Kuppler, D. J. Timmons, Q. R. Fang, J. R. Li, T. A. Makal, M. D. Young, D. Q. Yuan, D. Zhao, W. J. Zhuang and H. C. Zhou, *Coordin Chem Rev*, 2009, **253**, 3042-3066.
66. S. L. Qiu and G. S. Zhu, *Coordin Chem Rev*, 2009, **253**, 2891-2911.
67. J. Klinowski, F. A. A. Paz, P. Silva and J. Rocha, *Dalton T*, 2011, **40**, 321-330.
68. S. E. Park, J. S. Chang, Y. K. Hwang, D. S. Kim, S. H. Jhung and J. S. Hwang, *Catal Surv Asia*, 2004, **8**, 91-110.
69. S. H. Jhung, J. S. Chang, J. S. Hwang and S. E. Park, *Micropor Mesopor Mat*, 2003, **64**, 33-39.
70. S. H. Jhung, J. H. Lee, J. W. Yoon, J. S. Hwang, S. E. Park and J. S. Chang, *Micropor Mesopor Mat*, 2005, **80**, 147-152.
71. K. K. Kang, C. H. Park and W. S. Ahn, *Catal Lett*, 1999, **59**, 45-49.

72. S. H. Jhung, J. S. Chang, Y. K. Hwang and S. E. Park, *J Mater Chem*, 2004, **14**, 280-285.
73. Y. K. Hwang, J. S. Chang, S. E. Park, D. S. Kim, Y. U. Kwon, S. H. Jhung, J. S. Hwang and M. S. Park, *Angew Chem Int Edit*, 2005, **44**, 556-560.
74. S. H. Jhung, J. H. Lee and J. S. Chang, *B Korean Chem Soc*, 2005, **26**, 880-881.
75. P. Horcajada, T. Chalati, C. Serre, B. Gillet, C. Sebrie, T. Baati, J. F. Eubank, D. Heurtaux, P. Clayette, C. Kreuz, J. S. Chang, Y. K. Hwang, V. Marsaud, P. N. Bories, L. Cynober, S. Gil, G. Ferey, P. Couvreur and R. Gref, *Nat Mater*, 2010, **9**, 172-178.
76. S. H. Jhung, J. H. Lee, J. W. Yoon, C. Serre, G. Ferey and J. S. Chang, *Adv Mater*, 2007, **19**, 121-+.
77. K. M. L. Taylor-Pashow, J. Della Rocca, Z. G. Xie, S. Tran and W. B. Lin, *J Am Chem Soc*, 2009, **131**, 14261-+.
78. A. Centrone, Y. Yang, S. Speakman, L. Bromberg, G. C. Rutledge and T. A. Hatton, *J Am Chem Soc*, 2010, **132**, 15687-15691.
79. A. Centrone, T. Harada, S. Speakman and T. A. Hatton, *Small*, 2010, **6**, 1598-1602.
80. T. Ahnfeldt, J. Moellmer, V. Guillerm, R. Staudt, C. Serre and N. Stock, *Chem-Eur J*, 2011, **17**, 6462-6468.
81. P. Silva, A. A. Valente, J. Rocha and F. A. A. Paz, *Cryst Growth Des*, 2010, **10**, 2025-2028.
82. E. Haque, N. A. Khan, J. H. Park and S. H. Jhung, *Chem-Eur J*, 2010, **16**, 1046-1052.
83. D. O. Kim, J. Park, G. R. Ahn, H. J. Jeon, J. S. Kim, D. W. Kim, M. S. Jung, S. W. Lee and S. H. Shin, *Inorg Chim Acta*, 2011, **370**, 76-81.
84. S. H. Jhung, J. H. Lee, P. M. Forster, G. Ferey, A. K. Cheetham and J. S. Chang, *Chem-Eur J*, 2006, **12**, 7899-7905.
85. J. S. Lee, S. B. Halligudi, N. H. Jang, D. W. Hwang, J. S. Chang and Y. K. Hwang, *B Korean Chem Soc*, 2010, **31**, 1489-1495.
86. D. W. Jung, D. A. Yang, J. Kim, J. Kim and W. S. Ahn, *Dalton T*, 2010, **39**, 2883-2887.
87. J. Y. Choi, J. Kim, S. H. Jhung, H. K. Kim, J. S. Chang and H. K. Chae, *B Korean Chem Soc*, 2006, **27**, 1523-1524.
88. Z. Ni and R. I. Masel, *J Am Chem Soc*, 2006, **128**, 12394-12395.
89. J. S. Choi, W. J. Son, J. Kim and W. S. Ahn, *Micropor Mesopor Mat*, 2008, **116**, 727-731.
90. Z. H. Xiang, D. P. Cao, X. H. Shao, W. C. Wang, J. W. Zhang and W. Z. Wu, *Chem Eng Sci*, 2010, **65**, 3140-3146.

91. Y. K. Seo, G. Hundal, I. T. Jang, Y. K. Hwang, C. H. Jun and J. S. Chang, *Micropor Mesopor Mat*, 2009, **119**, 331-337.
92. M. Schlesinger, S. Schulze, M. Hietschold and M. Mehring, *Micropor Mesopor Mat*, 2010, **132**, 121-127.
93. N. A. Khan, E. Haque and S. H. Jhung, *Phys Chem Chem Phys*, 2010, **12**, 2625-2631.
94. T. J. Prior, B. Yotnoi and A. Rujiwatra, *Polyhedron*, 2011, **30**, 259-268.
95. H. K. Liu, T. H. Tsao, Y. T. Zhang and C. H. Lin, *Crystengcomm*, 2009, **11**, 1462-1468.
96. W. L. Liu, L. H. Ye, X. F. Liu, L. M. Yuan, X. L. Lu and J. X. Jiang, *Inorg Chem Commun*, 2008, **11**, 1250-1252.
97. X. F. Wang, Y. B. Zhang, H. Huang, J. P. Zhang and X. M. Chen, *Cryst Growth Des*, 2008, **8**, 4559-4563.
98. U. Mueller, M. Schubert, F. Teich, H. Puetter, K. Schierle-Arndt and J. Pastre, *J Mater Chem*, 2006, **16**, 626-636.
99. U. Mueller, I.Richter, M. Schubert, WO 2007131955A1, 2007.
100. R. Ameloot, L. Stappers, J. Fransaer, L. Alaerts, B. F. Sels and D. E. De Vos, *Chem Mater*, 2009, **21**, 2580-2582.
101. M. Y. Li and M. Dinca, *J Am Chem Soc*, 2011, **133**, 12926-12929.
102. K. Sumida, S. Horike, S. S. Kaye, Z. R. Herm, W. L. Queen, C. M. Brown, F. Grandjean, G. J. Long, A. Dailly and J. R. Long, *Chem Sci*, 2010, **1**, 184-191.
103. P. M. Forster, N. Stock and A. K. Cheetham, *Angew Chem Int Edit*, 2005, **44**, 7608-7611.
104. S. Bauer, C. Serre, T. Devic, P. Horcajada, J. Marrot, G. Ferey and N. Stock, *Inorg Chem*, 2008, **47**, 7568-7576.
105. T. Ahnfeldt, D. Gunzelmann, T. Loiseau, D. Hirsemann, J. Senker, G. Ferey and N. Stock, *Inorg Chem*, 2009, **48**, 3057-3064.
106. E. Biemmi, S. Christian, N. Stock and T. Bein, *Micropor Mesopor Mat*, 2009, **117**, 111-117.
107. A. Sonnauer, F. Hoffmann, M. Froba, L. Kienle, V. Duppel, M. Thommes, C. Serre, G. Ferey and N. Stock, *Angew Chem Int Edit*, 2009, **48**, 3791-3794.
108. M. Plabst, R. Kohn and T. Bein, *Crystengcomm*, 2010, **12**, 1920-1926.
109. R. Banerjee, A. Phan, B. Wang, C. Knobler, H. Furukawa, M. O'Keeffe and O. M. Yaghi, *Science*, 2008, **319**, 939-943.
110. P. Maniam and N. Stock, *Inorg Chem*, 2011, **50**, 5085-5097.
111. C. Volkringer, T. Loiseau, N. Guillou, G. Ferey, M. Haouas, F. Taulelle, E. Elkaim and N. Stock, *Inorg Chem*, 2010, **49**, 9852-9862.
112. H. Reinsch, M. Kruger, J. Wack, J. Senker, F. Salles, G. Maurin and N. Stock, *Micropor Mesopor Mat*, 2012, **157**, 50-55.

113. T. Ahnfeldt, N. Guillou, D. Gunzelmann, I. Margiolaki, T. Loiseau, G. Ferey, J. Senker and N. Stock, *Angew Chem Int Edit*, 2009, **48**, 5163-5166.
114. W. Kleist, F. Jutz, M. Maciejewski and A. Baiker, *Eur J Inorg Chem*, 2009, 3552-3561.
115. H. X. Deng, C. J. Doonan, H. Furukawa, R. B. Ferreira, J. Towne, C. B. Knobler, B. Wang and O. M. Yaghi, *Science*, 2010, **327**, 846-850.
116. H. Chun, D. N. Dybtsev, H. Kim and K. Kim, *Chem-Eur J*, 2005, **11**, 3521-3529.
117. T. Fukushima, S. Horike, Y. Inubushi, K. Nakagawa, Y. Kubota, M. Takata and S. Kitagawa, *Angew Chem Int Edit*, 2010, **49**, 4820-4824.
118. K. Koh, A. G. Wong-Foy and A. J. Matzger, *Chem Commun*, 2009, 6162-6164.
119. S. Marx, W. Kleist, J. Huang, M. Maciejewski and A. Baiker, *Dalton T*, 2010, **39**, 3795-3798.
120. J. A. Botas, G. Calleja, M. Sanchez-Sanchez and M. G. Orcajo, *Langmuir*, 2010, **26**, 5300-5303.
121. B. Jee, K. Eisinger, F. Gul-E-Noor, M. Bertmer, M. Hartmann, D. Himsl and A. Poppl, *J Phys Chem C*, 2010, **114**, 16630-16639.
122. S. Furukawa, K. Hirai, K. Nakagawa, Y. Takashima, R. Matsuda, T. Tsuruoka, M. Kondo, R. Haruki, D. Tanaka, H. Sakamoto, S. Shimomura, O. Sakata and S. Kitagawa, *Angew Chem Int Edit*, 2009, **48**, 1766-1770.
123. Y. Yoo and H. K. Jeong, *Cryst Growth Des*, 2010, **10**, 1283-1288.
124. S. Proch, J. Herrmannsdorfer, R. Kempe, C. Kern, A. Jess, L. Seyfarth and J. Senker, *Chem-Eur J*, 2008, **14**, 8204-8212.
125. T. Ishida, M. Nagaoka, T. Akita and M. Haruta, *Chem-Eur J*, 2008, **14**, 8456-8460.
126. M. Muller, S. Turner, O. I. Lebedev, Y. M. Wang, G. van Tendeloo and R. A. Fischer, *Eur J Inorg Chem*, 2011, 1876-1887.
127. H. L. Liu, Y. L. Liu, Y. W. Li, Z. Y. Tang and H. F. Jiang, *J Phys Chem C*, 2010, **114**, 13362-13369.
128. S. Hermes, M. K. Schroter, R. Schmid, L. Khodeir, M. Muhler, A. Tissler, R. W. Fischer and R. A. Fischer, *Angew Chem Int Edit*, 2005, **44**, 6237-6241.
129. M. Sabo, A. Henschel, H. Froede, E. Klemm and S. Kaskel, *J Mater Chem*, 2007, **17**, 3827-3832.
130. S. Hermes, F. Schroder, S. Amirjalayer, R. Schmid and R. A. Fischer, *J Mater Chem*, 2006, **16**, 2464-2472.
131. H. Kim, H. Chun, G. H. Kim, H. S. Lee and K. Kim, *Chem Commun*, 2006, 2759-2761.

132. F. Yu, P. Q. Zheng, Y. X. Long, Y. P. Ren, X. J. Kong, L. S. Long, Y. Z. Yuan, R. B. Huang and L. S. Zheng, *Eur J Inorg Chem*, 2010, 4526-4531.
133. N. V. Maksimchuk, M. N. Timofeeva, M. S. Melgunov, A. N. Shmakov, Y. A. Chesalov, D. N. Dybtsev, V. P. Fedin and O. A. Kholdeeva, *J Catal*, 2008, **257**, 315-323.
134. N. V. Maksimchuk, K. A. Kovalenko, S. S. Arzumanov, Y. A. Chesalov, M. S. Melgunov, A. G. Stepanov, V. P. Fedin and O. A. Kholdeeva, *Inorg Chem*, 2010, **49**, 2920-2930.
135. C. Y. Sun, S. X. Liu, D. D. Liang, K. Z. Shao, Y. H. Ren and Z. M. Su, *J Am Chem Soc*, 2009, **131**, 1883-1888.
136. Z. Y. Li, G. S. Zhu, G. Q. Lu, S. L. Qiu and X. D. Yao, *J Am Chem Soc*, 2010, **132**, 1490-+.
137. O. R. Evans and W. B. Lin, *Accounts Chem Res*, 2002, **35**, 511-522.
138. E. Y. Lee, S. Y. Jang and M. P. Suh, *J Am Chem Soc*, 2005, **127**, 6374-6381.
139. B. D. Chandler, D. T. Cramb and G. K. H. Shimizu, *J Am Chem Soc*, 2006, **128**, 10403-10412.
140. W. J. Rieter, K. M. L. Taylor, H. Y. An, W. L. Lin and W. B. Lin, *J Am Chem Soc*, 2006, **128**, 9024-9025.
141. Y. Liu, G. Li, X. Li and Y. Cui, *Angew Chem Int Edit*, 2007, **46**, 6301-6304.
142. G. J. Halder, C. J. Kepert, B. Moubaraki, K. S. Murray and J. D. Cashion, *Science*, 2002, **298**, 1762-1765.
143. D. Maspoch, D. Ruiz-Molina and J. Veciana, *J Mater Chem*, 2004, **14**, 2713-2723.
144. P. D. C. Dietzel, Y. Morita, R. Blom and H. Fjellvag, *Angew Chem Int Edit*, 2005, **44**, 6354-6358.
145. W. Ouellette, M. H. Yu, C. J. O'Connor, D. Hagrman and J. Zubieta, *Angew Chem Int Edit*, 2006, **45**, 3497-3500.
146. C. T. Yu, S. Q. Ma, M. J. Pechan and H. C. Zhou, *J Appl Phys*, 2007, **101**.
147. X. M. Zhang, Z. M. Hao, W. X. Zhang and X. M. Chen, *Angew Chem Int Edit*, 2007, **46**, 3456-3459.
148. Z. M. Wang, Y. J. Zhang, T. Liu, M. Kurmoo and S. Gao, *Adv Funct Mater*, 2007, **17**, 1523-1536.
149. T. Okubo, R. Kawajiri, T. Mitani and T. Shimoda, *J Am Chem Soc*, 2005, **127**, 17598-17599.
150. Q. Ye, Y. M. Song, G. X. Wang, K. Chen, D. W. Fu, P. W. H. Chan, J. S. Zhu, S. D. Huang and R. G. Xiong, *J Am Chem Soc*, 2006, **128**, 6554-6555.

151. Z. T. Xu, *Coordin Chem Rev*, 2006, **250**, 2745-2757.
152. M. Alvaro, E. Carbonell, B. Ferrer, F. X. L. I. Xamena and H. Garcia, *Chem-Eur J*, 2007, **13**, 5106-5112.
153. A. Kuc, A. Enyashin and G. Seifert, *J Phys Chem B*, 2007, **111**, 8179-8186.
154. R. Q. Zou, H. Sakurai, S. Han, R. Q. Zhong and Q. Xu, *J Am Chem Soc*, 2007, **129**, 8402-+.
155. W. B. Lin, *J Solid State Chem*, 2005, **178**, 2486-2490.
156. S. Horike, M. Dinca, K. Tamaki and J. R. Long, *J Am Chem Soc*, 2008, **130**, 5854-+.
157. D. F. Sava, V. C. Kravtsov, F. Nouar, L. Wojtas, J. F. Eubank and M. Eddaoudi, *J Am Chem Soc*, 2008, **130**, 3768-+.
158. E. Lee, J. Kim, J. Heo, D. Whang and K. Kim, *Angew Chem Int Edit*, 2001, **40**, 399-402.
159. M. D. Ward, *Science*, 2003, **300**, 1104-1105.
160. J. L. C. Rowsell and O. M. Yaghi, *Angew Chem Int Edit*, 2005, **44**, 4670-4679.
161. X. Lin, J. H. Jia, P. Hubberstey, M. Schroder and N. R. Champness, *Crystengcomm*, 2007, **9**, 438-448.
162. D. J. Collins and H. C. Zhou, *J Mater Chem*, 2007, **17**, 3154-3160.
163. R. E. Morris and P. S. Wheatley, *Angew Chem Int Edit*, 2008, **47**, 4966-4981.
164. S. Q. Ma, D. F. Sun, J. M. Simmons, C. D. Collier, D. Q. Yuan and H. C. Zhou, *J Am Chem Soc*, 2008, **130**, 1012-1016.
165. M. Dinca and J. R. Long, *Angew Chem Int Edit*, 2008, **47**, 6766-6779.
166. Q. M. Wang, D. M. Shen, M. Bulow, M. L. Lau, S. G. Deng, F. R. Fitch, N. O. Lemcoff and J. Semanscin, *Micropor Mesopor Mat*, 2002, **55**, 217-230.
167. R. Custelcean and B. A. Moyer, *Eur J Inorg Chem*, 2007, 1321-1340.
168. E. Biemmi, A. Darga, N. Stock and T. Bein, *Micropor Mesopor Mat*, 2008, **114**, 380-386.
169. M. D. Allendorf, R. J. T. Houk, L. Andruszkiewicz, A. A. Talin, J. Pikarsky, A. Choudhury, K. A. Gall and P. J. Hesketh, *J Am Chem Soc*, 2008, **130**, 14404-+.
170. A. Demessence, P. Horcajada, C. Serre, C. Boissiere, D. Grosso, C. Sanchez and G. Ferey, *Chem Commun*, 2009, 7149-7151.
171. S. Achmann, G. Hagen, J. Kita, I. M. Malkowsky, C. Kiener and R. Moos, *Sensors-Basel*, 2009, **9**, 1574-1589.
172. X. Q. Zou, G. S. Zhu, I. J. Hewitt, F. X. Sun and S. L. Qiu, *Dalton T*, 2009, 3009-3013.
173. G. Lu and J. T. Hupp, *J Am Chem Soc*, 2010, **132**, 7832-+.

174. L. E. Kreno, J. T. Hupp and R. P. Van Duyne, *Anal Chem*, 2010, **82**, 8042-8046.
175. T. Uemura, R. Kitaura, Y. Ohta, M. Nagaoka and S. Kitagawa, *Angew Chem Int Edit*, 2006, **45**, 4112-4116.
176. C. J. Chuck, M. G. Davidson, M. D. Jones, G. Kociok-Kohn, M. D. Lunn and S. Wu, *Inorg Chem*, 2006, **45**, 6595-6597.
177. T. Uemura, D. Hiramatsu, Y. Kubota, M. Takata and S. Kitagawa, *Angew Chem Int Edit*, 2007, **46**, 4987-4990.
178. P. Horcajada, C. Serre, M. Vallet-Regi, M. Sebban, F. Taulelle and G. Ferey, *Angew Chem Int Edit*, 2006, **45**, 5974-5978.
179. M. Vallet-Regi, F. Balas and D. Arcos, *Angew Chem Int Edit*, 2007, **46**, 7548-7558.
180. P. Horcajada, C. Serre, G. Maurin, N. A. Ramsahye, F. Balas, M. Vallet-Regi, M. Sebban, F. Taulelle and G. Ferey, *J Am Chem Soc*, 2008, **130**, 6774-6780.
181. M. D. Allendorf, C. A. Bauer, R. K. Bhakta and R. J. T. Houk, *Chem Soc Rev*, 2009, **38**, 1330-1352.
182. J. Rocha, L. D. Carlos, F. A. A. Paz and D. Ananias, *Chem Soc Rev*, 2011, **40**, 926-940.
183. P. Wang, J. P. Ma and Y. B. Dong, *Chem-Eur J*, 2009, **15**, 10432-10445.
184. M. Arruebo, *Wires Nanomed Nanobi*, 2012, **4**, 16-30.
185. J. Della Rocca, D. M. Liu and W. B. Lin, *Accounts Chem Res*, 2011, **44**, 957-968.
186. P. Horcajada, R. Gref, T. Baati, P. K. Allan, G. Maurin, P. Couvreur, G. Ferey, R. E. Morris and C. Serre, *Chem Rev*, 2012, **112**, 1232-1268.
187. R. C. Huxford, J. Della Rocca and W. B. Lin, *Curr Opin Chem Biol*, 2010, **14**, 262-268.
188. S. Keskin and S. Kizilel, *Ind Eng Chem Res*, 2011, **50**, 1799-1812.
189. Z. B. Ma and B. Moulton, *Coordin Chem Rev*, 2011, **255**, 1623-1641.
190. A. C. McKinlay, R. E. Morris, P. Horcajada, G. Ferey, R. Gref, P. Couvreur and C. Serre, *Angew Chem Int Edit*, 2010, **49**, 6260-6266.
191. R. B. Getman, Y. S. Bae, C. E. Wilmer and R. Q. Snurr, *Chem Rev*, 2012, **112**, 703-723.
192. Z. Y. Gu, C. X. Yang, N. Chang and X. P. Yan, *Accounts Chem Res*, 2012, **45**, 734-745.
193. Y. H. Hu and L. Zhang, *Adv Mater*, 2010, **22**, E117-E130.
194. J. R. Li, R. J. Kuppler and H. C. Zhou, *Chem Soc Rev*, 2009, **38**, 1477-1504.
195. J. R. Li, Y. G. Ma, M. C. McCarthy, J. Sculley, J. M. Yu, H. K. Jeong, P. B. Balbuena and H. C. Zhou, *Coordin Chem Rev*, 2011, **255**, 1791-1823.
196. J. R. Li, J. Sculley and H. C. Zhou, *Chem Rev*, 2012, **112**, 869-932.

197. X. A. Lin, N. R. Champness and M. Schroder, *Functional Metal-Organic Frameworks: Gas Storage, Separation and Catalysis*, 2010, **293**, 35-76.
198. J. Liu, P. K. Thallapally, B. P. McGrail, D. R. Brown and J. Liu, *Chem Soc Rev*, 2012, **41**, 2308-2322.
199. Y. Liu, W. M. Xuan and Y. Cui, *Adv Mater*, 2010, **22**, 4112-4135.
200. S. Q. Ma and H. C. Zhou, *Chem Commun*, 2010, **46**, 44-53.
201. L. J. Murray, M. Dinca and J. R. Long, *Chem Soc Rev*, 2009, **38**, 1294-1314.
202. J. Sculley, D. Q. Yuan and H. C. Zhou, *Energ Environ Sci*, 2011, **4**, 2721-2735.
203. M. Shah, M. C. McCarthy, S. Sachdeva, A. K. Lee and H. K. Jeong, *Ind Eng Chem Res*, 2012, **51**, 2179-2199.
204. M. P. Suh, H. J. Park, T. K. Prasad and D. W. Lim, *Chem Rev*, 2012, **112**, 782-835.
205. K. Sumida, D. L. Rogow, J. A. Mason, T. M. McDonald, E. D. Bloch, Z. R. Herm, T. H. Bae and J. R. Long, *Chem Rev*, 2012, **112**, 724-781.
206. H. H. Wu, Q. H. Gong, D. H. Olson and J. Li, *Chem Rev*, 2012, **112**, 836-868.
207. D. Zhao, D. Q. Yuan and H. C. Zhou, *Energ Environ Sci*, 2008, **1**, 222-235.
208. A. Corma, H. Garcia and F. X. L. Xamena, *Chem Rev*, 2010, **110**, 4606-4655.
209. D. Farrusseng, S. Aguado and C. Pinel, *Angew Chem Int Edit*, 2009, **48**, 7502-7513.
210. J. Lee, O. K. Farha, J. Roberts, K. A. Scheidt, S. T. Nguyen and J. T. Hupp, *Chem Soc Rev*, 2009, **38**, 1450-1459.
211. L. Q. Ma, C. Abney and W. B. Lin, *Chem Soc Rev*, 2009, **38**, 1248-1256.

Chapter 2: Metal Organic Frameworks as oxidation catalysts

Abstract

In this chapter, a state of the art of the use of MOFs as heterogeneous catalysts in liquid phase oxidation reactions will be presented. More specifically, their use in the oxidation of cycloalkanes, benzylic compounds, cycloalkenes, alcohols, sulfides and thiols will be discussed. Firstly, some general concepts on catalysis will be introduced.

2.1 What is catalysis?

The classical definition of a catalyst has been discussed many times[1]. In brief, a catalyst is a substance that changes the kinetics but not the thermodynamics of a chemical reaction[2]. In other words, a catalyst accelerates the reaction between reactants. To see how the catalyst accelerates the reaction, we need to look at the Gibbs free energy diagram in Fig. 2.1, which compares the non-catalytic and the catalytic reaction. For the non-catalytic reaction, the figure simply reflects the familiar way to visualize the Arrhenius equation: the reaction proceeds when A and B collide with sufficient energy to overcome the activation barrier in Fig. 2.1. The change in Gibbs free energy between the reactants, A + B, and the product P is ΔG [3].
The energy diagram of Figure 2.1 illustrates several important points[3, 4]:

- The catalyst offers an alternative path for the reaction, which is obviously more complex, but energetically much more favorable.
- The activation energy of the catalytic reaction is significantly smaller than that of the non-catalyzed reaction; hence, the rate of the catalytic reaction is much larger.
- The overall change in Gibbs free energy for the catalytic reaction equals that of the non-catalyzed reaction. Hence, the catalyst does not affect the equilibrium constant for the overall reaction of A + B to P. Thus, if a reaction is thermodynamically unfavorable, a catalyst cannot change this situation. So, as was mentioned earlier, a catalyst changes the kinetics but not the thermodynamics.
- The catalyst accelerates both the forward and the reverse reaction to the same extent. In other words, if a catalyst accelerates the formation of the product P from A and B, it will do the same for the decomposition of P into A and B.

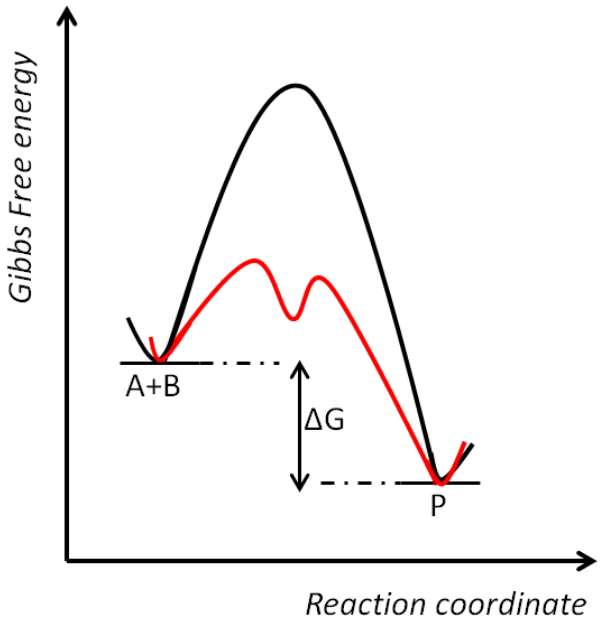

Fig. 2.1. Gibbs free energy diagram for a non-catalyzed (black curve) and catalyzed reaction (red curve).

2.2 Types of catalysts

Catalysts are usually subdivided in 3 categories: bio catalysts, homogeneous catalysts and heterogeneous catalysts. Each of them can be manmade of naturally occurring. Each of them will be briefly described.

2.2.1 Bio catalysis

The bio catalysts or enzymes play a crucial role in life. Enzymes can modify a particular molecule to give a product with 100 % selectivity in terms of chemo, regio and stereo selectivity. In spite of their high substrate and product selectivity, they usually exhibit a low stability under non-optimized conditions (optimized conditions: water, room temperature, atmospheric pressure), which makes them unsuitable in a wide range of processes in the chemical industry[3, 5].

2.2.2 Homogeneous catalysis

In homogeneous catalysis, the catalyst is present in the same phase as the reactants during the reactions, i.e. all molecules are in the gas or the liquid phase. They generally consist of metal centers surrounded by a variety of ligands. Homogeneous catalysts are highly versatile and can give very high selectivities. By varying the metal center and the surrounding ligands, the selectivities can be tuned toward a certain product. However, homogeneous catalysts suffer from one important drawback: the difficulty of separating the products at the end of the reaction, which makes them less attractive from the "Green Chemistry" point of view [3, 5].

2.2.3 Heterogeneous catalysis

Heterogeneous catalysts are solids that catalyze a reaction of molecules in the gas or liquid phase. So, the catalyst is present in a different phase than the reactants during the reactions. Usually metals, or metal oxides, are used as heterogeneous catalysts, which can drastically accelerate the rate of a reaction. They are resistant to high temperatures[3, 5].

The heterogeneous catalysis process can occur *via* two possible mechanisms: the Langmuir-Hinshelwood or Eley-Rideal mechanism (see Fig. 2.2). In the first mechanism (see Fig. 2.2, left), it is assumed that all species are adsorbed and accommodated onto the surface before they take part in any reaction. Hence, species react in the chemisorbed state on the surface. This is the prevailing situation in heterogeneous catalysis [3].
In the other mechanism, the so-called Eley-Rideal mechanism, one of the reactants reacts directly out of the gas phase, without being accommodated at the surface. However, this mechanism is rather rare [3].

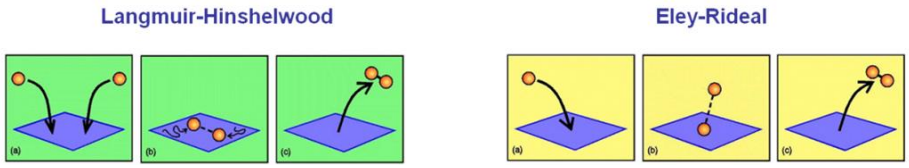

Fig. 2.2. LEFT: Langmuir-Hinshelwood mechanism, RIGHT: Eley-Rideal mechanism for a bimolecular heterogeneous catalytic reaction.

2.3 Importance of heterogeneous catalysis

There are several reasons that justify the use of a heterogeneous catalyst. Firstly, solid catalysts can be easily recovered at the end of the reaction, which makes it possible to reuse them afterwards. This implies that less waste is generated. Secondly, isolation and purification of the product become easier. Solid catalysts can be fixed in reactors in, for example, a fixed bed reactor. Hence, the reactants will flow over the bed of the catalyst and separation of the product is achieved simultaneously. Finally, the support can induce a selectivity in size and shape, as is observed in zeolites[5].

MOFs can shown great potential in catalysis, since they can combine different catalytic functions[6]:

- They can merge Brönsted or Lewis acidity and basicity, or both, and redox centers, thus making a "cascade" catalytic process possible.
- Their specific hydrophilic/hydrophobic properties might influence the adsorption of reagents, intermediates and products, driving the catalytic selectivity.
- The highly controlled 3D geometric organization can create a synergetic effect. Confinement of the reactants according to a specific arrangement of the catalytic centers will drive chemo- and regio-selective transformations, comparable to those observed in enzymes.
- The nanosized porosity permits shape selectivity by avoiding the production of undesired bulky intermediates or products.

The active sites in MOFs should be protected by the coordination bonds that prevent leaching to a higher extent.

2.4 Active sites in MOFs

The active sites in MOFs can be generated in several ways. First, the metal or metal cluster connecting points can be used to catalyze organic transformations.

As shown in Scheme 2.1, a metal connecting point with a free coordinating site can be used as a Lewis acid catalyst after removal of coordinating solvent molecules from the axial positions of the metal center[7]. Secondly, active sites can be generated from the functional groups within a MOF scaffold (Scheme 2.2)[8, 9]. However, unlike traditional immobilized catalysts, the active sites generated in this fashion are arranged in a predictable and tuneable manner due to the periodically ordered nature of porous MOFs. Thirdly, the catalytic activity of MOFs can result from entrapped active catalysts, such as palladium or ruthenium nanoparticles (Scheme 2.3)[10, 11].

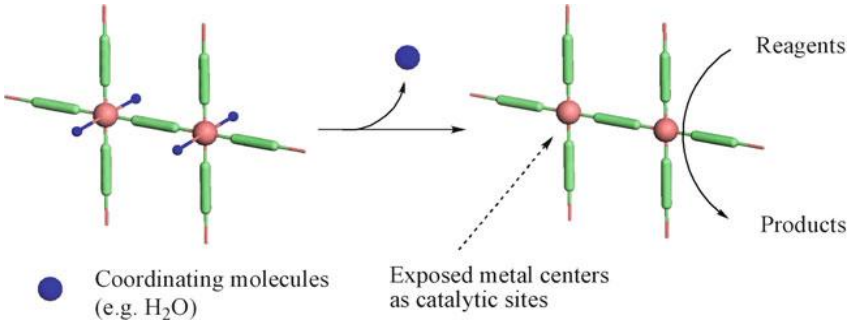

Scheme 2.1. Schematic representation illustrating the generation of unsaturated metal connecting points as active sites[12].

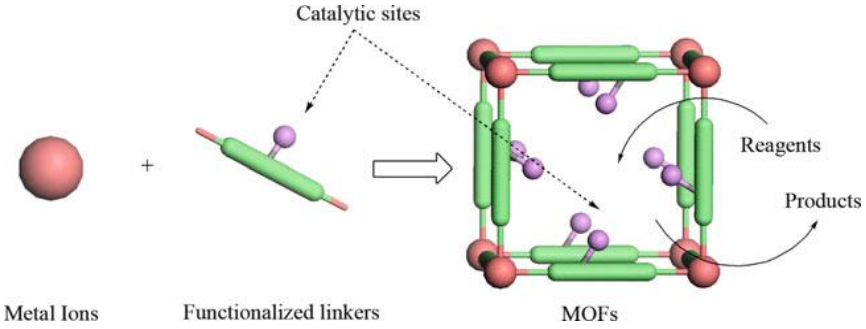

Scheme 2.2. Schematic representation showing the use of functional groups in the bridging ligands as active catalysts[12].

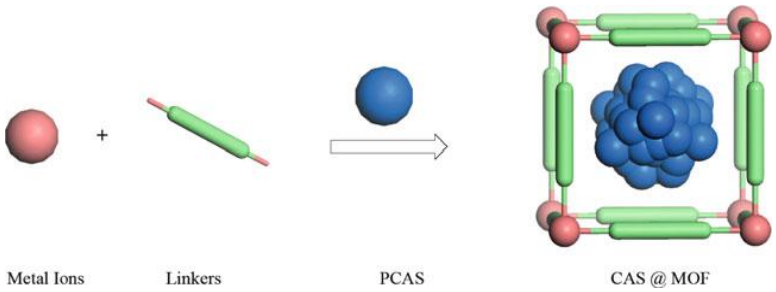

Scheme 2.3. Schematic representation of trapping catalytic active species inside MOFs[12].

2.5 Catalysis with MOFs

The very first demonstration of the catalytic potential of MOFs was made in 1994 for a two-dimensional Cd bipyridine lattice that catalyzes the cyanosilylation of aldehydes[13]. Yet, many other Lewis acid catalyzed reactions are reported for which MOFs have been examined: isomerization of alpha-pinene oxide, citronellal cyclization and rearrangement of ethylene acetal of 2-bromopropiophenone[14-16]. Beside Lewis acid catalysis, Brönsted acid catalysis like, for example, the Friedel-Crafts benzylation and base catalytic (Knoevenagel and transesterification reactions) studies have been carried out on MOFs[17-22]. Furthermore, the potential of MOFs as a bifunctional catalyst, e.g. in the oxidation of linalool, has been studied[23, 24]. Although the use of chiral MOFs is still in a very early stage, there are already a few reports that clearly have shown the advantages of a MOF as a chiral catalyst in comparison to the homogeneous analogue [25-29].

In this thesis the focus will be on oxidation catalysis with MOFs and more specifically the use of V-based MOFs in oxidation catalysis (see following chapters). First, a state of the art on MOFs as heterogeneous catalysts in liquid phase oxidation reactions will be presented. Particularly the potential of MOFs in the oxidation of cycloalkanes, benzylic compounds, alcohols, sulfides, thiols and cycloalkenes will be reported after a brief introduction to the types of oxidants applied in oxidation catalysis.

2.6 Types of oxidants

An important aspect in oxidation catalysis is the source of oxygen. In brief, there are four important processes of oxygen activation. Each of these mechanisms of oxygen incorporation into organic molecules will now be discussed.

2.6.1 Oxidation in the presence of pure O_2

Clearly gaseous O_2, often referred to as molecular oxygen or dioxygen, is the most desired oxidant due to its availability and low cost. The most well known catalytic system that can use molecular oxygen directly and efficiently is bulk silver [30]. It achieves this by dissociative adsorption into atomic oxygen species (see eq.1 scheme 2.4), which will give rise to selective epoxidation product.

$$O_2 + 4Ag \rightarrow 2O^{2-}_{ads} + 4Ag^{+} \quad (1)$$

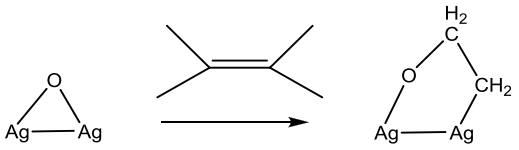

Scheme 2.4. Oxametallacycle mechanism for Ag catalysts.

By illumination of semi-conductors by an artificial or natural light in water (=photocatalysis), highly oxidizing OH· radicals can be created, which can be good oxidants. In Scheme 2.5, the basic mechanism of photocatalysis is shown for TiO_2. Many efforts have been devoted to clarify the oxidizing species generated at the irradiated TiO_2 surface. Oxidizing species, which have been suggested, include holes, ·OH and O^{-}_{2}· radicals, among others[31]. In first instance, in the basic process of photocatalysis, an electron is ejected from the valence band (VB) to the conduction band (CB) of the TiO_2 semiconductor, creating a h^+ hole in the valence band (eq. 1 Scheme 2.5) due to UV irradiation of TiO_2 with an energy equal or superior to the band gap.

This is followed by formation of extremely reactive radicals (like ·OH) and direct oxidation of the organic reactant. Furthermore, the ejected electrons react with electron acceptors such as molecular oxygen, which is dissolved in water (eq. 3 Scheme 2.5) [32]. These can in turn be oxidizing species.

$$TiO_2 + h\nu \rightarrow e^-_{cb} + h^+_{vb} \quad (1)$$

$$h^+_{vb} + H_2O \rightarrow \cdot OH + H^+ \quad (2)$$

$$e^-_{cb} + O_2 \rightarrow O^-_2\cdot \quad (3)$$

Scheme 2.5. Basic process of photocatalysis[32].

2.6.2 Oxidation in the presence of O_2 and aldehyde

The oxidation of alkenes in the presence of an aldehyde and O_2 appears to proceed via a mechanism related to aldehyde autoxidation, as can be seen in Scheme 2.6. In other words, the aldehyde plays a sacrificial role and undergoes co-oxidation (see eq.1 and 2 scheme 2.6). From literature, it is concluded that the predominant oxidizing species is an acylperoxy radical (see eq. 2 Scheme 2.6)[33, 34]. These radicals are known to preferentially react with the double bonds of alkenes yielding epoxides, whereas hydroxyl and alkylperoxy radicals tend to abstract allylic hydrogens, resulting in allylic oxidation products.

2.6.3 Oxidation in the presence of hydrogen peroxide or organic peroxides

In most catalytic systems the oxygen needs to be activated in some form. Examples of products of direct activation are hydrogen peroxide or organic peroxides like TBHP, which retain the O-O bond. Hydrogen peroxide is a very environment-friendly oxidant because the only by-product is water. It is, however, very hazardous to handle. In Scheme 2.7 an epoxidation mechanism is shown for a Mo based catalyst in the presence of H_2O_2. Early transition metal ions in their highest oxidation state, such as Ti(IV), V(V), W(VI) and Mo(VI), tend to be stable toward changes in their oxidation state.

Consequently, in epoxidation reactions with H_2O_2 or alkylhydroperoxides, they form adducts (M-OOH and M-OOR). These adducts are the key intermediates in the epoxidation, and the role of the metal ion is that of a Lewis acid. The metal center acts as a Lewis acid by removing charge from the O-O bond, facilitating its dissociation, and activating the nearest oxygen atom (*proximal* oxygen) for insertion into the olefin double bond, whereas the *distal* oxygen constitutes a good leaving group in the form of -OH or -OR (see Scheme 2.7)[30].

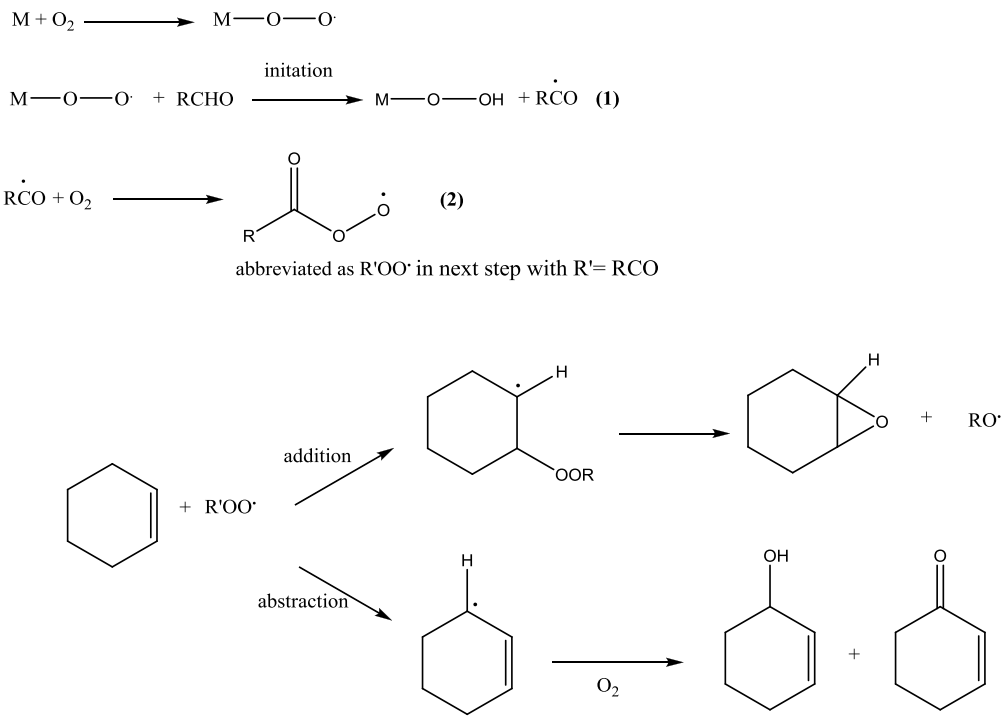

Scheme 2.6. General mechanism for the oxidation of cyclohexene with O_2 and aldehyde (RCHO)[34].

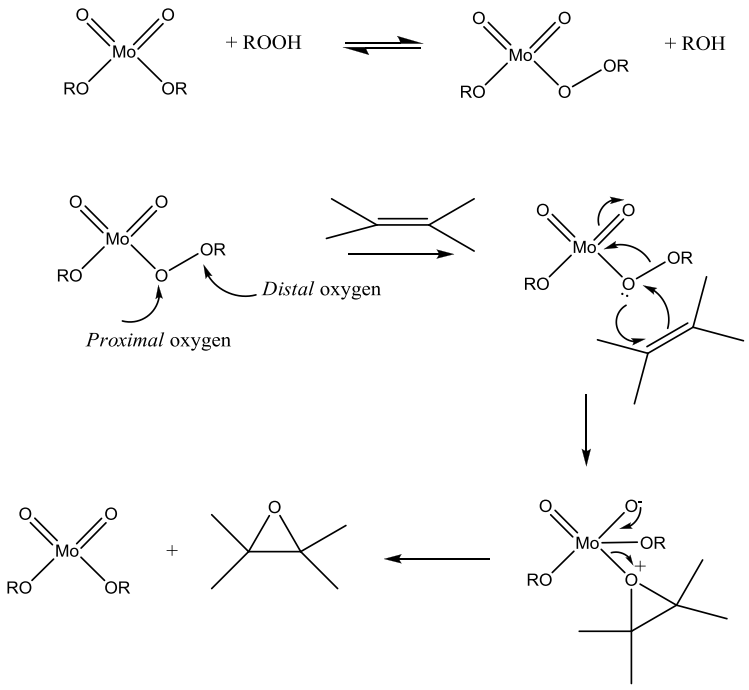

Scheme 2.7. Accepted alkylperoxo mechanism of Mo-catalyzed epoxidation with hydroperoxides[30]. It should be noted that this mechanism can be different for other transition metals.

2.6.4 Oxidation in the presence of N_2O, iodosyl aromatics and hypochlorite

Other examples of oxidants are N_2O, iodosyl aromatics and hypochlorite, which contain a single oxygen atom in a highly activated state. With these oxidants, a single oxygen atom is transferred to a metal ion to form a high oxidation state metal-oxo species (M=O), which in turn delivers the same oxygen to the reactant. These single oxygen transfers are seen in certain coordination compounds of Fe, Mn, and Cr, in which the metal undergoes successive oxidation state changes[30].

2.7 MOFs in oxidation catalysis

2.7.1 Oxidation of cycloalkanes and benzylic compounds

The investigated MOFs for the oxidation of cycloalkanes and/or benzylic compounds are presented in Table 2.1. Most reports describe the use of TBHP as oxidant (entries 1,4-15,19 Table 2.1). However, a small amount of studies carried out the oxidation under aerobic conditions (entries 2-3, 16-18 Table 2.1) or employed H_2O_2 as an oxidant (entries 20-21 Table 2.1). From Table 2.1 it can be seen that tetralin is a commonly applied reactant (see Fig. 2.3). First of all, Cr-MIL-101 has been evaluated for the oxidation of tetralin using TBHP as an oxidant, versus in situ generated acylperoxy radicals through trimethylacetaldehyde and O_2 (entry 1 Table 2.1).[35] From this investigation it was clear that the sources of oxidant played an important role in the activity and selectivity. The use of TBHP afforded higher conversion, whereas higher selectivities toward 1-tetralone were obtained with the other oxidant (93 vs. 86%). Another study on the oxidation of tetralin applied pure O_2 as the oxidant for the evaluation of the catalytic performance of a Cu and Co MOF (entries 2 and 3 Table 2.1)[36]. A significant difference was observed between both catalysts due to the different catalytic behaviour of the central metal ions. The authors observed that the Cu-based MOF was very efficient for the activation of tetralin to produce tetralinhydroperoxide and less efficient in reacting the peroxide, whereas the Co-MOF showed a long induction period for the formation of the peroxide. Nevertheless, once the peroxide was formed, it was rapidly converted. This study unambiguously shows that the metal is directly involved in the generation and reaction of the intermediate hydroperoxide species.

The influence of the metal ion on the oxidation performance was once more confirmed by the study of Dhakshinamoorthy *et al.*[37] (entries 4-7 Table 2.1). They observed a significant difference in activity between Fe(BTC), $Cu_3(BTC)_2$ and $Al_2(BDC)_2$. Furthermore, this report showed that the nature of the oxidant plays a crucial role. While molecular oxygen and hydrogen peroxide were inefficient to promote the xanthene oxidation, TBHP was a good oxidizing reagent in terms of the percentage yield to xanthenone.

However, the question whether or not the catalytic activity might be due to leaching of metal ions from the nodes of the MOFs into solution was not addressed.

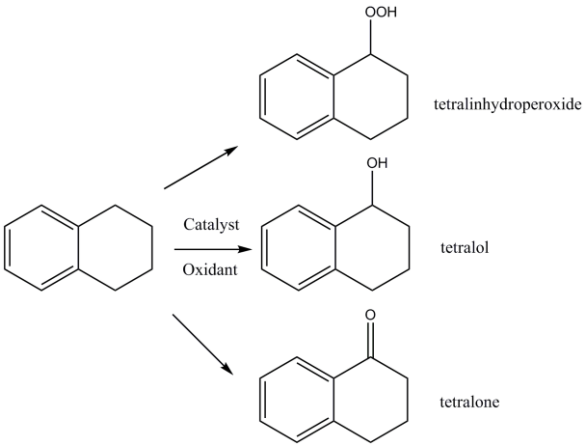

Fig. 2.3. Oxidation of tetralin toward tetralinhydroperoxide, tetralol and tetralone.

Instead of studying the influence of the metal centers, Wang *et al.* [38] studied the influence of the anion exchange on the oxidation of diphenylmethane and tetralin for Cu based MOFs (entries 8-11 Table 2.1). As can be observed from Table 2.1, a similar conversion of tetralin was obtained for both MOFs, whereas for the oxidation of diphenylmethane a significantly higher conversion was detected for the Cu-MOF-NO_3 in comparison to the Cu-MOF-SiF_6, suggesting that the catalysts are sensitive to the size and shape of the reactants. The openings of the channels on the surface may display distinct recognition and response to different reactants. As a consequence, the activity is regulated by the size of the surface openings of the Cu-MOFs with the counter anion varying from SiF_6^{2-} to NO_3^-.

Furthermore, some modified MOFs, obtained by the incorporation of species into the framework, were examined for the oxidation of cycloalkanes and/or benzylic compounds. Firstly, 4 POM based MOFs were examined for the oxidation of ethylbenzene (entries 12-15 Table 2.1)[39]. Also, this report demonstrated that the metal center, more specifically the valence of the metal ion in the POM, can significantly influence the catalytic performance of the 3D framework.

Secondly, *N*-hydroxyphthalimide (NHPI), a radical initiator, was incorporated in Fe(BTC) which was explored for the oxidation of several benzylic compounds and alkanes (see entries 16-18 Table 2.1)[40]. The authors assumed the occurrence of a radical oxidation mechanism with the aid of NHPI and the metal site of the MOF (see Scheme 2.8). Acceptable proof for this mechanism was noted: the presence of NHPI can generate phthalimide *N*-oxyl radical intermediates that act as a precursor for C-centered radicals which endure auto-oxidation. The significant difference between the reactivity of the linear alkanes and benzylic compounds (entries 17-18 Table 2.1) is explained by the unfavourable diffusion of the linear alkanes through the MOF due to the larger molecular dimensions[40].

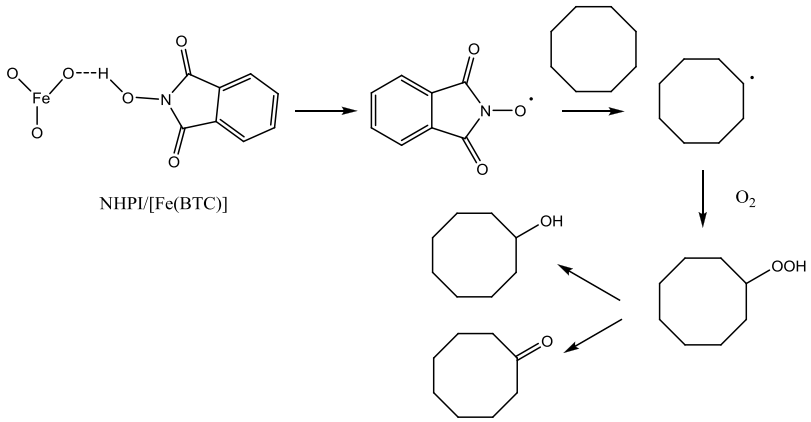

Scheme 2.8. Proposed mechanism for the oxidation of cyclooctane catalysed by NHPI@Fe(BTC)[40].

Finally, the report of Alkordi *et al.*[41] describe the incapsulation of a Mn-metallated porphyrin complex in an indium-imidazoledicarboxylate based MOF, *rho*-ZMOF (entry 19 Table 2.1)[41]. The resulting catalyst was explored for the oxidation of cyclohexane with TBHP as an oxidant, yielding a conversion of 91.5% after 24 hours of catalysis.

Table 2.1. Overview of the MOFs studied for the oxidation of cycloalkanes and/or benzylic compounds.

Entry	Catalytic MOF	Reactant	Oxidant	Conversion (%)	Main product (selectivity)	Take home message	Reference
1	Cr-MIL-101	Tetralin	TBHP/ O_2+aldehyde	55-73	Tetralone (86-93%)	Solvent and oxidant: influence on activity and selectivity	Kim *et al.*[35]
2	[Cu(2-pymo)$_2$]	Tetralin	air	52	Tetralinhydro peroxide	No induction period, low selectivity toward ketone	Xamena *et al.*[36]
3	[Co(PhIM)$_2$] (ZIF-9)	Tetralin	air	23	Tetralone	Induction period, high selectivity toward ketone	Xamena *et al.*[36]
4	Fe(BTC)	Xanthene	TBHP	90	Xanthone (99%)		Dhakshina-moorthy *et al.*[37]
5	$Cu_3(BTC)_2$	Xanthene	TBHP	82	Xanthone (85%)	O_2 and H_2O_2: inefficient to promote oxidation	Dhakshina-moorthy *et al.*[37]
6	$Al_2(BDC)_2$	Xanthene	TBHP	42	Xanthone (98%)	Influence of the metal ion on the activity: Fe>Cu>Al	Dhakshina-moorthy *et al.*[37]
7	Fe(BTC)	Benzylic compounds (tetralin, cyclooctane,…)	TBHP	28-96	Ketone (26-99%)		Dhakshina-moorthy *et al.*[37]
8	$[Cu^{II}(bped)_2(H_2O)_2(SiF_6)$	Tetralin	TBHP	88	Tetralone (77%)	Influence of the anion exchange: activity is regulated by the size of the surface openings of Cu-MOFs	Wang *et al.*[38]

9	$[Cu^{II}(bped)_2(H_2O)_2(NO_3)$	Tetralin	TBHP	92	Tetralone (71%)		Wang *et al.*[38]
10	$[Cu^{II}(bped)_2(H_2O)_2(SiF_6)$	Diphenylmethane	TBHP	28	Benzophe-none (>99)		Wang *et al.*[38]
11	$[Cu^{II}(bped)_2(H_2O)_2(NO_3)$	Diphenylmethane	TBHP	48	Benzo-phenone		Wang *et al.*[38]
12	$\{[Cu_2(4,4'\text{-bipy})_4(H_2O)_4](SiW_{12}O_{40})(H_2O)_{18}\}_n$	Ethylbenzene	TBHP	56.8	Acetophenone (88.1%)	Reaction occurs in the pores	Yu *et al.*[39]
13	$\{[Cu_2(4,4'\text{-bipy})_4(H_2O)_4](SiW_{12}O_{40})$ (4,4'-bipy)$_2(H_2O)_4\}_n$	Ethylbenzene	TBHP	37.9	Acetophenone (80.1%)	The activity is influenced by the valence of the metal ion in POM	Yu *et al.*[39]
14	$\{[Cu_2(4,4'\text{-bipy})_4(H_2O)_4](PW_{12}O_{40})$ $(H_2O)_{18}\}_n$	Ethylbenzene	TBHP	44.5	Acetophenone (82.2%)		Yu *et al.*[39]
15	$\{[Cu_2(4,4'\text{-bipy})_4(H_2O)_4]$-$(PMo_{12}O_{40})$ $(H_2O)_{18}\}_n$	Ethylbenzene	TBHP	45.1	Acetophenone (86.5%)		Yu *et al.*[39]
16	NHPI@Fe(BTC)	Cyclooctane	O_2	28	Cycloocta-none	No solvent, high selectivity toward alcohol and ketone	Dhakshina-moorthy *et al.*[40]
17	NHPI@Fe(BTC)	Benzylic compounds	O_2	17-33	Ketone	Undergoes desactivation (formation of FeO nanoparticles)	Dhakshina-moorthy *et al.*[40]

18	NHPI@Fe(BTC)	Linear alkanes	O_2	7-8	Ketone		Dhakshina-moorthy *et al.*[40]
19	Mn-porhyrin@rho-ZMOF	Cyclohexane	TBHP	91.5	Cyclohexa-none	Stable up to 11 cycles	Alkordi *et al.*[41]
20	$[Cu_3(\mu_3\text{-}OH)(\mu\text{-}pz)_3(EtCOO)_2(H_2O)]$	Cyclohexane/cyclopentane	H_2O_2	27.9/25.4	Alcohol	In absence of nitric acid: no activity	Di Nicola *et al.*[16]
21	$[Cu_3(\mu_3\text{-}OH)(\mu\text{-}pz)_3(EtCOO)_2(EtOH)]$	Cyclohexane/cyclopentane	H_2O_2	25.6/31.0	Alcohol		Di Nicola *et al.*[16]

2.7.2 Oxidation of alcohols

In Table 2.2 an overview is presented of the MOFs that have been examined for the oxidation of alcohols. As can be seen from this table, there is only one report of a Pd based MOF, denoted as $[Pd(2\text{-pymo})_2]_n$, studied for the aerobic oxidation of 3-phenyl-2-propen-1-ol (entry 1 Table 2.2)[42]. Total conversion of this reactant at atmospheric pressure was reached after 20 h and a selectivity of 74% toward the cinnamylaldehyde was obtained. This value was similar to the one found for other palladium-catalyzed oxidation reactions of allylic alcohols[42].

All the other reports (apart from one), describe the deposition of Au or Pt nanoparticles on a MOF. One report describes the gas-phase loading of MOF-177 with Pt nanoparticles, denoted as Pt@MOF-177, which was examined for the aerobic oxidation of allylic and aliphatic alcohols at room temperature in a base-free medium (entry 2 Table 2.2)[43]. For most reactants very high conversions and selectivities (TON>500) were observed. However, it was not possible to recycle the catalyst. Due to the presence of water (which is a by-product in the oxidation of alcohols), the host framework was destroyed[43].
Also Dhakshinamoorthy *et al.*[44] applied O_2 as an oxidant to examine the catalytic performance of $Cu_3(BTC)_2$ in combination with TEMPO as co-catalyst (entry 3 Table 2.2). The authors observed a somewhat low reactivity for some substituted benzylic alcohols and other alcohols, which they attributed to the inability of reactants to reach the active sites and to catalyst deactivation by poisoning and/or pore blocking.

As can be seen from Table 2.2, all Au@MOF materials were studied for the benchmark reaction: the oxidation of benzyl alcohol. Although it is not possible to make a fair comparison between the different Au@MOF catalyst, some features can be deduced. Firstly, some reports claim that the presence of a base is required. For example, Müller *et al.*[45] showed that if no base was added to the reaction mixture, the Au@MOF catalysts were inactive. Upon the addition of a base, the alcohol oxidation reaction is accelerated by deprotonation of the alcohol.[45] Nevertheless, in the report of Liu *et al.*[46] on Au@MIL-101 (entry 11 Table 2.2), the catalyst already showed a high catalytic performance without the presence of a base.

The authors explained that the high activity is due to the high dispersion of the Au nanoparticles in combination with a beneficial synergetic effect of the MIL-101 support. It is well known that the support may play a crucial role, either direct or indirect, in determining the activity of gold[47]. The role of the support is also illustrated in the work of Ishida *et al.*[48]: significant differences in alcohol conversions are observed for the Au@MOF-5, Au@Al-MIL-53 and $Au@Cu_3(BTC)_2$ (entry 4,5 and 6 Table 2.2).

Finally, in the work of Esken *et al.*[49] (entry 7 and 8 Table 2.2), it was shown that the Au nanoparticles may chemically interact with the functionalities on the organic linker. They observed a remarkable difference in catalytic activity between Au@ZIF-8, which exhibit a good conversion of 81% benzyl alcohol, whereas the Au@ZIF-90 shows a very weak activity (13%). The latter is due to in situ oxidation of the aldehyde functions of ZIF-90 by means of the Au nanoparticles imbedded in the MOF, making the active Au sites inaccessible for further reaction [49].

Table 2.2. Overview of the MOFs investigated for the oxidation of alcohols.

Entry	Catalytic MOF	Reactant	Oxidant	Conversion (%)	Main product (selectivity)	Take home message	Reference
1	$[Pd(2\text{-pymo})_2]_n$	3-phenyl-2-propen-1-ol	air	>99	3-phenylprop-2-enal (74%)	Selectivity similar to Pd based catalysts	Llabrés i Xamena *et al.*[42]
2	Pt@MOF-177	Allylic and aliphatic alcohols	air	>99	Ketone or aldehyde	RT, solvent- and base-free conditions, not recyclable	Proch *et al.*[43]
3	TEMPO/$Cu_3(BTC)_2$	Benzyl alcohol	O_2	90	Benzaldehyde (>98%)	Deactivation by poisoning and/or pore blocking	Dhakshina-moorthy *et al.*[44]
4	Au@MOF5	Benzyl alcohol and 1-phenylethanol	O_2	79-99	Methyl benzoate	In absence of a base: no activity	Ishida *et al.* [48] and Müller *et al.*[45]
5	Au@Al-MIL-53	Benzyl alcohol and 1-phenylethanol	O_2	56-98	Methyl benzoate	Influence of MOF support on the activity	Ishida *et al.*[48]
6	Au@$Cu_3(BTC)_2$	Benzyl alcohol	O_2	70	Benzaldehyde		Ishida *et al.*[48]
7	Au@ZIF-8	Benzyl alcohol	O_2	81	Methyl benzoate (98%)	Side reaction: oxidation of functional groups in framework by Au	Esken *et al.*[49]
8	Au@ZIF-90	Benzyl alcohol	O_2	13	Methyl benzoate (50%)		Esken *et al.*[49]
9	Au/ZnO@MOF-5	Benzyl alcohol	O_2	68	Methyl benzoate	In absence of a base: no activity	Müller *et al.*[45]
10	Au/TiO_2@MOF-5	Benzyl alcohol	O_2	74	Methyl benzoate	Au/oxide@MOF-5: higher activity and selectivity than Au@MOF-5	Müller *et al.*[45]
11	Au@MIL-101	Benzylic alcohols, allylic alcohols and aliphatic alcohols	O_2	23-99	Aldehyde or ketone (>99%)	High activity, selectivity, recyclability in absence of base or water	Liu *et al.*[46]

2.7.3 Oxidation of thiols and sulfides

In Table 2.3, a summary is presented of the MOFs studied for thiol and sulfide oxidation. It is immediately clear that the reports on MOFs for the oxidation of thiols are rather rare. To the best of our knowledge, only the report of Dhakshinamoorthy *et al.* [50] examined the commercially available Fe(BTC) for the oxidation of thiophenol (see Fig. 2.5).

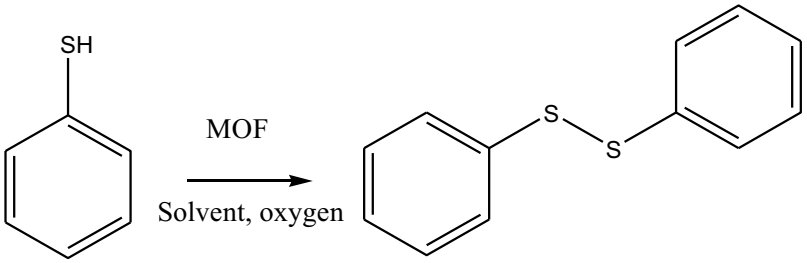

Fig. 2.5. Aerobic oxidation of thiophenol to diphenyldisulfide.

The solid catalyst showed moderate to high conversions at RT (44% of reactant conversion) and 70°C (87% of reactant conversion) in air using acetonitrile as solvent (entry 1 Table 2.3), whereas, $Cu_3(BTC)_2$ and $Al_2(BDC)_3$ exhibit a rather poor catalytic performance of 28% and 4% respectively. However, no clear explanation was given for this observation. The authors only mentioned the bad stability of the $Cu_3(BTC)_2$, which was evidenced by XRPD and EPR measurements[50].

Apart from the report on Cr-MIL-101 (entry 13, Table 2.3), the MOFs studied for the oxidation of sulfides are all rare-earth based MOFs, which can be divided into 2 main groups: the Yb and Sc based MOFs. For all these rare-earth MOFs, H_2O_2 was applied as the oxidant.
The Yb based MOF of Bernini *et al.*[51] (entry 4 Table 2.3) has been examined for the oxidation of methylsulfanylbenzene. After an induction period, a moderate conversion of 50% in the first run was observed. The authors state that the noted induction period is due to the Ln-O-OH species that are formed during the first run, which are the real active sites in the additional runs [51].

Furthermore, the same group reported much higher conversions for 2 other based Yb MOFs (entry 5 and 6 Table 2.3)[52]. Although the kinetic profile of both MOFs was different, complete conversion (>99%) was obtained, using methylphenylsulfide as the reactant. The difference in kinetic profile could be explained by the different charge density over the rare-earth cation, caused by the ligand nature. The authors claimed that a higher charge density on the Yb cation causes a slower formation of the active peroxo complex [52].

The same research group utilized this latter reactant also for the catalytic evaluation of their Sc based MOFs. Comparison of the Sc-terephthalate (entry 7 Table 2.3) with the Sc-succinate (entry 8, Table 2.3) shows that the reaction proceeds faster and more selectively for the terephthalate based framework under the same reaction conditions[53, 54].

To extend their study on Sc and Y based MOFs, the group of Monge presented in 2009 the synthesis of a novel Sc and Y-MOF, using 1,5- and 2,6-naphthalenedisulfonates as organic linkers [55]. Although the reaction takes place at the surface of the materials, even better results were obtained in comparison to their earlier reports (entries 7, 8 and 9 Table 2.3) with conversions up to 100 % in 60 minutes (entry 11 and 12, Table 2.3).

Table 2.3. Overview of the MOFs studied for the oxidation of thiols and/or sulphides.

Entry	Catalytic MOF	Reactant	Oxidant	Conversion (%)	Main product (selectivity)	Take home message	Reference
1	Fe(BTC)	Thiophenol	Air/O_2	44-87	Diphenyldisulfide	Fe(BTC) shows a better long term activity compared to iron nitrate	Dhakshinamoorthy *et al.*[50]
2	$Cu_3(BTC)_2$	Thiophenol	Air/O_2	28	Diphenyldisulfide	Activity: Fe>Cu>Al	Dhakshinamoorthy *et al.*[50]
3	$Al_2(BDC)_3$	Thiophenol	Air/O_2	4	Diphenyldisulfide		Dhakshinamoorthy *et al.*[50]
4	$[Yb(C_4H_4O_4)_{1.5}]$	Methylsulfanylbenzene	H_2O_2	50	Methyl phenyl sulfoxide (92%)	In first run: induction period due to formation of the active species	Bernini *et al.*[51]
5	$[Yb_4(OH)_{10}(H_20)_4]$[2,6-AQDS]	Methylphenylsulfide	H_2O_2	>99	Methyl phenyl sulfoxide (>99%)	Higher charge density yields in poorer activity	Gándara *et al.*[52]
6	[Yb(OH)(2,6-AQDS)(H_2O)]	Methylphenylsulfide	H_2O_2	>99	Methyl phenyl sulfoxide (>99%)		Gándara *et al.*[52]
7	$[Sc_2(C_8H_4O_3)_3]$	Methylphenylsulfide and (2-ethylbutyl) phenylsulfide	H_2O_2	~90	Sulfoxide (85%)	No loss in activity or selectivity for at least 4 runs	Perles *et al.*[52]
8	$[Sc_2(C_4H_4O_4)_{2.5}(OH)]$	Methylphenylsulfide and	H_2O_2	~85	Sulfoxide (90-99%)		Perles *et al.*[54]

		(2-ethylbutyl) phenylsulfide					
9	$[Y_2(C_4H_4O_4)_3(H_2O)_2].H_2O$	Methylphenylsulfide and (2-ethylbutyl) phenylsulfide	H_2O_2	>99 and 95	Sulfoxide (90-95%)	Every MOF: total conversion in 60 min. to the sulfoxide	Perles *et al.*[54]
10	$[La_2(C_4H_4O_4)_3(H_2O)_2].H_2O$	Methylphenylsulfide and (2-ethylbutyl) phenylsulfide	H_2O_2	>99 and 86	Sulfoxide (90-95%)	Better activity than the corresponding metal oxides	Perles *et al.*[54]
11	$[Sc_2(nds)(OH)_4]_n$	Methylphenylsulfide	H_2O_2	>99	Methyl phenyl sulfoxide (>99%)		Perles *et al.*[55]
12	$[Y(1,5\text{-nds})(OH)(H_2O)]_n$	Methylphenylsulfide	H_2O_2	>99	Methyl phenyl sulfoxide (>99%)		Perles *et al.*[55]
13	Cr-MIL-101	Benzenethiol, diphenylsulfide and isopropyl phenylsulfide	H_2O_2	88-99	Sulfoxide (>99%)	Reactants with electron-releasing groups enhance the activity	Hwang *et al.*[56]

2.7.4 Oxidation of cycloalkenes and linear alkenes

Catalytic studies on MOFs for the epoxidation of the C=C bond have received considerable attention as can be witnessed from Table 2.4. Commonly investigated reactants are cyclohexene, cyclooctene and styrene. The oxidation of cyclohexene will also be used in this thesis as the benchmark reaction to examine the catalytic performance of the synthesized V-MOFs. (see following chapters). During the oxidation of cyclohexene, many products can be formed, as can be seen from Scheme 2.9, using TBHP as oxidant.

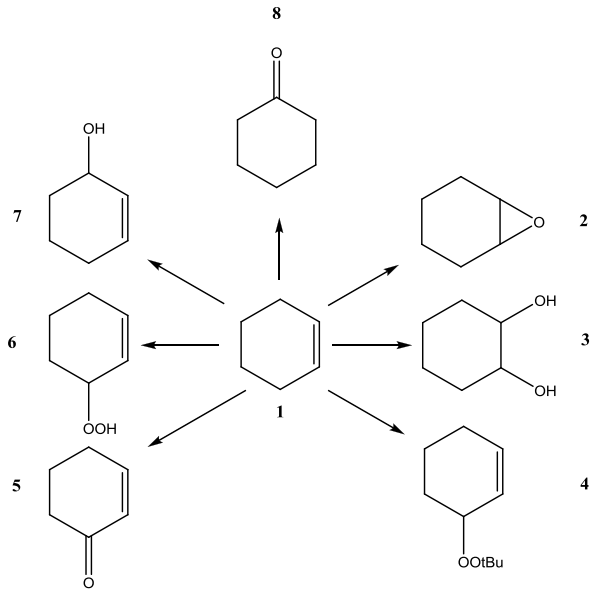

Scheme 2.9. Oxidation of cyclohexene **1** toward the products: cyclohexene oxide **2** cyclohexane-1,2-diol **3**, *tert*-butyl-2-cyclohexenyl-1-peroxide **4**, 2-cyclohexene-1-one **5**, cyclohexene hydroperoxide **6,** 2-cyclohexen-1-ol **7** and cyclohexanone **8**.

From Table 2.4, principally four classes of MOFs, studied in the oxidation of alkenes, can be distinguished. More specifically, Cu-, Co-, rare-earth and modified MOFs. Each of these classes will now be discussed in more detail.

Table 2.4. Overview of MOFs examined for the oxidation of cyclic and/or linear alkenes.

Entry	Catalytic MOF	Reactant	Oxidant	Conversion (%)	Main product (selectivity)	Take home message	Reference
1	$[Cu(bpy)(H_2O)_2(BF_4)_2(bpy)]$	Cyclohexene	O_2	8	Cyclohexene hydroperoxide (90%)	No solvent, high selectivity (90%) to cyclohexene hydroperoxide	Jiang *et al.*[57]
2	$\{[Cu(Pht)(Im)_2].1.5H_2O\}_n$	Cyclohexene	H_2O_2	75.2*	2-cyclohexen-1-one (75.2%)	Major product: 2-cyclohexen-1-one	Baca *et al.*[58]
3	$[Co(Pht)(Im)_2]_n$	Cyclohexene	H_2O_2	40.6*	2-cyclohexen-1-one (40.6%)	Yield of ketone: Cu-MOF>Co-MOF	Baca *et al.*[58]
4	$[Cu(H_2btec)(bipy)]_\infty$	Cyclohexene	TBHP	62	Cyclohexene oxide (68%)	Cyclohexene: higher conversion but lower selectivity toward epoxide	Aguirre *et al.* [59] and Brown *et al.*[60]
5	$[Cu(H_2btec)(bipy)]_\infty$	Styrene	TBHP	27	Styrene oxide (70.2%)	Styrene: lower conversion but higher selectivity toward epoxide	Aguirre *et al.* [59] and Brown *et al.*[60]
6	$[Co^{II}(bpb)].3DMF$	Cyclohexene	TBHP	62	Tert-butyl-2-cyclohexenyl-1-peroxide (83%)	83% selectivity toward tert-butyl-2-cyclohexenyl-1-peroxide	Lu *et al.*[61]
7	$[Co^{II}_4O(bdpb)_3]$ = MFU-1	Cyclohexene	TBHP	27.5	Tert-butyl-2-cyclohexenyl-1-peroxide (66%)	Reaction in the pores, high selectivity to allylic substitution (66%)	Tonigold *et al.*[62]
8	MFU-2	Cyclohexene	TBHP	16	Tert-butyl-2-cyclohexenyl-1-peroxide	MFU-2: catalysis due to metal leaching	Tonigold *et al.*[63]
9	NHPI@MFU-1	Cyclohexene	Air	35	Cyclohexene		Tonigold *et al.*[63]

					hydroperoxide		
10	Co-ZIF with imidazole as ligand	Cyclooctene	O_2+aldehyde	>99	Cyclooctene oxide (98.5%)	High selectivity to epoxide (99%): cooperative effect ligand and metal center	Zhang *et al.*[64]
11	Co-ZIF with imidazole as ligand	Cyclohexene	O_2+aldehyde	>99	Cyclohexene oxide (70.3%)		Zhang *et al.*[64]
12	Co-ZIF with imidazole as ligand	Styrene	O_2+aldehyde	>99	Styrene oxide (60.2%)		Zhang *et al.*[64]
13	Co-STA12	(E) stilbene	O_2	95	*Trans*-stilbene oxide (90%)	Induction period, catalysis mainly heterogeneous	Beier *et al.*[65]
14	$[Y_2(N_3)(nic)_2(OH)_3(Hnic)(H_2O)]_n$	Cyclooctene	TBHP	86	Cyclooctene oxide (>99%)		Sen *et al.*[66]
15	$[Gd_2(N_3)(nic)_2(OH)_3(Hnic)(H_2O)]_n$	Cyclooctene	TBHP	41	Cyclooctene oxide (>99%)		Sen *et al.*[66]
16	$[Sm_4(N_3)_2(nic)_4(OH)_6(Hnic)_2(H_2O)_2]_n$	Cyclooctene	TBHP	40	Cyclooctene oxide (>99%)		Sen *et al.*[66]
17	$[Y_2(N_3)(nic)_2(OH)_3(Hnic)(H_2O)]_n$	Styrene	TBHP	92	Styrene oxide	Influence of oxidant: no activity with H_2O_2 or NaOCl	Sen *et al.*[66]
18	$[Gd_2(N_3)(nic)_2(OH)_3(Hnic)(H_2O)]_n$	Styrene	TBHP	81	Styrene oxide	Activity: MOF> rare- earth oxides	Sen *et al.*[66]
19	$[Sm_4(N_3)_2(nic)_4(OH)_6(Hnic)_2(H_2O)_2]_n$	Styrene	TBHP	87	Styrene oxide	No induction period, surface catalysis	Sen *et al.*[66]
20	$[Y_2(N_3)(nic)_2(OH)_3(Hnic)(H$	Substituted styrene derivates and	TBHP	79-99	Epoxide		Sen *et al.*[66]

	$_2O)]_n$	linear alkenes					
21	$[Gd_2(N_3)(nic)_2(OH)_3(Hnic)(H_2O)]_n$	Substituted styrene derivates and linear alkenes	TBHP	65-95	Epoxide		Sen *et al.*[66]
22	$[Sm_4(N_3)_2(nic)_4(OH)_6(Hnic)_2(H_2O)_2]_n$	Substituted styrene derivates and linear alkenes	TBHP	81-99	Epoxide		Sen *et al.*[66]
23	$[Nd(HCOO)_3]_n$	Cyclopentene	TBHP	98	Cyclopentene oxide (>99%)		Sen *et al.*[67]
24	$[Pr(HCOO)_3]_n$	Cyclopentene	TBHP	>99	Cyclopentene oxide (>99%)		Sen *et al.*[67]
25	$[Nd(HCOO)_3]_n$	Cyclooctene	TBHP	78	Cyclooctene oxide (>99%)	Influence of oxidant: low activity with H_2O_2 or NaOCl	Sen *et al.*[67]
26	$[Pr(HCOO)_3]_n$	Cyclooctene	TBHP	86	Cyclooctene oxide (>99%)	Selectivity and conversion depends on steric hindrance of reactant	Sen *et al.*[67]
27	$[Nd(HCOO)_3]_n$	Styrene	TBHP	89	Styrene oxide	Activity: MOF> rare-earth oxides	Sen *et al.*[67]
28	$[Pr(HCOO)_3]_n$	Styrene	TBHP	91	Styrene oxide		Sen *et al.*[67]
29	$[Nd(HCOO)_3]_n$	Substituted styrene derivates and linear alkenes	TBHP	42-99	Epoxide		Sen *et al.*[67]
30	$[Pr(HCOO)_3]_n$	Substituted styrene derivates and	TBHP	38-98	Epoxide		Sen *et al.*[67]

		linear alkenes					
31	Co-POM@Cr-MIL-101	α-pinene	O_2	45	Verbenol (29%)	Conversion of α-pinene and cyclohexene to allylic product	Maksimchuk *et al.*[68]
32	Ti-POM@Cr-MIL-101	α-pinene	H_2O_2	40	Verbenol (32%)	Conversion of caryophyllene to epoxide	Maksimchuk *et al.*[68]
33	Ti-POM@Cr-MIL-101	Cyclohexene	H_2O_2	39	2-cyclohexene-1-one and 2-cyclohexen-1-ol	O_2: catalyst is stable, H_2O_2: MIL-101 matrix is destroyed	Maksimchuk *et al.*[68]
34	Ti-POM@Cr-MIL-101	Caryophyllene	H_2O_2	88	Caryophyllene 4,5-monoepoxide (>99%)		Maksimchuk *et al.*[68]
35	5% PW_4/Cr-MIL-101	Cyclohexene	H_2O_2	76	Cyclohexene oxide (74%)	Good selectivity toward epoxide (70-80%): depends on POM loading	Maksimchuk *et al.*[69]
36	5% PW_{12}/Cr-MIL-101	Cyclohexene	H_2O_2	72	Cyclohexene oxide (76%)	Stability of PW_{12} increased after immobilization	Maksimchuk *et al.*[69]
37	5% PW_{12}/Cr-MIL-101	Cyclic alkenes (cyclooctene, α-pinene, styrene..)	H_2O_2	30-76	Epoxide (71-99%)		Maksimchuk *et al.*[69]
38	NHPI@FeBTC	Styrene	O_2	10	Benzaldehyde (60%)	Conversion increased by electron donating substituents	Dhakshina-moorthy *et al.*[70]
39	NHPI@FeBTC	Substituted styrene derivates	O_2	12-60	Aldehyde (63-75%)		Dhakshina-moorthy *et al.*[70]

40	$NaHCO_3$/[$MoO_2Cl_2(H_2O)_2$].(H_2dipy-pra)Cl_2	Cyclooctene and other cyclic and linear alkenes	H_2O_2	86-99	Epoxide (>99%)	High selectivity toward the epoxide (>90%)	Luan *et al.*[71]
41	VO(acac)$_2$@IRMOF-3	Cyclohexene	TBHP	40	-	Low catalytic activity and stability	Ingleson *et al.*[72]
42	Mn(acac)$_2$@IRMOF-3	Cyclohexene	O_2+aldehyde	67.5	Cyclohexene oxide (92%)		Bhattacharjee *et al.*[73]
43	Mn(acac)$_2$@IRMOF-3	Cyclooctene	O_2+aldehyde	60.2	Cyclooctene oxide (95.8%)	High selectivities toward the epoxide (>80%) and good stability	Bhattacharjee *et al.*[73]
44	Mn(acac)$_2$@IRMOF-3	Styrene	O_2+aldehyde	52.3	Styrene oxide (80.7%)		Bhattacharjee *et al.*[73]
45	[Ni_2(dhtp)(H_2O)$_2$]. 8H_2O= Ni-CPO-27	Cyclohexene	H_2O_2	75.4	Cyclohexene oxide (39.7%)	Only heterogeneous catalysis at RT	Lee *et al.*[74]
46	[$MoO(O_2)_2$.4,4'-bipy]$_n$	Cyclohexene	H_2O_2	95	Cyclohexene oxide (>99%)	Retains activity and selectivity upon 5 additional cycles	Afsharpour *et al.*[75]
47	[$MoO(O_2)_2$.4,4'-bipy]$_n$	Cyclooctene	H_2O_2	40	Cyclooctene oxide (>99%)		Afsharpour *et al.*[75]

*selectivity toward the ketone product

2.7.4.1 Evaluation of the oxidation of alkenes with Cu based MOFs

To the best of our knowledge, only three studies have been carried out on Cu-MOFs for the oxidation of alkenes (entries 1-5 Table 2.4). In the first report pure O_2 was applied as an oxidant (entry 1, Table 2.4), in the second study H_2O_2 (entries 2-3 Table 2.4) and in the last study TBHP was employed as an oxidant (entries 4-5 Table 2.4). The aim of the first study was to demonstrate the feasibility of the allylic oxidation of cyclohexene [57]. In spite of the low cyclohexene conversion (8%), very good selectivities toward cyclohexene hydroperoxide were obtained (87%). This high selectivity to the allylic product is in good agreement with the above described study on the Cu- and Co containing MOFs for the oxidation of tetralin, in which the Cu-MOF was highly active in the activation of tetralin to tetralinhydroperoxide (entries 2-3 Table 2.1)[36].

Also the second study, employing H_2O_2 as an oxidant, mainly gave the allylic oxidation product 2-cyclohexene-1-one (entries 2-3 Table 2.4)[58]. Furthermore, this preliminary study showed that the yield of the ketone was higher for the Cu-based MOF in comparison to the Co-MOF.
While the previous studies showed good selectivity toward allylic oxidation products, the report of Aguirre *et al.*[59] obviously shows that also Cu-based MOFs can possess good selectivities toward the formation of the epoxide (entries 4-5 Table 2.4). Although a significant difference is observed in the conversion of both reactants (cyclohexene and styrene), a selectivity of approximately 70% toward the epoxide was detected in both cases. In an additional report, the authors proposed a mechanism for the formation of the epoxide (see Scheme 2.10) and they ascribed the difference in conversion for cyclohexene and styrene to the mechanism involved in the oxidation reaction [60].
When TBHP is applied as an oxidant, two mechanisms are reported for oxygen activation. Firstly a homolytic cleavage of the O-O bond can occur, generating the $C(CH_3)_3O\cdot$ radicals, which will result in a low chemoselectivity in the obtained products. In the second mechanism, a heterolytic cleavage of the O-O bond takes place, resulting in *tert*-butylperoxide radicals ($C(CH_3)_3OO\cdot$. The heterolytic mechanism proposed in Scheme 2.10, will give the epoxide as main product.

For the oxidation of cyclohexene, the allylic hydrogen is as reactive as the olefinic double bond, which will result in a higher conversion of cyclohexene in comparison to styrene [60].

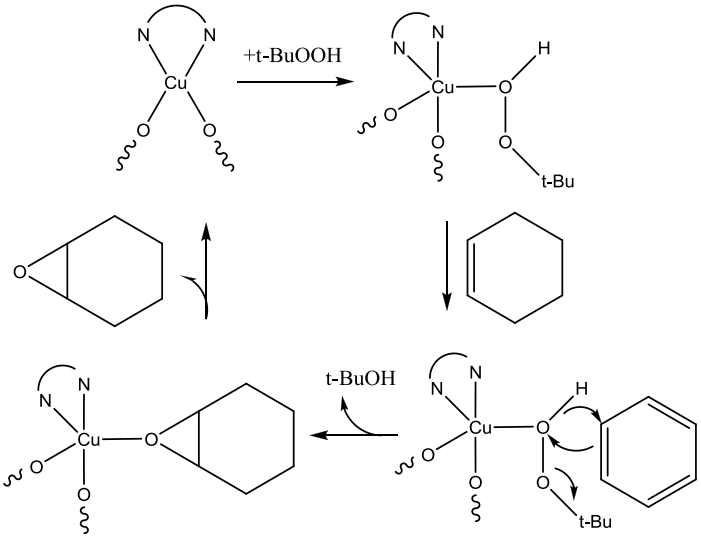

Scheme 2.10. Proposed general reaction mechanism for the formation of the epoxide by Brown *et al.*[60].

2.7.4.2 Evaluation of the oxidation of alkenes with Co-based MOFs

Several Co containing MOFs have been evaluated for the oxidation of alkenes (entries 6-13 Table 2.4). Since each research group applied different reaction conditions (oxidant, solvent, ...) it is unfeasible to draw general conclusions.
The first research group applied TBHP as an oxidant for the evaluation of their Co-MOFs (entries 6-7 Table 2.4)[61, 62]. In both studies very high selectivities were obtained toward the allylic substitution product, *tert*-butyl-2-cyclohexenyl-1-peroxide (83%), suggesting a reaction pathway in which freely diffusing peroxy radicals are generated by reductive cleavage of *tert*-butyl hydroperoxo ligands coordinating to Co(III) metal centers. By means of UV/Vis and XPS measurements, the authors established evidence for the presence of Co (III) metal centers.

In a later report of Tonigold *et al.* [63], more mechanistic insights were given and additional catalytic tests were executed. Whereas the MFU-1 demonstrated to be a stable catalyst, the catalytic activity of MFU-2 was due to the slow leaching of the Co centers using TBHP as an oxidant (entry 8 Table 2.4)[63].

The second research group applied O_2 combined with the sacrificial isobutyraldehyde to test their Co-ZIF for the oxidation of various alkenes (entries 10-12 Table 2.4)[64]. Whereas the previous research group of Volkmer attained the allylic substitution product, Zhang *et al.* observed the epoxide product with very high selectivities (98.5%). The authors ascribed these results to a cooperative effect of the N-containing basic ligand and the unsaturated metal center, since epoxides are relatively stable in a basic environment [64]. Similar to the previous research group, they suggested a radical mechanism (see Scheme 2.11). In first instance, an acylperoxy radical was generated *in situ* during the reaction of isobutyraldehyde (abbreviated as RCHO) with molecular oxygen initiated by Co-ZIF. In a second step, the acylperoxy radical reacts either with olefins to yield the epoxide directly, or with Co-ZIF to form Co-peroxy species, which will transform an oxygen atom directly to the olefins by the oxygen-oxygen bond cleavage of the peroxy group.

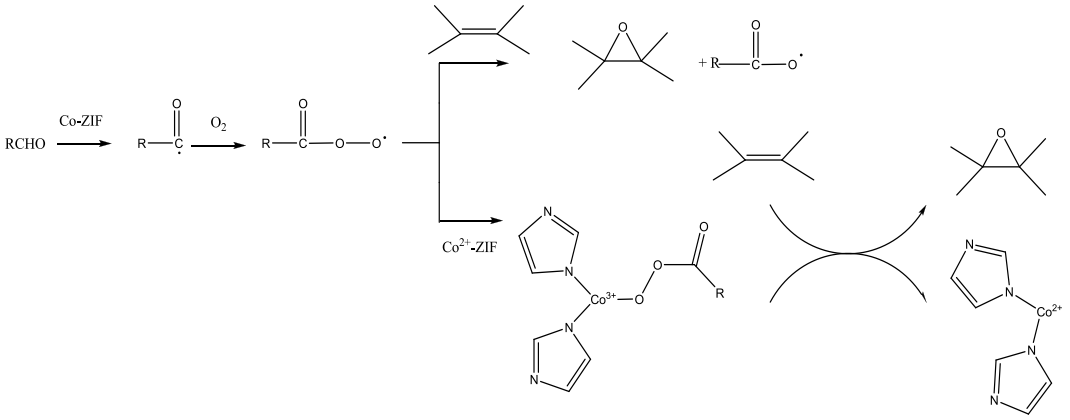

Scheme 2.11. Proposed pathway by Zhang *et al.*[64] for the selective epoxidation of olefins catalyzed by Co-ZIF.

In the third report of Beier *et al.*[65], pure O_2 was applied as an oxidant with DMF as a solvent (entry 13 Table 2.4). Former studies on Co-catalysts revealed that in the presence of DMF, a Co-DMF complex is formed that reacts with O_2 giving rise to Co-superoxo species [76-79]. As mentioned earlier, these species will afterwards transfer the oxygen to the olefin, resulting in the epoxide product. The catalytic evaluation of Co-STA-12 resulted in the formation of the epoxide with an excellent selectivity of 90%, which was in agreement with the proposed mechanism[65].

2.7.4.3 Evaluation of the oxidation of alkenes with rare-earth based MOFs

Although homogenous rare-earth salts have already shown to possess good catalytic performance for the oxidation of olefins, the reports using rare-earth MOFs in the epoxidation of alkenes are even rare as for the Cu-based MOFs [80, 81]. In recent years, Sen *et al.* reported two papers concerning the employment of rare-earth based carboxylate MOFs in the oxidation of alkenes (entries 14-30 Table 2.4) [66, 67]. Similarities between both studies were observed. Firstly, TBHP was seen as the most appropriate oxidant. Very little or no catalytic activity was observed when H_2O_2 or sodium hypochlorite was applied. Moreover, in both cases a higher conversion was noted for the MOF based catalysts than for the corresponding metal oxides.
In their first report, the catalysis took place at the surface of the materials due to the absence of porosity. Although the difference in reactant reactivity and in catalytic reactivity between the MOFs was not explained, it is very likely that the latter difference could be ascribed to the rare-earth center, since a similar trend (higher reactivity of Y in comparison to Gd and Sm) was observed for the corresponding metal oxides (entries 14-22 Table 2.4)[66].
In their second report (entries 23-30 Table 2.4), the authors attributed the divergence in reactant conversion to sterical hindrance. As the bulkiness of the cyclic alkene increases or the chain length of the linear alkene increases, the conversion and selectivity toward the epoxide decrease[67].

2.7.4.4 Evaluation of the oxidation of alkenes with modified MOFs

Furthermore, some modified MOFs were examined for the oxidation of alkenes. The modified MOFs can be divided into 2 groups.

The first group of MOFs encompass the POM based MOFs (entries 31-37 Table 2.4) and the second group of MOFs contain an immobilized homogeneous catalyst (entries 38-44 Table 2.4).
Firstly, Co and Ti –monosubstituted Keggin heteropolyanions were inserted into the nanocages of Cr- MIL-101 [68]. During the catalytic evaluation of the resulting materials, two types of oxidant were applied: O_2 for the Co-POM (entry 31 Table 2.4) and H_2O_2 for the Ti-POM (entries 32-34 Table 2.4). Both systems gave foremost the allylic product in the oxidation of α-pinene. In addition, in the oxidation of cyclohexene over Ti-POM@MIL-101, the allylic oxidation products cyclohexene-2-ol and cyclohexene-2-one were the main products as well. In turn, the oxidation of caryophyllene mostly gave the epoxide product. The authors state that this could be due to the deprotonation of the Ti-POM on immobilization within the MIL-101 cages which protect the acid-sensitive epoxide from the ring opening [68].
Later on, the same group reported the incapsulation of the polyoxotungstates $[PW_4O_{24}]^{3-}$ (PW_4) and $[PW_{12}O_{40}]^{3-}$ (PW_{12}) into MIL-101 which were examined for the oxidation of cyclohexene and other cyclic alkenes by means of H_2O_2 as an oxidant (entries 35-37 Table 2.4)[69]. For these POM@MOF materials, not the allylic but the epoxide product was observed as the main product in the oxidation of cyclohexene and other cyclic alkenes. Furthermore, the authors observed that the stability of the immobilized POM increased toward destruction in the presence of H_2O_2 [69].

For the second group of modified MOFs, Dhakshinamoorthy *et al.* reported the NHPI@FeBTC for the aerobic oxidation of styrene and styrene derivates (entries 38-39 Table 2.4)[70]. In earlier times this MOF was already investigated for the aerobic oxidation of cyclooctane and other benzylic compounds (see entries 16-18 Table 2.1)[40]. A similar mechanism was proposed (Scheme 2.8) with the generation of phtalimide N-oxyl radicals acting as precursors of C-centered radicals that would undergo auto-oxidation. Ingleson *et al.* [72] reported the two steps modification of IRMOF-3 to an imine grafted $VO(acac)_2$ complex (entry 41 Table 2.4). The authors carried out a preliminary catalytic investigation on this modified MOF structure for the oxidation of cyclohexene with TBHP as the oxidant. However, the $VO(acac)_2$@IRMOF-3 showed a rather low catalytic activity and stability[72].

The group of Battacharjee *et al.*[73] reported a more straightforward one step functionalization of the IRMOF-3 with $Mn(acac)_2$ (entries 42-44 Table 2.4). Instead of using TBHP as an oxidant they utilized O_2 in combination with trimethylacetaldehyde as a co-oxidant. Good conversions (even for the more bulky cyclooctene) were obtained with very high selectivities toward the epoxide (>80%) [73].

2.8 Conclusions

In this chapter it was shown that there is an expanding growth of reports on MOFs in oxidation catalysis. MOFs were examined as such or served as matrix for the incapsulation or post-modification with a homogeneous catalyst. However, from the reports described above, it can be seen that there is a lack of integrated strategy combining the design concepts with the target applications and specification. To be able to compete with the industrial catalysts, general statements like observing the same catalytic activity in a few additional cycles is not sufficient. The long term stability of the MOF in the catalytic conditions should be verified and continuous flow experiments should be carried out instead of batch reactions to see if MOFs can compete with the industrial catalysts. At this moment, very few papers address the comparison of the MOF material with catalysts used in industry (e.g. zeolites, zeotypes, silica based materials). Most of the reports compare the catalytic activity of the MOF with the homogeneous counterpart or metal oxides.
Furthermore, more in depth studies are definitely required on the nature of the active site. In other words, a combined experimental and theoretical study to elucidate the catalytic mechanism is of a paramount importance. Concerning the oxidizing reagents and within the concept of green chemistry, more efforts should be carried out to perform the oxidation reactions with H_2O_2. However, this requires the use of MOFs that are stable in water, which is rather rare. Moreover, the use of molecular oxygen as oxidant for the catalysis with MOFs should be further addressed in the near future.
Finally, the big advantage of MOFs compared to zeolites should be more and more exploited by employing reactants in which chemo, regio and stereo selectivity aspects can be achieved. Their use as chiral solid catalysts is still in an early stage but will probably be developed in the near future.

2.9 References

1. E. K. Rideal and H. S. Taylor, *Catalysis in Theory and Practice*, G. MacMillan, 1919.
2. M. Boudart, Blackwell, *Perspectives in Catalysis*, Oxford, 1992.
3. I. Chorkendorff and J. W. Niemantsverdriet, *Concepts of modern catalysis and kinetics*, Wiley, 2003.
4. G. B. Marin and G. S. Yablonsky, *Kinetics of Chemical Reactions: Decoding Complexity*, Wiley, 2011.
5. P. Barbaro and F. Liguori, *Heterogenized homogeneous catalysts for fine chemicals production*, Springer, 2010.
6. U. S. Ozkan, *Design of heterogeneous catalysts*, Wiley, 2009.
7. O. R. Evans, H. L. Ngo and W. B. Lin, *J Am Chem Soc*, 2001, **123**, 10395-10396.
8. S. Hasegawa, S. Horike, R. Matsuda, S. Furukawa, K. Mochizuki, Y. Kinoshita and S. Kitagawa, *J Am Chem Soc*, 2007, **129**, 2607-2614.
9. C. D. Wu, A. Hu, L. Zhang and W. B. Lin, *J Am Chem Soc*, 2005, **127**, 8940-8941.
10. Y. K. Hwang, D. Y. Hong, J. S. Chang, S. H. Jhung, Y. K. Seo, J. Kim, A. Vimont, M. Daturi, C. Serre and G. Ferey, *Angew Chem Int Edit*, 2008, **47**, 4144-4148.
11. F. Schroeder, D. Esken, M. Cokoja, M. W. E. van den Berg, O. I. Lebedev, G. van Tendeloo, B. Walaszek, G. Buntkowsky, H. H. Limbach, B. Chaudret and R. A. Fischer, *J Am Chem Soc*, 2008, **130**, 6119-6130.
12. L. Q. Ma and W. B. Lin, *Functional Metal-Organic Frameworks: Gas Storage, Separation and Catalysis*, 2010, **293**, 175-205.
13. M. Fujita, Y. J. Kwon, S. Washizu and K. Ogura, *J Am Chem Soc*, 1994, **116**, 1151-1152.
14. L. Alaerts, E. Seguin, H. Poelman, F. Thibault-Starzyk, P. A. Jacobs and D. E. De Vos, *Chem-Eur J*, 2006, **12**, 7353-7363.
15. K. Schlichte, T. Kratzke and S. Kaskel, *Micropor Mesopor Mat*, 2004, **73**, 81-88.
16. C. Di Nicola, Y. Y. Karabach, A. M. Kirillov, M. Monari, L. Pandolfo, C. Pettinari and A. J. L. Pombeiro, *Inorg Chem*, 2007, **46**, 221-230.
17. P. Horcajada, S. Surble, C. Serre, D. Y. Hong, Y. K. Seo, J. S. Chang, J. M. Greneche, I. Margiolaki and G. Ferey, *Chem Commun*, 2007, 2820-2822.
18. A. Vimont, J. M. Goupil, J. C. Lavalley, M. Daturi, S. Surble, C. Serre, F. Millange, G. Ferey and N. Audebrand, *J Am Chem Soc*, 2006, **128**, 3218-3227.

19. A. Vimont, H. Leclerc, F. Mauge, M. Daturi, J. C. Lavalley, S. Surble, C. Serre and G. Ferey, *J Phys Chem C*, 2007, **111**, 383-388.
20. N. L. Rosi, M. Eddaoudi, J. Kim, M. O'Keeffe and O. M. Yaghi, *Angew Chem Int Edit*, 2001, **41**, 284-+.
21. M. Savonnet, S. Aguado, U. Ravon, D. Bazer-Bachi, V. Lecocq, N. Bats, C. Pinel and D. Farrusseng, *Green Chem*, 2009, **11**, 1729-1732.
22. J. Gascon, U. Aktay, M. D. Hernandez-Alonso, G. P. M. van Klink and F. Kapteijn, *J Catal*, 2009, **261**, 75-87.
23. F. Gandara, A. Garcia-Cortes, C. Cascales, B. Gomez-Lor, E. Gutierrez-Puebla, M. Iglesias, A. Monge and N. Snejko, *Inorg Chem*, 2007, **46**, 3475-3484.
24. N. Snejko, C. Cascales, B. Gomez-Lor, E. Gutierrez-Puebla, M. Iglesias, C. Ruiz-Valero and M. A. Monge, *Chem Commun*, 2002, 1366-1367.
25. S. H. Cho, B. Q. Ma, S. T. Nguyen, J. T. Hupp and T. E. Albrecht-Schmitt, *Chem Commun*, 2006, 2563-2565.
26. F. J. Song, C. Wang and W. B. Lin, *Chem Commun*, 2011, **47**, 8256-8258.
27. F. J. Song, C. Wang, J. M. Falkowski, L. Q. Ma and W. B. Lin, *J Am Chem Soc*, 2010, **132**, 15390-15398.
28. Y. B. Huang, T. F. Liu, J. X. Lin, J. A. Lu, Z. J. Lin and R. Cao, *Inorg Chem*, 2011, **50**, 2191-2198.
29. W. B. Lin, *Top Catal*, 2010, **53**, 869-875.
30. S. T. Oyama, *Mechanisms in homogeneous and heterogeneous epoxidation catalysis*, Elsevier, 2008.
31. A. Fujishima, X. Zhang and D. A. Tryk, *Surface Science Reports*, 2008, **63**, 515-582.
32. D. Robert and S. Malato, *The Science of the Total Environment*, 2002, **291**, 85-97.
33. K. R. Lassila, F. J. Waller, S. E. Werkheiser and A. L. Wressell, *Tetrahedron Lett*, 1994, 8077-8080.
34. B. B. Wentzel, P. L. Alsters, M. C. Feiters and R. J. M. Nolte, *J Org Chem*, 2004, **69**, 3453-3464.
35. J. Kim, S. Bhattacharjee, K. E. Jeong, S. Y. Jeong and W. S. Ahn, *Chem Commun*, 2009, 3904-3906.
36. F. X. L. I. Xamena, O. Casanova, R. G. Tailleur, H. Garcia and A. Corma, *J Catal*, 2008, **255**, 220-227.
37. A. Dhakshinamoorthy, M. Alvaro and H. Garcia, *J Catal*, 2009, **267**, 1-4.
38. S. J. Wang, L. Li, J. Y. Zhang, X. C. Yuan and C. Y. Su, *J Mater Chem*, 2011, **21**, 7098-7104.

39. F. Yu, P. Q. Zheng, Y. X. Long, Y. P. Ren, X. J. Kong, L. S. Long, Y. Z. Yuan, R. B. Huang and L. S. Zheng, *Eur J Inorg Chem*, 2010, 4526-4531.
40. A. Dhakshinamoorthy, M. Alvaro and H. Garcia, *Chem-Eur J*, 2011, **17**, 6256-6262.
41. M. H. Alkordi, Y. L. Liu, R. W. Larsen, J. F. Eubank and M. Eddaoudi, *J Am Chem Soc*, 2008, **130**, 12639-12641.
42. F. X. L. I. Xamena, A. Abad, A. Corma and H. Garcia, *J Catal*, 2007, **250**, 294-298.
43. S. Proch, J. Herrmannsdorfer, R. Kempe, C. Kern, A. Jess, L. Seyfarth and J. Senker, *Chem-Eur J*, 2008, **14**, 8204-8212.
44. A. Dhakshinamoorthy, M. Alvaro and H. Garcia, *Acs Catal*, 2011, **1**, 48-53.
45. M. Muller, S. Turner, O. I. Lebedev, Y. M. Wang, G. van Tendeloo and R. A. Fischer, *Eur J Inorg Chem*, 2011, 1876-1887.
46. H. L. Liu, Y. L. Liu, Y. W. Li, Z. Y. Tang and H. F. Jiang, *J Phys Chem C*, 2010, **114**, 13362-13369.
47. A. Corma and H. Garcia, *Chem Soc Rev*, 2008, **37**, 2096-2126.
48. T. Ishida, M. Nagaoka, T. Akita and M. Haruta, *Chem-Eur J*, 2008, **14**, 8456-8460.
49. D. Esken, S. Turner, O. I. Lebedev, G. Van Tendeloo and R. A. Fischer, *Chem Mater*, 2010, **22**, 6393-6401.
50. A. Dhakshinamoorthy, M. Alvaro and H. Garcia, *Chem Commun*, 2010, **46**, 6476-6478.
51. M. C. Bernini, F. Gandara, M. Iglesias, N. Snejko, E. Gutierrez-Puebla, E. V. Brusau, G. E. Narda and M. A. Monge, *Chem-Eur J*, 2009, **15**, 4896-4905.
52. F. Gandara, E. G. Puebla, M. Iglesias, D. M. Proserpio, N. Snejko and M. A. Monge, *Chem Mater*, 2009, **21**, 655-661.
53. J. Perles, M. Iglesias, M. A. Martin-Luengo, M. A. Monge, C. Ruiz-Valero and N. Snejko, *Chem Mater*, 2005, **17**, 5837-5842.
54. J. Perles, M. Iglesias, C. Ruiz-Valero and N. Snejko, *J Mater Chem*, 2004, **14**, 2683-2689.
55. J. Perles, N. Snejko, M. Iglesias and M. A. Monge, *J Mater Chem*, 2009, **19**, 6504-6511.
56. Y. K. Hwang, D. Y. Hong, J. S. Chang, H. Seo, M. Yoon, J. Kim, S. H. Jhung, C. Serre and G. Ferey, *Appl Catal a-Gen*, 2009, **358**, 249-253.
57. D. M. Jiang, T. Mallat, D. M. Meier, A. Urakawa and A. Baiker, *J Catal*, 2010, **270**, 26-33.
58. S. G. Baca, M. T. Reetz, R. Goddard, I. G. Filippova, Y. A. Simonov, M. Gdaniec and N. Gerbeleu, *Polyhedron*, 2006, **25**, 1215-1222.

59. P. Aguirre, K. Brown, D. Venegas-Yazigi, V. Paredes-Garcia and E. Spodine, *Macromolecular Complexes*, 2011, **304**, 65-71.
60. K. Brown, S. Zolezzi, P. Aguirre, D. Venegas-Yazigi, V. Paredes-Garcia, R. Baggio, M. A. Novak and E. Spodine, *Dalton T*, 2009, 1422-1427.
61. Y. Lu, M. Tonigold, B. Bredenkotter, D. Volkmer, J. Hitzbleck and G. Langstein, *Z Anorg Allg Chem*, 2008, **634**, 2411-2417.
62. M. Tonigold, Y. Lu, B. Bredenkotter, B. Rieger, S. Bahnmuller, J. Hitzbleck, G. Langstein and D. Volkmer, *Angew Chem Int Edit*, 2009, **48**, 7546-7550.
63. M. Tonigold, Y. Lu, A. Mavrandonakis, A. Puls, R. Staudt, J. Mollmer, J. Sauer and D. Volkmer, *Chem-Eur J*, 2011, **17**, 8671-8695.
64. A. P. Zhang, L. Q. Li, J. Li, Y. Zhang and S. Gao, *Catal Commun*, 2011, **12**, 1183-1187.
65. M. J. Beier, W. Kleist, M. T. Wharmby, R. Kissner, B. Kimmerle, P. A. Wright, J. D. Grunwaldt and A. Baiker, *Chem-Eur J*, 2012, **18**, 887-898.
66. R. Sen, S. Koner, D. K. Hazra, M. Helliwell and M. Mukherjee, *Eur J Inorg Chem*, 2011, 241-248.
67. R. Sen, D. Saha and S. Koner, *Catal Lett*, 2012, **142**, 124-130.
68. N. V. Maksimchuk, M. N. Timofeeva, M. S. Melgunov, A. N. Shmakov, Y. A. Chesalov, D. N. Dybtsev, V. P. Fedin and O. A. Kholdeeva, *J Catal*, 2008, **257**, 315-323.
69. N. V. Maksimchuk, K. A. Kovalenko, S. S. Arzumanov, Y. A. Chesalov, M. S. Melgunov, A. G. Stepanov, V. P. Fedin and O. A. Kholdeeva, *Inorg Chem*, 2010, **49**, 2920-2930.
70. A. Dhakshinamoorthy, M. Alvaro and H. Garcia, *Acs Catal*, 2011, **1**, 836-840.
71. Y. Luan, G. Wang, R. L. Luck and M. Yang, *Eur J Inorg Chem*, 2007, 1215-1218.
72. M. J. Ingleson, J. P. Barrio, J. B. Guilbaud, Y. Z. Khimyak and M. J. Rosseinsky, *Chem Commun*, 2008, 2680-2682.
73. S. Bhattacharjee, D. A. Yang and W. S. Ahn, *Chem Commun*, 2011, **47**, 3637-3639.
74. J. S. Lee, S. B. Halligudi, N. H. Jang, D. W. Hwang, J. S. Chang and Y. K. Hwang, *B Korean Chem Soc*, 2010, **31**, 1489-1495.
75. M. Afsharpour, A. R. Mahjoub and M. M. Amini, *Appl Catal a-Gen*, 2007, **327**, 205-210.
76. Q. H. Tang, Y. Wang, J. Liang, P. Wang, Q. H. Zhang and H. L. Wan, *Chem Commun*, 2004, 440-441.
77. M. Salavati-Niasari, S. Abdolmohammadi and M. Oftadeh, *J Coord Chem*, 2008, **61**, 2837-2851.

78. M. V. Patil, M. K. Yadav and R. V. Jasra, *J Mol Catal a-Chem*, 2007, **277**, 72-80.
79. K. M. Jinka, J. Sebastian and R. V. Jasra, *J Mol Catal a-Chem*, 2007, **274**, 33-41.
80. D. Diez, M. G. Nunez, A. B. Anton, P. Garcia, R. F. Moro, N. M. Garrido, I. S. Marcos, P. Basabe and J. G. Urones, *Curr Org Synth*, 2008, **5**, 186-216.
81. M. Bougauchi, S. Watanabe, T. Arai, H. Sasai and M. Shibasaki, *J Am Chem Soc*, 1997, **119**, 2329-2330.

Chapter 3: The coordinatively saturated vanadium MIL-47 as a low leaching heterogeneous catalyst in the oxidation of cyclohexene

---

Abstract

In this chapter the catalytic performance of a coordinatively saturated V-MOF, MIL-47, is examined for the liquid phase oxidation of cyclohexene. Different oxidants and amounts of catalyst are applied and compared. If the oxidant TBHP is dissolved in water, a significant leaching of V-species into the solution is observed, and also radical pathways are prominently operative leading to the formation of an adduct between the peroxide and cyclohexene. If, however, the oxidant is dissolved in decane, leaching is negligible and the structural integrity of the V-MIL-47 is maintained during successive runs. The selectivity toward the epoxide is very high in these circumstances. Additionally, the catalytic activity of the V-MOF is compared with the homogeneous $VO(acac)_2$ catalyst, the zeotype VAPO-5 and the supported VO_x/SiO_2. Extensive computational modeling is performed on the MIL-47 to show that several reaction cycles are possible. EPR measurements confirm that at least two parallel catalytic cycles are co-existing: one with V^{+IV} sites and one with pre-oxidized V^{+V} sites, and this is in complete agreement with the theoretical predictions.

The results presented in this chapter are the outcome of a collaborative research effort involving several research groups :

- The synthesis and characterization of the catalysts and the catalytic testing were performed at COMOC (Ghent University) by Karen Leus.
- The modeling was done at the Center for Molecular Modeling (Ghent University) by Matthias Vandichel.

- The EPR analysis has been carried out by Prof Henk Vrielinck and Prof Freddy Callens from the Electron Magnetic Resonance (EMR) research group (Ghent University).

- Steven Pyl, a member from the Laboratory for Chemical Technology (Ghent University) analyzed the product mixture after catalysis with GCxGC TOF MS.

- Dr. Paul Wiper and Prof Yaroslav Khimyak from the University of Liverpool performed the solid state NMR measurements.

The results displayed in this chapter are described in 3 publications, indexed in the Web of Science:

K. Leus, I. Muylaert, M. Vandichel, G. B. Marin, M. Waroquier, V. Van Speybroeck, P. Van Der Voort, *The remarkable catalytic activity of the saturated metal organic framework V-MIL-47 in the cyclohexene oxidation*, Chemical Communications, **2010**, 46, 5085–5087.

K. Leus*, M. Vandichel*, Y.Y. Liu, I. Muylaert, J. Musschoot, S. Pyl, H. Vrielinck, F. Callens, G. B. Marin, C. Detavernier, P. V. Wiper, Y. Z. Khimyak, M. Waroquier, V. Van Speybroeck, P. Van Der Voort, *The coordinatively saturated vanadium MIL-47 as a low leaching heterogeneous catalyst in the oxidation of cyclohexene*, Journal of Catalysis, **2012**, 285, 196–207.
*=both authors contributed equally to this work

K. Leus, I. Muylaert, V. Van Speybroeck, G.B. Marin, P. Van Der Voort, *A coordinative saturated vanadium containing metal organic framework that shows a remarkable catalytic activity*, Studies in Surface Science and Catalysis, **2010**, 175, 329-332 (WOS proceeding paper).

3.1 Introduction

In this chapter, the potential of the V-MOF MIL-47 is examined in the oxidation of cyclohexene. In chapter 2 it was shown that during the oxidation of cyclohexene many products can be formed (see Scheme 2.9, chapter2, the same numbers of the products will be used in this chapter). One of these products is cyclohexene oxide, which is an important intermediate in the synthesis of several products such as enantioselective drugs, epoxy paints, rubber promoters and dyestuff. In chapter 2 the potential of MOFs in the oxidation of cyclohexene was already illustrated. Nevertheless, regarding the potential of vanadium in oxidation catalysis, a V-MOF was never investigated in the oxidation of cyclohexene, which will be the scope of this chapter.

In this chapter the potential of the reported V-MOF, MIL-47 $V^{IV}O(CO_2–C_6H_4–CO_2)$ is examined [1]. As can be seen from Fig. 3.1 MIL-47 has a three-dimensional framework, in which each V^{+IV} center is coordinated to four oxygen atoms from four carboxylate groups, and to two oxygen atoms on the O–V–O axis, thus forming a saturated octahedral coordination node. The nodes are further connected by sharing the carboxylate linkers and thus grow into a three-dimensional framework. 1D rhombus channels are along the a axis with sizes of about 10.5 x 11.0 Å (Van der Waals radii excluded) for the channel windows. The structure shows good thermal stability (stable up to 350 °C in air). In this chapter, the synthesis of MIL-47 will be described together with the reference catalysts VAPO-5 and VO_x/SiO_2. Their catalytic activity will be evaluated and compared using TBHP in water as oxidant. Additionally a more profound study on the catalytic performance of MIL-47 will be presented using respectively TBHP in water and TBHP in decane as oxidant. The latter has been chosen, as epoxidation reactions are known to be sensitive to water traces [2]. Computational modeling on the V-MOF is performed to elucidate the catalytic pathways, which were confirmed by EPR spectroscopy.

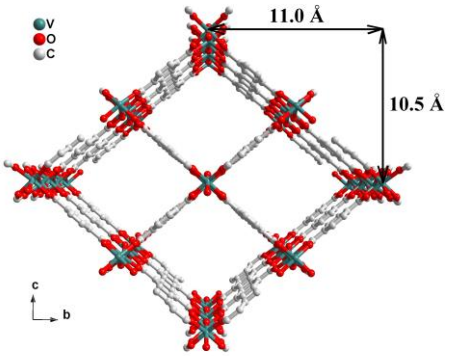

Fig. 3.1. Perspective view of the MIL-47.

3.2 Results and discussion

3.2.1 The catalytic performance of MIL-47 in the oxidation of cyclohexene using different catalyst loadings

In Fig. 3.2, the catalytic performance of MIL-47 is shown using respectively TBHP/water (left) and TBHP/decane (right) as oxidant. In this figure, two catalyst loadings (0.11 mmol and 0.42 mmol of V-centers) are considered. The reader should pay attention to the differences in the timescale of the x-axes, as all experiments were performed until a linear plateau in the conversion was reached or until a maximum time of 82 h. Moreover, the same numbers as in chapter 2 (Scheme 2.9) are used for the products.
Several general trends can be deduced from Fig. 3.2 (1) Convergence regimes for cyclohexene conversion are reached in all cases, provided sufficient large reaction time is taken into account. (2) The conversion tends toward 80% at the end of the reaction. The lower conversion in Fig. 3.2c is probably due to a too short reaction time. (3) In the initial stages, the cyclohexene conversion is almost linear in all cases. There are, however, differences in the slope of these linear sections: the 0.42 mmol V catalytic systems start clearly the fastest (approximately 20% conversion per hour for TBHP in water and 7% conversion per hour of TBHP in decane) whereas the 0.11 mmol V systems start much slower (4% conversion per hour for the TBHP in water and even slower for the TBHP in decane).

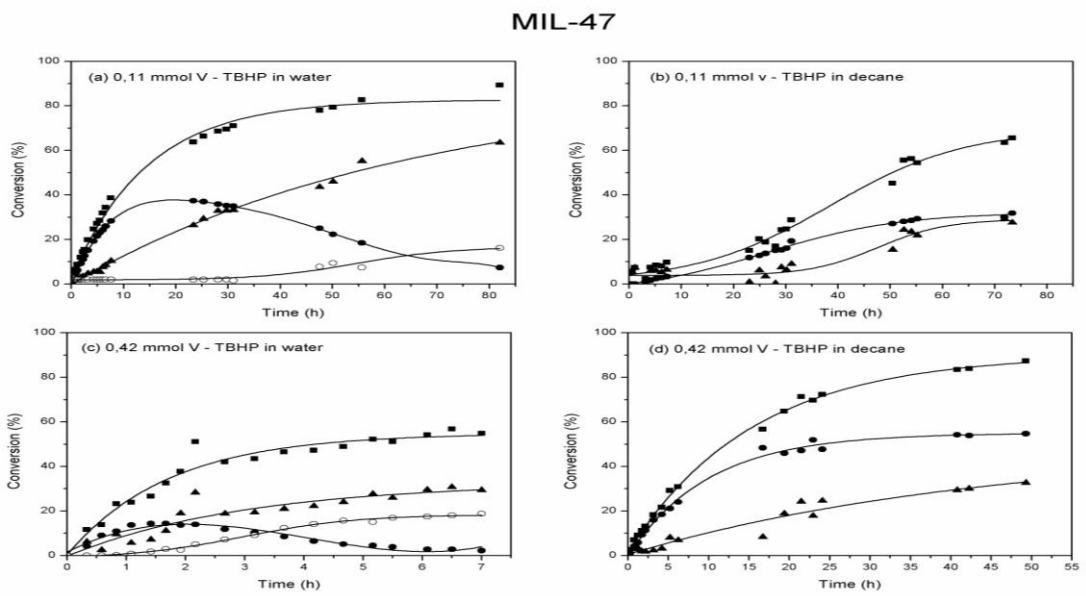

Fig. 3.2. Cyclohexene (**1**) conversion (■) and the yield of cyclohexene oxide (**2**) (●), *tert*-butyl-2-cyclohexenyl-1-peroxide (**4**) (▲) and cyclohexane-1,2-diol (**3**) (○) for MIL-47 in TBHP/water (Left) with 0.11 mmol V-sites (a) and 0.42 mmol V-sites (c); and for MIL-47 in TBHP/decane (Right) with 0.11 mmol V-sites (b) and 0.42 mmol V-sites (d). No cyclohexane-1,2-diol (○) is formed when TBHP in decane is used. The production of 2-cyclohexene-1-one is in all cases less than 5%, for the clarity of the figure this is not shown.

(4) In the systems that use TBHP in water, the cyclohexene oxide attains a maximum, after which the concentration gradually returns to zero. This is partly due to the transformation of the epoxide **2** into the diol **3** resulting from the reaction with water and terephthalic acid. (5) The byproduct **4**, formed via radicalar pathways, grows systematically and exceeds the concentration of the epoxide after sufficiently long reaction times. The crossing of those two yields occurs at relatively short reaction times for the TBHP in water systems and is heavily delayed by using the TBHP in decane. This is due to the particular role of water in the reaction medium in stabilizing the radical intermediates (see computational discussion, Section 3.2.5). (6) The formation of the ketone **5** is marginal in all cases.

(7) During the first 7 h of reaction, the selectivity toward the cyclohexene oxide is almost 100% in the 0.11 mmol V-sites with TBHP in water system. After that, the product distribution changes. The cyclohexene oxide reaches a maximum of 38% after 25 h of reaction. After that, the cyclohexane-1,2-diol **3** starts to be produced, and the tert-butyl-2-cyclohexenyl-1-peroxide **4** becomes dominant (see Table 3.1). The faster kinetics observed in Fig. 3.2c compared to Fig. 3.2a are mainly due to the higher V-loading. But in both cases, also a significant amount of leached V is observed. After 1 h of catalysis, with TBHP in water as oxidant, 12.8% of the V is leached out of the structure using 0.11 mmol of V-sites. This high leaching percentage was confirmed by a hot filtration experiment. The catalyst was separated from the reaction mixture after 1 h using a combined nylon-membrane filter. Fig. 3.3 presents the conversion curve of cyclohexene in the presence of MIL-47 and the cyclohexene conversion after filtration. Also the sum of products **2**, **3** and **5** is shown with and without the hot filtration. It is clear from this figure that both the conversion of cyclohexene and the formation of oxidized products are strongly reduced after filtration of the catalyst. This indicates that the catalytic reaction is predominantly heterogeneous. There is however some homogeneous catalytic activity left. This activity is due to a combination of radical mechanisms (formation of product **4** occurs via radical pathways (vide infra)) and leached V.

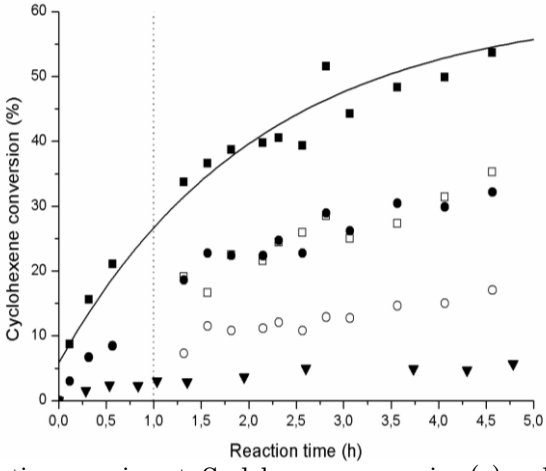

Fig. 3.3. Hot filtration experiment. Cyclohexene conversion (■) and yield of oxidized products (●) as a function of time. Cyclohexene conversion (□) and yield of oxidized products (○) after filtration of the catalyst. The catalytic activity of $VO(acac)_2$ corresponding to the 12.8% leached V-sites (▼).

In order to reduce this leaching, the catalytic performance of MIL-47 in the oxidation of cyclohexene was analyzed with TBHP/ decane as oxidant (see Fig. 3.2b and d). When the catalytic performance of MIL-47 in the water-based media is compared to the water-free media, it is clear that the cyclohexene conversion is approximately 30% after 7 h of reaction with TBHP/decane as oxidant, while the total cyclohexene conversion in the water dissolved TBHP system is much higher in the initial stage (55% after 7 h of reaction). Furthermore, it is interesting to note that, as the conversion is lower, the selectivity toward the cyclohexene oxide is remarkably higher.

In Table 3.1, the selectivity toward the cyclohexene oxide with TBHP/water and TBHP/decane as oxidant is shown for each V-loading, together with the TON and TOF of MIL-47 and $VO(acac)_2$. This Table 3.1 shows that the selectivity in TBHP/decane is significantly higher compared to the water-based equivalent. The presence of water during the catalytic test clearly affects both the rate of the epoxidation reaction and the stabilization of radical species toward the formation of the adduct **4**. More details about the reaction mechanisms for both systems are given in the computational section 3.2.5 (vide infra). The former effect might be partly due to vanadium leaching. Only a negligible amount (<3%) of vanadium was leached out of the structure when TBHP/decane was used as oxidant after 7 h of reaction, whereas with TBHP/ water, after the same time, a V-leaching of almost 50% was observed.

Table 3.1. Selectivity toward the cyclohexene oxide with TBHP/water and TBHP/decane as oxidant for each V- loading and the TON and TOF of MIL-47 and $VO(acac)_2$.

V-loading (mmol)	Oxidant	Catalyst	TON[a]	TOF (h^{-1})[b]	Selectivity (%)[c]
0.11	TBHP/water	MIL-47	150	30	70
0.42	TBHP/water	MIL-47	67	29	43
0.11	TBHP/decane	MIL-47	42	37	63
0.42	TBHP/decane	MIL-47	28	8	83
0.11	TBHP/water	$VO(acac)_2$	169	44	70
0.42	TBHP/water	$VO(acac)_2$	62	57	25
0.11	TBHP/decane	$VO(acac)_2$	112	35	87
0.42	TBHP/decane	$VO(acac)_2$	74	48	78

[a] TON was calculated after 7 hours; [b] TOF was calculated after 30 minutes; [c] The selectivity toward the cyclohexene oxide calculated at 40% cyclohexene conversion.

3.2.2 Catalytic performance of $VO(acac)_2$ in the oxidation of cyclohexene using different catalyst loadings

Next, the catalytic performance of MIL-47 in TBHP/water and TBHP/decane as oxidant was compared with the homogeneous catalyst $VO(acac)_2$ in identical conditions and V-loadings.

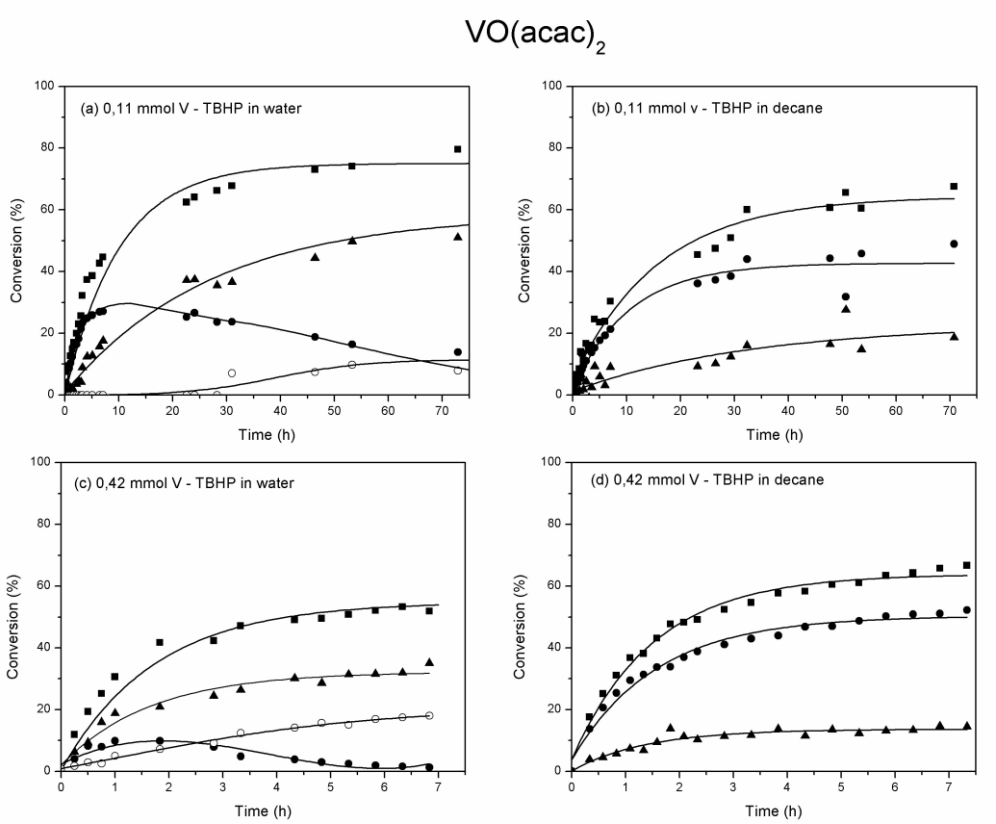

Fig. 3.4. Cyclohexene (**1**) conversion (■) and the yield of cyclohexene oxide (**2**) (●), *tert*-butyl-2-cyclohexenyl-1-peroxide (**4**) (▲) and cyclohexane-1,2-diol (**3**) (○) for $VO(acac)_2$ in TBHP/water (Left) with 0.11 mmol V-sites (a) and 0.42 mmol V-sites (c).; and for $VO(acac)_2$ in TBHP/decane (Right) with 0.11 mmol V-sites (b) and 0.42 mmol V-sites (d). No cyclohexane-1,2-diol (○) is formed when TBHP/decane is used. The production of 2-cyclohexene-1-one is in all cases less than 5%, for the clarity of the figure this is not shown.

In Fig. 3.4 the cyclohexene conversion and yield of cyclohexene oxide **2**, cyclohexane-1,2-diol **3**, and the tert-butyl-2-cyclohexenyl-1-peroxide **4** is shown for the $VO(acac)_2$ catalyst respectively in the water and water-free medium for total V-loadings of 0.11 and 0.42 mmol. The reader is again reminded that the x-axes have different timescales. The homogeneous catalyst shows a similar behaviour as MIL-47 in the water-based oxidant. Firstly, the cyclohexene conversion reach a plateau after approximately the same time (80% after 70 h for 0.11 mmol and 55% after 7 h of catalysis for 0.42 mmol V-sites). Secondly, for both V-loadings, the cyclohexene oxide **2** attains a maximum after 20 h for the 0.11 mmol V and 2 h for the 0.42 mmol V when the cyclohexane-1,2-diol **3** starts to be produced and the tert-butyl-2-cyclohexenyl-1-peroxide **4** becomes the main product. However, comparison of the homogeneous catalyst with the MIL-47 for TBHP/decane as oxidant clearly shows some differences. For the $VO(acac)_2$, the cyclohexene conversion is much faster compared to the MIL-47. After 7 h of reaction, a cyclohexene conversion of 65% is observed for the 0.42 mmol V sites compared to 30% for the microporous MOF. Likewise, with the lower V content, it can be seen that the cyclohexene conversion is much slower compared to the $VO(acac)_2$ catalyst. Nevertheless, the selectivity of both catalysts toward cyclohexene oxide is more or less the same as can be seen from Table 3.1.

Besides the homogeneous catalyst $VO(acac)_2$, two other V catalysts are tested for the oxidation of cyclohexene using TBHP in water as oxidant, namely the supported VO_x/SiO_2 and the microporous crystalline VAPO-5. The latter is a crystalline AlPO zeotype, containing vanadium(+IV) centers. We observed that VAPO-5 is completely catalytically inactive for the oxidation of cyclohexene. This observation is consistent with other research, outlining that VAPO-5 (and more generally MeAPOs) are not suitable as catalysts for liquid phase oxidation reactions [3]. In Fig. 3.5 the first and second run of the supported VO_x/SiO_2 catalyst is shown. As can be seen from this figure, the VO_x/SiO_2 shows a good conversion in a first run. However, after the first catalytic run, 40% of the vanadium was leached from the silica supported catalyst and no cyclohexene conversion was observed in its second run, indicating the reaction occurs basically homogeneous.

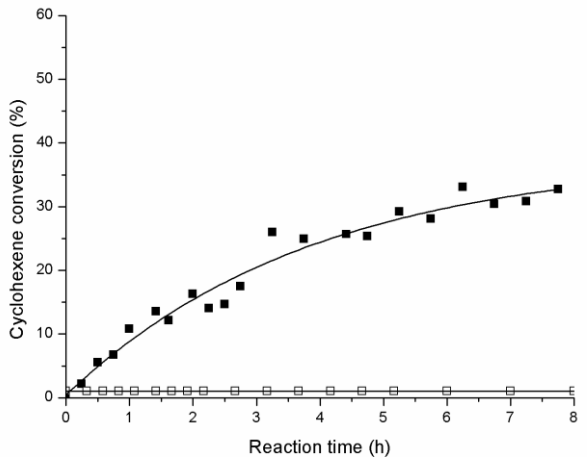

Fig. 3.5. Cyclohexene conversion curves of the VO_x/SiO_2 catalyst in its first (■) and second run (□) using 0.1g VO_x/SiO_2 catalyst (loading: 0.2 mmol V/g).

3.2.3 Stability and regenerability of the catalyst

The crystalline structure of the MOF was examined by X-ray diffraction to verify the stability of the MOF after a catalytic run. In Fig. 3.6, the XRPD pattern of MIL-47 is shown before and after a catalytic run, using TBHP/water or TBHP/decane as oxidant at a temperature of 50 °C. Furthermore, the XRPD pattern of the organic linker in MIL-47 (terephthalic acid or BDC, benzene dicarboxylic acid) is shown. As can be seen from this figure, the XRPD pattern of the MIL-47 after a first catalytic run with TBHP in water as oxidant (Fig. 3.6c) changes significantly compared to the original XRPD pattern (Fig. 3.6a). Especially, some new diffraction peaks, which can be assigned to the BDC linkers, appear after a first catalytic run. This observation indicates that the structure partially decomposes in the TBHP/water system. This also explains the significant V leaching that has been observed. To regenerate the catalyst a treatment in a tubular furnace under a nitrogen flow at 523 K for four hours was carried out to remove the organic compounds. After this calcination treatment the porosity was completely regenerated and the structure of MIL-47 was regained as shown in Fig. 3.6d.

Comparison of the XRPD pattern of MIL-47 before and after a catalytic run, using TBHP in decane (Fig. 3.6a and b) as oxidant, however, clearly demonstrates that in a water-free medium, the structural integrity of the MOF is entirely preserved. No peaks of free BDC can be observed, and no additional treatment is required to remove these free linkers.

To test the regenerability of the catalyst, four consecutive catalytic runs have been performed in TBHP/decane as oxidant. During each catalytic cycle, the cyclohexene conversion was monitored during at least 6 h. The XRPD patterns of the original MIL-47 and after each run are shown in Fig. 3.7 As can be seen from this figure, MIL-47 preserves its crystalline structure during these additional runs. The lower signal to noise ratio in run IV is due to the tiny amount of sample that was left for analysis.

In Table 3.2, the TON and TOF values are shown for MIL-47 in the four consecutive runs. Furthermore, the percentage of leached V in the filtrate is given after each catalytic test. Only in the first cycle, a negligible amount of leached V was observed (<3%), whereas in the following cycles, no leaching was detected. The TON and TOF drop after the first run but remain relatively constant during the next additional cycles. This observation can be explained by the fact that after each run, still some organic compounds of the previous catalytic test clog the pores. This was supported by nitrogen adsorption measurements that showed that the surface area of MIL-47 after a first run dropped from 1225 m^2/g to approximately 500 m^2/g; this will surely lead to a decrease of the reaction rate in the additional runs. Even in conditions of severe leaching (TBHP in water), these leached out species are relatively inert for the epoxidation mechanism as the building of epoxide stops almost completely after the hot filtration of the catalyst; whereas the radical formation of the adduct **4** continues (see Fig. 3.3).

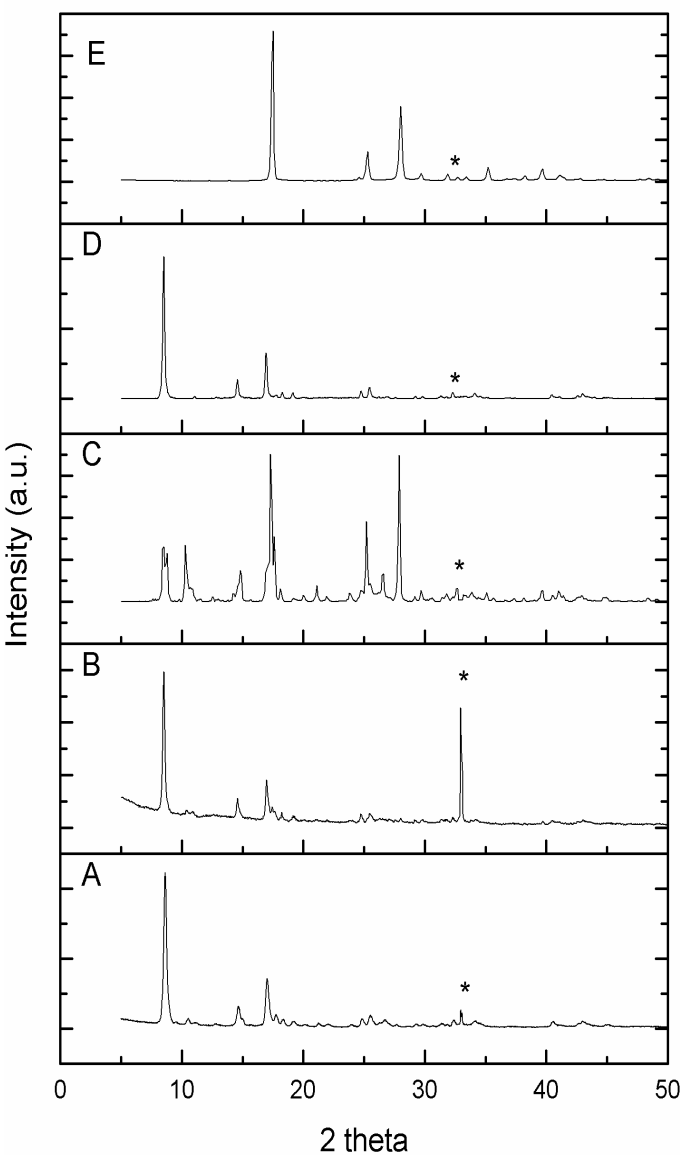

Fig. 3.6. XRPD pattern of (a) MIL-47, (b) MIL-47 after catalysis with TBHP in decane as oxidant, (c) MIL-47 after catalysis with TBHP in water as oxidant, (d) MIL-47 after regeneration and (e) terephthalic acid (* is due to the background of the sample holder at an angle of 32.9°).

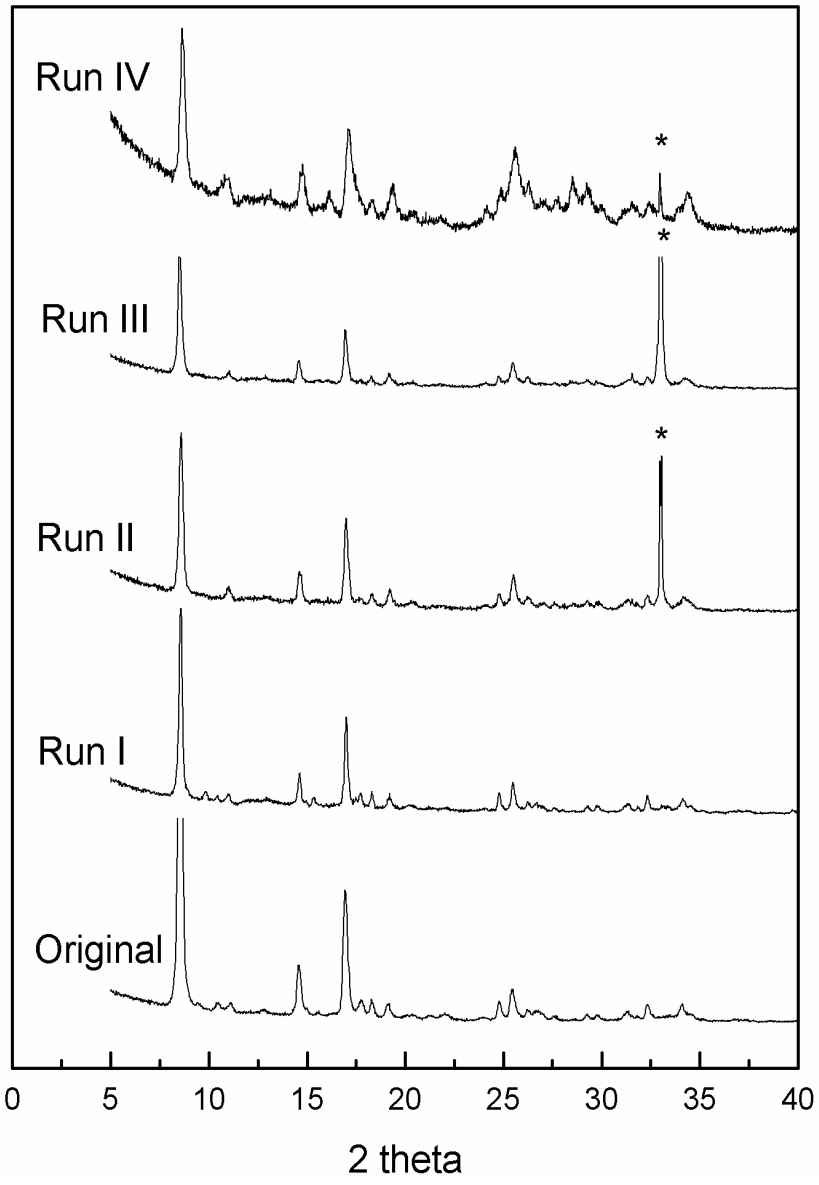

Fig. 3.7. XRPD pattern of the original MIL-47 before catalysis and the XRPD pattern of MIL-47 after the first, second, third and fourth catalytic run (* is due to the background of the sample holder at an angle of 32.9°).

Table 3.2. TOF, TON and the percentage of leached V for the consecutive catalytic runs with TBHP/decane as oxidant.

	TON[a]	TOF (h^{-1})[b]	Leaching (%)
Run I	23	7.8	<3
Run II	14	4.8	0
Run III	15.3	2.9	0
Run IV	12.7	3	0

[a] TOF was calculated after 38 minutes; [b] TON was calculated after 6 hours.

3.2.4 EPR results

In Fig. 3.8, the results of room temperature EPR measurements on dry powders of MIL-47 are shown as a function of catalytic reaction time for MIL-47 in TBHP/decane. The inset displays the EPR spectra of the MIL-47 powder and the MIL-47 powder after 3 h of catalytic performance. Both spectra appear as broad lines and can be well-fitted by single Lorentzians. The position, which is practically the same in the two spectra, is compatible with a signal assignation to V^{+IV} (g = 1.96) [4]. The absence of ^{51}V hyperfine structure is attributed to spin–spin interactions between the close-by V^{+IV} ions in the MIL-47 structure. The width of the spectra, however, is a point of significant difference between the spectra, which needs to be further addressed in future investigation. In this chapter, we are mainly interested in the evolution of the total spectral intensity. This was evaluated by double integration of the field-modulated spectra. In order to avoid possible influences of broad background signals, the total intensities were also calculated from the area of the best-fit Lorentzian to the singly integrated spectra. Intensities were normalized to that of the calcined MIL-47 powder.

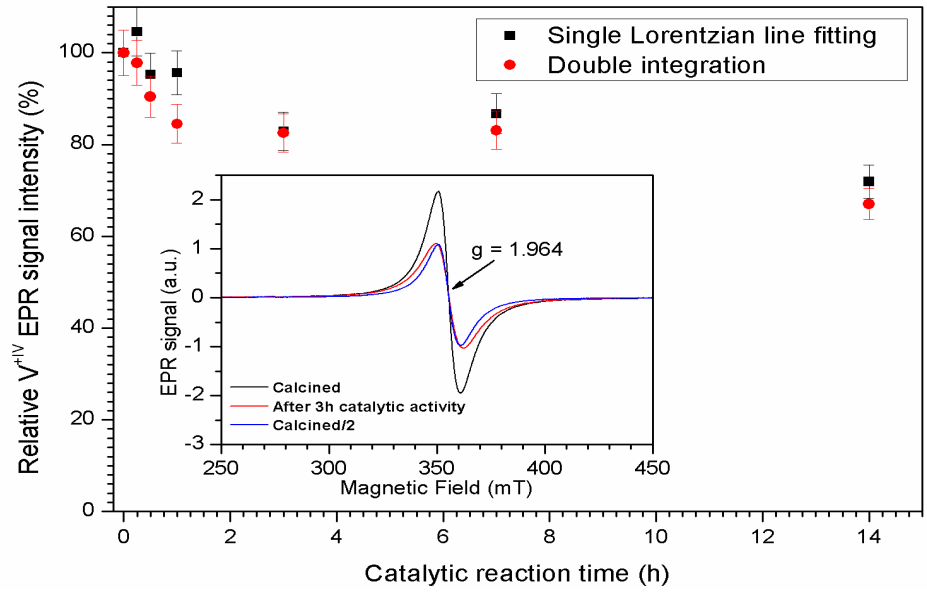

Fig. 3.8. Catalytic reaction time evolution of the intensity of the EPR spectrum for the MIL-47 in TBHP/decane system. EPR spectra were recorded on dry powders and intensities were evaluated by single Lorentzian fitting to the singly integrated spectra and by double integration. All intensities were normalized to that of the MIL-47 sample before catalysis. Inset – EPR spectra for MIL-47 before catalysis(black) and after 3 h of catalytic reaction in the MIL-47/TBHP/decane system (red). For better comparison of the line widths of the EPR spectra, the spectrum of the MIL-47 sample before catalysis is devided by 2 in intensity is shown in blue.

As seen in Fig. 3.8, the two methods lead essentially to the same conclusions. Within the investigated range of catalytic reaction times, the spectra experience an intensity drop by 20–30%, suggesting that approximately this percentage of the V^{+IV} centers observable with EPR is oxidized to V^{+V}. The major part of the intensity decrease is observed in the first few hours (1–3 h). In the later stages, the EPR intensity seems to stabilize or at least to change far more slowly.

3.2.5 Theoretical results on reactive pathways for epoxidation

This computational section aims at: (i) defining the active sites for catalysis, (ii) introducing a finite cluster representing the active site within the MIL-47, (iii) proposing plausible reaction pathways for the epoxidation of cyclohexene, and (iv) elucidating the role of the solvent (water versus decane) on the product selectivity in the cyclohexene conversion, as observed in the experiment. However, to get already some insights into the possible reaction mechanism and intermediates, first theoretical calculations were performed on the $VO(acac)_2$ catalyst, which showed a remarkable resemblance to the MIL-47 catalyst from the experimental results.

3.2.5.1 Computational results on the $VO(acac)_2$ catalyst

A comparison of the optimized geometries of the $VO(acac)_2$ system with the MIL-47 indicates that the surroundings of the vanadium atom are very similar geometrically wise (Fig. 3.9). The initial coordination of TBHP with vanadium is expected to occur in a similar fashion apart from steric constraints. The formation of the epoxide, the diol and the peroxide will now be discussed. Because the ketone is not present in large quantities, this reaction pathway will not be considered here.

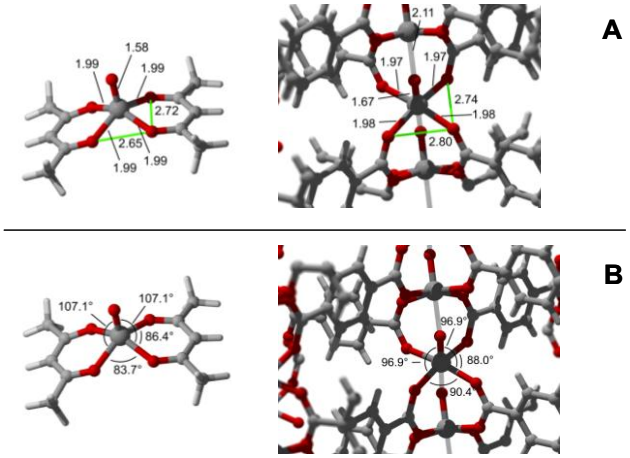

Fig. 3.9. A) Comparison of distances (in A°) for the homogeneous $VO(acac)_2$ (left) system and the metal organic framework MIL-47 (right) and B) Comparison of angles (given in °) for $VO(acac)_2$ (left) and MIL-47 (right).

Fig. 3.10 shows the epoxidation pathway with $VO(acac)_2$ with the final regeneration step of the catalyst included. The reaction cycle starts with an activation step (A) in which TBHP coordinates with $VO(acac)_2$. Here, an alkylperoxo species, namely VO(acac)(OOtBu), is formed.
All attempts to model an epoxidation cycle on a complex with two acac ligands failed, which suggests that first vacant coordination sites need to be generated, in accordance with earlier literature data on the activity of peroxo and alkylperoxo species for oxidations [5, 6].

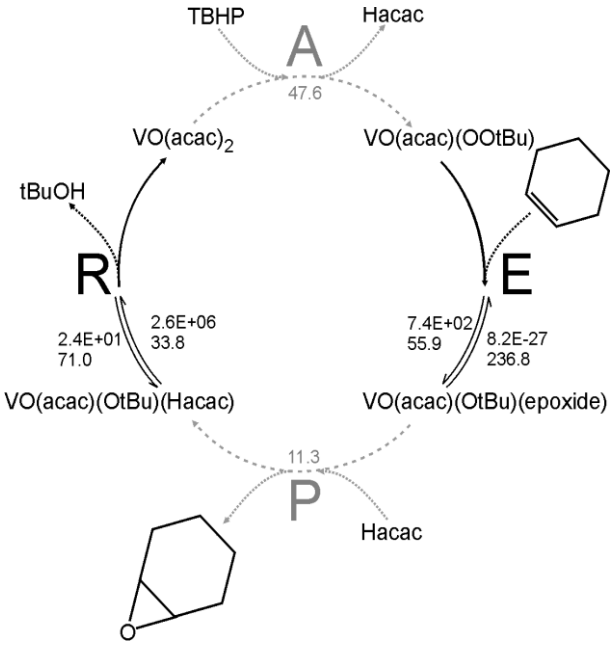

Fig. 3.10. $VO(acac)_2$ epoxidation cycle. Gray numbers indicate reaction energies (kJ mol^{-1}), while black numbers indicate reaction barriers (bottom, kJ mol^{-1}) and reaction rates (top, s^{-1}).

In a second step the actual epoxidation (E) toward cyclohexene oxide can occur easily with an activation barrier of 55.9 kJ mol^{-1} calculated at the B3LYP/6-311+g(3df,2p) level of theory. This step is irreversible which can be deduced from the reverse barrier which is very high (236.8 kJ mol^{-1}).

After epoxidation, Hacac can coordinate back to the vanadium center and cyclohexene oxide is split off (P). Notice that a similar ligand exchange with cyclohexene oxide could also occur with other species present in the reaction medium (tBuOH, H_2O, TBHP). The final regeneration step occurs fast *via* a proton transfer reaction. Both activation (A) and production (P) are endothermic from our calculations but the equilibrium could significantly shift on inclusion of a larger molecular environment. In the case of the $VO(acac)_2$ catalyst substantial amounts of acetic acids are formed upon decomposition of Hacac with TBHP [7]. The subsequent formation of the cyclohexane-1,2-diol can be explained by opening of the epoxide ring by an acid catalyzed hydrolysis mechanism [8]. In the MIL-47, a small fraction of terephthalic acid is anticipated to catalyze the opening of the epoxide ring. During the first catalytic cycle, a majority of the reaction product is tert-butyl-2-cyclohexenyl-1-peroxide. This product is formed due to a radical reaction pathway between the substrate and the oxidant TBHP and has been recently observed for unsaturated Co-MOFs [9]. Freely diffusing peroxy radicals can be generated by a variety of mechanisms in which the oxidation state of vanadium changes.

3.2.5.2 Selection of the cluster model

In an undamaged saturated MIL-47 framework, the coordination sphere around the metal ion is completely blocked by the organic linkers, leaving no free positions available for substrate chemisorptions. From the previously described calculations on the $VO(acac)_2$ catalyst, it was shown that first vacant coordination sites should be created to activate the catalyst [10]. This is in accordance with earlier literature data [5, 6]. For the MIL-47, free coordination positions should also be created by ligand removal or by folding one terephthalic acid ligand away from the vanadium center or by removing bridging oxygen between the neighboring vanadium centers from the O–V–O axis. In view of these structural defects in the periodic structure, we opted to simulate the reaction pathways in a cluster model. The numerical algorithms to search for transition states are better established in the computational programs used for the cluster calculations compared with their periodic equivalents. Of course the cluster should be chosen large enough to represent the real active environment within the MIL-47 topology. In view of this, we propose the extended cluster model as displayed in Fig. 3.11.

This model contains two vanadium atoms, bridged by two terephthalate linkers. On the vanadyl chain, only two V=O bonds are maintained, and the continuation to further terephthalate linkers is interrupted and replaced by terminating OH-groups. Starting from this cluster, one can search for the optimized geometry by relaxing all atoms or by fixing the outer carboxyl oxygen atoms at their crystal positions to prevent unphysical deformation of the cluster, while relaxing all other atoms during the geometry optimization. When taking into account dispersion interactions, the constrained geometry is favored by about 42 kJ/mol. Moreover, the obtained result is a realistic representation of the actual molecular environment around the active site in the MIL-47. The MIL-47 (with V^{+IV}) is one of the MOF structures that only shows a small degree of flexibility, and thus, this model should be well suited.

Although for completeness, we also performed all calculations in the model in which all atoms are relaxed, allowing as such too much conformational flexibility. In particular, the angle between the two terephthalate planes containing the two terephthalic linkers changes largely during such computational protocol. While this particular angle amounts to 98.5 ° when the outer atoms are fixed, this angle increases by 12° in the completely unconstrained model. The other geometrical parameters are not substantially different, even the distance between the two V-centers remains almost unaltered for both cluster models (3.80 versus 3.81 Å, compared to 3.42 Å in the MIL-47 crystal). As will be seen later, the deviancy in spatial orientation of the linkers leads to important changes in the kinetics of the reactions with non-negligible impact on the preferential pathways. The cluster model is schematically shown in Fig. 3.11c, where L represents a bidentate ligand (Fig. 3.11d) and hence shows a twofold coordination with V. Notice that the ligand L in the cluster model contains also a V atom, but this site is not regarded as catalytically active during the simulations. The upper vanadium atom as shown in Fig. 3.11c is taken as the active catalytic center. Both vanadium atoms have oxidation state +IV in the starting cluster model.

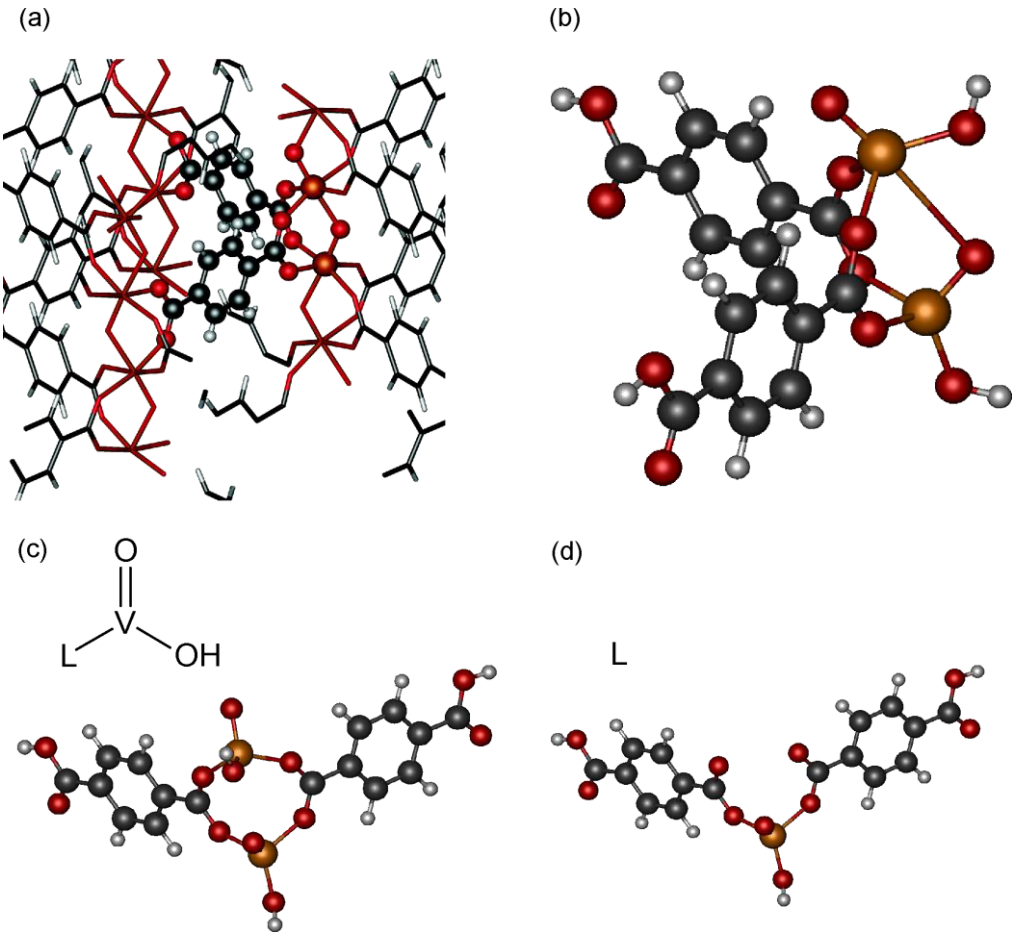

Fig. 3.11. (a) selected cluster (in balls) in the MIL-47 crystal structure, (b) cluster cut out from the crystal as indicated in (a) is now terminated with hydrogens and is chosen large enough to represent the active site in MIL-47, (c) schematical representation of the extended cluster as displayed in (a), (d)bidentate ligand represented by L. Geometry following the unconstrained model for (c) and (d).

3.2.5.3 Possible reaction pathways toward formation of cyclohexene oxide

As already observed for the $VO(acac)_2$ catalyst, the reaction cycle starts with an activation step, in which TBHP coordinates with the vanadium center to form an alkylperoxo species **7** (as shown in Scheme 3.1). The two most probable reaction routes toward epoxidation starting from this complex are displayed in Scheme 3.1. First, a direct pathway to epoxidation leads to the formation of cyclohexene oxide **2** and brings the catalyst to a less active complex **8**. Secondly, a radical mechanism is plausible (indicated as "radical" in Scheme 3.1). In this route, +V vanadium complexes **9** are formed by homolytic cleavage of the peroxy linkage that can then be further activated with TBHP. The generated V^{+V}-activated complexes **10** and **12** can again epoxidize cyclohexene. Both direct and radical routes are completed by a regeneration step that closes the cycle. Apart from the complexes given in Scheme 3.1, other possible V^{+V} (OOtBu) complexes can be formed, which also lead to cyclohexene epoxidation. All these plausible pathways have been investigated in this work, but they turned out not to be competitive with respect to those taken up in Scheme 3.1. We disregard them from further discussion.

3.2.5.4 Reaction kinetics: direct versus radical pathway.

For each reaction path energy barriers, Gibbs-free energies at 323 K and reaction rates have been computed in the two models for geometry optimization (unconstrained versus constrained) as outlined before. The results are given in Table 3.3 All energetics have been calculated within the B3LYP/6-311 + g(3df,2p)-D3//B3LYP/6-31 + g(d) level of theory. The B3LYP/6-311 + g(3df,2p) energies were further refined by including van der Waals interactions at the B3LYP-D3 level of theory with the Orca software package[11]. For the constrained model, we used the partial Hessian vibrational analysis (PHVA) method for the frequency calculations making use of the in-house developed software module TAMkin [12, 13]. The outer oxygen atoms, which were used to fix the cluster, were given an infinite mass [14-18]. All structures for starting geometries were built using ZEOBUILDER[13, 19]. The kinetics for all epoxidation reactions are obtained using the bimolecular approach in which the two reactants are treated in gas phase.

More details are also given by Van Speybroeck et al. [20] on the computational procedures for discriminating between intrinsic and apparent reaction kinetics.

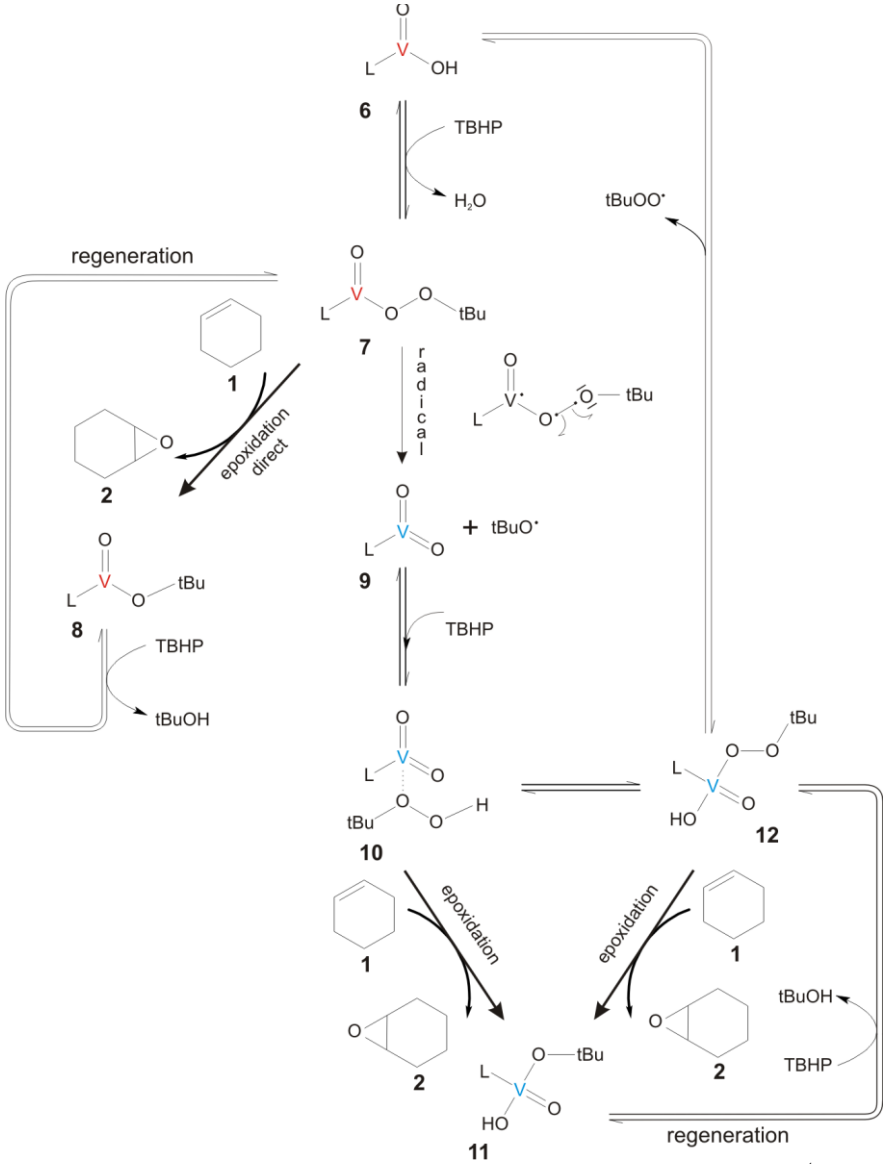

Scheme 3.1. Two competitive cyclohexene epoxidation pathways for MIL-47 (direct and radical). (V^{+IV} is shown in red, V^{+V} is shown in blue and V^{+III} is represented in black).

To give an idea on the values of the physisorption energy for the various species, the complete energy diagram is taken up in Fig. 3.12 for the direct path **7→8**. The physisorption energy of cyclohexene is of about -28 kJ/mol, while -70 kJ/mol for the epoxide. However, the position of the cyclohexene/epoxide in the adsorbed complex and the way these molecules are coordinated with the V-center is not always uniquely determined, and therefore, the reaction kinetics is performed starting from the gas-phase species in this study. The direct epoxidation reaction **7→8** is irreversible as can easily be seen from the energy diagram of Fig. 3.12. Similar large reaction energies are observed for the other epoxidation reactions. Therefore, only the rate constants for the forward reactions are taken up in Table 3.3. The transition state of the direct epoxidation reaction **7→8** is given in Fig. 3.14a. The cyclohexene molecule is located in the free spot that extends to a whole hemisphere in front of the two remaining linkers and the t-butoxy group, stressing once more that the epoxidation reaction can only take place if some ligands are removed.

Table 3.3 Energy barriers and Gibbs-free energy barriers for the epoxidation reactions (bimolecular) and the radical decomposition (unimolecular). Also the reaction energies are reported, as well the reaction Gibbs-free energies at 323 K.

	Unimolecular			Bimolecular				
	$\Delta E^{\ddagger}_{0,intr}$ (kJ/mol)	$\Delta G^{\ddagger}_{323,intr}$ (kJ/mol)	$k^{unimol}_{323,intr}$ (s^{-1})	$\Delta E^{\ddagger}_{0,app}$ (kJ/mol)	$\Delta G^{\ddagger}_{323,app}$ (kJ/mol)	$k^{bimol}_{323,app}$ ($m^3mol^{-1}s^{-1}$)	$\Delta E_{0,r}$ (kJ/mol)	$\Delta G_{323,r}$ (kJ/mol)
Unconstrained model								
Direct 7→8	-	-	-	-2.8	46.3	5.71E+03	-157.7	-174.8
Radical 7→9	37.1	32.9	3.22E+07	-	-	-	28.5	-34.7
10→11	-	-	-	35.1	89.6	5.73E-04	-219.4	-213.3
12→11	-	-	-	26.8	82.9	6.97E-03	-191.9	-187.2
Constrained model								
Direct 7→8	27.4	40.3	2.02E+06	-1.0	48.9	2.19E+03	-157.3	-171.2
Radical 7→9	38.0	35.2	1.37E+07	-	-	-	23.8	-37.3
10→11	-	-	-	29.1	90.2	4.69E-04	-226.5	-220.3
12→11	-	-	-	41.9	107.0	8.87E-07	-189.8	-177.8

The constrained and unconstrained models predict nearly the same reaction barriers and entropic contributions (see Table 3.3) as the geometries resulting from the models only differ in the spatial orientation of the two remaining linkers. The energy diagram of Fig. 3.12 learns that the reaction is strongly exergonic and thus irreversible. The direct route **7→8** is highly favored on basis of the energy barriers and Gibbs-free energies of activation.

The reactions **10**→**11** and **12**→**11** are higher activated (90.2 kJ/mol and 107.0 kJ/mol versus 48.9 kJ/mol for the Gibbs-free energy of activation $\Delta G^{\ddagger}_{323,app}$ following the constrained model Table 3.3) but are thermodynamically driven as the product **11** is very stable (Gibbs reaction-free energies of -220.3 and -177.8 kJ/mol). The epoxidation reactions **10**→**11** and **12**→**11** are initiated by a radical decomposition **7**→**9** thereby bringing the active V-site into an oxidation state +V followed by a reaction of the originally inactive V complex **9** with TBHP to an active complex **10** or **12**. The radical decomposition (**7**→**9**) is modeled as an unimolecular process with a reaction barrier of 37–38 kJ/mol or a Gibbs-free energy barrier of 33–35 kJ/mol at 323 K, which thus slightly decreases with temperature. This reaction will certainly take place, and in addition, it is also thermodynamically favored as the reaction becomes more and more exergonic with temperature due to entropic effects (see Fig. 3.12).

Some transformations taken up in Scheme 3.1 are modeled as equilibration steps and the values are taken up in Table 3.4.Starting from complex **9**, an equilibration step occurs in which the TBHP coordinates with species **9**, to form another V^{+V} species **10**. This step is thermodynamically controlled toward species **10** at lower temperatures. Species **10** can further transform to species **12**, in which TBHP covalently bonds to the vanadium center. The equilibrium of this step lies in the direction of V-cluster **12**. From species **10** and **12** that are both V^{+V} species, the epoxidation of cyclohexene can be initiated.

Overall, the whole reaction cycle starting from **7** to **11** is very exothermic and also irreversible as the backward reactions have very high activation barriers (up to 300 kJ/mol). In this "radical" pathway, which allows transformation of oxidation state from +IV to +V for vanadium, one of the epoxidation reactions **10**→**11** and **12**→**11** becomes the rate determining step. They are higher activated but eventually become also important as this reaction cycle is thermodynamically controlled. The reaction **12**→**11** requires some special interest as the results are more sensitive to the particular model used for the kinetics calculations, i.e., constrained versus unconstrained.

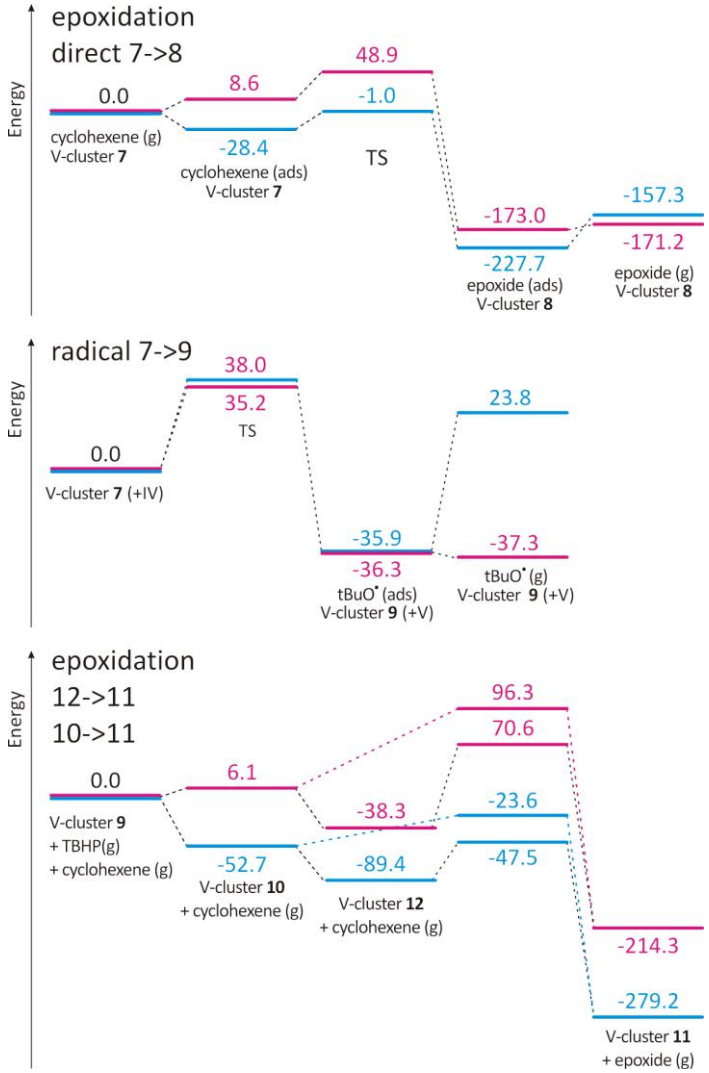

Fig. 3.12. Energy diagram for the direct epoxidation reaction 7→8, the radical reaction pathway 7→9 and the subsequent epoxidation reactions 10→11 and 12→11. Energies (at 0 K) are given in blue, Gibbs-free energies at 323 K are given in red. All energies in kJ/mol. The V-cluster appears as an activated complex in the reactants and as an inactivated complex in the products. In radical reaction 7→9 the oxidation number of vanadium changes from +IV to +V. Both energy (at 0 K) and Gibbs-free energy (at 323 K) profiles are drawn relative with respect to the first level in each scheme. Numerical results are obtained using the constrained cluster model.

In contrast to the direct pathway **7→8** with a V^{+IV} active complex, steric hindrance lies now on the origin of the significant increase of the barrier in the constrained cluster model. In this V^{+V} complex (Fig. 3.14d), the position of the cyclohexene in the transition state is slightly different with that in the V^{+IV} complex (Fig. 3.14a). In addition, the free spot for the coordination of cyclohexene is more limited in the V^{+V} complex, and in the constrained model, one of the linkers causes a steric repulsive effect on the cyclohexene, inducing an asymmetric spatial position with respect to the oxygen of the V complex. This unphysical situation causes too high barriers. Realistically, the values will lie in between the values of the two models and overall the conclusions on the most preferable pathway to epoxidation are not altered. The two geometries of the transition state are visualized in Fig. 3.14c and d where we can easily see that in the unconstrained case, the position of the linker is more relaxed allowing the cyclohexene to take the most favorable position in the transition state.

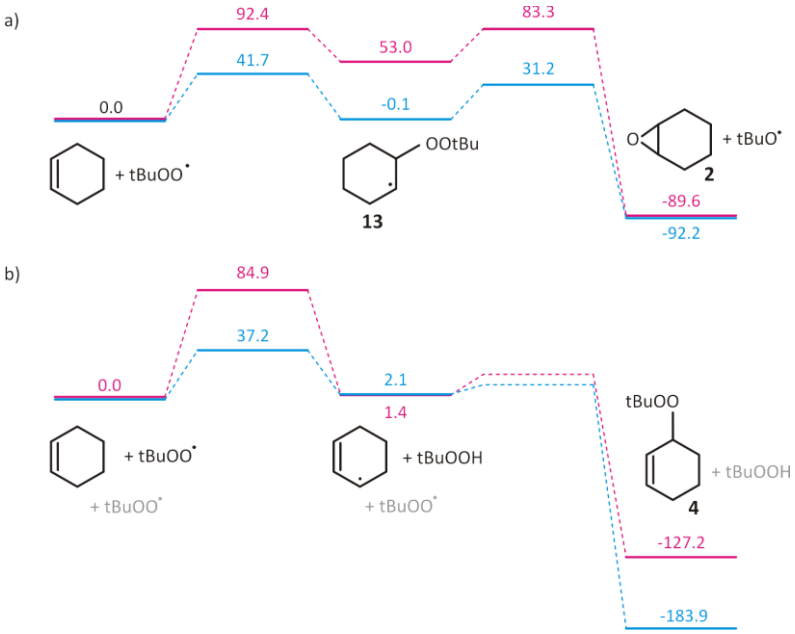

Fig. 3.13. Energy profiles for the reaction between cyclohexene and the tert-butylperoxy radical. Energies (at 0 K) are given in blue, Gibbs-free energies at 323 K are given in red. All energies in kJ/mol. (a) Pathway a leading to formation of cyclohexene oxide. (b) Pathway b leading to formation of the adduct 4. Electronic energies at 0 K are indicated in red. Energies in kJ/mol.

The regeneration reactions with TBHP go smoothly as they are mostly thermodynamically driven (see Table 3.4).

Table 3.4. Thermodynamical parameters for the reactions modeled as equilibrium steps. $\Delta E_{0,r}$ represents the reaction energy corrected with zero-point energies and dispersion, $\Delta G_{323,r}$ the reaction-free energy at 323 K. The equilibrium constant K_{323} at 323 K is obtained after a fitting procedure between 273 and 373 K.

	$\Delta E_{0,r}$ (kJ/mol)	$\Delta G_{323,r}$ (kJ/mol)	K_{323}	$[K_{323}]$
Unconstrained Model				
6 → 7	-59.8	-40.8	3.96E+06	-
8 → 7 (regeneration)	-27.5	-7.4	1.55E+01	-
11 → 12 (regeneration)	6.7	5.0	1.53E-01	-
9 → 10	-64.7	-4.8	1.60E-01	$m^3\ mol^{-1}$
10 → 12	-27.5	-26.1	1.67E+04	-
12 → 6 (V^{+V}-V^{+IV} recycling)	132.2	67.6	4.41E-10	m^{-3} mol
Constrained Model				
6 → 7	-60.3	-42.3	7.02E+06	-
8 → 7 (regeneration)	-27.9	-10.9	5.73E+01	-
11 → 12 (regeneration)	4.6	-4.3	4.94E+00	-
9 → 10	-52.7	6.1	2.74E-03	$m^3\ mol^{-1}$
10 → 12	-36.7	-42.5	7.54E+06	-
12 → 6 (V^{+V} - V^{+IV} recycling)	134.6	77.2	1.21E-11	m^{-3} mol

It is now interesting to couple our theoretical results to the available experimental data. The quantitative values of our calculations can indirectly be validated with the results of a kinetic study on the epoxidation of cyclohexene with $VO(acac)_2$. by Gould et al[21] suggested that vanadium is probably converted to the +V oxidation state and remains in that state throughout. This is in full agreement with the situation encountered in the epoxidation reactions **10→11** and **12→11**. The experiment reports values of 53.1 kJ/ mol for the enthalpy of activation and -82.8 J/K/mol for the entropy of activation.

For T = 323 K, this results to a Gibbs-free energy of activation of about 80 kJ/mol, which is in excellent agreement with the theoretical predictions for the pathways **10**→**11** and **12**→**11**, which proceed through a vanadium in oxidation state +V.

Summarizing, there are two pathways which are competitive and which form a closed cycle of epoxidation and regeneration and wherein the peroxide is systematically used to bring the inactive vanadium complex (species **6**) into an active complex with oxidation state +IV (species **7**) or an active complex with oxidation state +V (species **10** and **12**). The two epoxidation pathways start from a complex with another oxidation state for vanadium, but a switch from one cycle to the other is possible at any time. Once V^{+V} complexes are formed, a return to the V^{+IV}-cycle is possible via the equilibration step **12**→**6**, which we will call the V^{+V}–V^{+IV} recycling step for further reference. This step is energetically not favored ($\Delta E_{0,r}$ = 132–135 kJ/mol in Table 3.4) but becomes possible at temperatures of 323 K due to entropic contributions, which bring the free energy of reaction to reasonable values 67–77 kJ/mol. These barriers are of the same order as the barriers for epoxidation and are thus competitive with these pathways.

Thus far, no solvent effects have been taken into account. In the experimental part, the catalytic activity of the MIL-47 has been investigated with TBHP dissolved in water or in decane. One of the main differences was the much larger initiation time for cyclohexene conversion with decane as solvent. The proposed reaction scheme may serve to explain some of the experimental findings. The reaction cycle can only start once free coordination positions are created, either by folding a ligand away or by removing a terephthalic acid from vanadium.

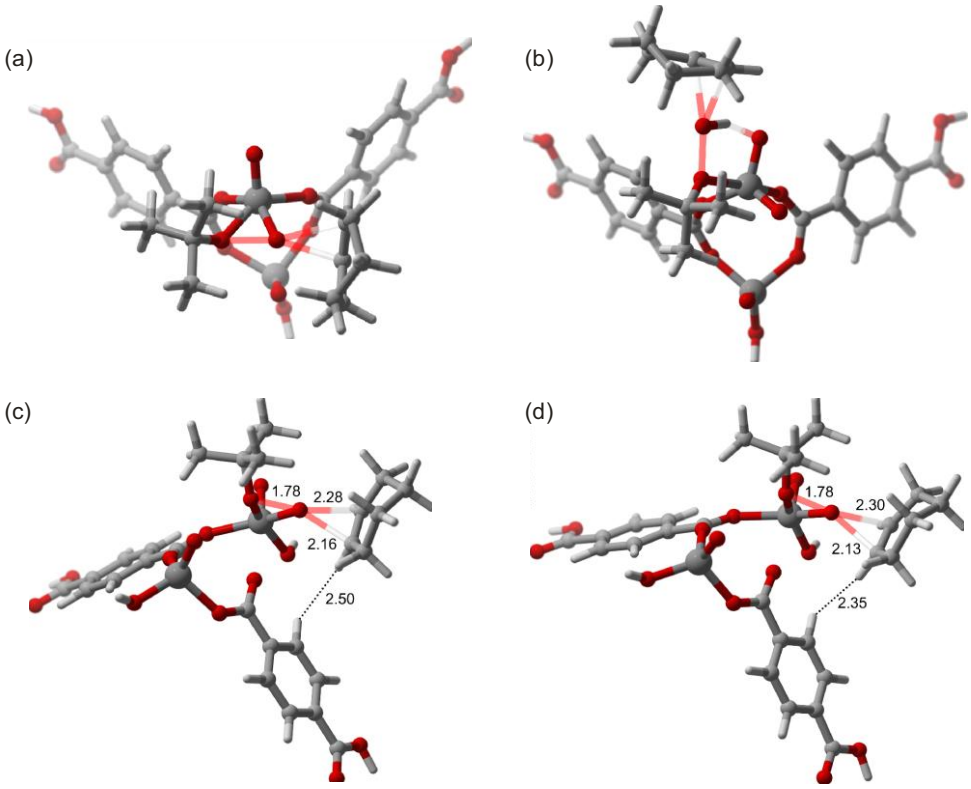

Fig. 3.14. Transition states of the three epoxidation reactions: (a) direct pathway 7→8, (b) pathway 10→11, (c) and (d) pathway 12→11. Use of the unconstrained model in (a)–(c); use of the constrained model in (d).

The structure **6** in Scheme 3.1 can be created by cleaving a terephthalate–vanadium bond and replacing the ligand by a hydroxyl group. Such hydroxyl groups can easily be introduced in a water-based medium and thus water helps in creating free coordination sites, enhancing the initial rate of cyclohexene conversion. In case of decane as solvent, such sites of type **6** are not formed as this solvent has no OH-group present. In this case, the activation should be induced by TBHP itself. This can either lead to the cleavage of a vanadium bond and an oxygen of the carboxylate group to form complex **7** immediately but also other species such as VO(L)(OtBu) could be formed, which can by ligand exchange with TBHP form the active species **7**.

Therefore, one can anticipate that the initiation time for epoxidation is larger in case of decane, as TBHP takes also an active role in the activation period. These findings are compatible with the observation that the measured experimental diffraction pattern does not change after reaction with TBHP/decane + cyclohexene. The bulk structure remains better conserved during the reaction cycle, whereas in case of water, more vanadium/terephthalic acid bonds are broken. The diffraction pattern of the catalyst with TBHP/water after catalysis (see Fig. 3.6) shows a broadening of the peaks that might be ascribed to further structure deterioration. Another feature observed experimentally is the formation of side products, such as diols, adducts, and cyclohexenones, which are manifestly present after a short reaction time on a MIL-47 catalyst with a V-loading of 0.42 mmol and with TBHP dissolved in water. The experiment with TBHP in decane as oxidant does not reveal any relevant by-product formation. The formation of the *tert*-butyl-2-cyclohexenyl-1-peroxide **4** must be ascribed to radical pathways between the substrate and the oxidant TBHP and was recently further investigated for unsaturated Co-MOFs [9, 22]. Freely diffusing peroxy radicals can be generated by a variety of mechanisms in which the oxidation state of vanadium changes. It is well known that radicals are better stabilized in water than in decane and thus such radical pathways are more prominently present in such polarisable media. Also the radicals tBuO• and tBuOO•, appearing in some pathways of Scheme 3.1, lie on the origin of the formation of the side products, and in particular that of the adduct **4** as schematically shown in Fig. 3.13 (pathway b). An enhanced concentration of radicals leads to more termination reactions and hence a larger production of adducts.

The increasing concentration of the tert-butylperoxy radical tBuOO• requires some attention, as it is also able to directly epoxidize cyclohexene following the so called Twigg mechanism as reported by Van Sickle et al. [23] (pathway a in Fig. 3.13). We examine the two competitive pathways.
In the first, a radical addition reaction takes place creating an intermediate cyclohexenyl radical **13** followed by cleavage of the tert-butylperoxy radical and formation of cyclohexene oxide. The energy profile is displayed in Fig. 3.13 (pathway a). The radical addition reaction shows a high free-energy barrier, while the reaction is strongly endergonic, indicating that the backward reaction (dissociation) goes much faster than the forward reaction (association).

In pathway b, a hydrogen abstraction occurs from the allylic position of cyclohexene forming the 3-cyclohexenyl radical, which can rapidly recombine with another tert-butylperoxy radical yielding the adduct **4**. The hydrogen abstraction also requires a high energy barrier (only 8 kJ/mol lower than in pathway a). The subsequent radical recombination reaction goes quite quickly since the reaction energy is strongly negative and heavily thermodynamically driven. These theoretical findings are in complete agreement with the suggestions made in a recent experimental work of Tonigold et al. [22] where pathway b has been proposed as the major pathway. Concluding, without excluding the direct epoxidation of cyclohexene by the tert-butylperoxy radical tBuOO•, the radical pathway will favor the adduct formation.

3.3 Conclusions

This study reveals that V-MIL-47 can be a highly selective catalyst in the epoxidation of cyclohexene using TBHP as the oxidant. Water should be avoided as the solvent for the peroxide, as it enhances strongly the leaching of the V-centers and as it accelerates an unwanted radical side reaction, forming an adduct between the peroxide and cyclohexene. When decane is used to dissolve the peroxide, the MIL-47 is a highly selective catalyst toward the epoxide, especially in the first linear regime of conversion. The leaching of V-centers is negligible in that case and the structural integrity of the MOF is preserved during successive runs. Computational studies show that several catalytic pathways co-exist and compete with each other, but every catalytic cycle starts with the breaking of two V-terephthalic bonds to coordinate with the peroxide. EPR studies confirm that approximately 20% of the V^{+IV} sites are oxidized to V^{+V} in the first minutes of the catalytic reaction and remain relatively constant afterward.

3.4 Experimental

3.4.1 Synthesis of MIL-47

MIL-47 was synthesized according to the original recipy described by Barthelet et al.[1] Typically, 1.37 g VCl_3 and 0.36 g terephthalic acid were mixed together with 15.7 mL of deionised H_2O.

The resulting mixture was transferred into a Teflon-lined stainless autoclave for 4 days at 200 °C. The *as*-synthesized MIL- 47 was filtered, washed with acetone, and calcined. Different procedures can be found in literature for the removal of uncoordinated terephthalic acid and the simultaneous oxidation of V^{III} to V^{IV}. In the procedure of Barthelet et al.[1], 250 mg of MIL-47 is calcined for 24 h at 573 K under a flow of air in a tubular furnace, while in the paper of Wang et al.[24] different procedures are described which consist of a calcination in air at 623 K with or without flow. To obtain the highest surface areas we followed the calcination procedure described by Alearts et al.[25] Activation of the MIL-47*as* was performed by spreading the sample in a porcelain cup. The sample was heated to 300 °C for 21.5 h, with a heating time of 2.5 h and a cooling down time of 8 h. Typical synthesis yield is approximately 15%.

3.4.2 Synthesis of VAPO-5

VAPO-5 was synthesized as follows[3] : a solution of 1.8 g oxovanadium (IV) sulphate-hydrate in 40 ml water was added to a solution of 27.0 g of ortho-phosphoric acid in 40 ml of water. While stirring, 15.5 g of pseudo boehmite (from Sasol) was added during 10 minutes. The suspension was vigorously stirred for 60 minutes at room temperature. To this viscous gel, 15.0 g of triethylamine was slowly added. The gel was stirred for 30 minutes and was then transferred into a teflon lined stainless autoclave and placed in an oven at 170 °C for 2 days. By centrifugation, the solid was recovered. Furthermore the catalyst was dried and calcined for 4 h under a O_2-flow at 550 °C (heating rate: 2 °C min^{-1})[3].

3.4.3 Synthesis of VO_x/SiO_2

For the synthesis of VO_x/SiO_2 catalyst, 1g porous silica (silicagel 60, Merck) was dried at 400 °C and subsequently stirred in a 30 ml 0.02M NH_4VO_3 solution at 80 °C for 2 hours. The as-made catalyst was filtered and dried, followed by a calcination step in air at 550 °C (heating rate: 1.5°C min^{-1}). The vanadium loading was determined spectroscopically and amounts 0.2 mmol g^{-1}.

3.4.4 Characterization of MIL-47, VAPO-5 and VO_x/SiO_2

In Table 3.5 the general porosity data of the synthesized VO_x/SiO_2, VAPO-5 and MIL-47 materials are shown.

Table 3.5. Surface area, pore volume and pore diameter of MIL-47, VAPO-5 and VO_x/SiO_2 based on the nitrogen adsorption isotherm.

	Surface area ($m^2\ g^{-1}$)	Pore volume ($cm^3\ g^{-1}$)	Pore diameter (nm)
MIL-47	1225	0.4	<2
VAPO-5	338	0.08	<2
VO_x/SiO_2	390	0.7	6

The Langmuir surface area of the synthesized MIL-47 is approximately 1225 m^2/g, which is consistent with literature[1]. The XRPD pattern of the synthesized MIL-47 and VAPO-5 is presented in Fig. 3.15 and compared to the XRPD pattern, generated from the original CIF-file[1]. The experimental XRPD pattern of MIL-47 matches perfectly with the simulated pattern, confirming the phase purity of the synthesized MIL-47. Some differences in reflection intensities between the simulated and experimental pattern are due to the variation in crystal orientation of the micro crystals. As can be seen in Fig. 3.15b the XRPD pattern of VAPO-5 is identical to the XRPD pattern of the AFI structure in the zeolite database[26] (aluminium phosphate AlPO-5) clearly indicating the purity of the material.

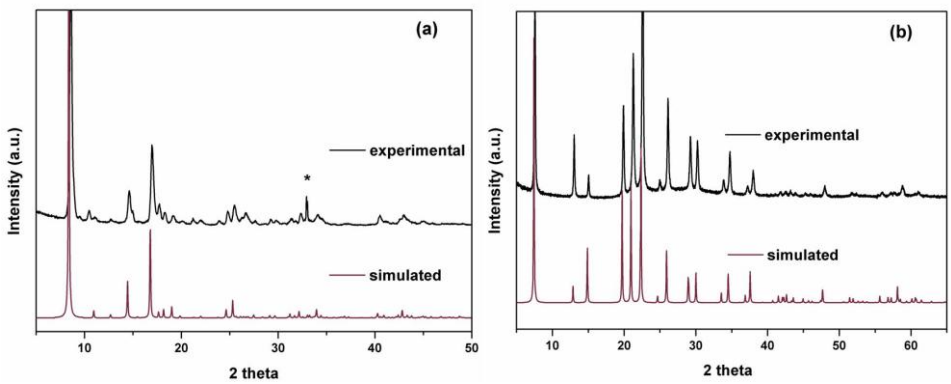

Fig. 3.15. XRPD patterns of (a) MIL-47 (experimental and simulated[1]) and (b) VAPO-5 (experimental and simulated[26]). (* is due to the background of the sample holder at an angle of 32.9°).

3.4.5. General procedure for the cyclohexene oxidation

During a typical catalytic test, a 100-mL round-bottom flask was charged with 30 mL of chloroform (anhydrous) used as solvent, 5 mL of cyclohexene, and 6.2 mL of 1,2,4-trichlorobenzene (used as internal standard for the GC analysis). The reactions were carried out with *tert*-Butyl hydroperoxide (70 wt% TBHP in water) or with TBHP in decane (5.5M solution) as oxidant. The molar ratio cyclohexene/oxidant was 1/2. All the catalytic tests were performed at a temperature of 50 °C and with an Ar-containing balloon on top of the condenser. Blank reactions at this temperature showed no catalytic conversion of cyclohexene. Aliquots were gradually taken out of the mixture, diluted with 500 µl ethylacetate, and subsequently analyzed by GC-FID and GC×GC TOF-MS. After a catalytic run, the catalyst was recovered by filtration on a combined nylon-membrane filter, washed with acetone, and vacuum dried overnight. The filtrate was analyzed by XRF to determine the leached vanadium.

3.5 References

1. K. Barthelet, J. Marrot, D. Riou and G. Ferey, *Angew Chem Int Edit*, 2001, **41**, 281-+.
2. J. Arfaoui, L. K. Boudali and A. Ghorbel, *Catal Commun*, 2006, **7**, 86-90.
3. M. J. Haanepen, A. M. ElemansMehring and J. H. C. vanHooff, *Appl Catal a-Gen*, 1997, **152**, 203-219.
4. A. Bruckner, *Top Catal*, 2006, **38**, 133-139.
5. E. P. Talsi, V. D. Chinakov, V. P. Babenko and K. I. Zamaraev, *J Mol Catal*, 1993, **81**, 235-254.
6. H. Mimoun, M. Mignard, P. Brechot and L. Saussine, *J Am Chem Soc*, 1986, **108**, 3711-3718.
7. L. P. Stepovik and M. V. Gulenova, *Russ J Gen Chem+*, 2009, **79**, 1663-1670.
8. A. Lundin, I. Panas and E. Ahlberg, *J Phys Chem A*, 2007, **111**, 9087-9092.
9. M. Tonigold, Y. Lu, B. Bredenkotter, B. Rieger, S. Bahnmuller, J. Hitzbleck, G. Langstein and D. Volkmer, *Angew Chem Int Edit*, 2009, **48**, 7546-7550.
10. K. Leus, I. Muylaert, M. Vandichel, G. B. Marin, M. Waroquier, V. Van Speybroeck and P. Van der Voort, *Chem Commun*, 2010, **46**, 5085-5087.

11. *ORCA. 2.6.35ed. <http://www.thch.uni-bonn.de/tc/orca/>.*
12. A. Ghysels, T. Verstraelen, K. Hemelsoet, M. Waroquier and V. Van Speybroeck, *J Chem Inf Model*, 2010, **50**, 1736-1750.
13. *CMM Code. <http://molmod.ugent.be/code/wiki>.*
14. A. Ghysels, D. Van Neck, V. Van Speybroeck, T. Verstraelen and M. Waroquier, *J Chem Phys*, 2007, **126**.
15. A. Ghysels, D. Van Neck and M. Waroquier, *J Chem Phys*, 2007, **127**.
16. A. Ghysels, V. Van Speybroeck, T. Verstraelen, D. Van Neck and M. Waroquier, *J Chem Theory Comput*, 2008, **4**, 614-625.
17. A. Ghysels, V. Van Speybroeck, E. Pauwels, D. Van Neck, B. R. Brooks and M. Waroquier, *J Chem Theory Comput*, 2009, **5**, 1203-1215.
18. A. Ghysels, V. Van Speybroeck, E. Pauwels, S. Catak, B. R. Brooks, D. Van Neck and M. Waroquier, *J Comput Chem*, 2010, **31**, 994-1007.
19. T. Verstraelen, V. Van Speybroeck and M. Waroquier, *J Chem Inf Model*, 2008, **48**, 1530-1541.
20. V. Van Speybroeck, J. Van der Mynsbrugge, M. Vandichel, K. Hemelsoet, D. Lesthaeghe, A. Ghysels, G. B. Marin and M. Waroquier, *J Am Chem Soc*, 2011, **133**, 888-899.
21. E. S. Gould, R. R. Hiatt and K. C. Irwin, *J Am Chem Soc*, 1968, **90**, 4573-&.
22. M. Tonigold, Y. Lu, A. Mavrandonakis, A. Puls, R. Staudt, J. Mollmer, J. Sauer and D. Volkmer, *Chem-Eur J*, 2011, **17**, 8671-8695.
23. Vansickl.De, F. R. Mayo and R. M. Arluck, *J Am Chem Soc*, 1965, **87**, 4824-&.
24. X. Q. Wang, L. M. Liu and A. J. Jacobson, *Angew Chem Int Edit*, 2006, **45**, 6499-6503.
25. L. Alaerts, M. Maes, P. A. Jacobs, J. F. M. Denayer and D. E. De Vos, *Phys Chem Chem Phys*, 2008, **10**, 2979-2985.
26. C. M. Baerlocher, L.B. , *Database of Zeolite Structures: Http://www.iza-structure.org/databases/*

Chapter 4: The influence of amino groups on the CO_2 adsorption capacity of metal organic frameworks: the case of NH_2-MIL-47

Abstract

In this chapter the synthesis of an amino functionalized vanadium-containing Metal Organic Framework, NH_2-MIL-47 will be presented. This MOF has been made by a hydrothermal reaction in an autoclave. Alternatively, a synthesis route via microwave enhanced irradiation has been optimized to accelerate the synthesis. The NH_2-MIL-47 exhibits the same topology as MIL-47, in which the V center is octahedrally coordinated. After an exchange procedure in DMF the V^{+III} center is oxidized to V^{+IV}, which is confirmed by EPR and XPS measurements. The CO_2 and CH_4 adsorption properties have been evaluated and compared to MIL-47, showing that both MOFs have a similar adsorption capacity and affinity for CO_2. DFT- based molecular modeling calculations were performed to obtain more insight into the adsorption positions for CO_2 in NH_2-MIL-47. Furthermore the calculated adsorption enthalpies agree well with the experimental values.

The results presented in this chapter are obtained by a collaborative effort between following research groups:

- The synthesis and characterization of the NH_2-MIL-47 was performed at COMOC by Karen Leus.

- Prof Depla from DRAFT (department of Solid State Sciences -UGent) analyzed the XRPD pattern of NH_2-MIL-47

- Dr Gauthier Vanhaelewyn from the EMR research group (UGent) performed the EPR measurements and Dr Els Bruneel from the

Department of Inorganic and Physical Chemistry executed the XPS measurements.

- Sarah Couck from the Vrije Universiteit Brussel (VUB – Chemical Engineering) carried out the CO_2 and CH_4 adsorption measurements and the breakthrough experiments on NH_2-MIL-47

- The molecular modeling was performed by Matthias Vandichel (Center for Molecular Modeling, UGent)

The results presented in this chapter are presented in following publication indexed in the Web of Science:

K. Leus, S. Couck, M. Vandichel, G. Vanhaelewyn, Y. Y. Liu, G. B. Marin, D. Depla, M. Waroquier, V. Van Speybroeck , J. Denayer, P. Van Der Voort, *Synthesis, Characterization and Sorption Properties of NH_2-MIL-47*, Physical Chemistry Chemical Physics, **2012**, 14, 15562-15570.

4.1 Introduction

The functionalization of porous materials with $–NH_2$ groups is of particular interest for the adsorptive separation of CO_2. For silica-based materials it was already demonstrated that functionalization of the surface of the mesopores with $–NH_2$ groups enhances the affinity toward CO_2 adsorption. This points to a strong interaction between CO_2 and the amino groups in the pores. Sometimes this even resulted in chemisorption, with the formation of carbonate, bicarbonate or carbamate species[1-6]. For MOF materials, the effect of $–NH_2$ groups is less straightforward and is still the subject of many discussions [7, 8]. For IRMOF-3 it was shown that the amino functionalization only had a marginal effect on the CO_2 sorption capacity and selectivity [7, 8]. Arstad et al. prepared three amino functionalized materials (USO-1-Al, USO-2-Ni, and USO-3-In) and they concluded that the capacity toward CO_2 is increased in comparison with the non-functionalized materials [9]. Pure phase amine functionalized MIL-101(Al) has been synthesized in the work of Serra-Crespo et al [10]. The separation properties have been assessed in terms of single component adsorption and mixture separation. The authors found that NH_2-MIL-101(Al) is an excellent candidate for the selective adsorption of CO_2 from methane and N_2. The functionalized material also displays a high CO_2 capacity, but lower than the unfunctionalized MIL-101 with Cr instead of Al. On the other hand NH_2-MIL-101(Al) performs better in CO_2/CH_4 separation than MIL-101(Cr) at low CO_2 pressures [10]. An amine-functionalized ZIF (ZIF-96) displays again higher CO_2 adsorption capacities[11].

In the specific case of MIL-53(Al), the functionalization of the framework with $–NH_2$ groups leads to a drastic increase in selectivity for CO_2 in mixtures with CH_4 as compared to the non-functionalized material, but this is not caused by a direct interaction (chemisorption) between CO_2 and the NH_2 groups [12, 13]. Lescouet et al. have shown that the adsorption capacity varies according to the fraction of amine functionalized linker [14].

Furthermore, the flexibility of the frameworks plays also an important role in adsorption processes. Several papers studied the difference in adsorption behaviour between the rigid MIL-47 in comparison to the flexible and breathing MIL-53. In a recent paper of Trung et al [15], MIL-53(Cr) and MIL-47(V) were studied for the adsorption of the apolar species, n-hexane and n-nonane.

While MIL-53(Cr) exhibits a sub-step during the sorption process explained by a structural transition of the framework, one obtains a I-type isotherm for MIL-47 as typically observed for non flexible microporous materials [15, 16]. In the recent paper of Leclerc et al [16], it has been shown that the oxidation state of the vanadium is decisive for the MIL-47 to show a breathing effect. If the vanadium resides in a +III state, a similar breathing effect as in MIL-53 has been observed whereas the presence of V^{+IV} centers inhibits the flexibility to a large extent [16].

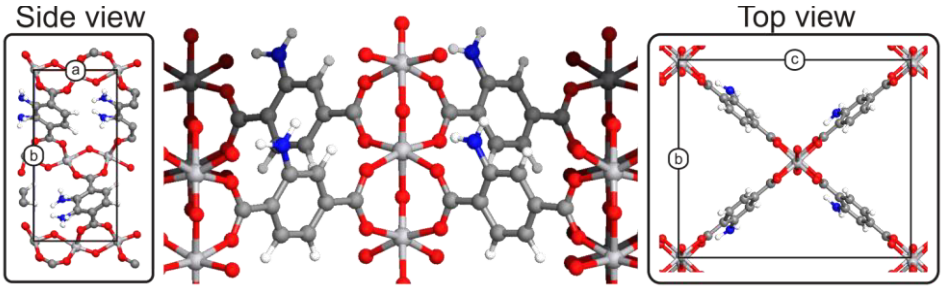

Fig. 4.1. Side, front and top view of the structure of NH_2-MIL-47.

To the best of our knowledge, amino functionalized MIL-47 has not yet been investigated. As can be seen from Fig. 4.1, NH_2-MIL-47 has a three-dimensional framework, where each V^{+IV} center is coordinated to four oxygen atoms from four carboxylate groups, and to two oxygen atoms on the O–V–O axis, thus forming a saturated octahedral coordination node. In the previous chapter it was already shown that the parent MIL-47 possesses good catalytic properties. Additionally MIL-47 displays also good adsorption properties [16-21].
In this chapter, the synthesis and the characterization of the amino functionalized V-MOF with MIL-47 topology is reported. The CO_2 and CH_4 adsorption properties of this NH_2-MIL-47 have been investigated and are compared to the parent MIL-47. Theoretical modeling can assist us in explaining the differences observed in adsorption behaviour between both materials.

4.2 Results and discussion

4.2.1 Structure analysis

XRPD measurements (Bragg-Brentano configuration) of both V-MOFs were executed. Based on the obtained XRPD spectra the corresponding d-spacings were calculated. The comparison between both samples together with the lines calculated from the MIL-47 structure as published by Barthelet et al.[22] (shown in grey) is presented in Fig. 4.2.

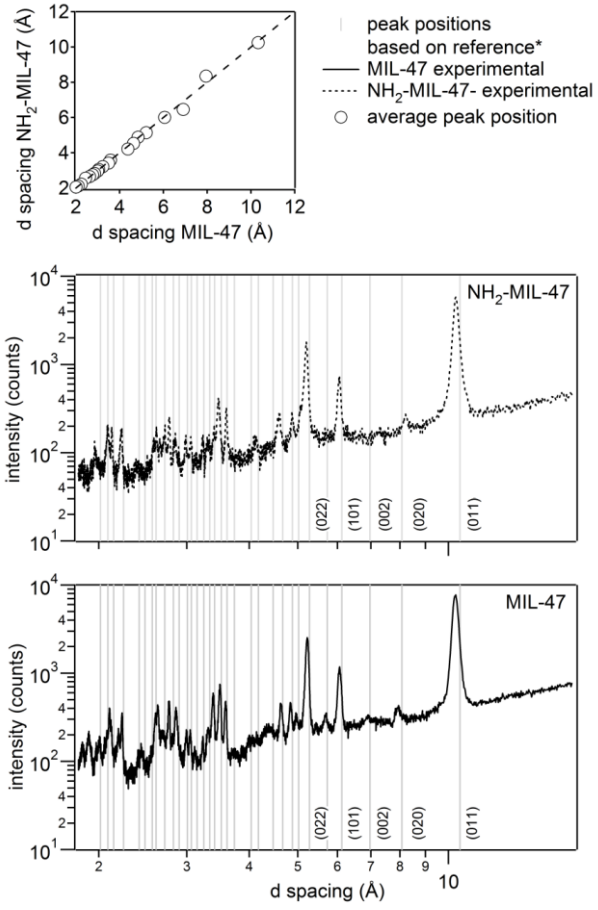

Fig.4.2. Calculated d-spacings for MIL-47 and NH_2-MIL-47 (*reference[22]).

Detailed analysis of both spectra shows that 20 of 21 lines of the modified MIL-47 structure correspond (within the error of the measurement) with the MIL-47 lines for which 26 lines were detected. This nice agreement is shown in Fig. 4.2 (top).
From this XRPD analysis one can conclude that the molecular structure of the modified MIL-47 is very similar with the original MIL-47 structure. The addition of the amino group hardly influences the molecular structure. The *as*-synthesized sample is formulated as $V^{+III}OH(C_8H_5NO_4)\ x(C_8H_7NO_4)$ (x~0.58) on the basis of the elemental analysis (calcd: C 43.11, H 2.88, N 6.28; found: C 43.10, H 2.86, N 6.39). After exchange with DMF, the elemental formula is $V^{+IV}O(C_8H_5NO_4)$ denoted as NH_2-MIL-47.

4.2.2 Thermal behaviour

To examine the thermal stability of NH_2-MIL-47, a TGA experiment has been carried out with a heating rate of 2°C/min in air. The resulting TGA curve is shown in Fig.4.3. Prior to this measurement the sample was dried under vacuum to remove DMF and H_2O molecules.

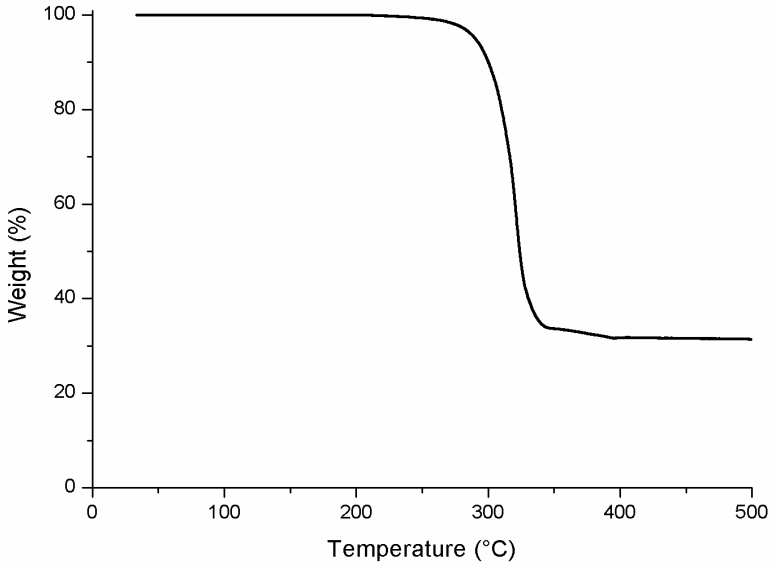

Fig.4.3. TGA curve of NH_2-MIL-47 obtained under an air flow with a heating rate of 2°C/min.

As can be seen from this figure, the first and only weight loss starts at 280°C, indicating that the V-MOF is stable up to 280 °C. Afterwards, the framework starts to decompose. The thermostability is in agreement with the earlier reported MIL-47 [22]. Thus, the introduction of functional groups does not influence the thermal stability. Moreover, we can conclude that the pretreatment step was successful to remove occluded guest molecules.

4.2.3 N_2 sorption measurements

Major efforts have been done to find the appropriate pretreatment of the V-MOF. An exchange procedure in DMF has been optimized to remove unreacted linkers and to obtain the highest surface area without loss of the integrity of the framework. The results of the exchange procedure are summarized in Table 4.1.

Table 4.1 Optimization of the exchange procedure in DMF for NH_2-MIL-47.

Time (minutes)	Exchange temperature (°C)	Langmuir surface area (m^2/g)
90	150	572
240	150	-
60	100	287
90	100	280
60	125	257
90	125	672
150	125	647
180	125	386

The optimal surface area was obtained at an exchange temperature of 125 °C during 90 minutes. Exchange experiments at 150 °C caused already significant structural damage. If the exchange experiment was carried out at 150 °C for 240 minutes the MOF structure was completely dissolved. However, at a lower temperature (100 °C), we were unable to completely remove the free linker from the pores. Longer exchange times at this temperature gave no improvement.

An exchange temperature of 125 °C for 90 minutes gave the highest surface area without structural damage, whereas a longer exchange time at 125 °C led already to damage of the structure. Furthermore, the presence of water and long exposure times to ambient conditions (in absence of any solvent) should be avoided as gradual decomposition will take place. The Langmuir surface area of MIL-47 was approximately 1200 m^2/g, which was comparable to the value reported in literature [22]. The isotherms of MIL-47 and the optimized NH_2-MIL-47 are shown in Fig.4.4.

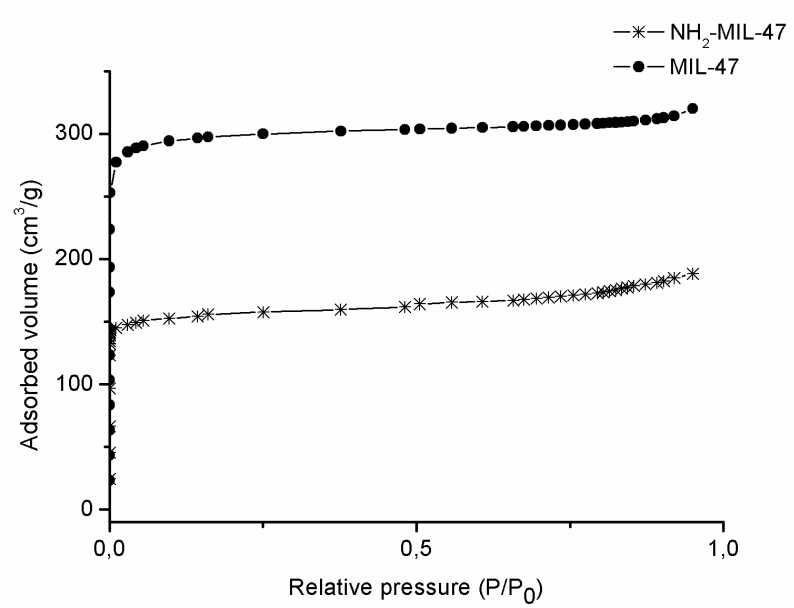

Fig. 4.4. Nitrogen adsorption isotherms of MIL-47 and NH_2-MIL-47.

4.2.4 Determination of the oxidation state

EPR measurements were performed to determine the oxidation state of the V in NH_2-MIL-47 *as* and NH_2-MIL-47. The measurements were carried out with a rectangular High Temperature EPR Cavity (HTC). In Fig. 4.5, the spectra of both samples are shown.

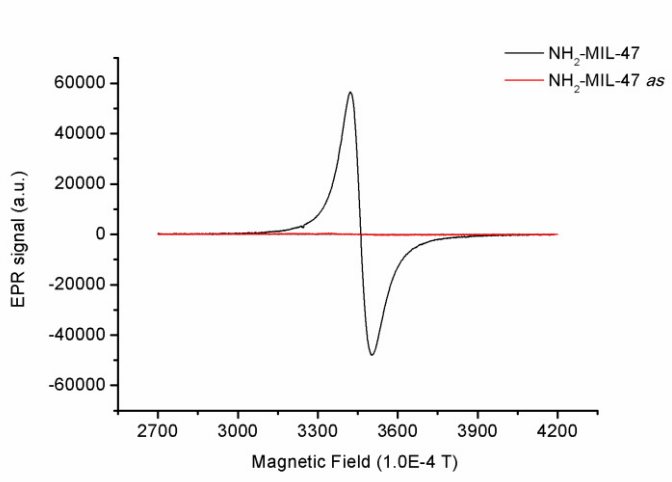

Fig. 4.5. EPR X-band spectrum of NH_2-MIL-47 *as* (red) and NH_2-MIL-47 (black).

As expected, the NH_2-MIL-47 *as* spectrum does not show any signal due to V^{+IV}. From this observation one can conclude that the metal is in the +III oxidation state. On the other hand, a manifest signal is observed in the NH_2-MIL-47 spectrum which can be attributed to V^{+IV}. The latter is the result of the exchange procedure in DMF. In the recent report of Leclerc et al. it was already suggested that the presence of DMF molecules could oxidize the V center in MIL-47 [16]. Moreover both observations are in agreement with the proposed structural formula obtained from elemental analysis. In addition, XPS measurements were performed (Fig.4.6). The binding energy for a V $^2p_{3/2}$ peak in NH_2-MIL-47 is observed at 516.8 eV. This coincides with the spectrum for MIL-47 (BE: 516.8 eV) and $VO(acac)_2$ (BE: 516.2 eV) both known as V^{+IV} [22, 23].

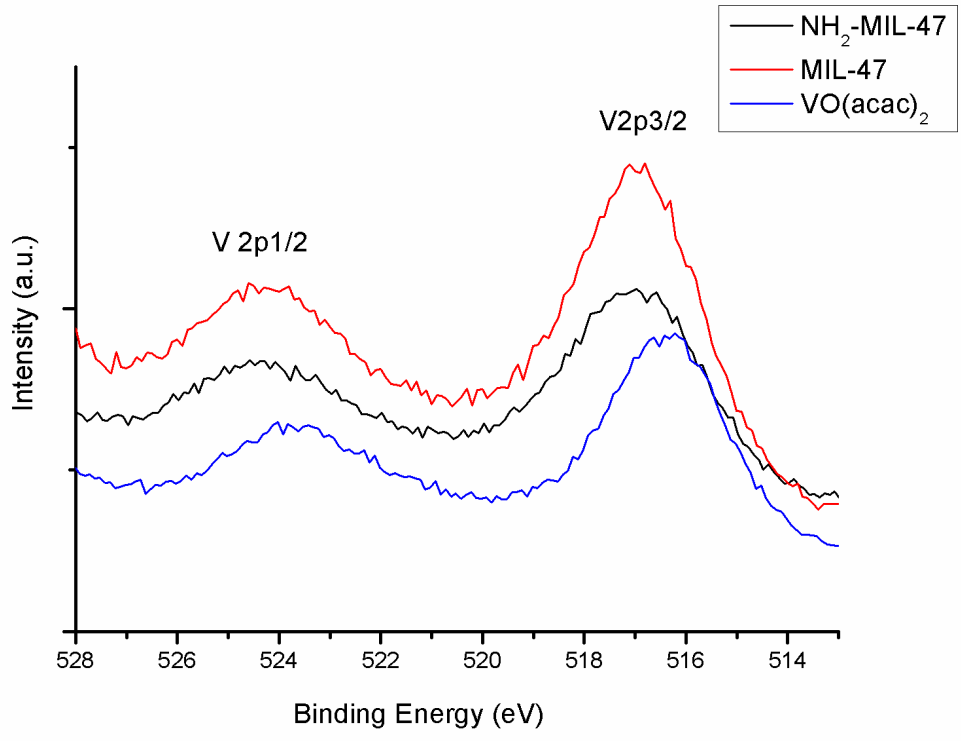

Fig.4.6. XPS spectra of V $^{2}p_{3/2}$ and V $^{2}p_{1/2}$ region of MIL-47, NH_2-MIL-47 and $VO(acac)_2$.

4.2.5 IR and SEM measurements

In Fig. 4.7, the DRIFT spectrum is shown of NH_2-MIL-47 *as* and NH_2-MIL-47. A distinct difference between both spectra, is the broad band at around 3630-3680 cm^{-1}, which is only present in the *as*-synthesized sample. This band corresponds to the stretching vibration of the μ_2-OH group and the free OH groups of the trapped linker [24]. This clearly demonstrates the complete removal of free linker after the optimized exchange procedure.

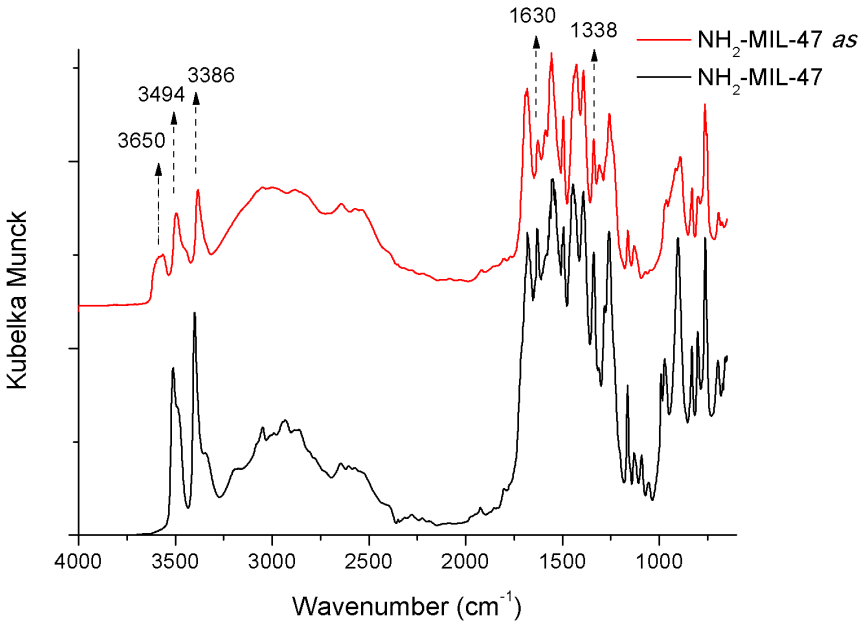

Fig.4.7. DRIFT spectrum of NH_2-MIL-47 *as* (shown in red) and NH_2-MIL-47 (shown in black).

The doublet at 3494 and 3386 cm^{-1} corresponds to the asymmetrical and symmetrical stretching of the amine groups, the vibration at 1630 cm^{-1} can be attributed to the N-H bending (scissoring) vibration. The C-N stretching absorption of the aromatic amines is located at 1338 cm^{-1} [25, 26]. Typical vibrations, due to the benzene linker can be observed: 1510-1450 cm^{-1} (aromatic ring stretch), 1225-950 cm^{-1} (aromatic C-H in plane bend) and 900-670 cm^{-1} (aromatic C-H out of plane bend) [27]. The vibrations in the region 1597-1616 cm^{-1} and 1415-1463 cm^{-1} can be assigned to the asymmetric and symmetric $-CO_2$ stretching vibrations respectively [28].

In Fig. 4.8, the SEM pictures of the materials obtained *via* microwave and autoclave procedure are presented. It can be seen that the structure, crystal size and morphology of the materials obtained *via* both synthesis routes are very similar (Fig. 4.8a en Fig. 4.8c). There are no significant changes observed of the materials after the exchange procedure (Fig. 4.8b and Fig. 4.8d) compared to the non treated sample. It is hard to give an exact size of the crystals because of the very broad crystal size distribution.

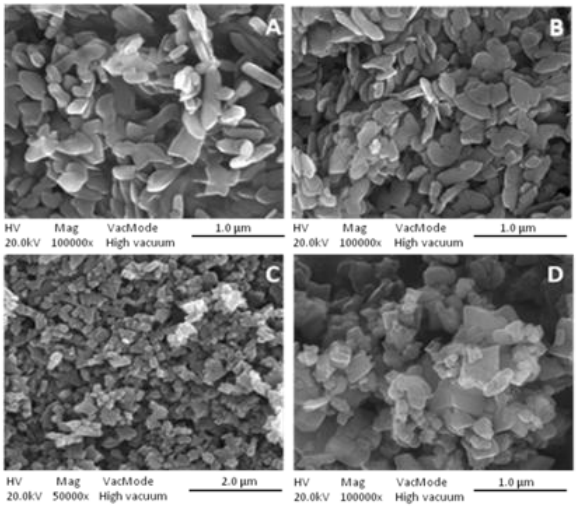

Fig.4.8. SEM pictures of NH_2-MIL-47 (a) synthesized via autoclave (b) after exchange via autoclave synthesis (c) synthesized via microwave (d) after exchange via microwave synthesis.

4.2.6 Adsorption tests: experimental and computational results

Adsorption isotherms of CO_2 and CH_4 on MIL-47 and NH_2-MIL-47 are displayed in Fig. 4.9. The presently obtained isotherms for CO_2 and CH_4 on MIL-47 show a somewhat lower capacity than was previously reported. Literature specifies a capacity for CO_2 and CH_4 of 10.1 and 5.5 mmol/g respectively, compared to 7.7 and 4.1 mmol/g obtained here [20, 29]. This difference should be attributed to differences in preparation methods and sample pretreatment, resulting in different micropore volumes. Calculated micropore volume for this material is 0.40 ml/g while for MIL-47 in literature it is 0.46 ml/g [22].

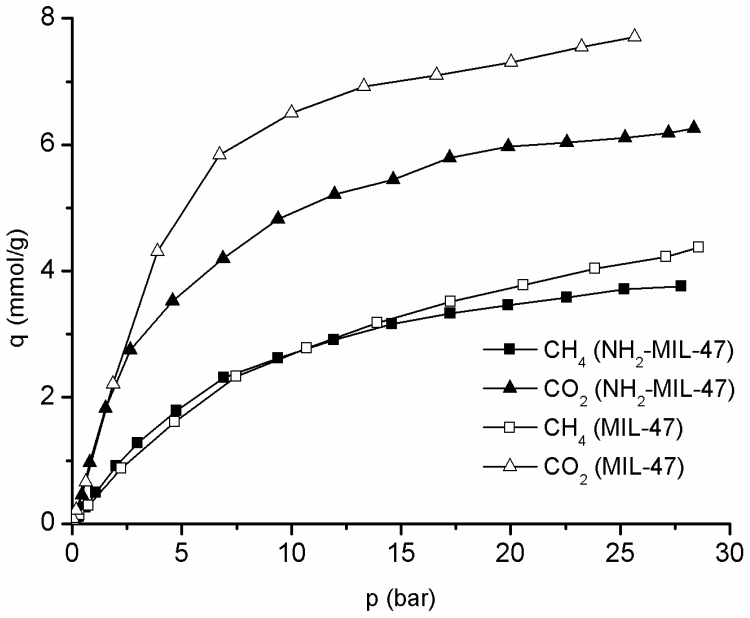

Fig. 4.9. Adsorption isotherms of CO_2 and CH_4 on MIL-47 (open symbols) and NH_2-MIL-47 (closed symbols) at 30 °C.

An interesting observation is the decrease in capacity (per gram adsorbent) for the amino version of the material, corresponding to 20% for CO_2 and 10% for CH_4 at 25 bar. This is in agreement with other amino functionalized MOFs [10, 12] where a capacity drop has also taken place per mass of sample. The presence of free-standing amino-groups in the pores results in a decrease in available pore volume. Even more interesting is that the isotherms on both materials completely coincide in the low-pressure regime; thus the presence of $–NH_2$ groups does not result in a significant increase in affinity for CO_2 or CH_4. This is confirmed by low coverage pulse-chromatography experiments. As shown in Table 4.2, adsorption enthalpies, Henry adsorption constants and separation factors of CO_2 and CH_4 are comparable on both materials. This strongly differs from what is observed with the MIL-53(Al) material, where functionalization with $–NH_2$ groups results in an increase in CO_2 adsorption enthalpy of 18 kJ/mol and a multiplication of the CO_2/CH_4 separation factor by orders of magnitude [12].

This is related to the structure of the materials. Pore size in the low coverage area can be estimated by using the pulse gas chromatographic technique[30]. In the paper of Couck et al. it was shown that the MIL-53 structure is probably in the large pore (lp) form when performing low coverage experiments [31] while NH_2-MIL-53 has narrower pores in this low coverage region[31, 32]. The narrower pore size is the reason for the higher adsorption enthalpy present in NH_2-MIL-53. As for MIL-47, it is known that this material does not show a flexible behaviour in the present experimental conditions, meaning that MIL-47 and MIL-53 have the same adsorption properties in the low coverage domain. Also NH_2-MIL-47 does not show flexibility and as a consequence behaves the same as its parent material MIL-47.

Table 4.2. Adsorption enthalpy (ΔH), Henry constant (K') at 30 °C of CO_2 and CH_4 and zero coverage separation factor ($\alpha_{K'}$) defined as the ratio of Henry adsorption constants of CO_2 over CH_4

	ΔH (kJ/mol)		K' (mol/kg/Pa)		$\alpha_{K'}$
	CO_2	CH_4	CO_2	CH_4	
MIL-47	-17.8	-11.1	$1.19\ 10^{-5}$	$4.68\ 10^{-6}$	2.5
NH_2-MIL-47	-22.0	-13.0	$9.83\ 10^{-6}$	$2.65\ 10^{-6}$	3.7

Finally, the adsorption behaviour of the parent MIL-47 and functionalized form of MIL-47 was evaluated in breakthrough adsorption experiments, in which CO_2/CH_4 mixtures of different composition, at a total pressure of 1 bar, were separated. Fig. 4.10 shows the amount of adsorbed CO_2 and CH_4 and the separation factor as a function of mixture composition. Capacity (per mass) for both CO_2 and CH_4, is slightly lower on NH_2-MIL-47 than on MIL-47. Again the selectivity, calculated from the breakthrough experiments, is comparable on both materials and is also in good agreement with the Henry selectivity (Table 4.2).

In addition to the experiments, the adsorption strength of CH_4 and CO_2 within the materials MIL-47 and NH_2-MIL-47 is investigated theoretically. Ramsahye et al. studied the adsorption behaviour of CO_2 in the unsubstituted materials MIL-53(Al,Cr) and MIL-47(V).

By means of periodic DFT calculations on the MIL-47(V) they concluded that there are no preferential adsorption sites for CO_2[33]. In a second publication, previous authors used grand canonical monte carlo simulations to study the adsorption mechanism. These simulations were based on partial atomic charges extracted from periodic DFT calculations and interatomic potentials between the adsorbate and host framework[34]. Simulation of adsorption phenomena can indeed be performed using molecular dynamics and Monte Carlo simulations with suitable force fields providing us information on the distribution on the position of adsorbates within the framework and giving average adsorption data. The derivation of a proper force field is a non-trivial task and is beyond the scope of this study. This is especially true for the derivation of polarisable force fields which are not standard available[35, 36].

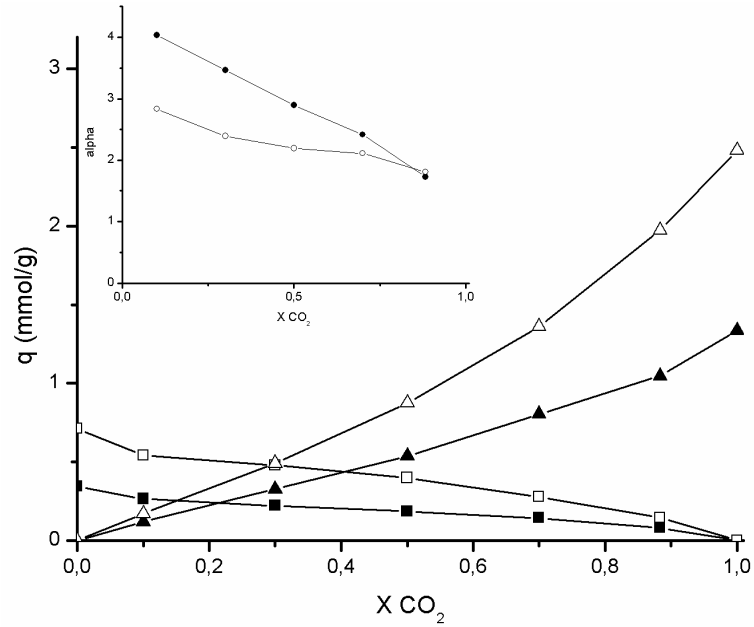

Fig. 4.10. Adsorption capacity for NH_2-MIL-47 (closed symbols: q CH_4 (■) and q CO_2 (▲)) and MIL-47 (open symbols: q CH_4 (□) and q CO_2 (△)). In the inset the selectivity for MIL-47 (○) and NH_2-MIL-47 (●) obtained via breakthrough experiments at 30 °C and a total pressure of 1 bar is shown.

Herein, we performed static calculations, based on DFT and complemented with dispersion corrections, to study the qualitative differences between adsorbate-host interactions. The computational protocol is outlined in section 4.4.3. A large number of adsorption structures has been investigated in the finite cluster model in order to determine the most stable configuration of the absorbate with respect to the linker. The most favorable positions are displayed in Fig.4.11 both for CH_4 and CO_2. The amino group has the largest effect on the position of the CO_2 adsorbate. The polar character of CO_2 lies at the origin of a stronger electrostatic attractive interaction between the adsorbate carbon and the negative charge of the nitrogen.

The electronic adsorption energy ΔE and adsorption enthalpy ΔH_{30} at 30 °C for both the terephthalic linkers and full periodic MIL-47 type materials are tabulated in Table 4.3. For both adsorbates the adsorption is stronger for the amino functionalized linker and CO_2 is more adsorbed than CH_4 by about 7 kJ/mol. Qualitatively this is in nice agreement with the experiment (Table 4.2). When taking into account the full topology of the MIL-47 the qualitative differences between CO_2 and CH_4 remain nearly the same, although overall the guest molecules are stronger adsorbed. This is probably the result of additional dispersion interactions between the adsorbate and the other linkers in the framework. For the periodic calculations the adsorption enthalpies have not been calculated in view of the difficulties encountered in the VASP calculations to obtain positive frequencies. To get an idea about the position of the CO_2 adsorbate in the periodic structure we refer to Fig. 4.12. Compared to the geometry obtained using the small cluster calculations CO_2 now takes a configuration in between the amino group of the one linker and the aromatic nucleus of another linker.

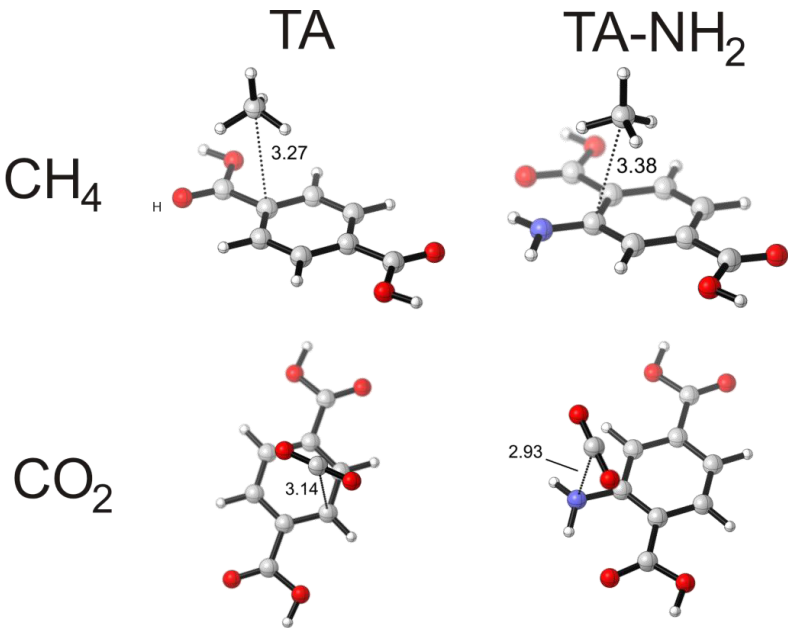

Fig. 4.11. Overview of the most stable adsorption positions of CO_2 and CH_4 on terephthalic acid (TA) and 2-aminoterephthalic acid (TA-NH_2) (cluster model). Shortest distances between the carbon of the adsorbate and the nearest linker atom are displayed in Ångström.

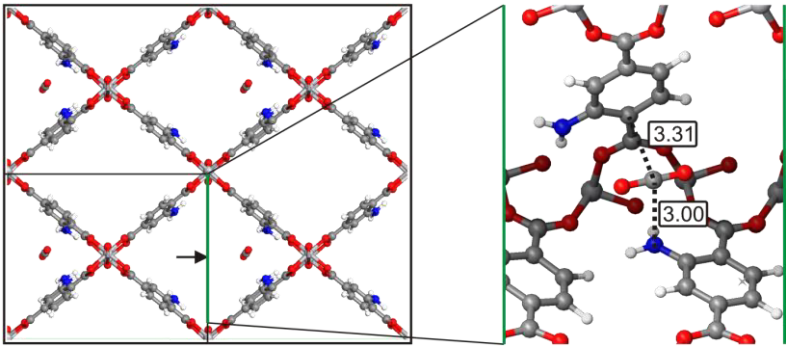

Fig.4.12. Most stable adsorption position of CO_2 in the periodic structure of NH_2-MIL-47. Distances displayed in Ångström.

Table 4.3. Calculated electronic adsorption energy (ΔE in kJ/mol) and adsorption enthalpy at 30 °C (ΔH_{30} in kJ/mol). Unit cell parameters in the periodic calculations have been optimized for the parent MIL-47 and for the NH_2-MIL-47 (NH_2-TA represents the 2-aminoterephthalic acid linker and TA the terephthalic acid linker)

	ΔE (kJ/mol)		ΔH_{30} (kJ/mol)	
	CO_2	CH_4	CO_2	CH_4
TA	-13.3	-11.0	-9.8	-5.9
NH_2-TA	-19.1	-12.4	-14.8	-7.2
MIL-47	-24.7	-13.2	-	-
NH_2-MIL-47	-25.6	-14.5	-	-

Summarizing, we have shown that the experimental adsorption enthalpies obtained from pulse chromatographic experiments (Table 4.2) follow the same trend as the corresponding adsorbate-linker interactions. Also within the framework, our geometrically similar adsorption spots show the same trend. We can thus conclude that the difference in linker-adsorbate interaction is the driving force between CO_2/CH_4 separation within MIL-47 and MIL-47-NH_2 rather than an interaction with the amino groups.

On specific MOFs, presence of NH_2 indirectly enhances CO_2 adsorption. In particular, for NH_2-MIL-53(Al), the amino groups play a key role in framework flexibility, and lead to the closure of the NH_2-MIL-53(Al) pores, hereby enhancing CO_2 adsorption due to stronger aspecific interactions on the one hand and exclusion of CH_4 molecules on the other hand [13]. Since MIL-47 and NH_2-MIL-47 are rather rigid and non-flexible, presence of amino groups does not result in pore contraction, and accordingly not in an increase in CO_2 affinity either.

4.3 Conclusions

An amino functionalized V-MOF, with MIL-47 topology, has been successfully synthesized via both autoclave and microwave enhanced irradiation. The NH_2-MIL-47 shows a similar thermal stability in comparison to the parent MIL-47, decomposing in one step at 280 °C. An optimization of the exchange procedure in DMF was performed, resulting in a Langmuir surface area of approximately 672 m^2/g.

CO_2 and CH_4 adsorption measurements have shown that the presence of additional NH_2 groups does not have a beneficial effect on the adsorption properties, which was also confirmed by the theoretical modeling results. For the NH_2-MIL-47, both experiment and theory clearly show that the amination of the linker does not result in an increased adsorption capacity per mass of adsorbent, nor in an increased CH_4/CO_2 separation factor. The slight increase in adsorption enthalpy for the NH_2-MIL-47 does not compensate for the loss in pore volume compared to the parent MIL-47. Contrary to other MOFs, the NH_2-MIL-47 and the MIL-47 are not triggered into breathing behaviour at the experimental conditions.

4.4 Experimental Section

4.4.1 Synthesis of NH_2-MIL-47 and MIL-47

NH_2-MIL-47 *as* has been synthesized in 2 possible manners. The first route was carried out in an autoclave. The molar ratio of VCl_3/ 2-aminoterephthalic acid/ H_2O was 1/1/100. Typically 9 mmol vanadium(III)chloride and 9 mmol 2-aminoterephthalic acid were mixed in a Teflon insert with 16.60 mL H_2O and placed in an autoclave for 4 days at 150 °C. Moreover, to accelerate the synthesis time, a procedure under microwave irradiation has been developed. For the microwave assisted synthesis 1.7 mmol VCl_3 was mixed with 1.7 mmol 2-aminoterephthalic acid in 3.02 mL H_2O. The reaction was carried out at 150 °C for 20 minutes, reducing the synthesis time significantly from 4 days to 20 minutes without loss in crystallinity. In a second step, an exchange procedure in DMF at 125 °C has been done for 90 minutes to remove unreacted linker. MIL-47 was synthesized according to the synthesis route described in the previous chapter.

4.4.2 Adsorption tests

Adsorption isotherms of pure CO_2 (purity of 99,99%) and CH_4 (purity of 99,95%) were determined at 30 °C, using the volumetric technique. About 0.5 g of MIL-47 or NH_2-MIL-47 was loaded in the sample container. Prior to the measurement the sample was out-gassed by heating it up to 80 °C under vacuum.

Breakthrough experiments have been performed using a column with a length of 30 cm and an internal diameter of 0.216 cm packed with 600 mg of MOF pellets. Pellets were obtained by pressing the powder to a solid disk, crushing the disk followed by sieving to the desired fraction of 500-630 μm. The adsorption capacity was calculated via the method of *Malek and Farooq (1996)* [37]. The same column was used for obtaining pulse gas chromatographic (pulse GC) data, i.e. Henry constants and adsorption enthalpies of CO_2 and CH_4. More details of this technique are reported elsewhere [38].

4.4.3 Computational details

The computational study comprises two types of ab initio calculations: first non-periodic cluster calculations to obtain initial insight into the active site of adsorption on the terephthalic linkers with and without amino functionalization. Secondly periodic calculations on the parent MIL-47 and NH_2-MIL-47 were done. The cluster geometries were optimized with the Gaussian09 package [39] using Density Functional Theory (DFT) with the hybrid M06-2X functional [40, 41] to study the initial adsorption of CH_4 and CO_2 on both linkers. This functional is the best choice to quantify the interactions of CH_4 and CO_2 with the organic linkers because it is utilized especially for medium range non-covalent interactions. The double-zeta Pople basis set 6–311+g(d,p) was applied. The optimized clusters were confirmed to be true minima on the potential energy surface by performing a vibrational frequency analysis, which confirmed that only positive frequencies were present. Afterwards, van der Waals corrections for the M06-2X functional were added to the energy [42 43]. The thermal corrections were added to the energy to determine the enthalpy, by an in-house developed software module TAMkin [44].
Secondly, the adsorbate molecules CH_4 and CO_2 were placed within the periodic V-MOF structures, in a position which corresponds to the most optimal geometries obtained with the cluster calculations. The geometry of the periodic system with inclusion of the guest molecules has been optimized by means of the Vienna Ab Initio Simulation Package (VASP) [45-48] making use of the PBE exchange correlation functional [49, 50]. In order to prevent self interactions between the adsorbates in neighbouring cells the unit cell has been doubled along the a direction.

The orientation of the amino group on the linkers is taken as in the crystallographic structure of NH_2-MIL-53(Fe) as reported in ref [24].

4.5 References

1. H. Y. Huang, R. T. Yang, D. Chinn and C. L. Munson, *Ind Eng Chem Res*, 2003, **42**, 2427-2433.
2. N. Hiyoshi, K. Yogo and T. Yashima, *Micropor Mesopor Mat*, 2005, **84**, 357-365.
3. Y. Belmabkhout, R. Serna-Guerrero and A. Sayari, *Ind Eng Chem Res*, 2010, **49**, 359-365.
4. C. Chen, W. J. Son, K. S. You, J. W. Ahn and W. S. Ahn, *Chem Eng J*, 2010, **161**, 46-52.
5. V. Zelenak, M. Badanicova, D. Halamova, J. Cejka, A. Zukal, N. Murafa and G. Goerigk, *Chem Eng J*, 2008, **144**, 336-342.
6. A. C. C. Chang, S. S. C. Chuang, M. Gray and Y. Soong, *Energ Fuel*, 2003, **17**, 468-473.
7. J. R. Karra and K. S. Walton, *J Phys Chem C*, 2010, **114**, 15735-15740.
8. A. R. Millward and O. M. Yaghi, *J Am Chem Soc*, 2005, **127**, 17998-17999.
9. B. Arstad, H. Fjellvag, K. O. Kongshaug, O. Swang and R. Blom, *Adsorption*, 2008, **14**, 755-762.
10. P. Serra-Crespo, E. V. Ramos-Fernandez, J. Gascon and F. Kapteijn, *Chem Mater*, 2011, **23**, 2565-2572.
11. W. Morris, B. Leung, H. Furukawa, O. K. Yaghi, N. He, H. Hayashi, Y. Houndonougbo, M. Asta, B. B. Laird and O. M. Yaghi, *J Am Chem Soc*, 2010, **132**, 11006-11008.
12. S. Couck, J. F. M. Denayer, G. V. Baron, T. Remy, J. Gascon and F. Kapteijn, *J Am Chem Soc*, 2009, **131**, 6326-+.
13. E. Stavitski, E. A. Pidko, S. Couck, T. Remy, E. J. M. Hensen, B. M. Weckhuysen, J. Denayer, J. Gascon and F. Kapteijn, *Langmuir*, 2011, **27**, 3970-3976.
14. T. Lescouet, E. Kockrick, G. Bergeret, M. Pera-Titus and D. Farrusseng, *Dalton T*, 2011, **40**, 11359-11361.
15. T. K. Trung, I. Deroche, A. Rivera, Q. Y. Yang, P. Yot, N. Ramsahye, S. D. Vinot, T. Devic, P. Horcajada, C. Serre, G. Maurin and P. Trens, *Micropor Mesopor Mat*, 2011, **140**, 114-119.
16. H. Leclerc, T. Devic, S. Devautour-Vinot, P. Bazin, N. Audebrand, G. Ferey, M. Daturi, A. Vimont and G. Clet, *J Phys Chem C*, 2011, **115**, 19828-19840.

17. K. Leus, I. Muylaert, M. Vandichel, G. B. Marin, M. Waroquier, V. Van Speybroeck and P. Van der Voort, *Chem Commun*, 2010, **46**, 5085-5087.
18. A. Phan, A. U. Czaja, F. Gandara, C. B. Knobler and O. M. Yaghi, *Inorg Chem*, 2011, **50**, 7388-7390.
19. N. A. Khan, J. W. Jun, J. H. Jeong and S. H. Jhung, *Chem Commun*, 2011, **47**, 1306-1308.
20. N. Rosenbach, A. Ghoufi, I. Deroche, P. L. Llewellyn, T. Devic, S. Bourrelly, C. Serre, G. Ferey and G. Maurin, *Phys Chem Chem Phys*, 2010, **12**, 6428-6437.
21. K. Leus, M. Vandichel, Y. Y. Liu, I. Muylaert, J. Musschoot, S. Pyl, H. Vrielinck, F. Callens, G. B. Marin, C. Detavernier, P. V. Wiper, Y. Z. Khimyak, M. Waroquier, V. Van Speybroeck and P. Van Der Voort, *J Catal*, 2012, **285**, 196–207.
22. K. Barthelet, J. Marrot, D. Riou and G. Ferey, *Angew Chem Int Edit*, 2001, **41**, 281-284.
23. B. Jarrais, A. R. Silva and C. Freire, *Eur J Inorg Chem*, 2005, 4582-4589.
24. T. Devic, P. Horcajada, C. Serre, F. Salles, G. Maurin, B. Moulin, D. Heurtaux, G. Clet, A. Vimont, J. M. Greneche, B. Le Ouay, F. Moreau, E. Magnier, Y. Filinchuk, J. Marrot, J. C. Lavalley, M. Daturi and G. Ferey, *J Am Chem Soc*, 2010, **132**, 1127-1136.
25. J. Gascon, U. Aktay, M. D. Hernandez-Alonso, G. P. M. van Klink and F. Kapteijn, *J Catal*, 2009, **261**, 75-87.
26. M. Kandiah, M. H. Nilsen, S. Usseglio, S. Jakobsen, U. Olsbye, M. Tilset, C. Larabi, E. A. Quadrelli, F. Bonino and K. P. Lillerud, *Chem Mater*, 2010, **22**, 6632-6640.
27. J. Coates, ed., *Interpretation of Infrared Spectra, A Practical Approach*, 2000.
28. T. Loiseau, C. Serre, C. Huguenard, G. Fink, F. Taulelle, M. Henry, T. Bataille and G. Ferey, *Chem-Eur J*, 2004, **10**, 1373-1382.
29. S. Bourrelly, P. L. Llewellyn, C. Serre, F. Millange, T. Loiseau and G. Ferey, *J Am Chem Soc*, 2005, **127**, 13519-13521.
30. J. F. M. Denayer and G. V. Baron, *Adsorption*, 2005, **11**, 85-90.
31. S. Couck, T. Remy, G. V. Baron, J. Gascon, F. Kapteijn and J. F. M. Denayer, *Phys Chem Chem Phys*, 2010, **12**, 9413-9418.
32. S. Couck, E. Gobechiya, C. E. A. Kirschhock, P. Serra-Crespo, J. Juan-Alcaniz, A. M. Joaristi, E. Stavitski, J. Gascon, F. Kapteijn, G. V. Baron and J. F. M. Denayer, *Chemsuschem*, 2012, **5**, 740-750.
33. N. A. Ramsahye, G. Maurin, S. Bourrelly, P. L. Llewellyn, C. Serre, T. Loiseau, T. Devic and G. Ferey, *J Phys Chem C*, 2008, **112**, 514-520.

34. N. A. Ramsahye, G. Maurin, S. Bourrelly, P. L. Llewellyn, T. Devic, C. Serre, T. Loiseau and G. Ferey, *Adsorption*, 2007, **13**, 461-467.
35. J. M. Castillo, T. J. H. Vlugt and S. Calero, *J Phys Chem C*, 2009, **113**, 20869-20874.
36. L. Vanduyfhuys, T. Verstraelen, M. Vandichel, M. Waroquier and V. Van Speybroeck, *J Chem Theory Comput*, 2012, **8**, 3217-3231.
37. A. Malek and S. Farooq, *J Chem Eng Data*, 1996, **41**, 25-32.
38. R. A. Ocakoglu, J. F. M. Denayer, G. B. Marin, J. A. Martens and G. V. Baron, *J Phys Chem B*, 2003, **107**, 398-406.
39. M. J. T. Frisch, G. W.; Schlegel, H. B.; Scuseria, G. E.; Robb, M. A.; Cheeseman, J. R.; Scalmani, G.; Barone, V.; Mennucci, B.; Petersson, G. A.; Nakatsuji, H.; Caricato, M.; Li, X.; Hratchian, H. P.; Izmaylov, A. F.; Bloino, J.; Zheng, G.; Sonnenberg, J. L.; Hada, M.; Ehara, M.; Toyota, K.; Fukuda, R.; Hasegawa, J.; Ishida, M.; Nakajima, T.; Honda, Y.; Kitao, O.; Nakai, H.; Vreven, T.; Montgomery, Jr., J. A.; Peralta, J. E.; Ogliaro, F.; Bearpark, M.; Heyd, J. J.; Brothers, E.; Kudin, K. N.; Staroverov, V. N.; Kobayashi, R.; Normand, J.; Raghavachari, K.; Rendell, A.; Burant, J. C.; Iyengar, S. S.; Tomasi, J.; Cossi, M.; Rega, N.; Millam, N. J.; Klene, M.; Knox, J. E.; Cross, J. B.; Bakken, V.; Adamo, C.; Jaramillo, J.; Gomperts, R.; Stratmann, R. E.; Yazyev, O.; Austin, A. J.; Cammi, R.; Pomelli, C.; Ochterski, J. W.; Martin, R. L.; Morokuma, K.; Zakrzewski, V. G.; Voth, G. A.; Salvador, P.; Dannenberg, J. J.; Dapprich, S.; Daniels, A. D.; Farkas, O.; Foresman, J. B.; Ortiz, J. V.; Cioslowski, J.; Fox, D. J. Gaussian 09, {R}evision {A}.02, Gaussian, Inc., Wallingford CT: , 2009.
40. Y. Zhao and D. G. Truhlar, *Theor Chem Acc*, 2008, **120**, 215-241.
41. Y. Zhao and D. G. Truhlar, *Accounts Chem Res*, 2008, **41**, 157-167.
42. S. Grimme, *J Comput Chem*, 2004, **25**, 1463-1473.
43. S. Grimme, J. Antony, S. Ehrlich and H. Krieg, *J Chem Phys*, 2010, **132**.
44. A. Ghysels, T. Verstraelen, K. Hemelsoet, M. Waroquier and V. Van Speybroeck, *J Chem Inf Model*, 2010, **50**, 1736-1750.
45. G. Kresse and J. Hafner, *Phys Rev B*, 1994, **49**, 14251-14269.
46. G. Kresse and J. Hafner, *Phys Rev B*, 1993, **47**, 558-561.
47. G. Kresse and J. Furthmuller, *Phys Rev B*, 1996, **54**, 11169-11186.
48. G. Kresse and J. Furthmuller, *Comp Mater Sci*, 1996, **6**, 15-50.
49. J. P. Perdew, K. Burke and M. Ernzerhof, *Phys Rev Lett*, 1996, **77**, 3865-3868.
50. J. P. Perdew, K. Burke and M. Ernzerhof, *Phys Rev Lett*, 1997, **78**, 1396-1396.

Chapter 5: Ti-functionalized NH_2-MIL-47: an effective and stable epoxidation catalyst

---

Abstract

In this chapter, the post-functionalization of NH_2-MIL-47 with $TiO(acac)_2$ to create a bimetallic oxidation catalyst is presented. The catalytic performance of this V/Ti-MOF was examined for the oxidation of cyclohexene using molecular oxygen as oxidant in combination with cyclohexanecarboxaldehyde as co-oxidant. A significantly higher cyclohexene conversion was observed for the bimetallic catalyst compared to the non-functionalized material. Moreover, the catalyst could be recycled at least 3 times without loss of activity and stability. No detectable leaching of V or Ti was noted. Electron paramagnetic resonance measurements were performed to monitor the fraction of V-ions in the catalyst in the +IV valence state. A reduction of this fraction by ~17% after oxidation catalysis is observed, which is in agreement with the general accepted mechanism for this type of reaction.

The results presented in this chapter were obtained in collaboration with the EMR research group of Ghent University who performed the EPR analysis.

The Solid State NMR measurements were performed by Dolores Esquivel (COMOC)

Thomas Bogaerts (COMOC/CMM) did the molecular modeling.

The results in this chapter are accepted for publication:

K. Leus, G. Vanhaelewyn, T. Bogaerts, Y. Y. Liu, D. Esquivel, F. Callens, G. B. Marin, V. Van Speybroeck, H. Vrielinck, P. Van Der Voort, *Ti-functionalized NH_2-MIL-47: an effective and stable epoxidation catalyst*, Catalysis Today, **accepted**

5.1 Introduction

In chapter 3, it was already shown that MIL-47, shows a remarkable catalytic activity in the liquid phase epoxidation of cyclohexene with TBHP as oxidant [1-3]. However, both the experimental results and theoretical calculations showed that the catalytic cycle starts with the breaking of at least one V-carboxylate bond to coordinate the peroxide. The structural defects created during this process contribute to the catalytic performance. Hence, a small amount of leaching was observed in the start of the catalysis. Our objective is to prevent leaching while maintaining or enhancing the catalytic performance by post-modification of the original MOF structure with a catalytic active and selective function. To the best of our knowledge, a Ti grafted V-MOF has not been reported so far. Nevertheless, bimetallic Ti-V catalysts are known to have a synergistic effect in oxidation catalysis [4].

In this chapter, a bimetallic V/Ti-MOF is presented via post-functionalization of the V-MOF, NH_2-MIL-47 with a Titanyl (IV) acetylacetonate complex (denoted as *NH_2-MIL-47 [Ti]* hereafter) (see Fig. 5.1). The obtained *NH_2-MIL-47 [Ti]* was examined in the oxidation of cyclohexene and was compared with the non-functionalized V-MOF as well as the homogeneous $TiO(acac)_2$ catalyst. Additionally regeneration and stability tests were carried out. In chapter 3, we used X-band (9.8 GHz) EPR measurements at RT to monitor the evolution in the fraction of V-ions of the MIL-47 in the paramagnetic +IV valence state[2]. A reduction of the V^{+IV} concentration by about 20% in the first few hours of reaction was observed, as a result of $V^{+IV} \rightarrow V^{+V}$ oxidation, confirming a radical parallel reaction pathway suggested by DFT calculations. In this chapter similar EPR experiments are performed in order to gain insight in the catalytic reaction mechanisms. In view of the absence of hyperfine (HF) structure in the spectra, the X-band measurements are complemented with Q-band experiments (34 GHz) and spectral simulations (Easyspin[5] library in Matlab®) in order to corroborate the assignment of the spectrum to V^{+IV}.

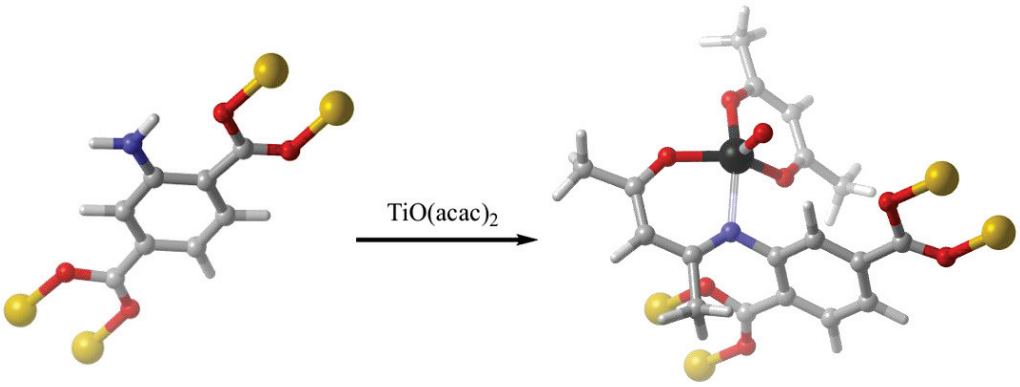

Fig. 5.1. Schematic representation of the post-functionalization of NH_2-MIL-47 with a Titanyl acetylacetonate complex (the carbon atoms are shown in grey, the oxygen atoms are depicted in red and the nitrogen, Ti and V atoms are shown in blue, black and yellow respectively).

5.2. Results and discussion

5.2.1 Characterization of the functionalized materials

5.2.1.1 XRPD analysis and determination of the Ti loading

By means of XRF the Ti loading was determined of the functionalized MOF materials (see Table 5.1). Approximately the same loading was obtained in each experiment, with an average of 1.25 mmol Ti/g, which indicates that almost 30% of the $–NH_2$ groups on the organic linker are modified. It should be noted that this loading is much higher compared to the earlier reported one step functionalization of $Mn(acac)_2$ on IRMOF-3, which was approximately 0.23 mmol Mn/g [6].

Table 5.1 Applied temperatures and reaction times during the grafting of $TiO(acac)_2$ onto NH_2-MIL-47 and the obtained Ti loading (mmol/g).

Sample	Temperature (°C)	Reaction time (h)	Ti (mmol/g)
NH_2-MIL-47 [Ti], 55°C,20h	55	20	1.21
NH_2-MIL-47 [Ti], 55°C,40h	55	40	1.25
NH_2-MIL-47 [Ti], 70°C,20h	70	20	1.26
NH_2-MIL-47 [Ti], 70°C,40h	70	40	1.21
NH_2-MIL-47 [Ti], 90°C,20h	90	20	1.38
NH_2-MIL-47 [Ti], 90°C,40h	90	40	1.31

Furthermore, the crystallinity of all the obtained Ti-grafted materials was verified by XRPD measurements (see Fig. 5.2). As can be seen from this figure, the XRPD pattern of each functionalized material presents the pure phase of the non-functionalized NH_2-MIL-47. This explicitly shows that the framework integrity of the parent MOF was well preserved during the post-functionalization.

5.2.1.2 DRIFTS, ^{13}C CP/MAS NMR and ^{1}H NMR measurements

DRIFTS, ^{13}C CP/MAS NMR and ^{1}H NMR measurements were carried out to verify if the $TiO(acac)_2$ complex was actually grafted onto the V-MOF. We selected the sample *NH_2-MIL-47 [Ti], 70°C, 20h*, for a detailed characterization and subsequent catalytic studies. In Fig. 5.3 the ^{13}C CP/MAS spectra of NH_2-MIL-47 and *NH_2-MIL-47 [Ti]* are presented. The ^{13}C CP/MAS spectrum of NH_2-MIL-47 gave several signals at 118, 125, 131 and 146 ppm associated with different sp^2 carbons of the organic linker and one peak at 171 ppm assigned to the carbonyl groups of the amino terephthalate linker[7]. In the non-functionalized NH_2-MIL-47 an additional signal at 162 ppm confirmed the not complete removal of solvent (DMF) used in the synthesis of the material. After functionalization, *NH_2-MIL-47[Ti]* showed new signals which corroborate the presence of the grafted $TiO(acac)_2$ complex on NH_2-MIL-47. An intense signal appeared at ca. 148 ppm.

As can be seen from Fig. 5.3 (inset 2), this signal could be deconvoluted into 3 peaks: the signal at 146 ppm corresponds to the C-N bond (non-functionalized material), whereas the signal at 147 and 149 ppm can be associated to the C-N and C=N groups of the bimetallic MOF respectively[7]. This clearly proves the success of the post-functionalization. Moreover, the *NH_2-MIL-47 [Ti]* showed several peaks in the aromatic region (120 – 130 ppm) and a new peak at ca. 191 ppm, which correspond to the C=C and C=O groups of the titanyl acetylacetonate complex, respectively[7]. The ^{1}H NMR spectrum (see Fig. 5.4) of the digested NH_2-MIL-47 *[Ti]* shows peaks at 2.06, 1.94 and 1.85 ppm due to the $-CH_3$ groups further confirming the presence of acac and imine-functionalized acac ligands grafted onto NH_2-MIL-47.

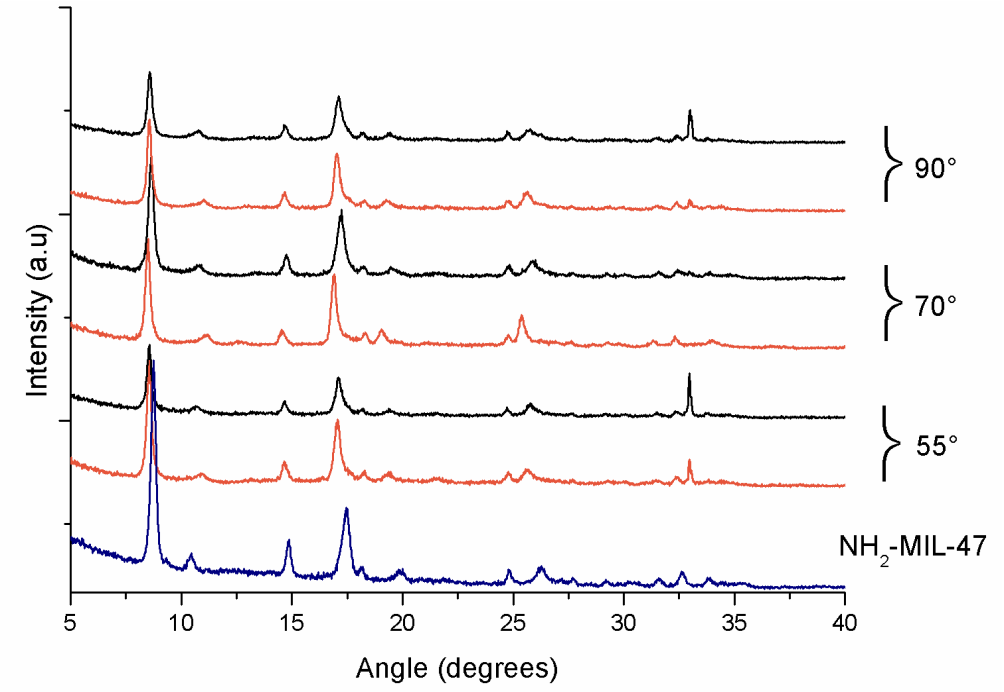

Fig. 5.2. XRPD pattern of NH_2-MIL-47 (blue) and the post functionalized *NH_2-MIL-47 [Ti]* materials, the *NH_2-MIL-47 [Ti]* stirred for 20 hours are shown in red and the samples stirred for 40 hours are depicted in black.

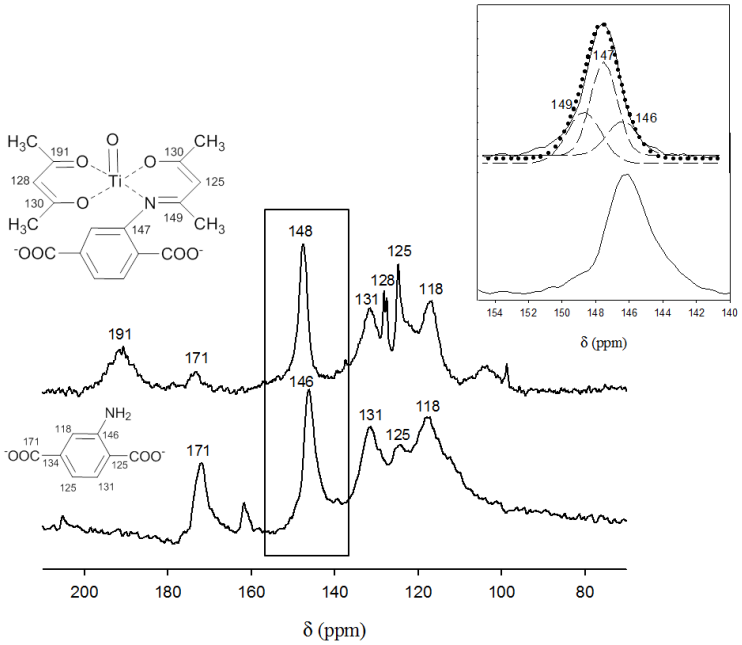

Fig.5.3. ^{13}C CP/MAS spectra of NH_2-MIL-47 and *NH_2-MIL-47 [Ti]*. **INSET 1**: detailed NMR spectrum of the signal at 148 ppm; **INSET 2**: deconvolution of the signal at 148 ppm.

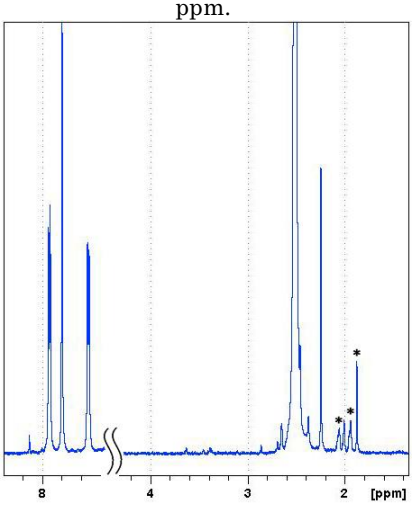

Fig. 5.4. ^1H spectrum of NH_2-MIL-47 *[Ti]*, the signals at 2.06, 1.94 and 1.85 ppm are indicated with an *.

Additionally the DRIFTS spectra of the NH_2-MIL-47 and *NH_2-MIL-47[Ti]*, 70°C, 20 h are shown in Fig. 5.5. From this figure it becomes clear that the characteristic vibrations of the parent MOF are still present. However, after the post-functionalization a decrease in intensity of some vibrations is observed, pointing toward a decrease of the -NH_2 groups. The typical vibrations of the benzene linker at 1510-1450 cm^{-1} (aromatic ring stretch), 1225-950 cm^{-1} (aromatic C-H in plane bend) and 900-670 cm^{-1} (aromatic C-H out of plane bend)[8] remain unchanged. Furthermore, the symmetric and asymmetric –CO_2 stretching vibrations in the region 1463-1415 cm^{-1} and 1616-1597 cm^{-1} are still present after grafting[9].

The principal changes in the spectrum before and after post-functionalization can be connected to the amine moiety. To obtain more insight in these changes, molecular modeling calculations were applied. The model of the catalyst was built by isolating the aromatic part of the linker with a $TiO(acac)_2$ substituent, as shown in Fig. 5.6. For comparison, the NH_2-MIL-47 was modelled as aniline. Only the relevant parts of the structure have been taken into account to calculate the spectra. Therefore, in both models the carboxylic acid group and its coordination with vanadium was not included since it would not contribute any relevant information to the calculated spectrum.
The vibrations at 1338 cm^{-1} (C-N stretch) and the doublet at 3494 cm^{-1} and 3386 cm^{-1} (NH_2 asymmetric and symmetric stretch) decrease in comparison to the non-functionalized V-MOF [10, 11]. Also the skeletal vibrations that contain NH_2 rocking at 1050 cm^{-1} and 1100 cm^{-1} decrease due to a partial modification of the amine groups. The presence of the $TiO(acac)_2$ modification can be seen by the vibrations at 735 cm^{-1} (C-C-H twisting) and 1026 cm^{-1} (C-CO-C wagging). The C=N vibration cannot be seen since it overlaps with the vibrations from the parent MOF between 1600 cm^{-1} and 1700 cm^{-1}. The new peak that appears at 1710 cm^{-1} could not be assigned with this model. This vibration could be due to free C=O vibrations, which are the consequence of some $TiO(acac)_2$ complexes that break during the post-functionalization. This would result in a ketone substituent which is not coordinated with titanium on the MOF.

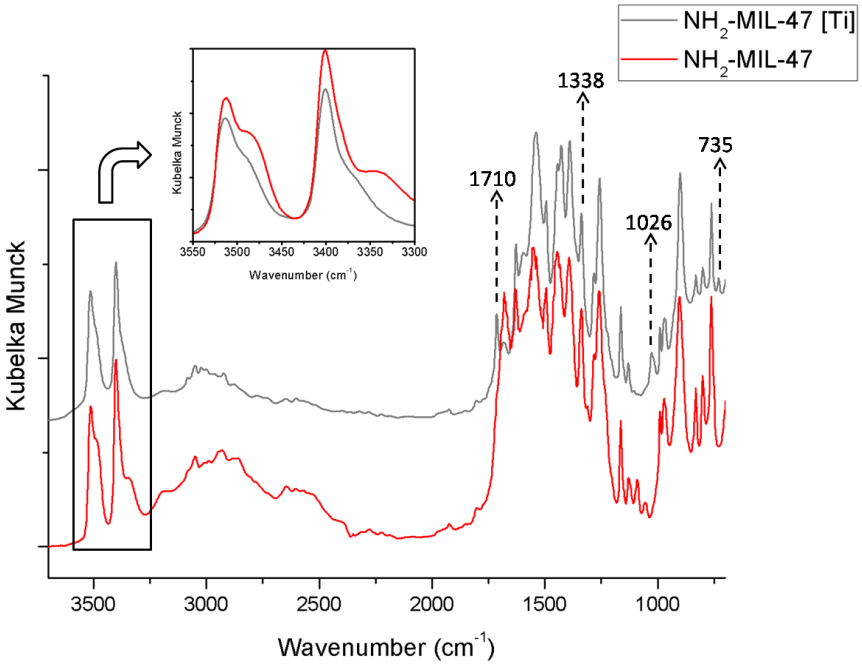

Fig. 5.5. DRIFTS spectra of NH_2-MIL-47 (shown in red) and *NH_2-MIL-47 [Ti], 70°C, 20 h* (shown in black) INSET: detailed DRIFTS spectra of both materials in the region 3550-3300 cm^{-1} (the spectra were normalized to the vibration at 800 cm^{-1} which corresponds to the aromatic C-H out of plane bend).

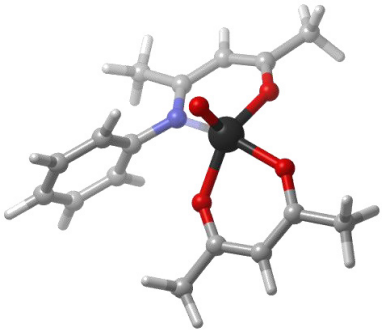

Fig. 5.6. Model used in the calculation of the IR vibrations after post-functionalization with the $TiO(acac)_2$ moiety (the C atoms are shown in grey, N atoms in blue, and the O and Ti atoms are depicted in red and black respectively).

5.2.1.3 Nitrogen sorption measurements

In Fig. 5.7 the nitrogen adsorption isotherms of NH_2-MIL-47 and *NH_2-MIL-47 [Ti], 70°C, 20h* are compared. The Langmuir surface area of the non-functionalized and post-functionalized material is 650 m^2/g and 190 m^2/g respectively. Despite the high loading of Ti (approximately 30 %), the post-functionalized MOF retains a partial porosity. In addition, the calculated pore volume of the parent and post-modified MOF is 0.30 ml/g and 0.10 ml/g respectively.

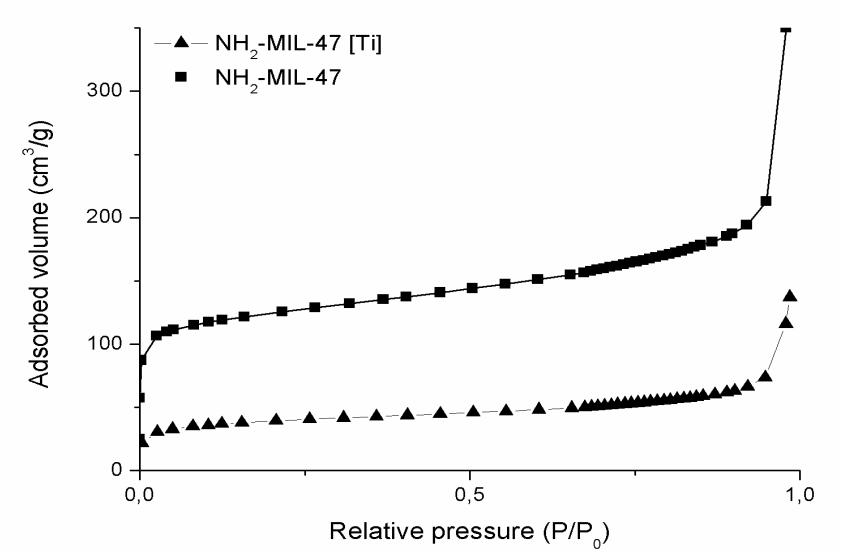

Fig. 5.7. Nitrogen adsorption isotherms of NH_2-MIL-47 and *NH_2-MIL-47 [Ti].*

5.2.2 Evaluation of the catalytic performance in the oxidation of cyclohexene.

The catalytic performance of NH_2-MIL-47 and *NH_2-MIL-47 [Ti], 70°C, 20h* was evaluated in the oxidation of cyclohexene. To make a fair comparison of both materials, the catalyst loading was chosen such that the number of V-sites was equal in the two experiments. Fig. 5.8 depicts the cyclohexene conversion and the detailed product distribution of both catalysts in the first run. Several features can be deduced from this figure.

(1) A cyclohexene conversion of approximately 14.1 % and 25 % is observed respectively for the non-functionalized and bimetallic material after 6 hours of reaction. This clearly shows that the bimetallic MOF exhibits a significantly higher catalytic performance than the (monometallic) V-MOF due to the presence of the extra active sites. (2) Moreover, faster conversion is observed for the bimetallic MOF. After 2 hours of reaction, 10 % of cyclohexene is already converted, whereas NH_2-MIL-47 shows only 6 % of conversion. (3) Finally, it can be noted that both materials show only 2 products: cyclohexene oxide and the radical product 2-cyclohexene-1-one, which are produced in almost equal amounts. This is in agreement with the proposed reaction mechanism (see section 5.2.5).

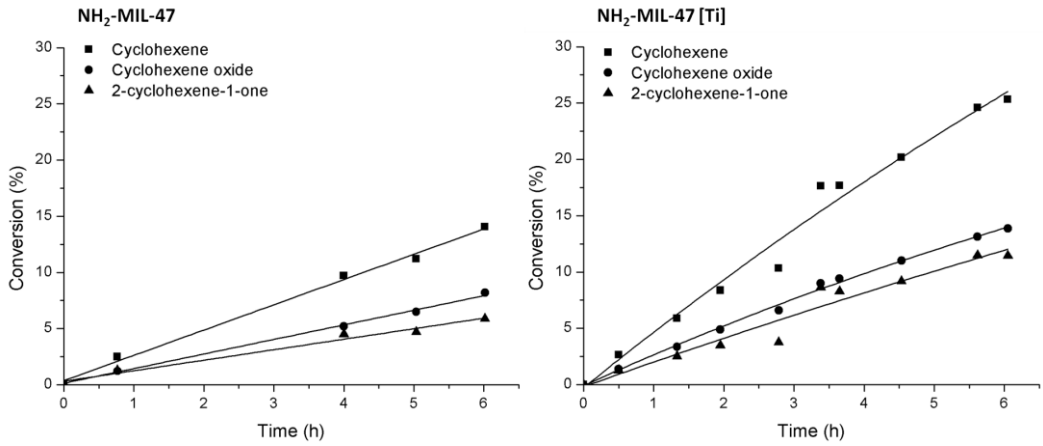

Fig. 5.8. Cyclohexene conversion (■) and the yield of cyclohexene oxide (●) and 2-cyclohexene-1-one (▲) for NH_2-MIL-47 and *NH_2-MIL-47 [Ti]* using acetonitrile as solvent and oxygen as oxidant in combination with the co-oxidant cyclohexanecarboxaldehyde at a temperature of 40°C. In both experiments a V loading of 0.42 mmol was applied.

Additionally, the homogenous catalyst $TiO(acac)_2$ has been tested using the same experimental conditions as for the MOF materials. The same amount of Ti has been used as in the post-functionalized material. The conversion pattern of this homogeneous catalyst is depicted in Fig. 5.9. From this figure it can be seen that after 6 hours of reaction a cyclohexene conversion of 25 % is reached, which is practically the same as for the Ti/V-MOF.

It is interesting to note that the product distribution observed for the homogeneous catalyst is very similar as for the NH_2-MIL-47 and *NH_2-MIL-47 [Ti]* almost equal percentages of the cyclohexene oxide and the ketone are observed.

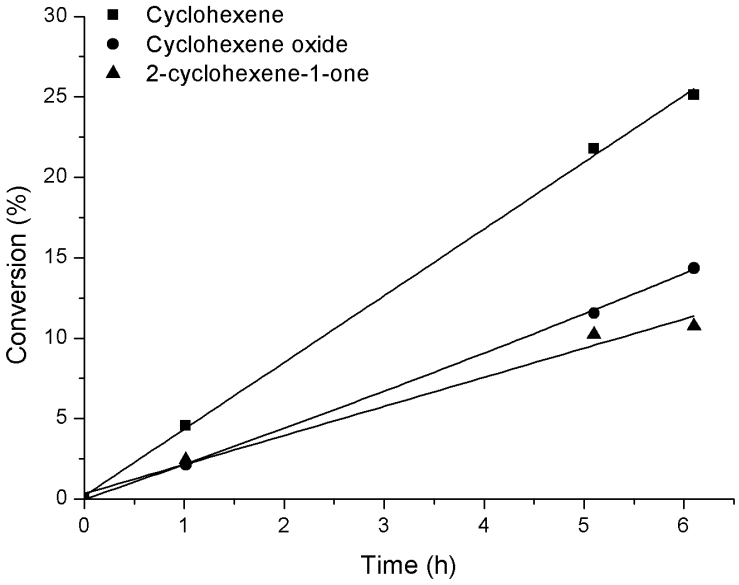

Fig.5.9. Cyclohexene conversion (■) and the yield of cyclohexene oxide (●) and 2-cyclohexene-1-one (▲) for $TiO(acac)_2$ using acetonitrile as solvent and oxygen as oxidant in combination with the co-oxidant cyclohexanecarboxaldehyde at a temperature of 40°C. The same Ti loading was applied as for the *NH_2-MIL-47 [Ti]* (0.22 mmol Ti).

5.2.3 Stability and regenerability of the catalysts

To test the regenerability of the V-MOFs, two additional runs have been executed on both materials. In Fig. 5.10, the cyclohexene conversion is shown after each run for the two catalysts, whereas in Table 5.2. the TON, TOF and leaching percentage are presented after each run for both materials. As can be seen from Fig. 5.10, the cyclohexene conversion for the post-functionalized material is slightly enhanced after the first run which is due to the generation of the extra catalytic V^{+V} sites (see section 5.2.4). However, for the non-functionalized V-MOF a significantly higher cyclohexene conversion is observed for the 2nd and the 3rd run (30 % and 24 %). This is due to the V leaching in

each run as can be noted from Table 5.2. In each run a small amount of V-leaching is observed (1,8 %, 2.5 % and 3.5 %) which gives rise to additional defects in the framework structure. Extra defects present in the structure can significantly influence the catalytic performance in the additional runs [2]. The *NH_2-MIL-47 [Ti]* did not show any detectable Ti or V leaching, which clearly demonstrates that the original MOF after post-functionalization becomes more stable. The exact reason for the enhanced leaching stability is currently unclear. Both shielding effects and electronic effects may influence the leaching behaviour and would require advanced modeling techniques [12].

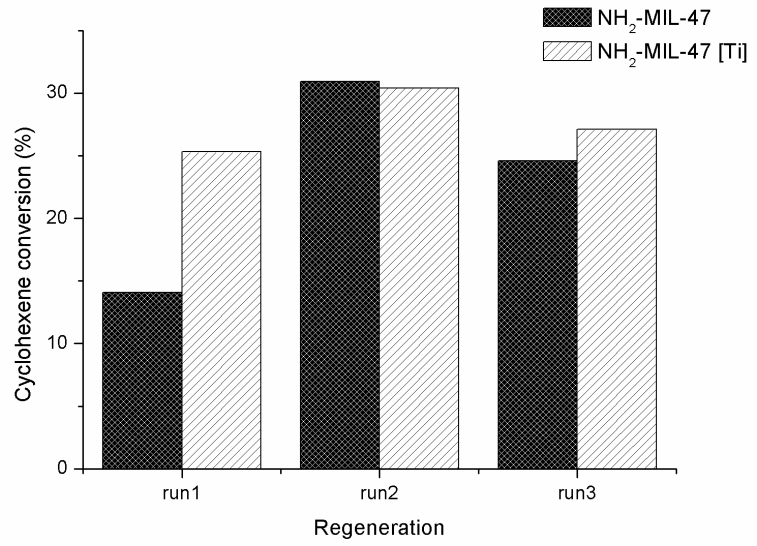

Fig. 5.10. Cyclohexene conversion for the executed additional runs on NH_2-MIL-47 and *NH_2-MIL-47 [Ti]*.

Table 5.2 TON, TOF and leaching percentage after each run for both V-based catalysts.

Sample	TON[a]	TOF[b] (h^{-1})	Leaching (%)
NH_2-MIL-47			
run 1	17.7	6.0	1.8
run 2	44.6	14.1	2.5
run 3	63.9	10.4	3.5
NH_2-MIL-47 [Ti]			
run 1	39.5	7.5	0
run 2	44.8	12.1	0
run 3	49.5	1.1	0

[a] TON was calculated after 6 hours of reaction, [b] TOF was calculated after 30 minutes of reaction.

Comparison of the XRPD pattern of *NH_2-MIL-47 [Ti]* before catalysis and after each run (see Fig. 5.11) clearly shows that the framework integrity of the MOF is well preserved.

5.2.4 EPR measurements

The aim of the EPR measurements is gaining insight in the reaction mechanisms by monitoring the fraction of paramagnetic V^{+IV} ions in the catalyst. Figure 5.12a shows the RT X-band spectra of *NH_2-MIL-47 [Ti]* dry powder samples before and after 2 and 4 hours of catalysis. The spectra of the samples prior to and after catalysis appear as single broad lines exhibiting widths of about 9.2 mT before and 10.4 mT after catalysis. No ^{51}V hyperfine (HF) structure is resolved in the spectra. The line position in the X-band spectra is practically the same for all samples, however, already suggests a signal assignation to V^{+IV} ($g=1.96 < g_e=2.0023$)[13]. Furthermore, spectra were recorded at higher microwave frequency (Q-band), which partially resolves the anisotropy of the $(V^{+IV}=O)O_4$ complexes.

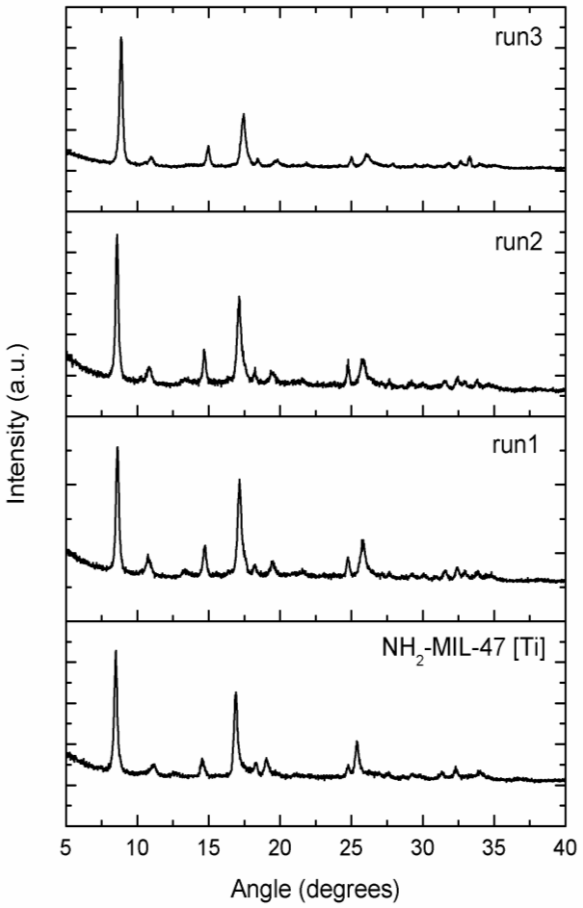

Fig. 5.11. XRPD pattern of the original *NH_2-MIL-47 [Ti]* before catalysis and the XRPD pattern of *NH_2-MIL-47[Ti]* after the first, second and third catalytic run.

In Fig. 5.13 the RT Q-band EPR spectrum of *NH_2-MIL-47 [Ti]* is compared with that of NH_2-MIL-47 and MIL-47. Spectrum simulations show that in all three samples the paramagnetic species have (approximately) axial symmetry. The $g_{\parallel}$ (along the V=O bond direction) and $g_{\perp}$ values obtained through fitting of the spectra are listed in Table 5.3. These values are typical for V^{+IV} species [13] and are in very good agreement with earlier EPR reports on V-MOFs [14]. It is worth noting that both in the work of Meilikhov *et al.* [14] and in our own previous investigations of V-MOFs (see chapter 3) [2, 3], no HF structure was resolved in

the spectra, most probably as a result of interactions between spins in these paramagnetically concentrated samples. The number of paramagnetic centers in the samples was estimated by comparing the signal intensity with that of a $VO(acac)_2$ grafted silica sample with known V^{+IV} loading. It was found to be comparable to the number of V-sites in the catalyst, indicating that at RT EPR provides information on the majority of the metal V-sites, and not only of a minority fraction, e.g. corresponding to defects. The intensity of the RT X-band spectra was evaluated by double integration of the EPR spectra over a range of 80.0 mT centered on the broad EPR line, in order to avoid errors due to non-perfect background correction in the broader range recorded. The data points in Fig. 5.12b represent the relative intensity with respect to the signal of *NH_2-MIL-47 [Ti]* prior to catalytic reaction. The error (one standard deviation) is estimated at 4 %, combining the effects of variations in consecutive measurements (sample positioning) and day-by-day changes in the spectrometer sensitivity. One observes that within the first 2 hours of catalysis, the spectrum intensity decreases about 17 %. Thereafter it remains stable or decreases more slowly. A very similar behaviour was observed for MIL-47 in the oxidation of cyclohexene with TBHP/decane as oxidant which was described in chapter 3[2]. Hence, we propose a similar interpretation: in the first few hours of catalysis a fraction of the V^{+IV} centers is oxidized to diamagnetic V^{+V} centers. Mechanistic considerations in Section 5.2.5 suggest a radical parallel pathway, involving a partial oxidation of the V-metal sites.

Table 5.3 Best fit principal g values for the V^{+IV} centers in MIL-47, NH_2-MIL-47 and *NH_2-MIL-47 [Ti]* at RT (see Fig. 5.13).

T	Sample	$g_\perp$	$g_\parallel$
RT	MIL-47	1.972	1.941
	NH_2-MIL-47	1.970	1.940
	NH_2-MIL-47 [Ti]	1.970	1.940

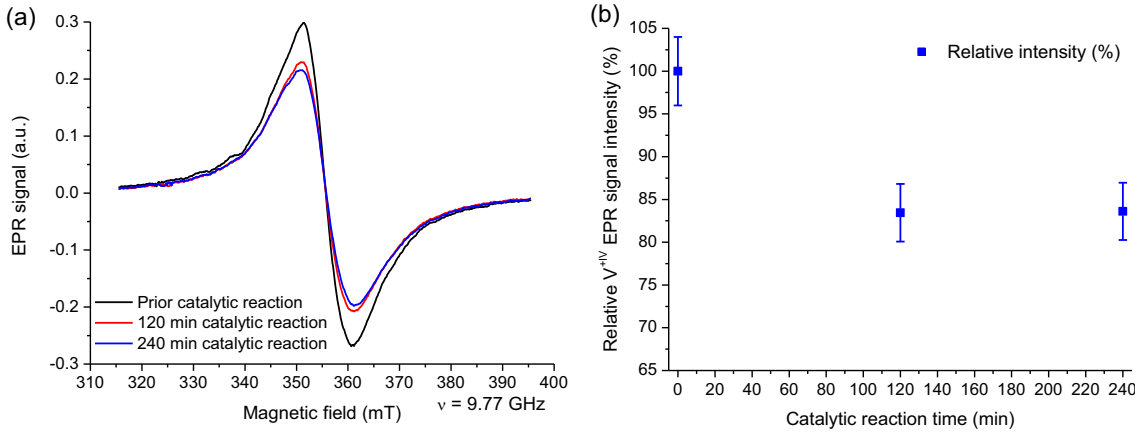

Fig. 5.12. (a) X-band EPR spectra at RT of the *NH_2-MIL-47 [Ti]* samples before and after catalysis; (b) Relative V^{+IV} EPR signal intensity with respect to the signal of *NH_2-MIL-47 [Ti]* prior to catalysis. The error (one σ) is estimated at 4 % (see text).

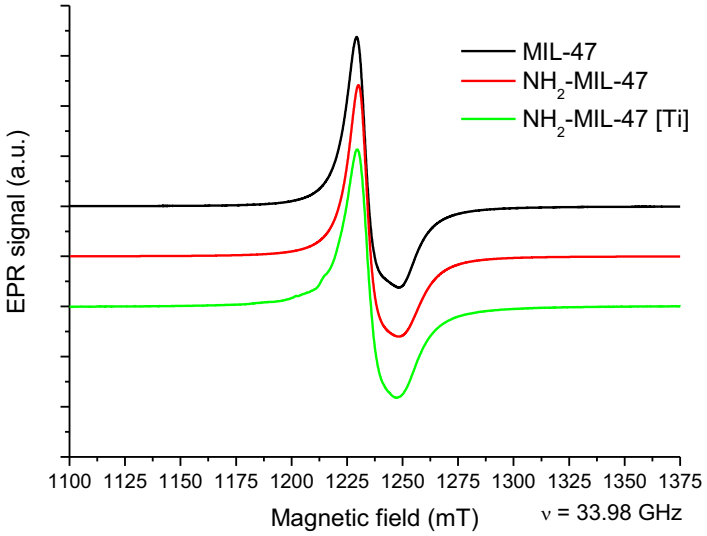

Fig. 5.13. Q-band (33.98 GHz) EPR spectrum of *NH_2-MIL-47 [Ti]* compared with the spectra of non-functionalized NH_2-MIL-47 and of MIL-47 at RT.

5.2.5 Reaction Mechanisms

Based on the above described EPR and catalytic results a plausible reaction mechanism is proposed. The mechanism of oxidation using molecular oxygen and a sacrificial co-oxidant has been the subject of many studies. A radical mechanism involving a peracid radical as primary oxidizing species has been generally accepted (Scheme 5.1) [15]. The role of the catalyst is considered to be the activation of molecular oxygen by the generation of radicals. However, a metal-oxygen moiety can be present as alternative, direct oxidizing species in the metal-catalyzed system[16, 17]. This oxidation pathway is generally accepted for late transition metals. Nevertheless, for metals like titanium and vanadium, this pathway is less likely as described by Sheldon et al[18]. The presence of metal-oxo species could explain the decrease of the V^{+IV} signal intensity in the EPR measurements since the generation of vanadium-oxo species is accompanied by an oxidation to V^{+V}, which corresponds to what was already reported for the V-MIL-47 in the cyclohexene oxidation using TBHP as oxidant (see chapter 3)[2].

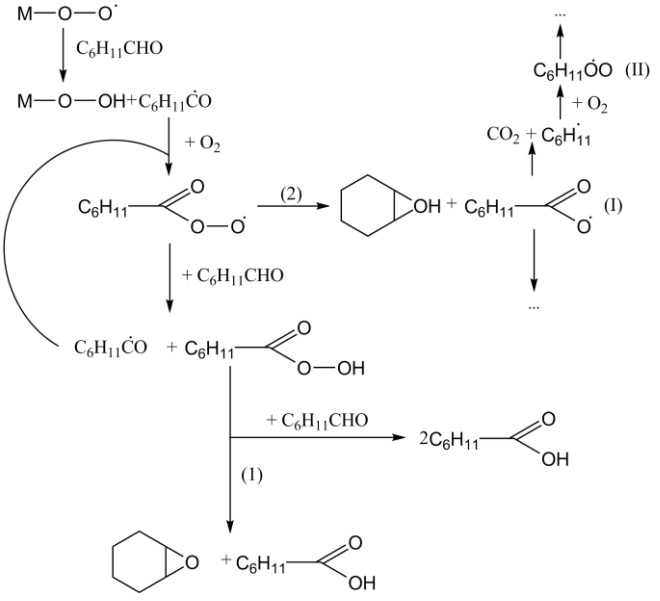

Scheme 5.1. General mechanism of the epoxidation with O_2 and aldehydes, most termination steps were omitted for clarity.

Another argument in favor for the mechanism shown in Scheme 5.1 is the presence of cyclohexanone in the product mixture. This is due to the formation of the peroxide radical ((II) in Scheme 5.1), followed by the formation of peroxide by a hydrogen abstraction. Afterwards, the obtained peroxide can react with another peroxide to form the cyclohexanone and oxygen (see Scheme 5.2).

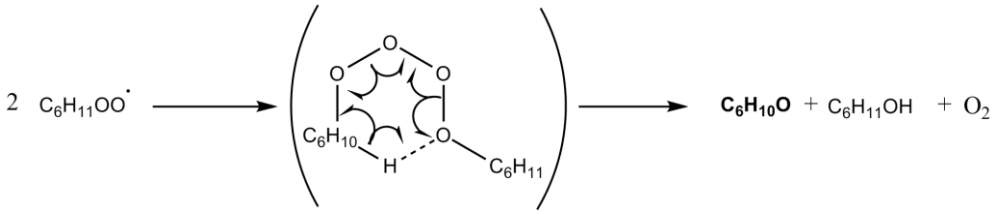

Scheme 5.2. Formation of cyclohexanone, which was observed in the product mixture.

This type of reaction generally exhibits a high (>80 %) selectivity toward the epoxide when it is catalyzed by complexes where the metal can only have a low oxidation state (maximum II or III)[19]. A MOF containing the same metals as those mostly used as homogeneous catalysts (Ni, Cu, Co) for this reaction gave similar results[16]. In the present system however, the selectivity towards the epoxide is significantly lower. It is known that the presence of carboxylic acid radicals and peroxo radicals ((I) and (II) in Scheme 5.1) can lead to oxidation in the allylic position[15, 16]. It is likely that these intermediates are stabilized by titanium and vanadium in the catalyst, leading to a decreased selectivity. Furthermore, the presence of M=O species and peroxide moieties can lead to the formation of cyclohexenol as shown in Scheme 5.3. Cyclohexenol can then be oxidized further to 2-cyclohexene-1-one, this conversion was also shown by Murahashi et al.[19].

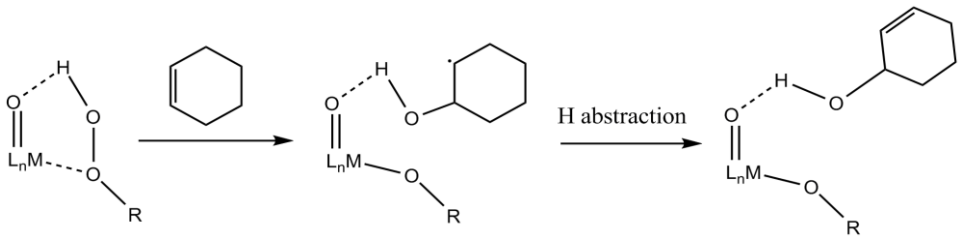

Scheme 5.3. Pathway to cyclohexenol formation.

5.3 Conclusions

We succeeded in the post-functionalization of NH_2-MIL-47 with $TiO(acac)_2$. ^{13}C CP/MAS, ^{1}H NMR and DRIFTS measurements clearly established the effectiveness of the grafting procedure, whereas XRPD measurements proved the stability of the bimetallic MOF during the grafting process. The obtained *NH_2-MIL-47 [Ti]* exhibits a significantly higher cyclohexene conversion compared to the non-functionalized material, probably mainly due to the extra active sites. Furthermore no leaching of V or Ti was detected. Regenerability tests have shown that only a slight increase in cyclohexene conversion is observed during the first 3 runs. EPR measurements indicate that about 17 % of the V^{+IV} sites are oxidized to V^{+V} in the first two hours of catalysis. In agreement with the latter, the general mechanism of the epoxidation with O_2 and aldehydes shows the generation of vanadium-oxo species which is accompanied by a partial oxidation of the V centers toward V^{+V}.

5.4 Experimental section

5.4.1 Synthesis of *NH_2-MIL-47 [Ti]*

In a first step NH_2-MIL-47 was prepared via a microwave synthesis route described in chapter 4. In a second step $TiO(acac)_2$ was grafted onto the V-MOF. Different temperatures and reaction times have been applied as shown in Table 5.1. In each experiment 0.0785 g $TiO(acac)_2$ was dissolved in 30 mL of dry toluene. After stirring the solution for 4 hours at 55 °C 0.15g NH_2-MIL-47 was added to the solution. Subsequently this mixture was stirred at a certain

temperature (55°C, 70°C and 90°C) for 20 or 40 hours under an inert argon atmosphere. Hereafter, the MOF was filtered on a combined nylon-membrane filter and washed several times with acetone to remove unreacted $TiO(acac)_2$. Afterwards the solid was dried overnight under vacuum.

5.4.2 Catalytic setup

In a typical catalytic test, a schlenk flask was loaded with 40.0 mL of acetonitrile as solvent, 7.0 mL cyclohexene (substrate) and 8.4 mL 1,2,4-trichlorobenzene used as internal standard. Oxygen (99.9% pure) was applied as the oxidant in combination with the co-oxidant cyclohexanecarboxaldehyde (7.6 mL). A constant oxygen flow of 7 mL/min was bubbled through the solution by means of a mass flow controller. Blanc reactions were carried out in the absence of catalyst which showed no conversion of cyclohexene. All the catalytic tests were carried out at a temperature of 40 °C in a schlenk flask equipped with a liquid condenser coupled with recirculating cooling liquid at -4 °C to prevent evaporation of the reaction mixture. Aliquots were gradually taken out of the mixture, diluted with 500 µl ethylacetate, and subsequently analyzed by GC-FID.

5.4.3 EPR measurements

For quantitative EPR analysis, spectra of dry powders, contained in quartz tubes with an outer diameter of 4 mm, filled to a height of approximately 6 mm (30-35 mg), were recorded at RT using a Bruker ESP300E X-band spectrometer (ER 4102-ST rectangular cavity). The sample tubes rested on the edge of an open tube inside the cavity for reproducible sample positioning. The microwave frequency was measured using a HP 5350 B microwave frequency counter. The magnetic field was modulated at 100 kHz with a peak-to-peak amplitude of 0.1 mT and the microwave power was set to 2 mW, avoiding saturation. A broad magnetic field range was swept (350 mT) around the free electron g-value (2.0023). All spectra were normalized to a microwave frequency of 9.77 GHz for comparison and corrected for the background spectrum of the empty cavity. For comparison of intensities, the spectra were divided by the sample mass. In order to resolve the anisotropy, selected powders were also measured in Q-band (≈34 GHz) at RT on a Bruker Elexsys E500 spectrometer equipped with a

Pendulum CNT-90XL frequency counter (spectra normalized to 33.98 GHz). These measurements were performed on powders contained in 2 mm outer diameter quartz tubes filled to a height of about 2 mm.

5.4.4 Computational details

Ab initio calculations are performed with the gaussian09 program[20]. All models were optimized with a B3LYP[21, 22] functional using a 6-31+G(d) Pople basis set. Frequency calculations were done at the same level of theory. To compare the calculated frequencies with the experimental DRIFTS spectrum a scale factor of 0.9648 was imposed as proposed by Merrick *et al.*[23]

5.5 References

1. K. Leus, I. Muylaert, M. Vandichel, G. B. Marin, M. Waroquier, V. Van Speybroeck and P. Van der Voort, *Chem Commun*, 2010, **46**, 5085-5087.
2. K. Leus, M. Vandichel, Y. Y. Liu, I. Muylaert, J. Musschoot, S. Pyl, H. Vrielinck, F. Callens, G. B. Marin, C. Detavernier, P. V. Wiper, Y. Z. Khimyak, M. Waroquier, V. Van Speybroeck and P. Van Der Voort, *J Catal*, 2012, **285**, 196–207.
3. Y. Y. Liu, K. Leus, M. Grzywa, D. Weinberger, K. Strubbe, H. Vrielinck, R. Van Deun, D. Volkmer, V. Van Speybroeck and P. Van der Voort, *Eur J Inorg Chem*, 2012, **16**, 2819–2827.
4. I. Muylaert, J. Musschoot, K. Leus, J. Dendooven, C. Detavernier and P. Van der Voort, *Eur J Inorg Chem*, 2012, 251-260.
5. S. Stoll and A. Schweiger, *J Magn Reson*, 2006, **178**, 42-55.
6. S. Bhattacharjee, D. A. Yang and W. S. Ahn, *Chem Commun*, 2011, **47**, 3637-3639.
7. E. Pretsch, P. Bühlmann, C. Affolter, A. Herrera and R. Martínez, Elsevier Masson, 2001.
8. J. Coates, ed., *Interpretation of Infrared Spectra, A Practical Approach*, 2000.
9. T. Loiseau, C. Serre, C. Huguenard, G. Fink, F. Taulelle, M. Henry, T. Bataille and G. Ferey, *Chem-Eur J*, 2004, **10**, 1373-1382.
10. J. Gascon, U. Aktay, M. D. Hernandez-Alonso, G. P. M. van Klink and F. Kapteijn, *J Catal*, 2009, **261**, 75-87.
11. M. Kandiah, M. H. Nilsen, S. Usseglio, S. Jakobsen, U. Olsbye, M. Tilset, C. Larabi, E. A. Quadrelli, F. Bonino and K. P. Lillerud, *Chem Mater*, 2010, **22**, 6632-6640.

12. J. M. Ho, C. J. Easton and M. L. Coote, *J Am Chem Soc*, 2010, **132**, 5515-5521.
13. R. Pilbrow, ed., *Transition Ion Electron Paramagnetic Resonance*, Clarendon Press – Oxford 1990.
14. M. Meilikhov, K. Yusenko, A. Torrisi, B. Jee, C. Mellot-Draznieks, A. Poppl and R. A. Fischer, *Angew Chem Int Edit*, 2010, **49**, 6212-6215.
15. B. B. Wentzel, P. L. Alsters, M. C. Feiters and R. J. M. Nolte, *J Org Chem*, 2004, **69**, 3453-3464.
16. E. Angelescu, O. D. Pavel, R. Ionescu, R. Birjega, M. Badea and R. Zavoianu, *J Mol Catal a-Chem*, 2012, **352**, 21-30.
17. P. Mastrorilli, C. F. Nobile, G. P. Suranna and L. Lopez, *Tetrahedron*, 1995, **51**, 7943-7950.
18. G. J. ten Brink, I. W. C. E. Arends and R. A. Sheldon, *Chem Rev*, 2004, **104**, 4105-4123.
19. N. Komiya, T. Naota, Y. Oda and S. I. Murahashi, *J Mol Catal a-Chem*, 1997, **117**, 21-37.
20. M. J. T. Frisch, G. W.; Schlegel, H. B.; Scuseria, G. E.; Robb, M. A.; Cheeseman, J. R.; Scalmani, G.; Barone, V.; Mennucci, B.; Petersson, G. A.; Nakatsuji, H.; Caricato, M.; Li, X.; Hratchian, H. P.; Izmaylov, A. F.; Bloino, J.; Zheng, G.; Sonnenberg, J. L.; Hada, M.; Ehara, M.; Toyota, K.; Fukuda, R.; Hasegawa, J.; Ishida, M.; Nakajima, T.; Honda, Y.; Kitao, O.; Nakai, H.; Vreven, T.; Montgomery, Jr., J. A.; Peralta, J. E.; Ogliaro, F.; Bearpark, M.; Heyd, J. J.; Brothers, E.; Kudin, K. N.; Staroverov, V. N.; Kobayashi, R.; Normand, J.; Raghavachari, K.; Rendell, A.; Burant, J. C.; Iyengar, S. S.; Tomasi, J.; Cossi, M.; Rega, N.; Millam, N. J.; Klene, M.; Knox, J. E.; Cross, J. B.; Bakken, V.; Adamo, C.; Jaramillo, J.; Gomperts, R.; Stratmann, R. E.; Yazyev, O.; Austin, A. J.; Cammi, R.; Pomelli, C.; Ochterski, J. W.; Martin, R. L.; Morokuma, K.; Zakrzewski, V. G.; Voth, G. A.; Salvador, P.; Dannenberg, J. J.; Dapprich, S.; Daniels, A. D.; Farkas, O.; Foresman, J. B.; Ortiz, J. V.; Cioslowski, J.; Fox, D. J. Gaussian 09, {R}evision {A}.02, Gaussian, Inc., Wallingford CT: , 2009.
21. A. D. Becke, *J. Chem. Phys.*, 1993, **98**, 5648-5652.
22. C. T. Lee, W. T. Yang and R. G. Parr, *Phys. Rev. B*, 1988, **37**, 785-789.
23. J. P. Merrick, D. Moran and L. Radom, *J Phys Chem A*, 2007, **111**, 11683-11700.

Chapter 6: Summary and general conclusions

Abstract

In this chapter the goals and results of this dissertation work are summarized. Firstly a short introduction on Metal Organic Frameworks is given. Then, the results on the synthesis of the V and V/Ti based MOF structures and their use in catalysis and adsorption will be summarized.

6.1 Metal Organic Frameworks: a new class of porous materials

Metal Organic Frameworks, abbreviated as MOFs, are a recent class of crystalline materials containing metal ions or metal clusters which are connected with each other by rigid organic linkers. The resulting structures can have a zero-dimensional (0D) one-dimensional (1D), two-dimensional (2D) or three-dimensional (3D) architecture. The first "MOF", denoted as MOF-5, was synthesized by the group of Yaghi (see Fig. 6.1). As can be seen from Fig. 6.1 MOF-5 consists of Zn_4O tetrahedral clusters connected which each other by 1,4-benzenedicarboxylate organic linkers[1].

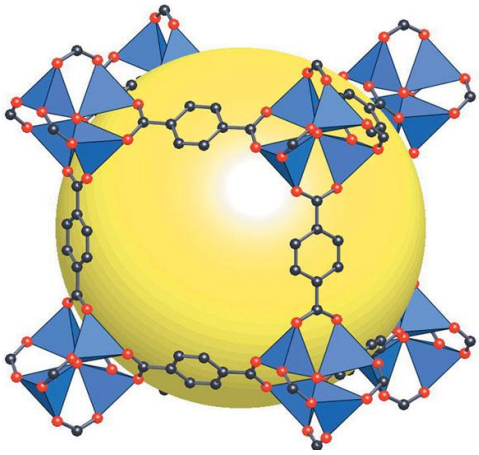

Fig. 6.1. Ball-and-stick representation of the framework of MOF-5[1].

There are many methods to synthesize MOFs. In general MOFs are synthesized using well soluble salts as the source for the metal compounds e.g. metal nitrates, sulfates or acetates together with the organic linker (mostly carboxylic acids or pyridyl-based linkers) in a solvent or mixture of solvents. Next to the classical synthesis method: microwave synthesis, electrochemical synthesis and high-throughput synthesis are applied. For a detailed description of these synthesis strategies the reader is referred to chapter 1.

6.2 Properties of Metal Organic Frameworks

Besides their exceptionally high porosities and surface areas, MOFs posses the advantage of allowing to tune the dimensionality of the pores. Pioneering work to enlarge the pores has been done by the group of Yaghi resulting in the isoreticular serie of MOF-5 in which the pores could be incrementally varied from 3.8 to 28.8 angstroms[2]. Another interesting property of these materials is that some MOFs reveal a flexible "breathing" framework. These compounds are categorized as soft porous crystals, having a highly ordered network and reversible structural transformability. Their relative poor thermal stability and hydrothermal stability are the most important disadvantages of MOFs.

6.3 Applications of Metal Organic Frameworks

While the initial focus in the field of MOFs was the synthesis and structural characterization, an increasing number of MOFs are now being explored for their interesting properties, including optic, magnetic, and electronic properties as well as their various potential applications such as catalysis, ion exchange gas storage, separation, polymerization and drug delivery. In chapter 1, the reader may find some important reviews on each application.

The main focus of this thesis is the use of MOFs in catalysis and adsorption. We aimed very specifically at the use of vanadium and vanadium/titanium based MOFs in oxidation catalysis or adsorption of CO_2/CH_4. At the beginning of this dissertation work, very few vanadium MOFs were known in literature. Additionally these V-MOFs were never tested in catalysis, although vanadium based catalysts are known in oxidation catalysis. During this thesis, there was a close collaboration with the Center for Molecular Modeling that performed the computational modeling presented in this work.

6.4 Active sites in MOFs

The active sites in MOFs can be generated in several ways. Firstly, the metal or metal cluster connecting points can be used to catalyze organic transformations.

As shown in Fig. 6.2, a metal connecting point with a free coordinating site can be used as a Lewis acid catalyst after removal of coordinating solvent molecules from the axial positions of the metal center. Secondly, active sites can be generated from the functional groups within a MOF scaffold (Fig. 6.3). However, unlike traditional immobilized catalysts, the active sites generated in this fashion are arranged in a predictable and tuneable manner due to the periodically ordered nature of porous MOFs. Thirdly, the catalytic activity of MOFs can result from entrapped active catalysts, such as palladium or ruthenium nanoparticles (Fig. 6.4).

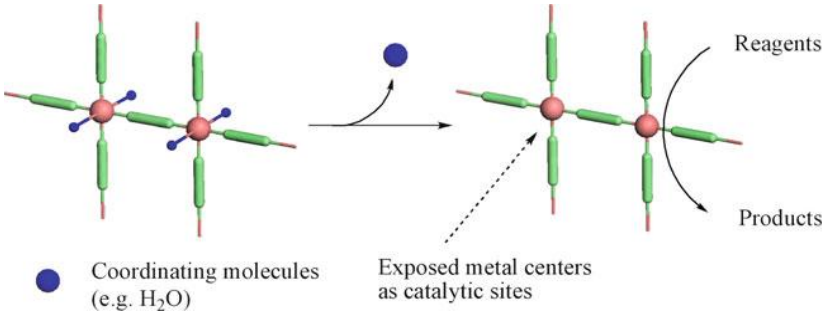

Fig. 6.2. Schematic representation illustrating the generation of unsaturated metal connecting points as active sites[3].

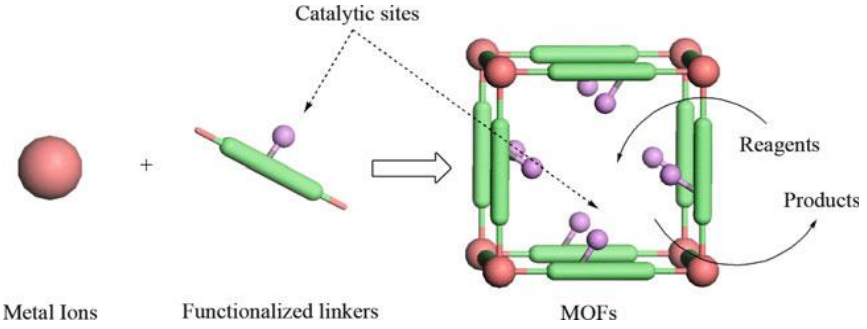

Fig. 6.3. Schematic representation showing the use of functional groups in the bridging ligands as active catalysts[3].

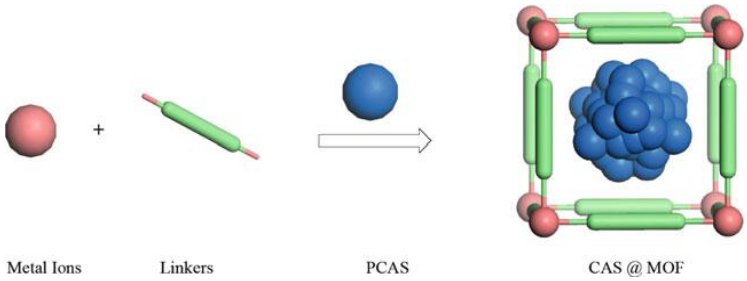

Fig. 6.4. Schematic representation of trapping catalytic active species inside MOFs[3].

6.5 The V-based Metal Organic Framework, MIL-47, acting as a heterogeneous catalyst in the oxidation of cyclohexene

In chapter 3, a detailed examination is presented of the MOF, MIL-47, in the oxidation of cyclohexene, applying TBHP in water or TBHP in decane as oxidant. MIL-47 has a three-dimensional framework, in which each V^{+IV} center is coordinated to four oxygen atoms from four carboxylate groups, and to two oxygen atoms on the O–V–O axis, thus forming a saturated octahedral coordination node (see Fig. 6.5)[4].

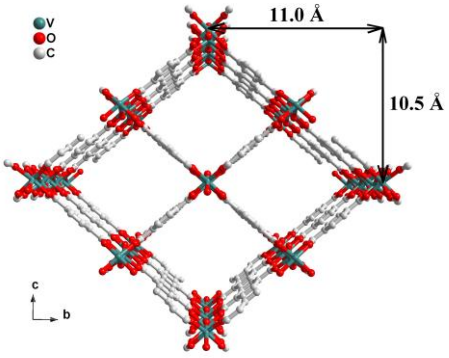

Fig. 6.5. Perspective view of the MIL-47.

During the oxidation of cyclohexene many products can be formed as can be seen from Fig. 6.6.

Throughout this investigation we observed that by applying TBHP in water as oxidant, a high conversion of cyclohexene was observed (55% after 7 hours of reaction). This high conversion was accompanied with a high leaching percentage (13% after 1 hour of reaction). With TBHP in decane as oxidant, the leaching could be highly reduced (3% after 7 hours of reaction). However, a lower cyclohexene conversion was observed with the former oxidant (30% after 7 hours of reaction). Additionally regenerability and stability tests were carried out with the latter oxidant, demonstrating that the MIL-47 catalyst was stable up until 5 cycles.

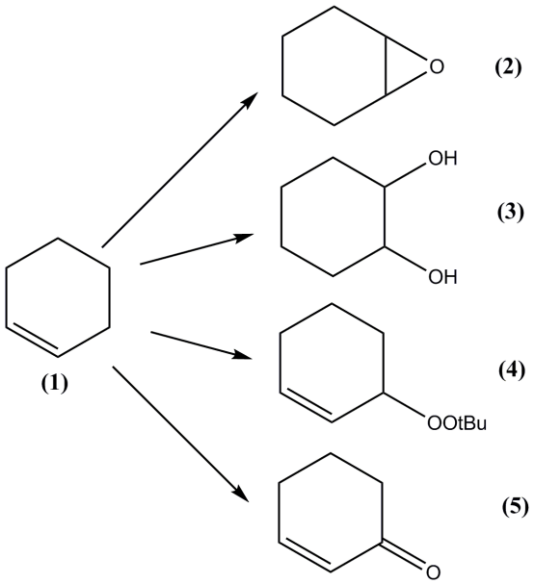

Fig.6.6. Oxidation of cyclohexene (1) to cyclohexene oxide (2), cyclohexane-1,2-diol (3), *tert*-butyl-2-cyclohexenyl-1-peroxide (4) en 2-cyclohexene-1-one (5).

In a second part of this chapter, the catalytic performance of MIL-47 was compared with two other V-based reference catalysts: VAPO-5 and VO_x/SiO_2. It was concluded that (1) VAPO-5 showed no catalytic activity and (2) the catalytic activity of the silica based catalyst was only due to the leached V. In other words, only homogeneous catalysis took place.

In a last part of this chapter we tried to define the active sites for catalysis and determine the plausible reaction pathways for the epoxidation of cyclohexene.

From the theoretical modeling we could conclude that (1) at least two V-organic linker bonds needs to be broken to allow a coordination with the oxidant and (2) that at least two parallel catalytic cycles are co-existing: one with V^{+IV} sites and one with pre-oxidized V^{+V} sites.

6.6 Investigation of the NH_2 functionality on the CO_2 adsorption capacity: comparison of MIL-47 and NH_2-MIL-47

The functionalization of porous materials with $–NH_2$ groups is of particular interest for the adsorptive separation of CO_2. For silica-based materials it was already demonstrated that functionalization of the surface of the mesopores with $–NH_2$ groups enhances the affinity toward CO_2 adsorption. This points to a strong interaction between CO_2 and the amino groups in the pores. For MOF materials, the effect of $–NH_2$ groups is less straightforward and is still the subject of many discussions. In some reports an increase is observed in the CO_2 adsorption capacity, whereas other research groups describe a decrease of the adsorption[5-7]. Furthermore, the flexibility of the frameworks plays also an important role in adsorption processes. While MIL-53 shows a two step adsorption process due to structural changes, the structurally rigid MIL-47 shows a Type I isotherm[8].

In chapter 4 of this dissertation work, the synthesis and characterization of the amino functionalized V-MOF with MIL-47 topology is reported. Moreover, the CO_2 and CH_4 adsorption properties of this NH_2-MIL-47 have been investigated and are compared to the parent MIL-47 (see Fig. 6.7). An interesting observation is the decrease in capacity for the amino version of the material, corresponding to 20% for CO_2 and 10% for CH_4 at 25 bar. Even more interesting is that the isotherms on both materials completely coincide in the low-pressure regime; thus the presence of $–NH_2$ groups does not result in a significant increase in affinity for CO_2 or CH_4.

Additionally, the adsorption enthalpies were determined by means of pulse-chromatography measurements for MIL-47 and NH_2-MIL-47. The experimental adsorption enthalpies follow the same trend as the corresponding adsorbate-linker interactions, determined by theoretical modeling.

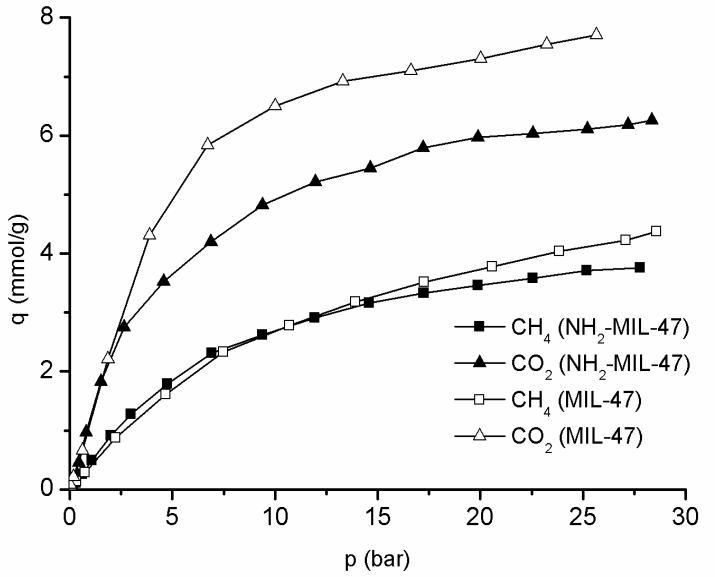

Fig. 6.7. Adsorption isotherms of CO_2 and CH_4 on MIL-47 and NH_2-MIL-47 at 30 °C.

From this investigation we can conclude that, in contrast with the flexible MIL-53, the additional NH_2 groups do not have a beneficial effect on the adsorption properties of the rigid NH_2-MIL-47, which was also confirmed by the theoretical modeling results.

6.7 Ti-functionalized NH_2-MIL-47: an effective and stable epoxidation catalyst

The introduction of extra functional groups on the organic linker can have a significant influence on the adsorption capacity as was illustrated in chapter 4. Also in the field of catalysis, it has been shown that the introduction of additional functional groups can generate a significant alteration in the catalytic performance compared to the parent framework.

In a first part of chapter 5, the post-modification of NH_2-MIL-47 with $TiO(acac)_2$ has been carried out (see Fig. 6.8). The obtained Ti loading was almost independent of the applied temperature and reaction time and amounts to 1.25 mmol Ti/g.

By means of DRIFTS, ^{1}H NMR and ^{13}C CP/MAS NMR measurements it was shown that the Ti complex was grafted onto the V-MOF. More details on the characterization can be found in chapter 5.

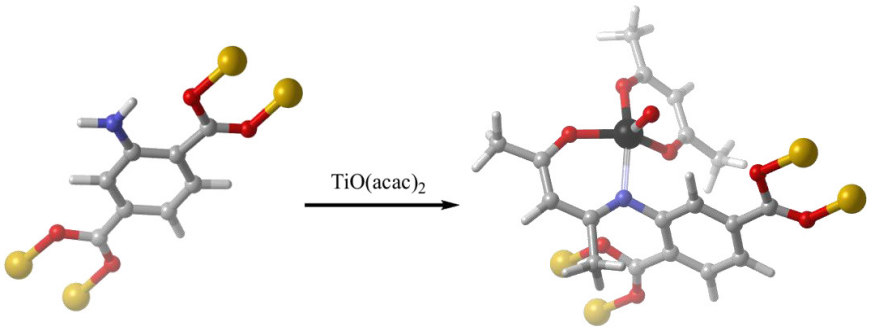

Fig. 6.8. Schematic representation of the post-functionalization of NH_2-MIL-47 with a Titanyl acetylacetonate complex (the carbon atoms are shown in grey, the oxygen atoms are depicted in red and the N, Ti and V atoms are shown in blue, black and yellow respectively).

Additionally, the obtained *NH_2-MIL-47 [Ti]* was examined in the oxidation of cyclohexene applying O_2 as oxidant in combination with cyclohexanecarboxaldehyde as a co-oxidant. The catalytic performance of the bimetallic MOF was compared with the non-functionalized V-MOF as well as with the homogeneous $TiO(acac)_2$ catalyst. Comparison of the TON and TOF values reveal that the Ti/V-MOF shows a higher catalytic activity in the first cycle in comparison to the NH_2-MIL-47, whereas in the additional cycles a slightly higher activity is observed for the NH_2-MIL-47. The latter is due to the leaching of V in the non-modified V-MOF, which causes defects in each run, enhancing the catalytic performance. The Ti/V-MOF shows no detectable leaching of V or Ti. The increased activity of the bimetallic MOF is due to a partial oxidation of V^{+IV} to V^{+V} in the first run. In other words, at least two parallel catalytic cycles are co-existing: one with V^{+IV} sites and one with pre-oxidized V^{+V} sites, which was also observed in chapter 3.

6.8 Conclusions

In this thesis it was shown that there is an expanding growth in the use of MOFs for many applications.

Two of these applications, more specifically, the utilization of MOFs in oxidation catalysis and adsorption/separation of CO_2/CH_4 were highlighted in this dissertation. Firstly, a thorough literature investigation on the use of MOFs in oxidation catalysis showed that MOFs are examined as such or served as matrix for the incapsulation or post-modification with a homogeneous catalyst. However, at this moment, very few papers address the comparison of the MOF material with catalysts used in industry (e.g. zeolites, zeotypes, silica based materials). Most of the reports compare the catalytic activity of the MOF with the homogeneous counterpart or with metal oxides. In this thesis, the investigation of V-MOFs and V/Ti-MOFs in the oxidation of cyclohexene was carried out. From this study we could conclude that the V-MOF, MIL-47, shows a high amount of V-leaching and a low stability in a water based oxidant. However, in a water-free oxidant, we were able to exclude the leaching to a higher extent. In other words, the choice of the oxidant is crucial to obtain a low-leaching and stable catalyst. Comparison of MIL-47 with silica and zeotype vanadium based reference catalysts showed that the MIL-47 shows a rather good performance in terms of activity and stability.
Furthermore, we observed that the stability could be enhanced during the catalytic performance by a post-modification of the V-MOF, NH_2-MIL-47, with a Ti-complex. Whereas the non-modified NH_2-MIL-47 showed a gradual leaching of V in each run, no leaching of V or Ti was observed for the Ti/V-MOF. However, at this moment we are unable to explain the latter observation.

Our entire catalytic study on V and V/Ti MOFs has been performed in close collaboration with the Center for Molecular Modeling to elucidate the catalytic mechanism and determine the active sites. For the V and V/Ti based MOF it was observed that at least two parallel catalytic cycles are co-existing: one with V^{+IV} sites and one with pre-oxidized V^{+V} sites.

In a second part of this dissertation work, the adsorption capacity and affinity was determined for CO_2/CH_4 for the V-MOF, NH_2-MIL-47. Whereas for silica materials it was already demonstrated that there is a strong interaction between CO_2 and the amino groups in the pores, for MOF materials, the effect of – NH_2 groups on the adsorption capacity is less straightforward and is still the subject of many discussions.

From our study we could conclude that, in contrast to the flexible MIL-53, the presence of additional NH_2 groups does not have a beneficial effect on the adsorption properties of the rigid NH_2-MIL-47 in comparison to the parent MIL-47, which was also confirmed by the theoretical modeling results. For the NH_2-MIL-47, both experiment and theory clearly show that the amination of the linker does not result in an increased adsorption capacity per mass of adsorbent, nor in an increased CH_4/CO_2 separation factor.

In conclusion, this thesis is a pioneering work, in the exploration of V-MOFs and V/Ti MOFs in catalysis and/or separation/adsorption processes. In the coming years, it may be expected that this research field will further expand as the research on MOFs and more specifically on V and V/Ti-MOFs is still in its infancy and most of the research is still performed on the academic level.
In the future a continuous synergy between experimentalists and theoreticians will stay of a paramount importance to obtain more insights in the applications of MOFs.

6.9 References

1. H. Li, M. Eddaoudi, M. O'Keeffe and O. M. Yaghi, *Nature*, 1999, **402**, 276-279.
2. M. Eddaoudi, J. Kim, N. Rosi, D. Vodak, J. Wachter, M. O'Keeffe and O. M. Yaghi, *Science*, 2002, **295**, 469-472.
3. L. Q. Ma and W. B. Lin, *Functional Metal-Organic Frameworks: Gas Storage, Separation and Catalysis*, 2010, **293**, 175-205.
4. K. Barthelet, J. Marrot, D. Riou and G. Ferey, *Angew Chem Int Edit*, 2001, **41**, 281-284.
5. B. Arstad, H. Fjellvag, K. O. Kongshaug, O. Swang and R. Blom, *Adsorption*, 2008, **14**, 755-762.
6. J. R. Karra and K. S. Walton, *J Phys Chem C*, 2010, **114**, 15735-15740.
7. A. R. Millward and O. M. Yaghi, *J Am Chem Soc*, 2005, **127**, 17998-17999.
8. T. K. Trung, I. Deroche, A. Rivera, Q. Y. Yang, P. Yot, N. Ramsahye, S. D. Vinot, T. Devic, P. Horcajada, C. Serre, G. Maurin and P. Trens, *Micropor Mesopor Mat*, 2011, **140**, 114-119.

Chapter 7: Nederlandstalige samenvatting

Proloog

In dit hoofdstuk wil ik de doelstellingen en bereikte resultaten in deze scriptie samenvatten. In eerste instantie belicht ik in een korte inleiding de materialen, meer bepaald Metaal-Organische Roosters, waarover dit proefwerk handelt. Enkele karakteristieke eigenschappen van deze materialen alsook hun mogelijke toepassingen worden kort aangehaald. Vervolgens schets ik in een summier overzicht de bereikte resultaten gedurende dit proefwerk op de gesynthetiseerde vanadiumhoudende en vanadium- en titaniumbevattende Metaal-Organische Roosters met betrekking tot hun gebruik als heterogene katalysator of adsorbens.

7.1 Metaal-Organische Roosters: een geavanceerde klasse van poreuze materialen

Sinds de ontdekking van hoog poreus geordende materialen in 1992 door de Exxon Mobil groep kent dit onderzoeksgebied een enorme expansie. Een belangrijke recente ontwikkeling in dit onderzoek zijn de Metaal-Organische Roosters (MOFs). MOFs zijn kristallijne materialen met op de knooppunten overgangsmetalen die door organische liganden verbonden zijn. De meest frequent gebruikte overgangsmetalen zijn zink, cadmium en koper. Als mogelijke organische liganden maakt men gebruik van allerlei benzeenderivaten zoals difenyl-, trifenyl- en tetrafenyl tetracarbonzuur, 1,4-benzeendicarbonzuur en 1,3,5-benzeentricarbonzuur. Deze materialen beschikken doorgaans over een groot oppervlakte en poriën in het hogere microporiëngebied.
Een pionier in het onderzoek naar MOFs is Omar Yaghi. MOF-5, gesynthetiseerd in het jaar 2000 door deze onderzoeksgroep, kan men beschouwen als het prototype voor nieuwe MOFs[1]. Het is een zinkhoudende MOF, met 1,4-benzeendicarbonzuur als organische linker (zie figuur 7.1).

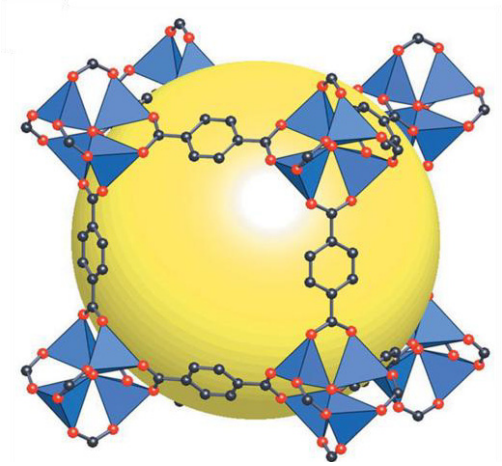

Figuur 7.1. MOF-5, het alom gekende prototype binnen de MOFs[1].

Er zijn diverse synthesestrategieën gekend voor de bereiding van deze materialen.

De klassieke hydrothermale of solvothermale synthese bestaat erin een metaalzout, in een welbepaalde verhouding, op te lossen samen met het geconjugeerde zuur van een organisch ligand. In een tweede stap plaatst men de oplossing gedurende een aantal uren bij een constante temperatuur in een autoclaaf. In een laatste stap worden de kristallen, na afkoeling tot kamertemperatuur, gewassen met water en vervolgens gedroogd. Naast deze klassieke syntheseweg voert men ook steeds meer syntheses uit met behulp van een microgolfoven of op basis van elektrochemie. Vandaag de dag worden zelfs volledig geautomatiseerde high throughput methodes aangewend. Voor een meer gedetailleerde beschrijving van deze alternatieve synthesestrategieën verwijs ik naar hoofdstuk 1.

7.2 Eigenschappen van Metaal-Organische Roosters

Naast een hoge specifieke oppervlakte bezitten MOFs ook het voordeel, in tegenstelling tot zeolieten, dat men de grootte van hun poriën kan variëren. Een porie expansie verkrijgt men door het gebruik van grotere organische liganden, zonder dat hierbij de oorspronkelijke structuur verandert. Dit noemt men *isoreticular* synthese. Een gekend voorbeeld hiervan is de *isoreticular* serie van MOF-5 waarin de grootte van de porie gevarieerd kan worden van 3.8 tot 28.8 Ångström[2].
Verder bezitten sommige MOFs de eigenschap dat men hun ruimtelijke structuur kan wijzigen. Meer bepaald kan een structuurverplaatsing optreden van enkele Ångström onder invloed van welbepaalde externe stimuli zoals bv. druk en temperatuur. Dit fenomeen is gekend onder de naam "*breathing*". Naast deze interessante voordelen bezitten MOFs ook enkele nadelen, waarbij hun beperkte thermische stabiliteit en hydrothermale stabiliteit de belangrijkste vormen.

7.3 Toepassingen van Metaal-Organische Roosters

In het begin lag de essentie van het onderzoek naar MOFs bij de synthese en de karakterisering. Door de jaren heen is het accent meer verschoven naar onderzoek van potentiële toepassingen voor deze veelbelovende materialen. De belangrijkste toepassingen zijn optische activiteit, magnetische en elektronische eigenschappen.

Ook katalyse, ionenuitwisseling, medicijnafgifte, gasopslag en gasscheiding zijn belangrijke onderzoeksgebieden (zie figuur 7.2).

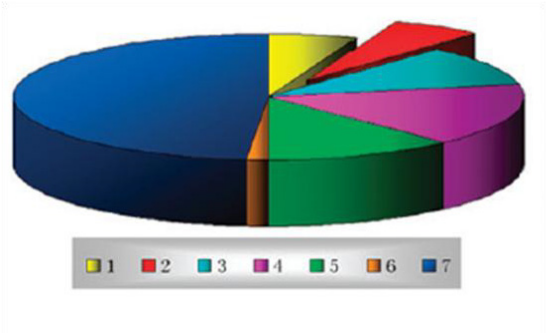

Figuur 7.2. Schematische weergave van de belangrijkste toepassingen van MOFs[3].

In deze doctoraatscriptie heb ik ervoor geopteerd om vanadiumhoudende en vanadium/titaniumbevattende MOFs te synthetiseren, waarbij hun katalytische activiteit of adsorptiecapaciteit werd geëvalueerd. Het aantal studies over vanadiumhoudende en titaniumhoudende MOFs was bij aanvang van deze dissertatie nog vrij beperkt. Zij werden bovendien nog nooit onderzocht op hun katalytische activiteit, niettegenstaande vanadium en titanium gekende transitiemetalen zijn in oxidatieve katalyse. Naast enkele adsorptietesten is de rode draad door deze scriptie dan ook katalyse. Gedurende dit hele proefschrift is er een nauwe samenwerking met het Centrum voor Moleculaire Modellering geweest voor de computationele modellering.

7.4 De actieve katalytische zones in MOFs

Er zijn verschillende strategieën om katalytisch actieve zones te genereren in MOFs. Een eerste mogelijkheid bestaat erin de metaalionen of de metaalionenclusters te gebruiken als actieve zones. Zoals in Figuur 7.3 weergegeven, kan een metaalion met een vrije coördinatiezone worden gebruikt als een Lewiszuur katalysator, nadat de coördinerende solventmoleculen van de axiale plaatsen van het metaalion zijn verwijderd.

In vele MOFs zijn echter alle coördinatiezones rond de metaalionen bezet door de organische liganden. Hierdoor zijn deze metaalionen niet meer toegankelijk als katalytische zone. Een alternatief hiervoor bieden de functionele groepen die aanwezig zijn op de organische liganden van de MOFs (zie Figuur 7.4). Een derde mogelijkheid is dat men de katalytische activiteit van de MOF kan verwerven door een actieve katalysator zoals palladium- of rutheniumpartikels in de MOF in te sluiten (zie Figuur 7.5).

Voor een uitgebreid overzicht omtrent het gebruik van MOFs als katalysator en meer bepaald het aanwenden van deze materialen in oxidatieve katalyse verwijs ik naar hoofdstuk 2. Hieruit valt duidelijk te concluderen dat er een explosieve groei waar te nemen is in dit toepassingsgebied. Diverse transitiemetaal- en lanthanidehoudende MOFs zijn al getest voor de oxidatie van cycloalkanen, benzeenhoudende verbindingen, cycloalkenen, alcoholen, sulfiden en thiol verbindingen. Maar er is een diepere studie rond de katalytische activiteit en stabiliteit over een langere periode (enkele jaren) vereist om inzicht te verkrijgen in de vraag of deze materialen in competitie kunnen treden met de gangbare industriële katalysatoren zoals bv. silica materialen, zeolieten, zeotypen, etc.

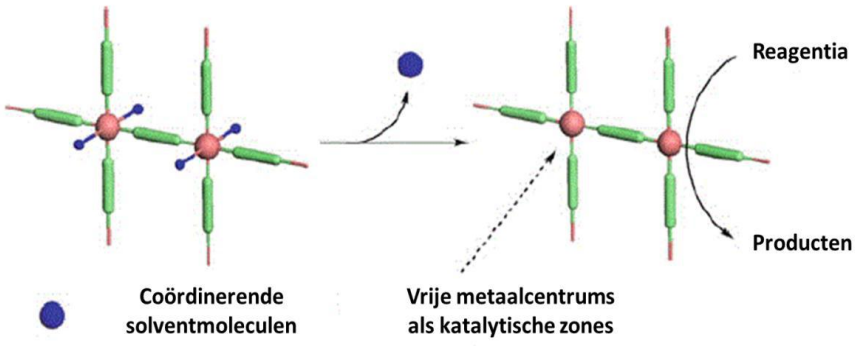

Figuur 7.3. Metaalion met een vrije coördinatiezone dat dienst doet als katalytisch centrum[4]

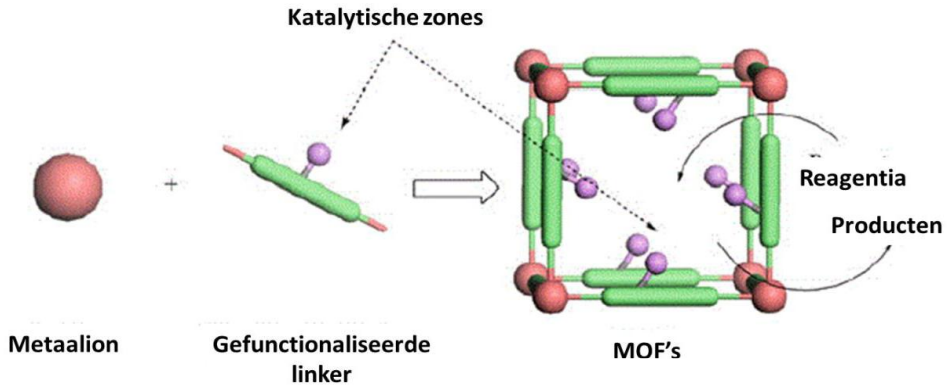

Figuur 7.4. Functionele groepen op de organische liganden die fungeren als actieve centra[4].

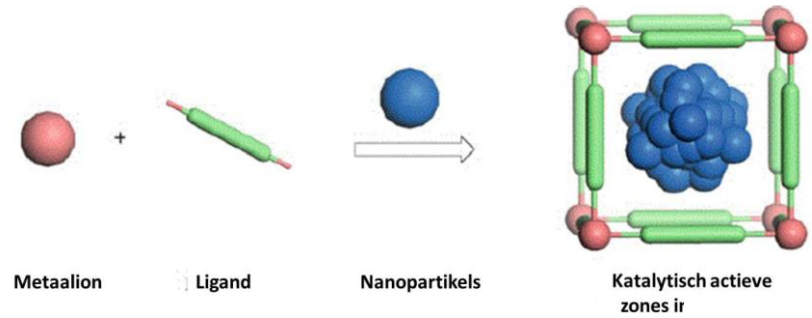

Figuur 7.5. Ingesloten metaalpartikels in MOFs als actieve centra[4].

7.5 De vanadiumhoudende MOF, MIL-47: een heterogene katalysator in de oxidatie van cyclohexeen

In hoofdstuk 3 presenteer ik een analyse van de vanadiumhoudende MOF, MIL-47, in de oxidatie van cyclohexeen. In deze studie wordt gebruik gemaakt van TBHP in water of TBHP in decaan als oxidans. MIL-47 is opgebouwd uit een 3-dimensioneel netwerk, waarin iedere metaalsite (V^{+IV}) wordt gecoördineerd door 4 zuurstofatomen van 4 organische liganden en door 2 zuurstofatomen gelegen op een O-V-O as (zie figuur 7.6)[5].

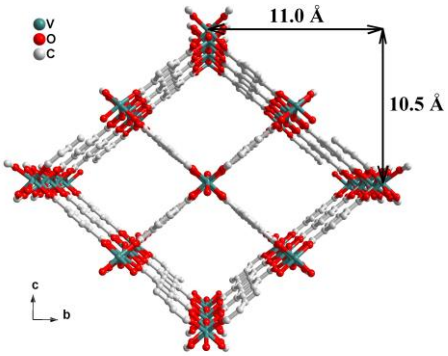

Figuur 7.6. Afbeelding van de vanadiumhoudende MOF, MIL-47.

Tijdens de oxidatie van cyclohexeen kunnen diverse producten worden gevormd, zoals te zien is in figuur 7.7. Een van deze reactieproducten is cyclohexeen oxide, dat een veelzijdige bouwsteen is in de organische synthese.
Uit dit onderzoek is gebleken dat men met het gebruik van TBHP in water als oxidans een hoge conversie van cyclohexeen (55% na 7 uur reactietijd) verkrijgt. Dit is echter ook gepaard gegaan met een hoog uitlogingspercentage (13% na 1 uur reactie). Met het gebruik van TBHP in decaan als oxidans is de uitloging beperkt gebleven tot slechts 3% na een reactietijd van 7 uur. Niettemin werd hierbij slechts een cyclohexeen conversie van 30% na dezelfde tijd bereikt. Verder zijn nog regeneratie- en stabiliteitstesten uitgevoerd met dit watervrije oxidans, waaruit duidelijk is gebleken dat MIL-47 geen verlies aan stabiliteit vertoont gedurende minstens 5 opeenvolgende cycli.

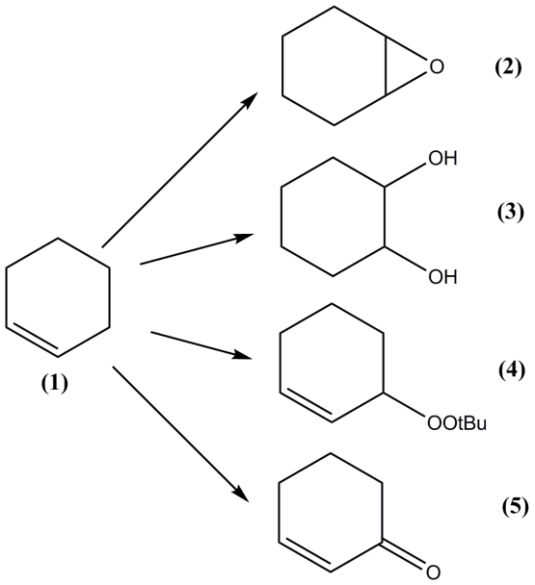

Figuur 7.7. Oxidatie van cyclohexeen (1) naar cyclohexeen oxide (2), cyclohexane-1,2-diol (3), *tert*-butyl-2-cyclohexenyl-1-peroxide (4) en 2-cyclohexene-1-one (5).

In een tweede luik van dit hoofdstuk heb ik de katalytische activiteit van de MIL-47 vergeleken met 2 vanadiumhoudende referentiekatalysatoren VAPO-5 en VO_x/SiO_2. Hieruit is gebleken dat VAPO-5 geen katalytische activiteit bezit en dat de katalytische activiteit van de silica katalysator enkel afkomstig is van het uitgeloogde vanadium. Er is met andere woorden enkel homogene katalyse opgetreden.

Tot slot zijn door middel van computationele berekeningen de actieve sites in MIL-47 bepaald en is het reactiemechanisme ontrafeld van de cyclohexeen oxidatie met behulp van MIL-47. Hieruit kan men ten eerste concluderen dat iedere cyclus start met het breken van minstens 2 V-organische linkerverbindingen zodat coördinatie van het oxidans met het V mogelijk wordt. De tweede conclusie luidt dat er minstens 2 parallelle reactiewegen optreden: één met V^{+IV} als actieve centra en één reactieweg met V^{+V} als actieve centra.

7.6 NH_2-MIL-47: onderzoek van de invloed van de NH_2-functionalisatie op de CO_2 adsorptiecapaciteit

Het aanbrengen van extra groepen op de organische liganden van MOFs, zoals bijvoorbeeld NH_2-groepen, kan een significante invloed uitoefenen op de resulterende adsorptiecapaciteit. Onderzoek heeft in het verleden al aangetoond dat NH_2-gefunctionaliseerde silica materialen een verhoogde CO_2 adsorptiecapaciteit bezitten in vergelijking met niet-gefunctionaliseerde silica materialen. Dit is het gevolg van een sterke interactie tussen het CO_2 en de NH_2 groepen in de poriën. Voor MOF materialen is de invloed van extra NH_2-groepen echter niet zo eenduidig. Bepaalde onderzoeken tonen een verhoging aan van de adsorptiecapaciteit van CO_2, terwijl andere onderzoeksgroepen een daling van de adsorptiecapaciteit rapporteren[6-8]. Naast het aanbrengen van deze extra groepen speelt de flexibiliteit van de MOF structuur ook een belangrijke rol in de resulterende adsorptiecapaciteit. Een typisch voorbeeld hiervan is de flexibele MIL-53 die een 2-staps adsorptieproces vertoont door de structurele veranderingen die optreden tijdens het adsorptieproces, terwijl de structureel gelijke maar rigide MIL-47 een typische Type I isotherm vertoont[9].

In hoofdstuk 4 bespreek ik in eerste instantie de synthese en karakterisering van de NH_2-gemodificeerde MIL-47. Ten tweede wordt de adsorptiecapaciteit van deze NH_2-MIL-47 bepaald voor CO_2 en CH_4 en vergeleken met de niet-gefunctionaliseerde MIL-47 (zie figuur 7.8). In deze figuur ziet men ten eerste dat de NH_2-MIL-47 een lagere adsorptiecapaciteit vertoont voor CO_2 en voor CH_4 in vergelijking met MIL-47. Ten tweede is op de figuur zichtbaar dat bij lage druk de adsorptie-isothermen voor beide materialen samenvallen. Anders geformuleerd, de extra NH_2-groepen geven geen aanleiding tot een verhoogde adsorptiecapaciteit voor CO_2 en CH_4.

Verder zijn ook nog de adsorptie enthalpie waarden bepaald aan de hand van puls-chromatografie experimenten voor MIL-47 en NH_2-MIL-47. Er is een mooie overeenkomst gebleken tussen deze experimenteel bepaalde enthalpie waarden en de berekende adsorbaat- linker interacties, bepaald aan de hand van moleculaire berekeningen.

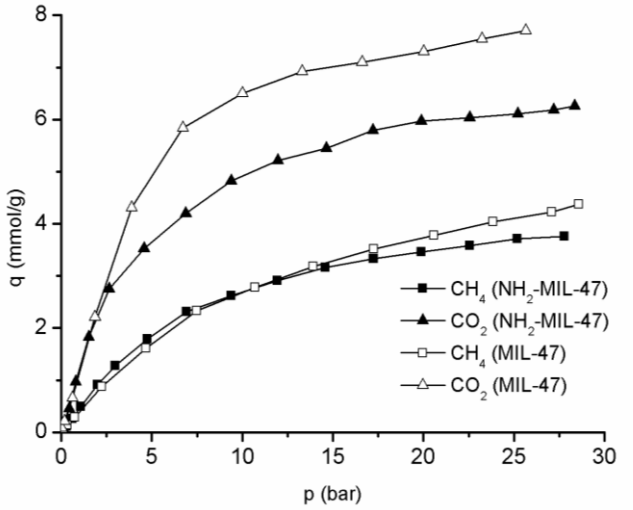

Figuur 7.8. Adsorptie isothermen voor CO_2 en CH_4 van MIL-47 en NH_2-MIL-47.

Uit deze studie kan men dus besluiten dat in tegenstelling tot de flexibele MIL-53 de extra NH_2- groepen geen positief effect teweegbrengen op de adsorptiecapaciteit van NH_2-MIL-47. Dit laat vermoeden dat NH_2-groepen enkel de adsorptiecapaciteit verhogen als de MOF een flexibel netwerk heeft.

7.7 Verankering van $TiO(acac)_2$ op NH_2-MIL-47: een stabiele en herbruikbare katalysator in de oxidatie van cyclohexeen

Zoals beschreven in hoofdstuk 4 kunnen extra groepen op de organische linker, een significante invloed teweegbrengen op de resulterende adsorptiecapaciteit. Hiernaast kunnen deze extra groepen ook katalytische processen beïnvloeden. Dit is onder meer aangetoond door de onderzoeksgroep van De Vos[10] waarin de katalytische activiteit van UiO-66 vergeleken werd met een hele reeks UiO-66-X gefunctionaliseerde materialen (met X= H, NH_2, CH_3, OCH_3, F, Cl, Br, NO_2). Hieruit is gebleken dat de aanwezigheid van NO_2 groepen op de organische linker de katalytische activiteit verhoogde in vergelijking met het niet gefunctionaliseerd materiaal. Een tweede alternatief, om de katalytische activiteit te beïnvloeden, bieden het inbrengen van extra actieve sites in de holtes van de MOF of het verankeren van extra actieve sites op functionele groepen, aanwezig op de organische linkers.

Een voorbeeld van dit laatste is terug te vinden in het artikel van Ingleson[11], waarbij men de NH_2-houdende MOF, IRMOF-3, modificeerde met $VO(acac)_2$ met de vorming van een imine groep. De resulterende katalysator vertoonde echter een lage katalytische en thermische stabiliteit. In een andere studie voerde men een postmodificatie uit van IRMOF-3 met $Mn(acac)_2$[12]. In tegenstelling tot de $VO(acac)_2$@IRMOF-3 vertoonde deze $Mn(acac)_2$@IRMOF-3 wel een goede conversie en stabiliteit. Het nadeel van deze studie was dat er slechts een klein percentage (8%) van $Mn(acac)_2$ verankerd kon worden op IRMOF-3.
In een eerste luik van hoofdstuk 5 heb ik de postmodificatie van NH_2-MIL-47 besproken met behulp van een Ti complex, $TiO(acac)_2$ (zie figuur 7.9). Het percentage aangebracht Ti-complex (1.25 mmol Ti/g) was vrijwel onafhankelijk van de aangewende reactietemperatuur en reactietijd. Door middel van DRIFTS, ^1H NMR en ^{13}C CP/MAS NMR metingen werd duidelijk aangetoond dat het Ti-complex covalent gebonden zat op de V-MOF. Voor verdere details en gedetailleerde karakterisering verwijs ik naar hoofdstuk 5.

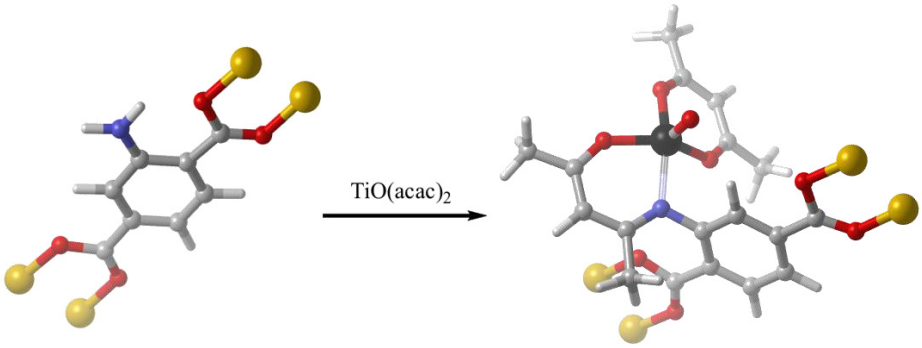

Figuur 7.9. Een vereenvoudigde voorstelling van de postmodificatie van NH_2-MIL-47 met $TiO(acac)_2$. De grijze atomen stellen de koolstofatomen voor, de gele en de rode atomen stellen respectievelijk de vanadium- en zuurstofatomen voor en de atomen in zwart en blauw zijn de titanium- en stikstofatomen.

Na een grondige karakterisering is de katalytische activiteit van de Ti/V- MOF geëvalueerd voor de oxidatie van cyclohexeen. In tegenstelling tot hoofdstuk 3 heb ik in deze studie O_2 in combinatie met cyclohexaancarboxaldehyde als oxidans aangewend.

De katalytische activiteit van de Ti/V-MOF heb ik in tweede instantie vergeleken met de niet-gemodificeerde NH_2-MIL-47 en de homogene katalysator $TiO(acac)_2$. Uit een vergelijking van de TON en TOF waarden is duidelijk te zien dat de Ti/V-MOF een hogere activiteit vertoont dan de NH_2-MIL-47 in de eerste cyclus, terwijl er in de twee daaropvolgende cycli een vrij gelijkaardige tot licht verhoogde activiteit is vast te stellen voor de NH_2-MIL-47. Deze hogere activiteit voor NH_2-MIL-47 is het gevolg van een sterke uitloging van vanadium in iedere cyclus. Dit zorgt voor de creatie van extra defecte sites, die op hun beurt een verhoging van de katalytische activiteit teweegbrengen. Daarentegen vertoont de Ti/V-MOF geen detecteerbare uitloging, en de verhoogde activiteit voor deze MOF in de extra cycli is dan ook te verklaren door een gedeeltelijke oxidatie van de V sites naar V^{+V} tijdens de eerste cyclus. Dus met andere woorden, net zoals beschreven in hoofdstuk drie treden er ook hier twee parallelle reactiepaden op: één met V^{+IV} en één met V^{+V} actieve sites.

7.8 Conclusie en toekomstperspectieven

Metaal-Organische Roosters zijn ondanks hun vrij recente bestaan al voor vele toepassingen onderzocht. In dit onderzoekswerk heb ik een overzicht gegeven van het gebruik van MOFs als heterogene katalysator en meer bepaald hun gebruik in oxidatie katalyse. Het onderzoek werd hierbij toegespitst op de studie van vanadiumhoudende en vanadium/titaniumhoudende MOFs in de oxidatie van cyclohexeen. Hieruit is gebleken dat veel aandacht dient besteed aan het gebruikte oxidans, gezien de beperkte stabiliteit van de V-MOFs. Modificeren van deze V-MOFs met een Ti-complex resulteerde niettemin in een verhoogde stabiliteit.
Verder bestudeerde ik ook de invloed van welbepaalde functionele groepen van de organische linkers op de resulterende adsorptiecapaciteit. Hieruit is duidelijk gebleken dat er vaak een samenspel heerst tussen de organische liganden en flexibiliteit van de MOF.
Tot slot kan men stellen dat het onderzoek rond MOFs nog in zijn kinderschoenen staat en dat het meeste onderzoek zich nog steeds situeert op academisch niveau. Vele vragen dienen nog beantwoord, zeker die met betrekking tot het gebruik van deze materialen in industriële toepassingen.

In de toekomst blijft een harmonieuze samenwerking tussen theoretici en experimentele scheikundigen hiervoor onontbeerlijk.

7.9 Referenties

1. H. Li, M. Eddaoudi, M. O'Keeffe and O. M. Yaghi, *Nature*, 1999, **402**, 276-279.
2. M. Eddaoudi, J. Kim, N. Rosi, D. Vodak, J. Wachter, M. O'Keeffe and O. M. Yaghi, *Science*, 2002, **295**, 469-472.
3. J. R. Li, R. J. Kuppler and H. C. Zhou, *Chem Soc Rev*, 2009, **38**, 1477-1504.
4. L. Q. Ma and W. B. Lin, *Functional Metal-Organic Frameworks: Gas Storage, Separation and Catalysis*, 2010, **293**, 175-205.
5. K. Barthelet, J. Marrot, D. Riou and G. Ferey, *Angew Chem Int Edit*, 2001, **41**, 281-+.
6. B. Arstad, H. Fjellvag, K. O. Kongshaug, O. Swang and R. Blom, *Adsorption*, 2008, **14**, 755-762.
7. J. R. Karra and K. S. Walton, *J Phys Chem C*, 2010, **114**, 15735-15740.
8. A. R. Millward and O. M. Yaghi, *J Am Chem Soc*, 2005, **127**, 17998-17999.
9. T. K. Trung, I. Deroche, A. Rivera, Q. Y. Yang, P. Yot, N. Ramsahye, S. D. Vinot, T. Devic, P. Horcajada, C. Serre, G. Maurin and P. Trens, *Micropor Mesopor Mat*, 2011, **140**, 114-119.
10. F. Vermoortele, M. Vandichel, B. Van de Voorde, R. Ameloot, M. Waroquier, V. Van Speybroeck and D. De Vos, *Angewandte Chemie International Edition*, 2012, **51**, 4887 –4890.
11. M. J. Ingleson, J. P. Barrio, J. B. Guilbaud, Y. Z. Khimyak and M. J. Rosseinsky, *Chem Commun*, 2008, 2680-2682.
12. S. Bhattacharjee, D. A. Yang and W. S. Ahn, *Chem Commun*, 2011, **47**, 3637-3639.

Glossary

A

Activation barrier	For an exothermic elementary step, it is the difference in internal energy between transition state and reactants.
Activation energy	For an elementary step, it is the difference in internal energy between transition state and reactants.
Active sites	Groups responsible for the catalytic activity.
Autoclave	A high pressure, high temperature vessel for carrying out catalytic reactions and making catalysts.
Adsorption isotherm	The quantity of molecules adsorbed or desorbed as a function of the relative pressure is known as the adsorption or desorption isotherm respectively.
Activated complex	See *transition state.*
Activated carbon	Activated carbon or activated coal is a porous carbon containing material and is used in gas purification, decaffeination, gold purification, metal extraction, water purification, medicine and air filters in gas masks and respirators.
Ambient pressure	The pressure of the surrounding medium, such as a gas or liquid, which comes into contact with the object.
Arrhenius equation	This is an equation that represents the dependence of the rate constant k of a reaction on the absolute temperature T: $k = A \exp(-E_a/RT)$ In its original form the pre-exponential factor A and the activation energy E_a are considered to be temperature independent.
Aerobic	Requiring molecular oxygen.
Auto-oxidation	Any oxidation that occurs in open air or in presence of oxygen and/or UV radiation and forms peroxides and hydroperoxides.
Adsorbate	The adsorbed species.
Adsorbent	Surface on which adsorption occurs.

As-synthesized The material obtained directly after synthesis and before any pretreatment.

B

Bronsted acid site Surface site that has a tendency to give up a proton.

Bimetallic catalyst Catalyst for which two active metals are present.

Blanc reactions(catalysis) Performing the catalytic reaction without the presence of the catalyst.

Bifunctional catalyst Represented by catalytic reactions which proceed by a sequence of elementary processes, certain of which occur at one set of sites, while other occur at sites which are of a completely different nature.

Binding energy The mechanical energy required to disassemble a whole into separate parts. A bound system typically has a lower potential energy than its constituent parts; this is what keeps the system together—often this means that energy is released upon the creation of a bound state.

C

Catalysis The phenomenon in which a relatively small amount of a foreign material, called a catalyst, augments the rate of a chemical reaction without itself being consumed.

Catalyst A source of active centers regenerated at the end of a closed reaction sequence.

Catalytic reaction A closed sequence which owes it propagation to a substance called a catalyst.

Chiral catalyst See *enantioselective.*

Calcination Heating in air or oxygen (most likely to be applied to a step in the preparation of a catalyst).

Crystalline Crystallinity refers to the degree of structural order in a solid. In a crystal, the atoms or molecules are arranged in a regular, periodic manner.

Coating A covering that is applied to the surface of an object, usually referred to as the substrate. In many cases coatings are applied to improve surface properties of the substrate, such as appearance, adhesion, corrosion resistance, and scratch resistance.

	In other cases, in particular in printing processes and *semi-conductor* device fabrication (where the substrate is a wafer), the coating forms an essential part of the finished product.
Crystallization	The (natural or artificial) process of formation of solid crystals precipitating from a solution.
Centrifugation	The process of separating lighter portions of a solution, mixture, or suspension from the heavier portions by centrifugal forces.
Chemo selectivity	Refers to the selective reactivity of one functional group in the presence of others; often this process in convoluted and protecting groups are used to ensure that this outcome can be attained.
Chemisorbed	See *Chemisorption.*
Cyanosilylation	An addition reaction in which a cyano (nitrile) group and a silyl group are added across a double bond or triple bond.
Chemisorption	Adsorption in which the forces involved are valence forces of the same kind as those operating in the formation of chemical compounds. Chemisorption strongly depends on the surface and the adsorptive, and only one layer of chemisorbed molecules is formed.

D

Deposition	The settling of particles (atoms or molecules) or sediment from a solution, suspension and mixture or vapor onto a pre-existing surface.
Doping	Treated or impregnated with a foreign substance.
Defect	Any deviation in a crystal from a perfect periodic lattice or structure.
Dead volume	Defined as the total volume minus the volume occupied by the *adsorbent*.
Diffuse Reflectance Infrared Fourier Transform Spectroscopy (DRIFTS)	Diffuse reflectance is a technique used in infrared (IR) spectroscopy. When an IR beam strikes a surface this results in two types of reflections: specular reflectance which directly reflects off the surface and diffuse reflectance in which the light that penetrates is reflected in all directions.
Deactivation(of catalyst)	The decrease in conversion in a catalytic reaction with time of run under constant conditions of reaction. Also known as catalyst decay.

E

Eley-rideal mechanism	Catalytic mechanism in which the rate-determining step is the reaction of a gas-phase molecule with a molecule adsorbed on the catalyst.
Enzyme	Protein molecules that possess exceptional catalytic properties.
Epitaxy	The growth of one crystal on the surface of another crystal in which the growth of the deposited crystal is oriented by the lattice structure of the substrate.
Electron paramagnetic Resonance (EPR)	EPR spectroscopy is used to investigate paramagnetic species, which contain one or more unpaired electrons. The nature of the information deduced from EPR may vary from a simple confirmation of the presence of a given paramagnetic species in a sample to a more detailed description of an intermediate or the coordination sphere of a particular paramagnetic ion.
Entropic effects	In thermodynamics, entropy is commonly associated with the amount of order, disorder, and/or chaos in a thermodynamic system.
Enantioselective	An enantioselective reaction is one in which one enantiomer is formed in preference to the other, in a reaction that creates an optically active product from an achiral starting material, using either a *chiral catalyst*, an *enzyme* or a chiral reagent. The degree of selectivity is measured by the enantiomeric excess.
Elemental analysis	An analysis technique to determine the empirical formula of a material.
Endothermic/endergonic	A process or reaction in which the system absorbs energy from the surroundings in the form of heat.
Exothermic/exergonic	A process or reaction that releases energy from the system, usually in the form of heat, but also in the form of light (e.g. a spark, flame, or explosion) and electricity (e.g. a battery).
Energy profile	An energy profile, or reaction profile is a schematic plot of the energy of a reacting system as a function of the reaction coordinate. The term energy may refer to *enthalpy*, free energy or internal energy. Energy profiles are intended to illustrate the energies of reactant, intermediate, transition and product states of the system in the order in which they are formed; they are useful for depicting reaction mechanisms.

Enthalpy The total energy of a *thermodynamic* system.

F

Fixed bed reactor Reactor in which the catalyst is stationary (usually packed in a tube) and the reactants pass over the catalyst.

Filtrate The product of filtration; a gas or liquid that has been passed through a filter.

G

Gas chromatography The process in which the components of a mixture are separated from one another by injecting the sample into a carrier gas which is passing through and over a bed of packing. Different components move through the bed of packing at different rates and so appear one after another at the effluent end, where they are detected and measured.

Gibbs free energy The Gibbs energy (also referred to as ΔG) is the chemical potential that is minimized when a system reaches equilibrium at constant pressure and temperature.

Green Chemistry Technology is called "green" if it uses raw materials efficiently, such that the use of toxic and hazardous reagents and solvents can be avoided while formation of waste or undesirable byproducts is minimized.

H

Heterogeneous catalysis Catalysis in which the catalyst constitutes a separate phase. Usually the catalyst is a crystalline or amorphous solid and the reactants and products are in one or more fluid phases.

Homogeneous catalysis Catalysis in which all reactants and the catalyst are dispersed in one phase.

Hysteresis A hysteresis is observed as the desorption of the *adsorbate* occurs at lower relative pressures than the adsorption.

Hydrophilic A hydrophilic molecule or portion of a molecule is one that has a tendency to interact with or be dissolved by water and other polar substances.

Hydrophobic Opposite of *hydrophilic.*

Homolytic The breaking of a single (two-electron) bond in which one electron remains on each of the atoms.

Heterolytic Breaking a chemical bond to produce two oppositely charged fragments.

Hydrothermal synthesis See *Solvothermal synthesis.*

Henry adsorption constants The Henry adsorption constant is the constant appearing in the linear adsorption isotherm, which formally resembles Henry's law; therefore, it is also called Henry's adsorption isotherm. This is the simplest adsorption isotherm in that the amount of the surface adsorbate is represented to be proportional to the partial pressure of the adsorptive gas:

$X=K_H P$

where: X= surface coverage

P=partial pressure

K_H= Henry's adsorption constant

Hot filtration (catalysis) Involves filtration of the catalyst part during a reaction, followed by continuation of the reaction in the absence of the (solid) catalyst. This experiment is used to demonstrate the heterogeneity of a catalyst.

Hydrolysis Decomposition of a chemical compound by reaction with water.

I

Induction period The time during which the extent of an reaction remains below experimental detection.

Initiation A step in which active centers are produced.

Irreversible A reaction is irreversible if the rate of the reverse reaction can be neglected as compared to the rate in the forward reaction.

Isomerization The reaction of a molecule to form another molecule with the same number and kinds of atoms but in different configurations.

Interpenetration Two lattices that grow in each other. Synonym: catenation.

Internal standard An internal standard in analytical chemistry is a chemical substance that is added in a constant amount to samples.

	This substance can then be used for calibration by plotting the ratio of the analyte signal to the internal standard signal as a function of the analyte concentration of the standards.
Initiator	A substance introduced into a reaction system in order to bring about an initiation reaction is known as an initiator.
Intermediate	Any reaction species that is neither an initial reactant nor a final product is referred to as an intermediate.

L

Langmuir isotherm or Type I isotherm	This type of isotherm is observed for materials with pores in the micro range (< 2nm). During the physical adsorption, the *micropores* are filled at low relative pressure. Once the pores are filled there is mainly adsorption at the exterior of the material.
Langmuir-Hinshelwood mechanism	In this mechanism it is assumed that both reactants must be adsorbed on the catalyst in order to react.
Lewis acid site	Site capable of receiving a pair of electrons, site which has an unoccupied orbital with a high electron affinity for an electron pair.
Leaching	Extraction of certain materials from a carrier into a liquid.

M

Mechanism	A vague term, related to Latin "machine", used loosely to describe a reaction network, or a reaction sequence. Sometimes called a "model". If based on kinetic arguments, it is occasionally called a "kinetic mechanism".
Model	See *Mechanism*
Mesopore	Pores with widths between 2.0 and 50nm.
Micropore	Pores with widths not exceeding 2.0 nm.
Metal Organic Framework (MOF)	A recent class of crystalline materials containing metal ions or metal clusters which are connected which each other by rigid organic linkers.
Morphology	The study of the form or shape of a catalyst.

Magic Angle Spinning (MAS NMR)	For solid or viscous samples, Magic Angle Spinning (MAS) NMR is used. This technique is based on the appropriate averaging of the various solid-state interactions by spinning the sample at a certain angle to the applied magnetic field. In a MAS NMR experiment the sample is placed in a rotor and is spinned at high speed around an axis at 54.74° to the axis of the applied magnetic field.

N

Nanoporous	According to IUPAC, porosity is defined in 3 areas: micro-, meso- and macroporosity. Porous materials are classified according to the pore diameter into one of these 3 classes: micropores: < 2 nm, mesopores: 2 nm < 50 nm and macropores: > 50 nm.
Nucleation	The initial process that occurs in the formation of a crystal from a solution, a liquid, or a vapor, in which a small number of ions, atoms, or molecules become arranged in a pattern characteristic of a crystalline solid, forming a site upon which additional particles are deposited as the crystal grows.
Nitrogen adsorption	An analysis technique used to determine specific surface and pore characteristics of solid materials. The main characteristics that can be qualified by physical sorption include surface area, pore volume and pore size distribution.
Nuclear Magnetic Resonance (NMR)	The fundamental principle of the NMR technique centers on the induction of transitions between different nuclear Zeeman levels of a particular nucleus.

O

Oxidation	A redox reaction involves oxidation where there is an increase in oxidation number, and reduction where there is a decrease in oxidation number.
Oxidant	An oxidant is a substance that accepts or receives electron from another substance, hence, is consequently reduced. Since it accepts electrons it is also called an electron acceptor. Also called: oxidizing agent or oxidizer.
Out-gassed	Heating a catalyst in vacuum to remove adsorbed or dissolved gas. Also used to refer to the gas desorbing when any solid is heated in vacuum.

P

Pretreatment	A treatment applied to a solid material before the start of catalytic run or another test. For MOF materials, the pretreatment step is often heating under vacuum.
Pore volume	Total internal void volume per unit mass of *adsorbent*.
Porosity	See *Nanoporous.*
Polyoxometalate (POM)	A polyoxometalate is a polyatomic ion, usually an anion, that consists of three or more transition metal oxyanions linked together by shared oxygen atoms to form a large, closed 3-dimensional framework.
Particle size (crystallite size)	The approximate diameter of a particle.
Paramagnetic	A substance which, when placed in a magnetic field, is magnetized parallel to the field to an extent proportional to the field (except at very low temperatures or in extremely large magnetic fields).
Poisoning	*Chemisorption* of reactants, products or impurities (alone or in combination) which occupy sites otherwise available for *catalysis*, resulting in reduced activity.
Physisorption	Also called physical adsorption, is accompanied by low heats of adsorption with no violent or disruptive structural changes occurring to the surface during the adsorption measurement. Physical adsorption may lead to surface coverage by more than one layer of *adsorbate.*
Periodic calculations	The limits of the cluster approach can be solved by using the periodic approach. Zeolites and MOF structures are build up by a certain unit cell, which is periodically repeated. In the periodic approach, there is no small piece cut away, but the whole unit cell is modeled or a multiplication of the unit cell (to prevent self interactions). Using a periodic repetition of the unit cell, an infinite crystal is mimicked.

R

Rate constant	The constant of proportionality that does not depend on composition, in the expression for the rate of a reaction. Also called “specific rate constant”.

Rate-determining step — If, in a reaction sequence, consisting of n steps (n-1) steps are reversible and if the rate of each one is very much larger in either direction than the rate of the n^{th} step, the latter is said to be rate-determining. It is also sometimes called the slow step.

Reaction rate — The number of moles of a substance created by a chemical reaction per unit time.

Regeneration — A special operation to reverse catalytic deactivation and restore catalytic activity.

Reticular synthesis — Reticular: form a net, described as the process of assembling designed rigid secondary building units (SBU) into predetermined ordered structures (networks) which are held together by strong bondings.

Reversible — A reaction is reversible if the rates in the forward and reverse direction are of the same order of magnitude.

Radical — Radicals are atoms, molecules, or ions with unpaired electrons.

Regio selectivity — Regio selectivity is the preference of one direction of chemical bond making or breaking over all other possible directions.

Reaction kinetics — Deals with the rates of chemical processes.

S

Step — The irreducible act of reaction in which reactants are transformed into products.

Structure (of a catalyst) — The distribution in space of the atoms or ions in the material part of the catalyst.

Substrate — In homogeneous catalysis: the substance undergoing reaction. In heterogeneous catalysis: any solid material on which adsorption or on which a layer or coating of a different material is deposited.

Support (carrier) — Material, usually of high surface area, on which the active catalytic material, present as the minor component, is dispersed. The support may be catalytically inert, but it may contribute to the overall catalytic activity.

Single crystal — A solid with its atoms arranged in a perfect, periodic lattice structure.

Scanning electron microscopy (SEM)	A technique for obtaining highly magnified images of solids. It is used to record catalyst structure and measure supported-catalyst particle size distribution.
Selectivity	Describes the relative rates of two or more competing reactions on a catalyst. For a single reactant taking part in two or more reactions, it may be defined in two ways: (1) fractional selectivity: the rate of the desired reaction dived by the sum of the rates of all the reactions; (2) relative selectivity: for each pair of products, the rate of the desired reaction divided by the rate of another reaction.
Stereo selectivity	The property of a chemical reaction in which a single reactant forms an unequal mixture of stereoisomers during the non-stereospecific creation of a new stereocenter or during the non-stereospecific transformation of a pre-existing one. The selectivity arises from differences in *steric* effects and electronic effects in the mechanistic pathways leading to the different products.
Shape selectivity	The ability to accommodate only molecules of a particular shape and size within the pores of a framework. This is observed for example in *zeolites*.
Surface area	see *Nitrogen adsorption.*
Semi-conductor	An insulator in which, in thermal equilibrium, some charge carriers are mobile.
Synergistic/synergetic	The joint action of agents, that when taking them together increase each other's effectiveness (in contrast to antagonism).
Saturation	Has diverse meanings in chemistry. However they are all based on reaching a maximum capacity.
Solvothermal synthesis	A method of producing chemical compounds. It is very similar to the *hydrothermal* route, the only difference being that the precursor solution is usually not aqueous.
Static calculations	The search toward the most stabile geometry of atoms (without taking into account their movements).
Steric hindrance	Steric hindrance occurs when the large size of groups within a molecule prevents chemical reactions that are observed in related molecules with smaller groups. Although steric hindrance is sometimes a problem, it can also be a very useful tool, and is often

exploited by chemists to change the reactivity pattern of a molecule by stopping unwanted side-reactions.

T

Termination — A step which destroys active centers in a chain reaction.

Transition state — The configuration of highest potential energy along the path of lowest energy between reactants and products. Synonymous with *activated complex*.

Thermogravimetric analysis — A technique whereby the weight of a substance heated in an environment at a constant rate is recorded as a function of temperature.

Turnover number (TON) (turnover frequency (TOF)) — The number of molecules reacting per active site in unit time.

Topology — Arrangement of the various elements (links, nodes, etc.) to build up a MOF.

Templating agents — The term template is associated with the liquid-crystal because it determines the structure of the solid material.

Thin films — A layer of material ranging from fractions of a nanometer (monolayer) to several micrometers in thickness.

Thermodynamics — The branch of natural science concerned with heat and its relation to other forms of energy and work. It defines macroscopic variables (such as temperature, entropy, and pressure) that describe average properties of material bodies and radiation, and explains how they are related and by what laws they change with time.

U

UV/Vis spectroscopy — Refers to absorption spectroscopy or reflectance spectroscopy in the ultraviolet-visible spectral region. UV/Vis spectroscopy is routinely used in analytical chemistry for the quantitative determination of different analytes, such as transition metal ions, highly conjugated organic compounds, and biological macromolecules. Spectroscopic analysis is commonly carried out in solutions but solids and gases may also be studied.

Unimolecular reaction — A chemical reaction involving only one molecular species as a reactant.

V

Van Der Waals Interactions	Sum of the attractive or repulsive forces between molecules (or between parts of the same molecule) other than those due to covalent bonds, the hydrogen bonds, or the electrostatic interactions of ions with one another or with neutral molecules.
Vacancy	An imperfection in a crystal structure in which an atom or ion is missing.

X

X-ray photoelectron Spectroscopy (XPS)	A nondestructive technique for analyzing the elemental chemical composition of solids by directing a monochromatic X-ray beam at the solid and analyzing the energy of the generated photoelectron. Chemical shifts can be measured, thus an elucidation of the chemical environment of the elements present can be obtained.
X-ray fluorescence (XRF)	Emission of X-rays by the material when an electron drops down to a vacant level and releases energy.
X-ray Powder Diffraction (XRPD)	XRPD is a non-destructive analytical method for the identification of crystalline phases and estimation of phase fractions.

Y

Yield	Ratio of the amount of a desired product formed to the amount of reactant consumed.

Z

Zeolite	Naturally occurring crystalline aluminosilicates which are composed of ordered arrangements of SiO_4 and AlO_4 tetrahedra and metal cations. They can also be prepared synthetically and their small pore structure allows them to be used as molecular sieves.
Zeotype	Materials with zeolitic structure and properties. It are synthetic molecular sieves containing other elements than Si and Al. The first in line were the aluminophosphates (AlPO), consisting of Al and P. Other zeotypes are, silico-aluminophosphates (SAPO) and metal-aluminophosphates (MeAPO).